

University of Southampton Research Repository ePrints Soton

Copyright © and Moral Rights for this thesis are retained by the author and/or other copyright owners. A copy can be downloaded for personal non-commercial research or study, without prior permission or charge. This thesis cannot be reproduced or quoted extensively from without first obtaining permission in writing from the copyright holder/s. The content must not be changed in any way or sold commercially in any format or medium without the formal permission of the copyright holders.

When referring to this work, full bibliographic details including the author, title, awarding institution and date of the thesis must be given e.g.

AUTHOR (year of submission) "Full thesis title", University of Southampton, name of the University School or Department, PhD Thesis, pagination

University of Southampton

Faculty of Engineering, Science & Mathematics

School of Engineering Sciences

**Performance Analysis of a Reduced Cost Manufacturing Process for Composite Aircraft
Secondary Structure**

by

Duncan Andrew Crump

Thesis for the degree of Doctorate of Engineering

April 2009

University of Southampton

Abstract

Faculty of Engineering, Science and Mathematics

School of Engineering Sciences

Doctor of Engineering

Performance Analysis of a Reduced Cost Manufacturing Process for Composite Aircraft

Secondary Structure

by Duncan Andrew Crump

In the current, environmentally-aware, climate aircraft designers are under increasing pressure to produce fuel efficient vehicles. Weight reduction is an important method for increasing fuel efficiency. Fibre reinforced polymer (FRP) composites are known to offer weight savings over traditional metallic components, due to their excellent stiffness and strength to weight ratios. However, the major limiting factor for the use of aerospace quality composites is the manufacturing cost. The costs incurred in the conventional process of prepreg cured in an autoclave are well documented. The research in this thesis is concerned with reducing the cost of manufacturing aircraft standard carbon fibre composite sandwich panels, whilst maintaining mechanical performance.

The overall aim of the EngD is to provide a unified approach for assessing the performance of carbon fibre sandwich secondary structure that are manufactured using several different techniques. Cost and performance criteria are defined so that an optimal panel can be produced. The work has been motivated by the industrial sponsor, GE Aviation Systems. Five combinations of raw material and processing techniques, manufacturing options (MOs) were considered in incremental steps from the baseline of unidirectional prepreg cured in an autoclave to the non-crimp fabric (NCF) infiltrated using resin film infusion (RFI) and cured in a conventional oven. For cost and performance analysis a generic panel has been designed that is representative of secondary wing structure on commercial passenger aircraft. The cost was estimated by monitoring the manufacture of generic panels using each MO, whilst the performance was measured by both mechanical characterisation tests and by full scale tests on a custom designed rig. The rig applies a pressure load using a water cushion and allows optical access to the surface of the panel enabling the use of optical techniques, i.e. thermoelastic stress analysis (TSA) and digital image correlation (DIC). Feasibility tests on TSA and DIC demonstrated their use on the materials considered in this thesis, and were used to validate finite element (FE) models.

The RFI out-of-autoclave process was found to reduce generic panel manufacture time by almost 30%, and the material cost was reduced by almost 40%. The mechanical characterisation tests suggested the 'new' process could produce laminates with a similar fibre volume fraction to that of the original process and similar in and out-of-plane mechanical properties. The in-plane stiffness was slightly reduced by 7 %, but the strength showed an increase of 12%. Full scale tests on the generic panels using point out-of-plane deflection measurements and full field TSA demonstrated the panel produced using the 'new' process has adequate performance. Moreover the full-field tests indicated an improvement in performance. Further work is required to optimise the design of the panel for weight, in particular the weight of the raw material, and investigating methods for modelling the NCF for certification.

Contents

List of Figures	vii
List of Tables.....	xii
Acknowledgements	xiv
Notation	xv
Abbreviations	xvi
1. Introduction	1
1.1 Background.....	1
1.2 Industrial Sponsors	4
1.3 Aims and Objectives.....	4
1.4 Novelty.....	5
1.5 Structure of Thesis	7
2 An overview of current practice and recent developments in composite manufacture	10
2.1 Introduction	10
2.2 Materials.....	10
2.2.1 Matrix materials	11
2.2.2 Reinforcements.....	12
2.2.3 Materials databases	14
2.3 Manufacturing.....	14
2.3.1 Raw materials	14
2.3.2 Processing methods	15
2.3.3 Curing methods	18
2.3.4 Automation.....	21
2.3.5 Design.....	23
2.4 Summary	24
3 GE Aviation Systems Current Practice	28
3.1 Introduction	28
3.2 Survey of Design and loads	28

3.3	Current manufacturing procedure	29
3.3.1	Overview.....	29
3.3.2	Goods-in.....	30
3.3.3	Prepreg Cutting.....	31
3.3.4	Core Cutting.....	31
3.3.5	Lay-up.....	32
3.3.6	Cure Process.....	33
3.3.7	De-Bag	33
3.3.8	Trim/Drill.....	33
3.3.9	Inspection and NDT.....	34
3.3.10	Observations	35
3.4	Current costing analysis.....	37
4	Cost of manufacture and its analysis.....	39
4.1	Introduction	39
4.2	Cost of composite parts	40
4.2.1	Autoclave/out-of-autoclave.....	40
4.2.2	Materials.....	41
4.3	Cost analysis	43
4.3.1	Cost model types	43
4.3.2	Traditional Costing Methods.....	44
4.3.3	Case-based reasoning.....	45
4.3.4	Activity Based Costing (ABC)	45
4.3.5	Parametric cost models.....	48
4.3.6	Feature Based cost models.....	50
4.4	Linking design and cost optimisation.....	51
4.5	Summary	53
5	Generic Panel Manufacture	56
5.1	Introduction	56
5.2	Manufacturing Options	57

5.3	Generic Panel Design	58
5.4	Manufacture of Generic Panels.....	58
5.4.1	Manufacturing Option 1.....	58
5.4.2	Manufacturing Option 2.....	61
5.4.3	Manufacturing Option 3.....	63
5.4.4	Manufacturing Option 4.....	64
5.4.5	Manufacturing Option 5.....	65
5.4.6	Relative Cost of each MO	65
5.5	Test panels manufactured	67
5.6	NDT of generic panels	69
5.7	Summary	72
6	Face sheet material characterisation	74
6.1	Introduction	74
6.2	Fibre volume fraction	75
6.3	In-plane tests	79
6.4	Out-of-plane tests.....	81
6.5	Summary	83
7	Design and commissioning of a full scale test rig.....	84
7.1	Introduction	84
7.2	Initial FE analysis of generic panel.....	85
7.3	Concept Design of Test Rig	89
7.4	Detailed Design of Rig	92
7.4.1	Flexible pressure cushion:	92
7.4.2	Fixed structure:	93
7.4.3	Moving structure	93
7.5	Commissioning of the test rig	95
7.5.1	Static Testing.....	95
7.5.2	Cyclic Testing.....	97
7.6	Summary	97

8	Digital Image Correlation (DIC).....	99
8.1	Introduction	99
8.2	Brief overview of application of DIC	100
8.3	Correlation cell size	103
8.4	Correlation pattern	106
8.5	Full-scale test.....	108
8.5.1	Experimental approach	108
8.5.2	FE for comparison.....	109
8.5.3	Full-scale – Natural pattern.....	110
8.5.4	Full-scale – Recommended pattern	112
8.5.5	Full-scale – Recommended pattern/reduced area of interest	114
8.6	Summary	118
9.	Thermoelastic stress analysis (TSA)	120
9.1	Introduction	120
9.2	Brief overview of application of TSA	121
9.3	Tensile feasibility tests	123
9.3.1	Strain measurement.....	123
9.3.2	Experimental calibration	127
9.3.3	Full scale experimental approach.....	129
9.4	FE Models	130
9.5	Comparison of generic panels.....	137
9.5.1	Maximum deflection results.....	137
9.5.2	Full-field TSA results	142
9.6	Summary	153
10.	Optimisation of panel.....	155
10.1	Introduction	155
10.2	Summary of previous chapters.....	156
10.2.1	Manufacturing and material costs	156
10.2.2	Mechanical characterisation	156

10.2.3	Generic panel comparison	157
10.3	Application of out-of-autoclave manufacture to GE	160
10.4	Greenfield site analysis	161
10.5	Summary	163
11.	Conclusions and future work	165
	References.....	170
	Appendices	176
	Appendix A – Drawings of Test Rig design.....	176
	Appendix B – Matlab code.....	193
	Appendix C –Future generic panel designs	199
	Appendix D – List of Publications	200

List of Figures

Figure 1.1 : Diagram of an aircraft wing and the position of secondary structure	3
Figure 1.2: Scheme to compare processes through cost and performance.....	7
Figure 2.1: Coordinate systems for lamina and laminate	11
Figure 2.2: Examples of woven fibre reinforcements	13
Figure 2.3: Schematic of the hand lay-up process	15
Figure 2.4: Schematic of RTM	16
Figure 2.5: Schematic of the VARI process	17
Figure 2.6: Schematic of the RFI process.....	18
Figure 2.7: Example of the cure cycle used for aerospace composites.....	19
Figure 2.8: Schematic of Quickstep process	20
Figure 3.1: Baseline process for the manufacture of composite sandwich structure at GE	30
Figure 3.2: Photograph illustrating core crush.....	33
Figure 3.3: Flow diagram of the autoclave based manufacturing process.....	35
Figure 3.4: Bottleneck caused by autoclave cure	37
Figure 4.1 : Cost Model Approaches.....	44
Figure 4.2 :Implementation of an ABC method	46
Figure 4.3: Example of results from costing a range of products with ABC and traditional approaches	47
Figure 4.4 :An example of a component split into features	50
Figure 5.1: Geometry of generic panel design	58
Figure 5.2: Photograph of small section of Nomex honeycomb core.....	59
Figure 5.3: Photograph of an example of the stabilised honeycomb core.....	60
Figure 5.4: Photograph of foam core.....	68
Figure 5.5: Ultrasound C-scan images of MO1 panels.....	69
Figure 5.6: Ultrasound C-scan images of MO2 panels.....	70
Figure 5.7: Ultrasound C-scan images of MO3 panels.....	70
Figure 5.8: Ultrasound C-scans images of MO4 panels	71

Figure 5.9: Ultrasound C-scans images of MO5 panels	71
Figure 5.10: Ultrasound C-scans images of other panels	72
Figure 6.1: Microscopy images of consolidated laminates from MO 1	77
Figure 6.2: Microscopy images of consolidated laminates from MO 2	77
Figure 6.3: Microscopy images of consolidated laminates of MO 3	77
Figure 6.4: Microscopy images of consolidated laminates of MO 4	78
Figure 6.5: Microscopy images of consolidated laminates from MO 5	78
Figure 6.6: Bar chart showing Young's modulus and strength data normalised against MO1	81
Figure 6.7: Typical stress-strain curves of specimens manufactured from MO1 and MO5	81
Figure 6.8: Bar chart showing flexural data normalised against MO1	83
Figure 7.1: Graph demonstrating convergence of FE model with element size.....	87
Figure 7.2: FE model mesh with loads and boundary conditions	88
Figure 7.3: Predicted out of plane deformation from FE model	88
Figure 7.4: Predicted ϵ_x strain field from FE model	88
Figure 7.5: Concept of pressure test rig.....	90
Figure 7.6: Initial design of pressure test rig	91
Figure 7.7: Design of pressure cushion.....	92
Figure 7.8: Photographs of the rig installed on the test machine	95
Figure 7.9: Plots of static tests.....	96
Figure 7.10: Cyclic tests	97
Figure 8.1: Photos of LaVision system set-up for a test	101
Figure 8.2: Demonstration of cell size and cell overlap and its application to correlation.....	101
Figure 8.3: Example of working volume calculated using calibration step	102
Figure 8.4: Example of a calibration plate used with the LaVision system.....	103
Figure 8.5: Recommended paint speckle pattern on the tensile specimen.....	104
Figure 8.6: DIC strain data normalised to the extensometer for each of the processing parameter combinations	105
Figure 8.7: Longitudinal DIC stain map of tensile specimen using 64 x 64 pixels with 50 % overlap	106

Figure 8.8: Coefficient of variation of DIC strain along the centreline of the tensile specimen for each of the processing parameter combinations	106
Figure 8.9: Representative plots of surface patterns on specimens MO 1 and MO 2	107
Figure 8.10: Normalised DIC strain values for the different correlation patterns and materials...	108
Figure 8.11: Photograph of DIC cameras supported over the generic panel	109
Figure 8.12: FE predicted out-of-plane deformation in the area of interest.....	110
Figure 8.13: FE predicted in-plane strain in the area of interest.....	110
Figure 8.14: Raw reference images of the first feasibility test with a natural correlation pattern...	111
Figure 8.15: Surface height correlated with natural surface pattern	111
Figure 8.16: 3D representation of the measured panel's deformation	112
Figure 8.17: Raw reference images of the second feasibility test with a recommended correlation pattern	112
Figure 8.18: Surface height correlated with recommended surface pattern.....	113
Figure 8.19: 3D representation of the measured panel's deformation with recommended pattern	113
Figure 8.20: DIC strain map using recommended pattern using (a) 128 x 128, (b) 64 x 64	114
Figure 8.21: Raw reference images of the second feasibility test with a recommended correlation pattern and reduced area of interest	115
Figure 8.22: Surface height correlated with recommended surface pattern and reduced area of interest.....	115
Figure 8.23: 3D representation of the measured panel's deformation with recommended pattern and reduced area of interest.....	115
Figure 8.24: DIC strain map using recommended pattern and reduced area of interest using (a) 128 x 128, (b) 64 x 64	116
Figure 8.25: FE and DIC strain maps interpolated on to a regular grid for comparison	117
Figure 8.26: Line plot of FE and DIC strain along line in Figure 8.25 for comparison.....	117
Figure 9.1: Schematic of application of TSA to test specimen	122
Figure 9.2: TSA images of tensile specimens; (a) M1 with surface ply at 0°, (b) M1 with surface ply at 90°, (c) M2, (d) M3, (e) M4, (f) M5	124
Figure 9.3: Graphs of measured and calculated temperature changes for (a) MO 1, (b) MO 2, (c) MO 4	126
Figure 9.4: TSA images to measure the calibration constants for each of the MOs	128
Figure 9.5: Predicted longitudinal and transverse stresses from FE model.....	134

Figure 9.6: Processed stress data from FE models using both homogeneous and ply-by-ply face sheet models	134
Figure 9.7: Lines of stress from (a) homogenous model (b) ply-by-ply model	135
Figure 9.8: Processed stress data for MO2 from FE models using both homogenous and ply-by-ply face sheets	136
Figure 9.9: Processed stress data for MO4 from FE models using both homogeneous and ply-by-ply face sheets	136
Figure 9.10: Processed stress data for (a) MO3 and (b) MO5, from homogeneous FE models....	137
Figure 9.11: Maximum displacement from transducer for crossply panel	138
Figure 9.12: Maximum displacement from transducer for panels made from MO 1	138
Figure 9.13: Maximum displacement from transducer for panels made from MO 2	139
Figure 9.14: Maximum displacement from transducer for panels made from MO 3	140
Figure 9.15: Maximum displacement from transducer for panels made from MO 4	140
Figure 9.16: Maximum displacement from transducer for panels made from MO 5	141
Figure 9.17: Example of full-field data from MO1	143
Figure 9.18: Example of full-field data from MO 2.....	143
Figure 9.19: Example of full-field data from MO 3.....	144
Figure 9.20: Example of full-field data from MO 4.....	144
Figure 9.21: Example of full-field data from MO 5.....	145
Figure 9.22: FE and TSA comparison for MO 1	146
Figure 9.23: FE and TSA comparison for MO2	146
Figure 9.24: FE and TSA comparison for MO3	147
Figure 9.25: FE and TSA comparison for MO4	147
Figure 9.26: FE and TSA comparison for MO5	148
Figure 9.27: Example line plot through stress concentration at the corner of the core for MO 1	149
Figure 9.28: Example line plot through stress concentration at the corner of the core for MO 2	149
Figure 9.29: Example line plot through stress concentration at the corner of the core for MO 3	150
Figure 9.30: Example line plot through stress concentration at the corner of the core for MO 4	151
Figure 9.31: Example line plot through stress concentration at the corner of the core for MO 5	151
Figure 10.1: Maximum displacement using transducer of MO 5 other panels	159

Figure 10.2: Maximum displacement using transducer of MO 4 other panels	159
Figure 10.3: Full-field TSA on MO 5 of other panels	160

List of Tables

Table 2.1: Advantages and limitaions of methods for composite manufacture.....	24
Table 3.1: Breakdown of costs in autoclave cured prepreg manufacture.....	36
Table 4.1: Advantages and disadvantages of the costing approaches	53
Table 5.1: Operations in the core stabilisation procedure and their duration	59
Table 5.2: Operations in the MO1 manufacturing process and their duration	61
Table 5.3: Operations in the MO2 and MO4 manufacturing processes and their duration	63
Table 5.4: Operations in the MO3 and MO5 manufacturing processes and their duration	64
Table 5.5: Time to manufacture panels for each MO and the relative cost of each process	66
Table 5.6: Estimation of material costs of manufacture of a panel using each MO	67
Table 5.7: List of generic test panels	68
Table 6.1: Volume fraction of the face sheets produced by each MO obtained from thickness measurements and image analysis.....	76
Table 6.2: Elastic properties of the face sheet lamina material for MO1, MO2 and MO4.....	80
Table 6.3: Tensile properties of the face sheet materials produced from each MO.....	80
Table 6.4: Out of plane properties of the face sheet material produced from each MO	82
Table 7.1: Material properties used for initial FE model	86
Table 9.1: Comparison of the measured temperature change at 10 Hz against calculated	125
Table 9.2: TSA calibrations constant K_L and K_T for the five Mos.....	129
Table 9.3: Predicted maximum deflection for each MO.....	131
Table 9.4: Experimental and FE deflections of panels produced using the five MOs	142
Table 9.5: Values of variation in stress sum in each MO	152
Table 10.1: Average mass per unit area of generic panels	157
Table 10.2: Cost of individual items	162
Table 10.3: Capital cost of greenfield autoclave site	162
Table 10.4: Capital cost of greenfield out-of-autoclave site	163

DECLARATION OF AUTHORSHIP

I, Duncan Andrew Crump, declare that the thesis entitled

Performance Analysis of a Reduced Cost Manufacturing Process for Composite Aircraft Secondary Structure

and the work presented in the thesis are both my own, and have been generated by me as the result of my original research. I confirm that:

this work was done wholly or mainly while in candidature for a research degree at this University;

where any part of this thesis has previously been submitted for a degree or any other qualification at this University or any other institution, this has been clearly stated;

where I have consulted the published work of others, this is always clearly attributed;

where I have quoted from the work of others, the source is always given. With the exception of such quotations, this thesis is entirely my own work;

I have acknowledged all main sources of help;

where the thesis is based on work done by myself jointly with others, I have made clear exactly what was done by others and what I have contributed myself;

parts of this work have been published (Appendix D)

Signed:

Date:

Acknowledgements

I would first like to thank my supervisors Professor Janice Dulieu-Barton and John Savage for their support, perseverance and advice during the last few years. I would also like to acknowledge the help of Dr Paul Cunningham in getting the project started. I would like to recognise the financial support offered by both the Engineering and Physical Sciences Research Council (EPSRC) and GE Aviation Systems.

Thanks too for the technical advice from members of University of Southampton and GE: Steve, Ed, Colin and Paul at GE for guidance on composite manufacture and making me feel welcome on site; James Chitty, Mike Street, Pete Sellen and the rest of the team in the EDMC for assistance on the rig design and its final manufacture. Finally, Erik Roszkowiak, Dave Beckett and Chris Wagg for helping with lab work and importantly giving some elbow grease to assembling and dismantling the large test rig each time.

I am very grateful to the other lab users who have at times provided a sounding board and training on test equipment, in particular Jimmy, Trystan, Richard, Helen, Djallal and Chen. I would also like to thank all the people in the fluid structures interaction group, past and present.

Special thanks should go to the many housemates and friends who have helped to make the last few years a fun and enjoyable experience. With particular thanks to: Suk, who still holds the meanest housemate award; Polly, for all the Sambucca and smiles; Lily, with whom I had many ‘heated’ debates; Ian, for his practical skills and almost fixing the boiler; Mike for his cakes; and Adam and Adele for the fun times and allowing me to sleep on the living room floor rather than a long cold walk home. They have also been there during the not so fun past few months spent writing up.

Finally, I would like to extend my gratitude to my parents and family for their continued support, even though I have rarely been present in the past year. The EngD and thesis would never have reached fruition were it not for the love and advice of my girlfriend the Lovely Lucy.

So what I’m trying to say, I guess, is Thanks everyone!

Notation

A_w	Areal fibre weight
A	Coefficient of linear thermal expansion
C_p	Specific heat at constant pressure
$Cost_{Material}$	Material cost
$Cost_{Rate}$	Charging rate for an operation including overheads
$Cost_{Total}$	Total manufacturing cost
ΔC	Change in cost
ΔT	Change in surface temperature
ΔW	Change in weight
E	Young's Modulus
E_f	Flexural Young's modulus
ϵ	Strain
K	Thermal calibration constant
L	Longitudinal
ν	Poisson's ratio
n	Number of plies
Q	Laminate stiffnesses
ρ	Density
ρ_f	Fibre density
σ	Stress
σ_F	Failure stress (strength)
σ_{Ff}	Flexural failure stress
T	Transverse or temperature
t	Thickness
t_{avg}	Average thickness
$Time_{Operation}$	Time for each operation
V_f	Fibre volume fraction

Abbreviations

ABC	Activity Based Costing
ACCEM	Advanced Composite Cost Estimating Model
ATL	Automated Tape Layer
CAD	Computer Aided Design
CAM	Computer Aided Manufacture
CBR	Case-Based Reasoning
CCD	Charge Couple Device
CER	Cost Estimating Relationship
CFRP	Carbon Fibre Reinforced Polymer
CLT	Classical Laminate Theory
CNC	Computer Numerically Controlled
DFP	Direct Fibre Preforming
DIC	Digital Image Correlation
EBC	Electron Beam Curing
FE	Finite Element
FRP	Fibre Reinforced Polymer
ILSS	InterLaminar Shear Strength
LVDT	Linear Variable Differential Transformer
MCMC	Manufacturing Cost Model for Composites
MO	Manufacturing Option
NCF	Non-Crimp Fabric
NDT	Non-Destructive Testing
PFE	Precision Feed Endeffector
PPT	Pulse Phase Thermography
QI	Quasi-Isotropic
RFI	Resin Film Infusion
RTM	Resin Transfer Moulding
TSA	Thermoelastic Stress Analysis
UD	UniDirectional
UV	Ultra-Violet
VARI	Vacuum Assisted Resin Infusion
VARTM	Vacuum Assisted Resin Transfer Moulding
VICONOPT	Vibration and Instability analysis with CONstraints OPTimisation

Chapter 1

1. Introduction

1.1 Background

In the current, environmentally-aware climate, aircraft designers are under increasing pressure to produce fuel efficient vehicles to reduce the impact of air travel and transportation. Any saving in the empty weight of an aircraft allows the end user to include more fuel mass, for increased range, or transport a larger payload. Therefore the structure of an aircraft is weight critical. The weight savings afforded by fibre reinforced polymer composites are one means available to the designer. Composites are materials made from two or more constituent parts that, together, form a material that has better mechanical properties than those of the constituent parts [1]. For the purposes of this work, ‘composites’ refers to fibre reinforced polymers (FRP). These use stiff and strong fibres that are consolidated with a polymer matrix to form a structural material. Such materials can be designed to provide material properties tailored to a particular application. The designer can define the mechanical properties by controlling the orientation of the fibres that provide directional stiffness and strength. Composites also provide excellent stiffness and strength to weight ratios when compared to standard engineering materials such as steel or aluminium [1]. It is for this reason that composites are increasingly used in the structure of commercial passenger aircraft. The first use of composite structure in a commercial passenger aircraft was as part of NASA’s aircraft energy efficiency program, between 1975 and 1986 [2]. In the previous generation (early 1990s) of medium sized passenger aircraft, e.g. Airbus A320 and Boeing 777, between 10 and 20% of the total airframe was manufactured from composites by weight [3]. The airframe can be defined as the structure of an aircraft, not including the engines. However, the airframe of the Airbus A380

(Super Jumbo), now in-service, is constructed of 22% composites by weight [4]. The Boeing 787 Dreamliner, in the design stage, is expected to use approximately 50% composites by weight [4]. The use of composites on the modern airframe is diverse; primary and secondary components in the fuselage, tail and wing have been manufactured from composites [4-6]. Jones [7] suggested the life-cycle value weight reduction of a single kg for an aircraft was \$880. This was the value in 1999, and is therefore expected to be much higher in today's economic climate.

The major limiting factor for the use of composite structure in the aircraft industry is the material and manufacturing costs compared with metals. This is particularly important for the aerospace industry, where high quality, well consolidated composites necessitate an expensive manufacturing process. The traditional approach for the production of aerospace quality composites uses a uni-directional (fibres aligned in one direction) mat pre-impregnated with resin (pre-preg) that is cut into individual plies. The plies are laid on to a tool, one on top of another, and the whole component is sealed into a vacuum bag to assist in consolidation. The tool and vacuum bag are placed into an autoclave, where a controlled application of heat and pressure (a cure cycle) cures the component. The sources of cost in the process have been investigated in the literature, and it has been shown that the process incurs a cost premium [8, 9]. The prepreg is an expensive form of raw material due to the extensive pre-processing that is necessary. The lay-up process is labour intensive and therefore a large number of man hours are required to manufacture a panel. Finally, autoclaves are expensive to run and have a high capital and setup cost [8, 10]. Therefore, investigations to alter the process or material are important to reduce the cost to manufacture.

The majority of recent research into cost reduction has concentrated on optimising the manufacture of primary composite structures [10-14]. However, there has been less interest in the manufacture of composites used for secondary structure. This research particularly focuses on secondary wing structure panels highlighted in Figure 1.1. Such panels are manufactured from composite sandwich. A sandwich structure uses thin, but stiff, face sheet materials (in this case composite) around a thick but less stiff core (often in the aerospace industry this is a Nomex paper honeycomb) [15]. The thick core increases the distance between the face sheets creating a structure that acts as an 'I' Beam and provides excellent flexural properties. Therefore, the sandwich structure allows similar flexural performance from a structure that is much lighter than a monolithic structure [15]. For example, it is possible to increase the bending strength of a structure by approximately six times by increasing the thickness by two and half times. By using a core material, this barely increases the overall weight of the structure [15].

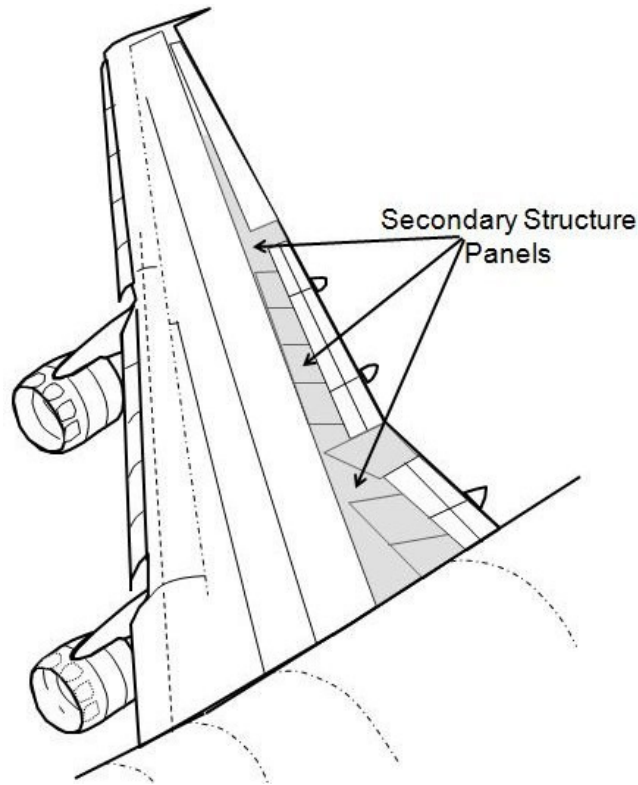


Figure 1.1 : Diagram of an aircraft wing and the position of secondary structure

The research in this thesis is concerned with reducing the cost of manufacturing aircraft standard composite sandwich panels, whilst maintaining a mechanical performance similar to that of the original manufacturing process. To achieve the required reduction in cost, the process for manufacturing the sandwich panels will be altered, with particular focus on the face sheet material. Several different face sheet material configurations will be investigated, using different combinations of raw material and manufacturing processes. The material and process combinations will be referred to as Manufacturing Options (MOs) throughout this thesis. In particular five MOs will be investigated: MO1 is the traditional process, prepreg cured in an autoclave; MO2 is the current ideal process, using woven prepreg; MO3 combines a ‘new’ material with an autoclave cure; MO4 uses woven prepreg with an out-of-autoclave cure; and MO5 combines a ‘new’ material with an out-of-autoclave cure. Each of the face sheet materials produced using the MOs is examined in detail considering both cost of manufacture and the mechanical performance. Therefore, this work investigates both a method to measure the cost of producing a sandwich panel using a process/material combination and a method to measure the mechanical performance of the resulting panel. In this thesis, techniques are defined to provide these measures that are combined to produce a means of defining an optimised panel based on a reduced cost MO and adequate mechanical performance. These measures are tested on a specifically designed component that is representative of secondary wing structure panels (see Figure 1.1) which is referred to as the generic panel.

1.2 Industrial Sponsors

The industrial sponsors of this EngD were GE Aviation Systems Aerostructures Hamble Ltd, who are part of the GE Aviation group and based locally in Hamble, Southampton. Their main business is the design and manufacture of metallic and composite parts for aircraft and the automotive industry, for example, parts for the military aircraft C17 and the McLaren Mercedes SLR. GE Aviation Hamble employs approximately 1000 people, from designers and production engineers to technicians. Their customers include companies such as Airbus, Boeing and Bombardier. As part of their research and development into future projects, GE were interested in investigating methods to reduce the cost of composite component manufacture. In particular, they expressed an interest in the out-of-autoclave process resin film infusion (RFI), with a view to using it in their newly constructed factory in China. During this EngD the author worked within the research and development (R&D) laboratory of GE, alongside technicians and engineers. The R&D department function is to test the feasibility of producing components for new contracts, test the manufacture of components before they are put into full production and test novel processes and materials. All of the composite samples used for the research described in this thesis have been manufactured by the author within the R&D department of GE. In addition, the samples were cured in the autoclaves used for full production, and scanned for initial structural integrity in the non-destructive testing (NDT) facilities. To better understand the full production process, time was also spent observing the individual areas that make up the manufacturing process of composites at GE. Finally, some assistance was provided from designers at GE while constructing FE models of the composite panels.

1.3 Aims and Objectives

The overall aim of this EngD is to provide a unified approach for assessing the performance of composite sandwich structures that are manufactured using several different techniques. Cost and performance criteria are defined so that an optimised panel can be produced. The motivation for this work has been provided by the industrial sponsor GE Aviation. The outcome of the EngD will enable GE Aviation to define competitive solutions for composite structure manufacture, whilst maintaining essential high standards of structural performance.

To accomplish this aim a number of objectives must be achieved:

1. Review existing composite manufacture
 - a. Review the existing and new methods for the manufacture of composites, including the areas that add to the overall cost. Also analyse the areas where cost may be reduced.

- b. Review the current manufacturing approach used at GE Aviation, and investigate the level of cost incurred in each area.
2. Design a generic component that models a typical secondary structure panel that can be manufactured and tested to allow a cost and performance comparison of different manufacturing techniques.
3. Compare the cost of different processes
 - a. Review the current approaches for assessing the cost of manufacturing composite components.
 - b. Define the manufacturing costs of the generic component for each of the five MOs.
4. Compare the mechanical performance of material produced using different processes
 - a. Establish the material characteristics of five different face sheet materials.
 - b. Design an approach to characterise the performance of each type of generic panel using full-field optical techniques to measure the complex response.
 - c. Design a rig to characterise the performance of generic panels, allowing access for optical measurement techniques.
 - d. Test the panels manufactured using different processes, using the rig and optical techniques.
 - e. Produce FE models of the generic panels and validate these using results from the full-scale tests.
5. Combine the cost and performance data to optimise the panel production.

1.4 Novelty

The work in this EngD has considered several novel concepts. The manufacture of composite sandwich panels using different material and process combinations has been monitored in detail to define the cost and provide a new means of comparing the relative cost for manufacture. To measure the performance of the generic panels, a unique full-scale test rig has been designed. The rig applies a cyclic pressure load to the surface of the composite panels. The design is unique as it allows cyclic loading, and optical access to the surface of the test panel to enable the application of full-field techniques. The application of full-field optical techniques to large structures under complex loading configurations and made from such complex materials is also novel. In particular,

this work has used digital image correlation (DIC) [16, 17] and thermoelastic stress analysis (TSA) [18] in a new way to validate FE models.

The overarching novelty in this EngD project is linking the structural performance to the cost of production. Figure 1.2 shows a scheme that captures each step in the process in the form of a flow chart, which enables the comparison of the manufacturing processes that have been devised as part of this project. The scheme contains different operations, where the colour groups the operations into activities that are linked. The outcome of the scheme is a component that is optimised for manufacturing cost, whilst retaining the necessary structural performance and is indicated by the light blue box; this fulfils objective 5. The first stage in the procedure is to review current practice, including existing designs of aircraft secondary sandwich structure (green boxes); this will inform the definition of the geometry of the generic panel. It is necessary to investigate the current manufacturing process, and establish the costs in order to identify other MOs. The steps considered in the green boxes fulfil objectives 1a and 1b. The next step considers the manufacture of the generic panels (yellow boxes) and includes the definition of the five MOs, the design of the generic panel (objective 2), and the results of monitoring the manufacture of the generic panels for cost (objective 3b). During the production of the generic panels, characterisation specimens are obtained, for each of the face sheet materials, to enable an initial material performance assessment based on tensile, flexural and through-thickness properties of the face sheet material (orange boxes, objective 4a). To provide a link between the performance of the generic panels, which cannot be assessed through specimen coupon testing, it is necessary to carry out mechanical testing of the panels. To make this full-scale assessment of the generic panels the review of existing designs provided information on the service-loading. This enabled the design and commissioning of a test rig for full-scale testing that replicates the in-service loads (dark orange boxes, objectives 4b and c). The generic panels manufactured using the five MOs are tested on the full-scale rig and the experimental data is used to validate FE models of the generic panel (red boxes, objectives 4d and e).

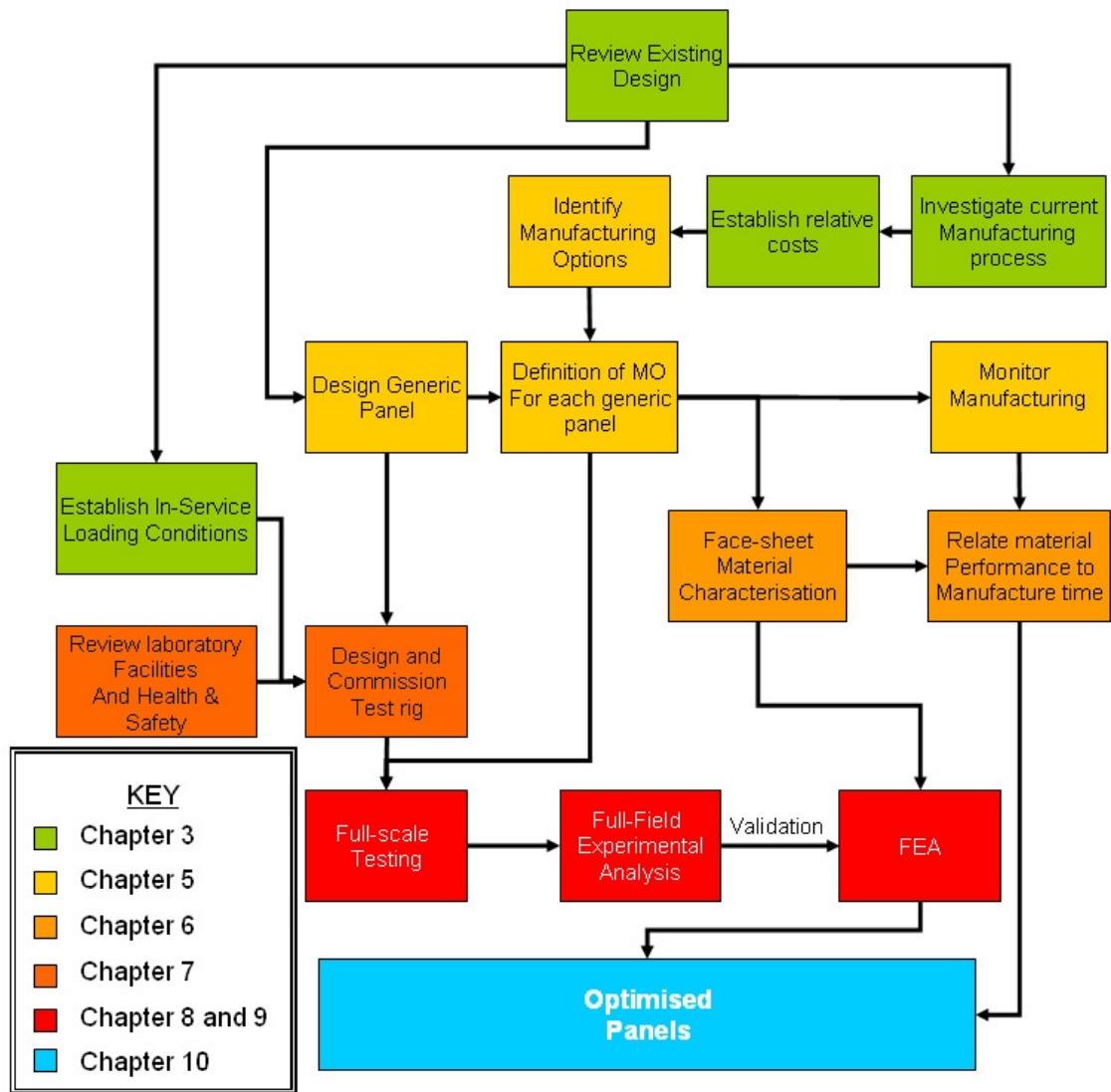


Figure 1.2: Scheme to compare processes through cost and performance

1.5 Structure of Thesis

This thesis consists of eleven chapters, dealing with different parts of the scheme in Figure 1.2, where the colour of the boxes represents the different parts and is related to the chapter in which they appear. The scheme illustrates the tasks required to provide a comparison between MOs, the order in which they must be completed and how the outcome of each affects the next. It is expected that once the FE model has been fully validated as an outcome of the work in the thesis it will be possible to remove the full-scale testing and the FE would be sufficient to provide a measure of the mechanical performance.

Chapter 2 contains a review of the literature on the subject of the current practice of composite manufacture and the recent developments. This includes a discussion of the types of raw material

available for composites, and the different processing techniques. The advantages and limitations of each material and process are presented, and the resulting conclusions help to inform the decision of which material and process combinations to consider in this thesis.

Chapter 3 considers the current practice at GE Aviation. This initially investigates the manufacture of aerospace composite components at GE. An insight into composite manufacturing techniques and the sources of the cost associated with manufacturing is provided. Finally the chapter concludes with a presentation of a study of wing secondary structure panels that are manufactured at GE. The design and geometry data obtained from this study forms the basis of the design of the representative panel described in Chapter 5.

Chapter 4 reviews the literature on the cost of composite manufacture and its analysis. The sources of cost in the use of each of the materials and processes are investigated and a discussion of the opportunity to reduce cost is provided. The chapter continues to review methods for cost analysis of manufacturing processes, which is an important part of the work described in this thesis.

Chapter 5 defines the manufacturing options and the design of a generic panel for analysis. The manufacture of generic panels using the five MOs is described and an estimation of the relative costs between them is presented. This includes a breakdown of time to manufacture and material cost. Finally, the result of non-destructive testing (NDT) is provided.

Chapter 6 contains the results of mechanical characterisation tests on the face sheet material produced using each MO. The results include the fibre volume fraction, as a measure of material consolidation, and the in- and out-of-plane mechanical properties. These results provide an initial comparison between the processes and also material data for production of FE models.

Chapter 7 describes the design of a test rig to apply a representative pressure load to the generic panels, allowing for access for optical measurement techniques. The chapter starts with the production of an FE model of the generic panel, using material properties from Chapter 6, to inform the rig design. Finally, initial tests are performed to prove the operation of the rig.

Chapter 8 presents results from feasibility tests of the use of DIC for the full field analysis of the strains in the generic panels subjected to the pressure load applied by the test rig. The tests first performed on tensile specimens to investigate the optimum processing parameters and correlation patterns used for application of the DIC to the composites considered in this thesis. This is followed by the application of DIC to a portion of a generic panel to assess the ability of the technique to provide full field strain data. The DIC measurement is compared to the FE model in Chapter 7 for the purposes of validation.

The results from similar feasibility tests are provided in Chapter 9 for TSA. Once the TSA technique has been proven, the chapter continues to show the production and results of individual FE models of generic panels manufactured using each MO. Point deflection measurements from a displacement transducer, and full field calibrated TSA data are used to compare the performance of the MOs and validate the FE models.

Chapter 10 discusses the optimisation of a process to manufacture the secondary structure component for cost and performance. Chapter 10 brings together the conclusions from Chapters 5, 6 and 9. Finally Chapter 11 offers some conclusions for the work and defines areas for further work.

Chapter 2

2 An overview of current practice and recent developments in composite manufacture

2.1 Introduction

This chapter aims to review the literature on the subject of composite manufacture and summarise the methods to produce aerospace composite materials. The review will inform of the current state of composite manufacture and the advantages and limitations of each. The summary includes a brief definition of fibre reinforced polymer composites considered in this thesis, and the types of constituents. This is followed by a discussion of the raw materials used for composite manufacture and the techniques for processing and curing them. At each stage, the recent developments of manufacture are included for consideration. The chapter will bring together information of the current manufacturing processes and the alternatives. The knowledge gained on composite manufacture will be used to inform a decision into the processes to be considered in this thesis, whilst realising the limitations that each may have.

2.2 Materials

Composites are made from two or more materials, ‘where mechanical performance and properties are designed to be superior to those of the constituent materials acting independently’ [1]. This thesis is concerned with carbon fibre reinforced polymers (CFRPs). CFRPs combine stiff carbon fibres as the reinforcement, with polymer resins acting as the continuous matrix binding the fibres together. The distribution, orientation, and size of the reinforcement have dramatic affects on the

mechanical properties of the whole composite or laminate. Of particular importance to the laminate properties is the proportion of fibre to matrix, often referred to as fibre volume fraction (V_f). Laminates of aerospace quality typically have a V_f greater than 52% [19]. A laminate is constructed by layering individual plies or lamina of composite material to produce a stack that must be consolidated and cured to produce the final laminate or component. The composites considered in this thesis use continuous fibres. In its most simple form, the CFRP is a unidirectional (UD) single ply in which the fibres are aligned along one axis. The single UD plies can be built up into laminates to produce a tailored component. The single ply will have directionally dependent properties. In the primary or longitudinal direction the material is much stiffer and stronger than the secondary or transverse direction. As a laminate may have a number of plies, orientated in different directions, the component axes may be different to the material axes of the individual plies. The properties of the laminate depend upon the individual ply orientations and their positions within the laminate. The coordinate systems illustrated in Figure 2.1 will be used throughout this thesis, unless otherwise stated. For a single ply the coordinate system has axes 1 and 2, where 1 is aligned with the fibre direction and 2 is perpendicular to the fibre. The laminate uses the coordinate system L (longitudinal), T (transverse) and Z.

2.2.1 Matrix materials

The matrix material in a composite is used to bind the reinforcement together. For the purposes of this research the matrix is a resin, and is characterised by relatively high ductility, low strength and low stiffness. The resin provides the composite with some other useful properties; toughness, damage tolerance, impact resistance, chemical resistance and thermal stability.

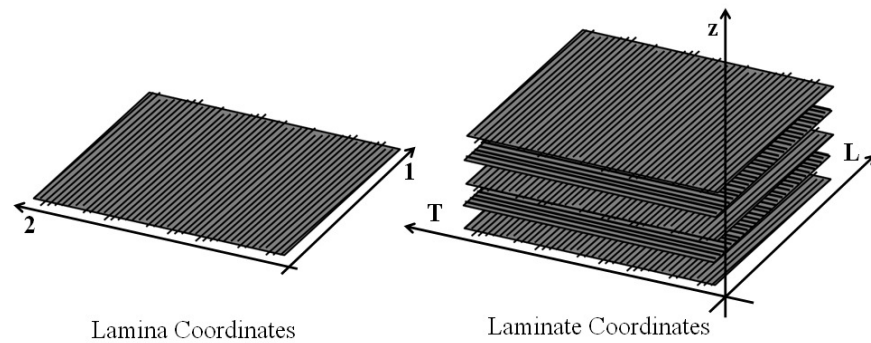


Figure 2.1: Coordinate systems for lamina and laminate

There are two main types of resin used for the matrix; thermosets and thermoplastics. Thermoplastics offered a toughness an order of magnitude higher than thermosets [20] and although improvements have been made to the toughness of thermosets, thermoplastics still remain tougher [21]. Some of the other characteristics of thermoplastics made them an attractive proposition for early aerospace composite pioneers. The manufacturing cycle for a thermoplastic is shorter than that for thermosets [21, 22], thermoplastics can be stored at room temperature indefinitely [19-21], and, because thermoplastics can be reprocessed, it is feasible to recycle

composite parts manufactured from such resins [19-21]. The initial attempts to manufacture composites from thermoplastic resins found some major limitations, in particular high cure temperature and lack of drapeability when used as a prepreg (pre-impregnated fibres) [20]. It is for these reasons that thermosets were developed by the aerospace industry in preference to thermoplastics. Further disadvantages to thermoplastics also hinder their use: they are expensive, even when compared to thermosets; they have poor chemical resistance [22]; and high resin viscosity makes impregnation of fibres more difficult [23]. More recently thermoplastics have found uses in the automotive industry [24], and limited use in the aerospace industry [25].

Thermoset composites are extensively used in the aerospace industry in a wide range of applications [26]. The cross-linked structure of thermoset polymers provides the potential for higher stiffness and service temperature [23]. It is also easier to obtain a good surface finish when using thermosets [23]. However the cure procedure for the cross-linking thermoset resins creates a significant disadvantage. Once the cross-linking process has begun it will continue until it is complete. Therefore in many of the forms that are used in the aerospace industry, e.g. prepreg or resin film, the resin has a limited shelf-life [27]. This can be of the order of just a few hundred hours and, although it is possible to extend the shelf-life of the resin to about 6-12 months by refrigeration [27], this is an extra expense for the composite manufacturer [21]. Larger composite part manufacturers can rely on 'Just-in-time' (JIT) delivery that removes the requirement for freezer storage. However for a company the size of GE Aviation this is not an option. A challenge facing aerospace composite manufacturers and users is the disposal of old stock of thermoset parts because thermosets have a limited possibility of recyclability due to the irreversibility of the cross-linking process [23].

Most high quality conventional prepreg with thermoset resin systems require an autoclave cure at high temperatures (up to 180 °C). There is an economic advantage for reducing this temperature, therefore [28] reports the development of a low temperature cure resin system. Here, the resin blend was designed to match the fracture toughness of the high temperature cure resins. The resulting resin required an extended cure of fourteen hours at 85 °C with a 2 hour post cure at 175 °C in a conventional oven.

2.2.2 Reinforcements

The reinforcement provides the composite with strength and stiffness. In the current work the reinforcement takes the form of continuous carbon fibres. In its simplest form fibres or filaments are held parallel together by a binder to form unidirectional (UD) tape. UD tape is thin, typically

around 0.125 mm to 0.250 mm [29], and therefore many layers can be used in a laminate to closely control the orientation of the fibres and hence tailor the directional material properties [30]. However, the large number of layers required to produce a laminate makes it time consuming and therefore expensive [29]. Hence, many applications use carbon fibres in the form of a fabric. Fabrics use bundles of untwisted filaments in tows. Tows have a specific fibre count, e.g. 12000 (12K). A collection of parallel tows without twisting is known as a roving. The reinforcing fibres can come in the form of woven fabric, e.g. plain or satin weave (Figure 2.2). Tows in both the longitudinal (warp) and transverse (fill or weft) directions are woven together. Plain weave uses a single warp tow and a single fill tow. There is equal reinforcement in both directions and therefore a laminate constructed from the fabric will usually have a uniform strength in both directions, although some crimp effects may be present. It also has the advantage of resistance to in-plane shear.

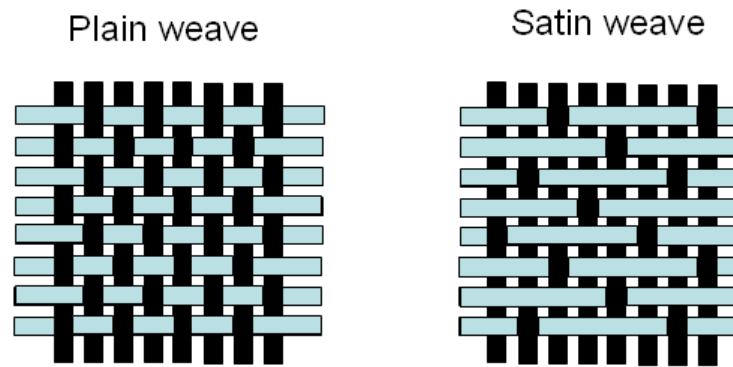


Figure 2.2: Examples of woven fibre reinforcements

Another example of a woven fabric is the harness satin weave. One type, the five-harness satin weave, has one warp tow over four fill tows and then under one fill tow. This fabric offers a high degree of drape and formability in all directions and is widely used for aircraft applications. Weaving the tows produces waviness as one tow passes over another, this waviness reduces the in-plane properties of a composite produced using the fabric [31]. Non-crimp fabrics (NCFs) that use loose stitching to hold together layers of UD fibres offers a compromise between UD tape and woven fabrics. NCFs still give comparably good drape but often have less fibre distortion than may be seen in woven fabrics [31]. NCFs require separate thread to bind the tows together to keep the shape during processing. NCFs use a secondary yarn (polyester or aramid) to bind ‘bundles’ of fibres together. The bundles form a blanket where fibres are in a near zero crimp state [32]. The secondary yarn stitches several non-crimped layers together, often with different fibre orientations in each to offer a degree of tailoring. Despite the name, these materials do have a small amount of crimp due to the stitching from the secondary yarn [29] and this crimp does have a knockdown affect on material properties compared with UD tape. The main advantage of NCFs is the ability to vastly increase the deposition rate when compared to UD prepreg [29, 30, 32].

NCFs can have areal weights as heavy as 2 kgm^{-2} , compared to approximately 190 gm^{-2} for UD prepregs [29].

2.2.3 Materials databases

Material databases allow designers to make an informed selection from such a wide range of combinations of matrices and reinforcements. Raw materials manufacturers often supply some mechanical properties and material information of the different combinations. For example, Hexcel and Cytec have extensive data on the raw materials on their websites. In [33] a material selection methodology is presented that uses a database of possible solutions that are tested using a finite element (FE) model. The methodology is aimed at the earliest stages of product design, where all possible material combinations are included. The approach uses ‘Ashby maps’, which are plots of particular materials on axes that represent the objectives, for example a map of weight against cost. These maps allow the designers to quickly assess a range of ‘best’ solutions. The methodology forms a database of all materials, and combinations of lay-up, etc, the combinations are then run through a relatively simple FE model to offer an initial analysis of the performance of such a solution. The relative performance of each solution is added to the database, along with component weight and any other parameter that the end user may find of interest. The results can be plotted on to ‘Ashby maps’ and by applying constraints, such as weight lower than a particular value, it is possible to reduce the solution population to a more manageable number from which the designer can choose. This is an excellent tool for the early stages of component design, although once the population has been reduced to a manageable number further, more in-depth, FE and analysis would be required to find the ‘optimal’ solution.

2.3 Manufacturing

2.3.1 Raw materials

The form of the raw materials is linked to the processing method to be used, and to a lesser degree the cure method. The most common form for carbon fibre reinforced thermoset polymer in the aerospace industry is prepreg [23]. Prepregs are produced by impregnating a fibre bed with a resin matrix, where the resin is such that its viscosity will drop during heating, which initiates first stage of cross linking. With increasing cure time the viscosity increases but reaction is controlled enabling prepreg to be stored (using sub-ambient temperatures). In the final cure, the material is heated to reinitiate the reaction, the viscosity drops until cross-linking increases and the matrix material ‘gels’ whereupon viscosity becomes infinite [23]. Prepregs are supplied on continuous rolls of widths up to 2 m [30] with a protective backing film on either side to avoid contamination and tacking to itself [34]. The prepreg has resin in a partially cured state impregnated into the fibres. Once the cross-linking cure process has begun it can only be slowed, not halted. Therefore prepregs have a life at room temperature of typically up to around 30 days before they must be

scrapped. To extend this it is necessary to store the prepreg in a freezer at approximately -20 °C [30, 35].

Increasingly, aerospace composite manufacturers are considering the use of dry fibre preforms [36]. These may take the form of layers of dry fibre mats that can be combined to the size and shape of the final component, or a 3D textile that is woven, braided or knitted [36]. The resin, in liquid or partially cured film form, is then infiltrated under vacuum through the fibre preform to produce the final component [36], using methods discussed in section 2.3.2.

2.3.2 Processing methods

The processing method for composites is required to turn the raw materials into the geometry and lay-up of the final component. Once the laminate has been formed it will be ready for curing, the final process that allows the resin to infiltrate the fibres and cross-link to give a consolidated component. The choice of forming process will be heavily dependent on the nature of the raw material selected. In section 2.3.1 it was highlighted that traditionally, aerospace standard composites require thermoset prepreg. To produce the final component, individual thin layers of prepreg are placed on to a mould tool by hand, before a flexible vacuum bag is formed around the component [35] (Figure 2.3). The vacuum bag process requires the use of non-re-useable materials, known as consumables. Once the prepreg stack has been formed on the mould tool, a layer of perforated or non-perforated release film is applied. The release film is designed to stop the composite component from adhering to the other consumables during cure, and is often perforated to allow volatiles to be removed from the part. The release film is covered with breather blanket (or bleed cloth). The breather blanket consists of a fibrous material in loose mats, and assists with air flow and ensure an even pressure across the composite part. Finally a polymeric vacuum bag is sealed to the mould tool using ‘tacky’ tape. Some applications require other materials, for example peel ply may be used to assist with resin bleed and surface finish. The process is labour intensive, requires a degree of skill from the operator [35] and is known as hand lay-up.

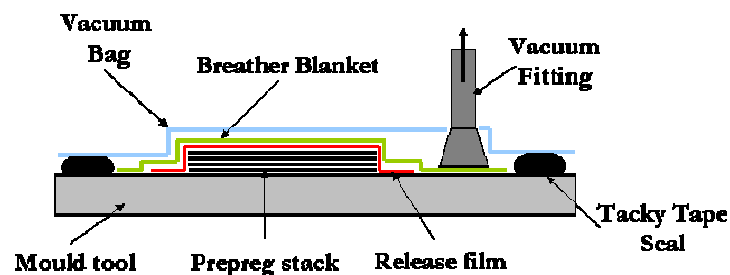


Figure 2.3: Schematic of the hand lay-up process

Resin transfer moulding (RTM), and vacuum assisted resin transfer moulding (VARTM), are liquid resin moulding techniques. The dry reinforcement is set into a matched metal heated tool [36]. It is necessary to preheat the dry reinforcement in the tool before infusion is initiated [37]. The resin is pumped through the reinforcement in the tool (RTM), or drawn through under vacuum pressure (VARTM) until the part is fully wetted out (Figure 2.4). It is possible to produce net-shape complex curved structures from RTM, but it is limited by the tooling required to manufacture large parts [36]. RTM is used for the manufacture of components in the automotive industry for performance vehicles [37], and is also considered an alternative to prepreg for the aerospace industry [6, 37]. However the reported V_{fs} possible using RTM vary; in [36] it is claimed that it is possible to achieve high V_{fs} , while [38] suggest V_{fs} of only 40% are possible. However, the V_f achievable is highly dependent upon the process setup used. In [6] a limitation for the process is highlighted. RTM materials cannot match the toughness of prepregs, as the toughening agents required limit the resin flow and increase resin viscosity. It has been shown that RTM requires a viscosity lower than 50cPs [6]. There is also potential for resin and void rich areas, and reinforcement deformation caused during injection [26].

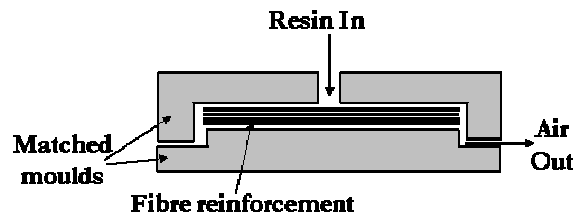


Figure 2.4: Schematic of RTM

Another liquid moulding technique to be considered is vacuum assisted resin infusion (VARI), which is similar to the VARTM described above. The process uses one-sided rigid tooling, whilst the other is bordered by a flexible polymeric vacuum bag as used in RFI and prepreg hand lay-up [26]. The dry reinforcement is set on to the rigid tooling. Then the part is sealed in the vacuum bag along with a perforated layer, known as the distribution mesh, which aids the resin path (Figure 2.5). The dry reinforcement is consolidated under vacuum before the liquid resin is drawn through, along the length of the part, using the pressure of the vacuum pump. To provide the best laminates using VARI it is crucial that the liquid resin is degassed prior to infusion. This involves applying a vacuum to the resin to draw out any latent air bubbles to avoid voids in the final part [26]. The resin path must be such that the entire component is infiltrated quickly, before the resin starts to cure. Laminates produced using VARI may have modest mechanical properties [26], depending on resin used and V_f , but are now being used in some major aerospace applications, e.g. A400M cargo door. Although resin systems used for VARI undergo an exothermic reaction on cure, another limitation for the process in the aerospace industry is the need to pre-heat the resin system prior to infusion to reduce the viscosity adequately [26]. This is a particular concern for

aerospace where the resin systems required to offer the necessary final laminate properties have a high viscosity at ambient temperatures.

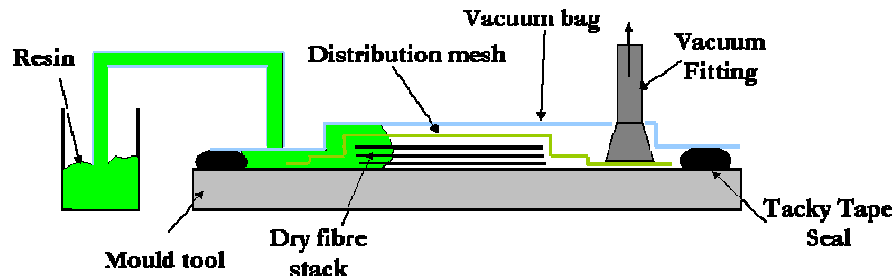


Figure 2.5: Schematic of the VARI process

Resin film infusion (RFI), combines dry fibre preforms or fabrics with semi-cured resin films [36]. Hexcel has developed a resin system, M36, particularly designed for use in a RFI process [39]. This is a relatively new process and, although the first cited work [40] was 30 years ago, much of the progress in this technique has happened more recently. Resin film and dry preforms are laid on to a mould tool, using a similar hand lay-up process to that described for the traditional prepreg process. Again the process uses a one-sided tool, with a flexible polymeric vacuum bag to seal the other side [41]. The vacuum bag is utilised to remove much of the air by debulking and compacting the preform before the resin is infused into the laminate. After debulking the resin is allowed to infuse under vacuum pressure to fully infiltrate the reinforcement and eliminate any remaining air voids (Figure 2.6). Unlike other resin infusion techniques, RFI has the advantage of only needing to draw the resin through the thickness of the reinforcement [41]. This is a much shorter infusion path than other techniques that draw the resin along the length of a structure; hence leading to better wetting. Studies have been performed into the permeability of the fibre preforms to investigate the control of the infusion process [42]. If the resin flows too fast it can lead to damage in the fibre structure or air voids [41]. In [43] the limits of the processes used in the production of 3D structure were considered. By numerically simulating different processing parameters, e.g. temperature, it was possible to estimate the maximum thickness that can be infused. It was found that a higher temperature will lead to a faster infusion, but a lower maximum height. RFI is seen as an attractive alternative to prepreg hand lay-up.

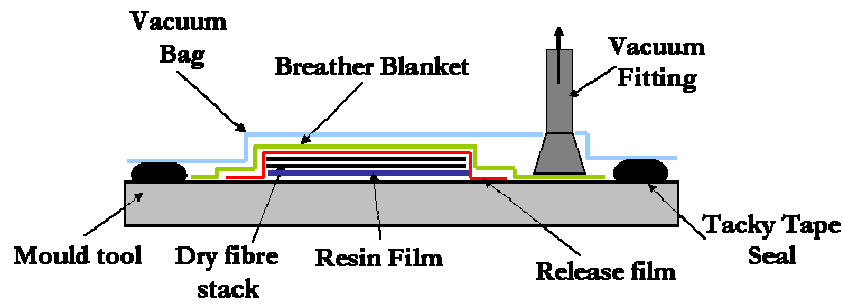


Figure 2.6: Schematic of the RFI process

Other forming techniques include 3D textiles (discussed in section 2.2.1) [36], automatic tape layers (ATLs) [6] and filament winding [26]. 3D textiles have been found to improve the damage tolerance of laminates. 3D textiles can also reduce machining and scrap if they are near net shape [36]. However no machine can make all architectures and when using carbon it is necessary to use a slow speed machine. ATLs use prepreg in UD tape form and remove the need for hand lay-up. Finally filament winding machines can form complex shapes by continually placing individual filaments.

2.3.3 Curing methods

The final stage in the manufacture of CFRPs is to cure the laminate such that the resin is fully cross-linked and the laminate is correctly consolidated. At its most basic, the cure may be carried out at room temperature for an extended period of time. However, resins used within the aerospace industry require a cure at an elevated temperature. This is crucial for obtaining the necessary material properties and to ensure the component can operate at the elevated temperature. Typically, aerospace standard composites require the use of an autoclave cure. The autoclave allows close control of temperature and pressure of the internal environment. The increased pressure of an autoclave cure assists in removing air from components, and helps to compact the laminate to increase the V_f improving final mechanical properties. Pressures of up to 1.5 MPa in autoclaves are reported [6], but typically range from around 0.2 MPa (30 psi) for honeycomb sandwich panels to around 0.7 MPa (100 psi) for monolithic laminates. An autoclave allows the application of heat and pressure in a controlled way known as a cure cycle (Figure 2.7). The cure cycle can be split into five main sections; first an initial ramp, where the temperature is gradually increased, second a consolidation dwell, where the temperature is held, third a secondary ramp, fourth a cure dwell and finally a cooling period. It is characteristic of thermosetting resins that there is a sharp reduction in viscosity when the temperature is raised above a certain point (typically 40-50°C for epoxies) [44]. It is important to control the flow of the resin within the part while the viscosity is decreasing, so the heating ramp rate must be carefully controlled. The temperature in the autoclave is held at a set temperature for a set period of time, known as an initial dwell. The initial dwell aids the consolidation of the part. After a second heating ramp a

second dwell period allows the resin to cure as the chemical cross-linking of the resin system is completed. It is vital that the temperatures and periods of dwell are both closely matched to the resin system used and closely controlled to avoid premature ‘gelling’ [44]. Under premature gelling the resin system will stop flowing and will begin to cure, and it is likely to produce laminates that are too thick and have excess resin [44], although with modern zero bleed systems this is less likely. Conversely, excessive resin flow can lead to a resin starved laminate that has reduced mechanical properties. The pressure aids consolidation of the laminate and typically can produce laminates of high quality with void contents less than 1% [6].

Recently, out-of-autoclave cures using a conventional thermal oven have been investigated for use in the aircraft business [6]. The oven cure uses only vacuum pressure to consolidate the laminate, whilst the temperature follows a similar cure cycle to that used in an autoclave.

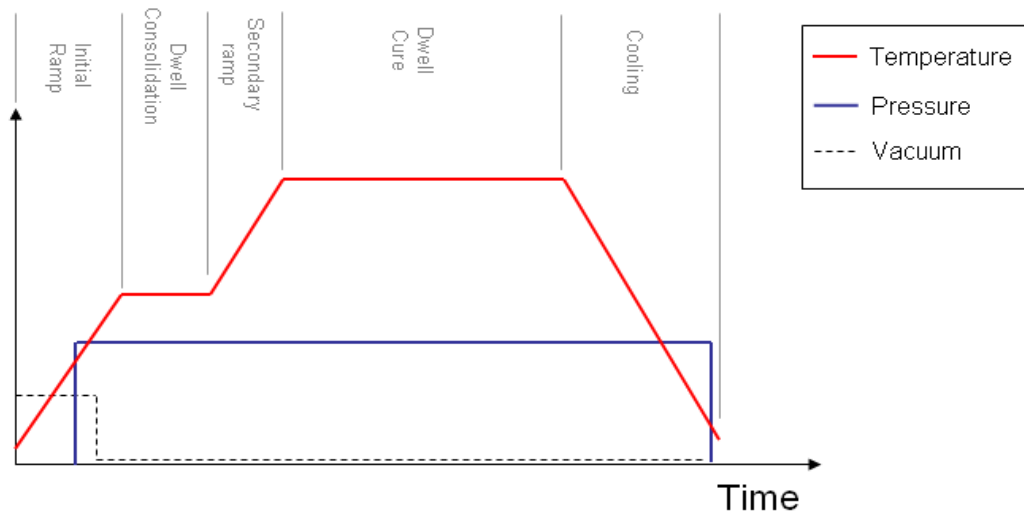


Figure 2.7: **Example of the cure cycle used for aerospace composites**

There is little literature reporting on the mechanical properties of laminates produced using oven cures. However Margueres *et al* [45], reported mechanical properties of glass fibre specimens manufactured using RFI (see section 2.3.2). The results were compared with those cured in an autoclave. Both sets of specimens had a V_f of approximately 40%. This is low for aerospace standard laminates, but the vacuum cure does not appear to have affected the V_f . The autoclaved specimens averaged approximately 1.5% void content and the vacuum only cure specimens averaged over 3 % [45]. If this is used as a measure of a good quality laminate, then the removal of the autoclave cure does appear to have had an effect on the quality of the final laminates. The mechanical properties correlate with the void content, and show a small reduction when using vacuum only. A similar set of tests were performed in [46], this time comparing autoclaved specimens to RTM (see section 2.3.2) specimens. These tests again used glass fibres. The autoclaved specimens had a V_f of approximately 55 %, whilst RTM could only produce 50 %. The

lower V_f is indicative of the individual set-up and not the process itself. This demonstrated a reduction in laminate quality from the out-of-autoclave specimens. This was mirrored by the mechanical property tests. Most of the properties were reduced by between 10 and 20 % by removing the autoclave. Both of these examples [45, 46] illustrate the difficulty in matching the performance of laminates produced using an autoclave with those produced using a vacuum only cure. However, with so few examples in the literature, and the lack of CFRP data, it is not possible to gauge the limit of out-of-autoclave processing.

Silcock *et al* [47] describes a novel process for rapid cure of laminates out-of-autoclave, known as Quickstep. Quickstep utilises a unique fluid filled mould tool that forms around the component to be cured (Figure 2.8). The fluid offers exceptional heat transfer that offers temperature control and reduced cure times. The cure cycle for a part using the Quickstep process is of the order of 10 minutes; a 95 % reduction from an autoclave cure. In [47], a demonstration component manufactured using the Quickstep process was also discussed. In this example the component had void contents > 5 %. This is too high for an aerospace standard part, although it could be used in the automotive industry. This process is still in the developmental stages, and therefore some improvement can be expected. The process may be important in the future.

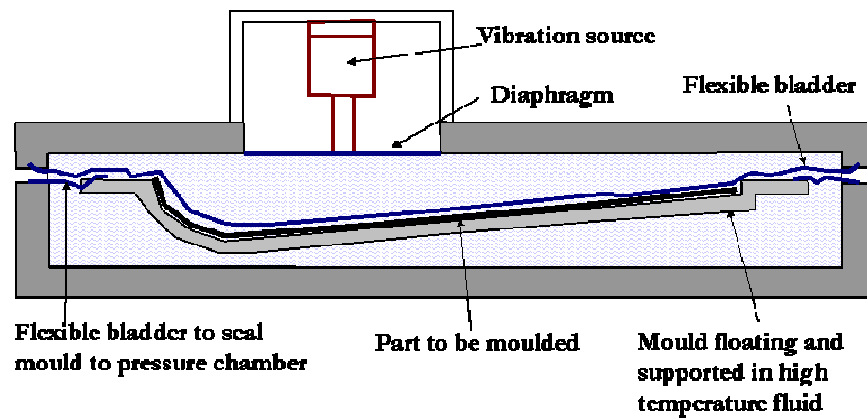


Figure 2.8: Schematic of Quickstep process

Further to vacuum only cure in a conventional oven there is much literature on the use of non-thermal processing for composite manufacture. There are two main approaches, both based on radiation curing that uses the radiation to create positive charged ions from initiator molecules, embedded in the resins designed for the process, to start the polymerisation process. Electron beam curing (EBC) [48], offers short cure times, and a reduction in the cost of tooling. So far the properties are low compared to autoclave laminates [48], although [49] have shown properties up to 80 % of those found from autoclaves are possible. The other radiation curing approach is ultra-violet (UV). [50], demonstrated laminates with V_f of 55 %, but only on small specimens and, even with laminates just 2 mm thick, a large amount of energy is required to achieve full cure. UV

curing is also better suited for use on glass fibre composites, through which the light can travel more easily than carbon [51]. Finally, some research has been conducted into the use of microwave curing [52]. The use of microwave curing has been quoted to offer reduced cycle times and energy requirements and because the heat is generated internally, a better cure can be expected. However, it is limited by non-uniform heating and poor process control. In this study [52] laminates produced using a microwave RTM technique were compared to those manufactured using the conventional thermal RTM approach. The microwave cure laminates had a significantly higher thickness, and hence a lower V_f . However, the void content was consistent with conventional thermal curing and when the mechanical properties are normalised for V_f , these are also comparable. It was concluded that it would be possible to produce good quality laminates with a 50% reduced cure cycle time.

2.3.4 Automation

The current state of the art of manufacturing techniques for aerospace quality composite components uses a prepreg material that is cut into kits (see section 2.3.1) using automated cutting machines. Automating cutting includes the use of nesting plies to minimise wastage. Besides the kit cutting, the manufacture of the components is still a labour intensive process. The kits are laid up manually on to tools, but this requires a degree of skilled labour to ensure the stacks produced are correctly laid up and consolidated. There is, therefore, a large amount of scope for removing labour. The literature reflects this, with varying levels of automation suggested through various approaches.

Research into automation of composite manufacture using conventional materials can be split into two distinct areas: (i) automating the conventional manual prepreg lay-up process e.g. by using computer numerically controlled (CNC) tape laying or tow placement, and (ii) moving away from the conventional process to automate the production of dry preforms for use in resin infusion processes e.g. RTM, VARTM (see section 2.3.2). While the removal of labour to reduce cost is the most important to the current research, other advantages to automation have also been highlighted in the literature, for example, removing operators from an unpleasant and dangerous environment and therefore allowing the prepreg to be worked at lower temperatures and increase the out-life. It was noted [34] that automation of the lay-up would reduce the scrap and error rate of production, as humans cannot produce an exactly identical part every time. However, this may be academic in a process that requires a certain degree of tolerance and inspection. It may also be possible to use novel material forms to assist in automation.

Chestney [8] outlines the development of an automated manufacturing cell to produce dry preforms. The operations required are as follows: roll-out material, cut ply profiles, pick ply, place ply on stack, inspect ply and tack ply. To undertake all these operations the cell is designed with: cutting table, handling robot with gripping device, lay-up table, tacking robot and cell controller with visual system for inspection. This process still requires human intervention to load and unload the system and to respond to errors. The system has one major limitation; it is designed to produce flat preforms which are to be formed into the tool prior to final RTM processing, and therefore will struggle with complicated curved structures. In [53] the control system for the manufacturing cell was considered by using an interface between a CAD program to produce a CAM file capable of controlling an automatic preform manufacturing process. The objective was to write code that could process, plan, and automatically obtain information such as individual ply profiles from a CAD drawing. The result is a system that can produce components ranging from 0.3 m² to over 3 m² and up to 20 layers. The current limitation on speed is the tacking operation that limits the speed to 15kg/hr. Research has also been conducted into 3-D preform manufacture [36, 54], using a tape layer with movable tape head to lay-down the material and movable supports for the tool to enable varying orientations or spraying of chopped strand mat. It was found that the machine could lay material down at ten times the rate of current prepreg tape-laying machines, but double curvature was a problem with the tolerance of tape laying position likely to lead to small gaps. A cost saving of 52-60% was reported although no details of how this conclusion was reached were given [55].

The automating of conventional prepreg material deposition raises additional concerns. Modern prepreg is tacky to assist with hand lay-up and therefore any gripping system would require a mechanism for releasing the material once it has been positioned. With an increase in automation the demand for non-tacky prepreps would also increase. Secondly, due to the inherent tackiness, suppliers cover the prepeg in a backing film that must be removed before the stack is produced. It is crucial that all the backing film is removed from each layer of prepreg because any film left in the component will form voids, degrading the mechanical performance [34]. In [56] the build and testing of a system was reported, which was successfully operated for three component shapes; a shallow sphere, a more concave access door, and a saddle shape. These shapes represent different degrees of curvature and the saddle shape also includes double curvature. The system cannot cope with the introduction of core material for sandwich structures, and still requires human intervention for placement of rolls in the de-reeling machine, response to warnings from the inspection system, response to system failure, control and monitoring interface, and removal of final components. A solution to this was offered by a device called the precision feed endeffector

(PFE), which enables the placement of core material in a prepreg component by utilising robotic arms together with tracks and gantries within the factory [57].

To ensure the plies are correctly handled and laid down, it is important that the behaviour of the raw materials is understood. For that reason [58] undertook a number of mechanical tests to determine the following properties: shear, bending, friction, transverse compression and tensile. A numerical procedure was then applied to assess the drape of a ply over a shaped tool. The work provided information to aid in the production of complex, curved parts where ply distortions may be a problem. By modelling the application of plies over a shaped tool, it is possible to advise operators to the best approach to laying down that ply to minimise ply distortion.

2.3.5 Design

It is widely accepted that the decisions made in the design process have a profound effect on the total product manufacturing costs, although the actual figure varies from source to source: 80% [59], 80-90% [60], 75% [61] and 70% [62]. The main advantage composite parts have over traditional aluminium components from a design perspective is the potential to remove the assembly costs by parts consolidation. It is possible to manufacture a large, complex component to replace a number of small and simple ones. However, any increase in complexity will increase manufacturing cost [63]. The drawback of combining components to reduce the number of parts is an increase in process risk. If one moulding failed the cost of scrap would be large. The greatest consideration in the design process is the manufacturability of the component. Edwards *et al* [64] reiterates the difficulty for designers to improve design for manufacture, when they have little understanding of the manufacturing processes to be used. This clearly impacts on how composite materials can be used in an optimal manner and underlines the need for a design team that is fully conversant with what is achievable in manufacturing.

There has been much literature published investigating methods to optimise the design of composite components for a number of factors. These optimisation codes would be useful tools for the designers of composite structure where the range of possible permutations of design solution provides a difficult, often uninformed, decision. An optimisation model was presented [65] to investigate the configuration of stiffeners on a stiffened composite panel under compressive loading. The model varies the size, shape and spacing of the stiffeners, and calculates the weight and cost of the panel with these parameters that will offer adequate buckling performance. The model uses a simplistic costing code assuming the panel will be manufactured using standard hand lay-up and autoclave of prepreg. The model does not take any account of lay-up or varying

manufacture process, but is aimed at the design configuration of the stiffeners. The paper also reports results of use of the model to provide an optimal solution, and highlights that the ideal configuration is expensive and therefore a compromise must be made. A similar approach was used for a helicopter fuselage [66, 67], considering four fabrication methods: sheet metal, high speed machined aluminium, composite hand lay-up and RTM. The panel was optimised for weight and cost for each fabrication method in turn, using a different costing code for each. The optimisation process found that by including composites it was possible to significantly reduce the weight over metal designs. For the lightly loaded structure the process, selected automated preform RTM as the lowest cost configuration, but for higher loaded structure a high speed machined aluminium was preferred.

2.4 Summary

A review of the literature pertaining to the manufacture of composite materials, with particular emphasis on those used in the aerospace industry, has identified the problems with the current ‘ideal’ process and investigated the advantages and disadvantages of the alternatives. Manual lay-up of prepregs cured in an autoclave remains the process of choice for producing the highest quality composite components with superior mechanical properties for use in aircraft. The current process is expensive, but in the past aircraft manufacturers have accepted the cost premium to provide high mechanical performance with considerable weight saving over aluminium parts. The review highlighted characteristics of the material, forming and curing processes used that contribute to the high cost inherent with aerospace standard composite production. Table 2.1 summarises the advantages and limitations of each of the processes described above.

Table 2.1: Advantages and limitations of methods for composite manufacture

Processes	Advantages	Limitations
Matrix		
• Thermoplastic	High toughness	Notch sensitivity
	Short manufacturing cycle	High forming temperature
	Store at room temperature indefinitely	In prepreg form drapeability is poor
	Recycling is a possibility	Expensive
		Poor chemical resistance
• Thermoset		High viscosity, therefore impregnation is difficult
	Cross-linked, therefore higher stiffness and service	Cross-linking is irreversible, and can only be slowed not

	temperature	halted
	Good surface finish	Limited shelf-life, requires cold-storage
		Limited recyclability
Reinforcement		
• UD	Simplest form Excellent tailoring of design	Thin – requires numerous layers Hard to form
• Fabric	Faster to lay-up than UD Good drapeability	Crimp affects mechanical properties Less tailorability of design
• NCFs	Thick laminates can be made quickly Some crimp, therefore some degradation of mechanical properties Reasonable drapeability can be better than woven fabrics	Secondary yarn can cause crimp With current usage only certain NCFs available, however as production rate increases this will no longer be an issue
Forming Methods		
• Hand lay-up	Produces high V_f Very flexible poorly controlled	Requires high operator skill Labour intensive
• RTM	Can be automated Can produce high quality laminates	Expensive matched tooling Resins used have low toughness Potential for fibre distortion as resin is injected Resin requires degassing
• VARI	Cheaper tooling	Modest mechanical properties Requires high degree of skill Resin requires degassing Care must be taken to minimise voids and premature

		curing
		Difficulty in achieving high V_f
		Aerospace resins need pre-heating
• RFI	Cheaper tooling	Possible damage to preform if resin infiltrates too fast
	Faster than hand lay-up	
	Less labour intensive	Fibre deformation in dry perform must be avoided
	High V_f	
	Less voids than VARI	
• 3D textiles and filament winding etc	Automated	Machines required are expensive
	Damage tolerance	
	Reduce machining due to near net shape	No one machine can make all architectures

Curing Methods

• Room temperature cure	Cheap/easy	Not suitable for aerospace resins
• Autoclave	Very high V_f	Requires pressurisation
	Very low void content	Expensive capital
	Careful control of curing	Expensive running
• Oven	No need for pressurisation	Historically reduced mechanical properties
	No need for expensive autoclave	
• Quickstep	Vastly reduced cure cycle	Reported high void contents
• Non-thermal processing	Short cure times	Reported properties are only 80 % of autoclave laminates
	Reduced tooling costs	
	No need for autoclave/oven	Particularly for UV cure, carbon and thick specimens are an issue

In light of the conclusions reached by reviewing the literature on composite manufacture, the use of NCFs infiltrated using RFI seems to be an attractive proposition. In the next chapter the standard process used at GE Aviation will be fully investigated and the applicability of introducing the RFI process into their procedures will be assessed. In Chapter 4, a detailed discussion of the

cost associated with manufacturing procedures will be presented along with different cost modelling procedures and some suggestions for design optimisation.

Chapter 3

3 GE Aviation Systems Current Practice

3.1 Introduction

The traditional approach for aerospace standard composite sandwich structure is hand lay-up of many individual plies of prepreg followed by an autoclave cure (Chapter 2). Manufacture of composite sandwich panels at GE Aviation Systems (GE) uses this proven method. In this chapter, observations of the current GE practice are discussed, including the current manufacturing procedure, the current costing approach and a review of the loads that the component design must withstand. At each stage, some consideration will be given to changes that may be required to accommodate a new out-of-autoclave process using RFI on NCFs and resin films. Throughout this thesis, the current manufacturing procedure at GE will be referred to as the baseline process, to which all ‘new’ processes will be compared for cost and performance.

3.2 Survey of Design and loads

GE manufactures composite components for aircraft producers such as Airbus, Boeing and Bombardier. The production begins with a bidding process that involves both design and manufacture analysis to provide a quote. A design team is involved, to a varying degree, in the analysis of parts and load depending on the particular project. The level of design involvement will be arranged as part of the bidding process. The components currently manufactured are secondary structure and mainly of sandwich construction. The following section reviews the current secondary structure manufactured at GE. The review will consider the design of components currently in use on medium sized commercial passenger aircraft, such as Airbus A320, and their

position and function. The review investigates the generic features in panels with a view to including them in new materials and processes. The information from the review will also assist in the design of a generic panel, for full-scale testing, that is representative of current designs. The review of existing designs identified trailing edge access panels (see Figure 1.1), classified as wing secondary structure on a commercial passenger aircraft, as a suitable basis for the design of the generic panel. The trailing edge access panels are typically fixed to the main wing spar and A-frame ribs via butt straps along three sides, allowing one of the longer edges to be free to deflect under service load. The panels are subjected to aerodynamic out-of-plane loads across their surface. The review of previous designs identified a number of ‘common’ features as follows:

- Sandwich construction
- Face sheets are of quasi-isotropic lay-up with 12 plies of UD carbon tape prepreg at 0.125 mm per ply,
- Panels are long and narrow – between 700 and 1500 mm long by 300 wide,
- Cut-outs and notches are used to account for neighbouring structure,
- Inserts and solid pucks are used for attachments,
- Simplistic block-like core geometry.

3.3 Current manufacturing procedure

3.3.1 Overview

The baseline process at GE can be split into nine sections: goods-in, prepreg cutting, core cutting, lay-up, cure process, debagging, trim and drill, non-destructive testing (NDT) and assembly. The following section will describe the manufacture of a component as it moves through these areas to provide an accurate and in-depth analysis of the baseline process (Figure 3.1). The schematic of the baseline process demonstrates how the raw materials and components move through the different areas that form the process during manufacture. Starting in the top left, at Goods-in, the red arrows show the direction of movement of materials and components. The process flows from left to right then back right to left on the lower level in a backwards ‘C’ shape. The key underneath the main figure decodes the symbols that represent each object. Currently, all aerospace parts at GE are manufactured from prepreg. Prepreg comes in the form of rolled sheets, approximately 1 m wide and many metres long. The prepreg is stored in cold storage to extend its useful life, as described in Chapter 2.

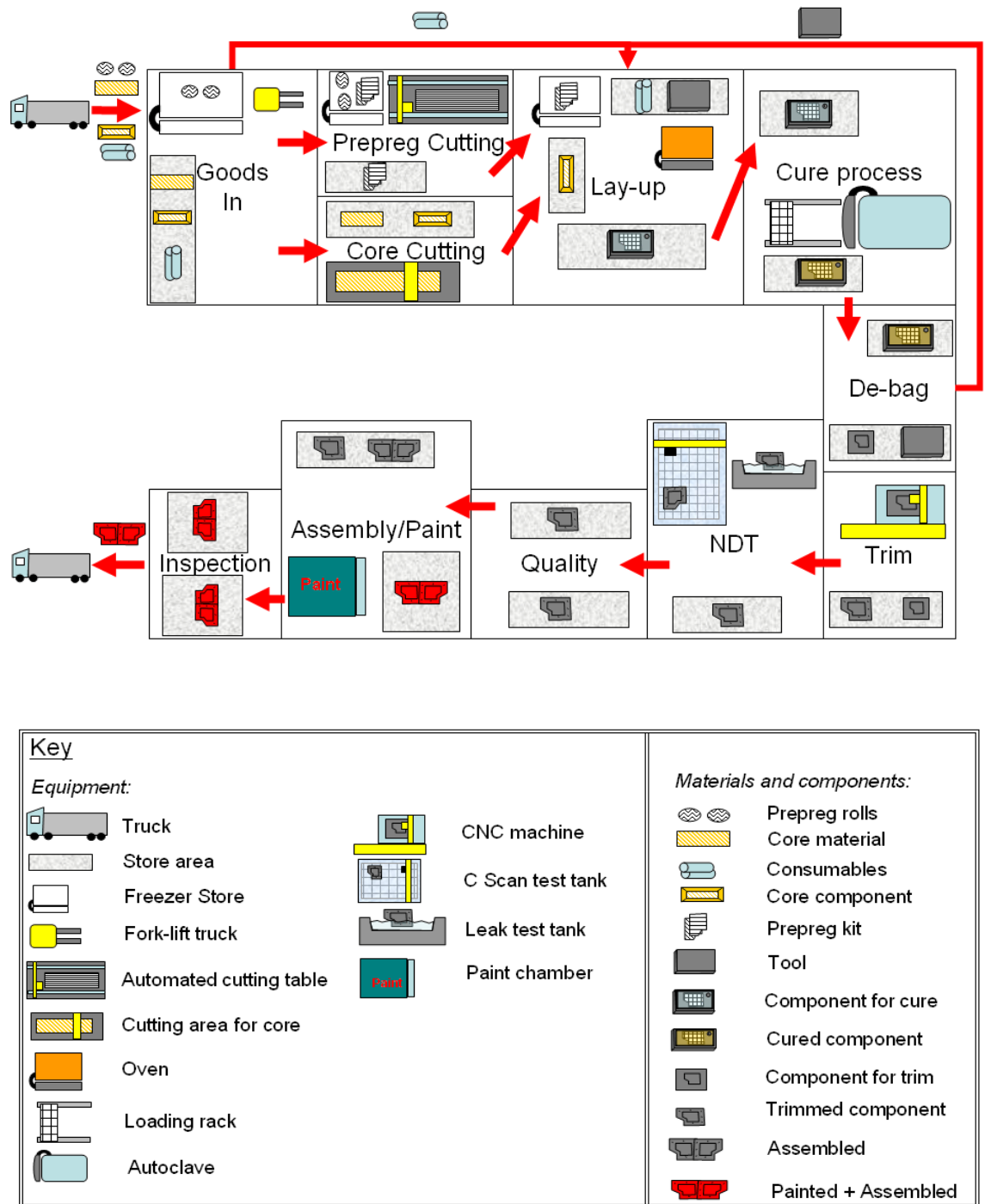


Figure 3.1: Baseline process for the manufacture of composite sandwich structure at GE

3.3.2 Goods-in

The process begins when material is delivered, by road, to goods-in. The raw materials can be separated into three categories: those that need cold-storage, those that do not need cold-storage, and consumables. Before prepreg is used, it is necessary to remove the roll from the freezer to fully defrost before unsealing and unrolling. This is important for two reasons. Firstly, if the roll is unrolled whilst frozen it may damage the prepreg and secondly, if the roll is unsealed while still

frozen, moisture may form which will cause problems during cure. The prepreg has a limited time when it can be left out of the freezer. To ensure the quality of the end part, the time the prepreg is stored at room temperature is recorded. This allows the prepreg to be used for the full specified 'out-life', whilst ensuring it is not exceeded. The freezer storage adds costs both in terms of running and monitoring time out of freezer and, the defrosting significantly increases the time for manufacturing, with an average time for defrosting being about 8 hours depending on the size of the roll. Removing or partially removing the freezer storage from the process by using dry fibre materials instead of pre-preg would give significant cost benefits. Consumables are materials such as vacuum bag and breather blanket, which are used during the manufacture of the component and then disposed of. The materials that require cold-storage, such as prepregs, should be returned to a freezer as soon as possible after they arrive. At this stage, an initial quality control is undertaken to ensure the materials supplied are undamaged and free from defects. The raw materials are held in storage, and distributed around the site as required. There would be little alteration needed to accommodate the use of separate NCFs and resin films for goods-in or storage, as it is usual for a number of materials to be required for a component. However, it may be possible to reduce the volume of freezers required; the rolls of resin film will be significantly smaller than rolls of prepreg.

3.3.3 Prepreg Cutting

The rolls of prepreg lend themselves to automated cutting. At GE an ultrasonic cutting machine, where high frequency vibration of the cutting blade is used to assist the path through the material, is used to cut the roll of prepreg into individual ply shapes. The stable nature of the material in its pre-impregnated form allows the use of a vacuum bed to hold the sheet in place during cutting to prevent wrinkling or distortion. The effect that the vacuum bed would have on dry fibre mats is unclear and this would require some investigation before adopting such a material into production. The resin film and NCF fabric could be cut simultaneously to reduce the cutting time. The individual plies that make up a 'kit' (i.e. a number of plies, possibly of different shapes, that when laid-up will form one component) may be of various shapes, sizes and orientations. To ensure the expensive raw material is used optimally, it is useful to use nesting software to determine the cutting profile. The material utilisation percentage is dependent upon the size and shape of the plies. Simple square geometries can allow towards 90 % utilisation, but more complex shapes can lead to percentages as low as 60 %. The material waste must be considered when costing any component. Prepreg cutting is performed as a batch process, and several kits may be produced at once with some returned to freezer for storage.

3.3.4 Core Cutting

GE has the facility to form simple core shapes from large sheets of honeycomb or foam. The dust hazards of the cutting process, mean operators cutting or forming cores must wear protective

clothing and dust extraction is required. More complex core shapes are currently sourced ready formed from the manufacturer at additional cost.

3.3.5 Lay-up

All the raw materials, core, prepreg and consumables, are delivered to the lay-up area. The lay-up is undertaken in a controlled area to avoid contaminants being transferred to the final laminate. A risk in composite sandwich structure, particularly cured in an autoclave, is a phenomenon called ‘core crush’, shown in Figure 3.2. Under the pressures applied during cure of a sandwich component, the fragile honeycomb core may become deformed in-plane, particularly on long straight edges. To counter this risk, a pre-manufacture process of core stabilisation is often performed. The core stabilisation process includes techniques such as applying foaming adhesive to the perimeter, filling in the empty cells, and covering the entire core in a layer of film adhesive. The adhesives are cured under partial vacuum pressure in a conventional oven. The process aims to give the core some lateral rigidity to protect it during the final cure of the sandwich component. This extra manufacturing stage obviously adds time and expense to the manufacturing process as a whole.

To form the component from the individual plies of prepreg material, each is hand laid on to a mould tool. The mould tools are prepared with a release agent, in this case Frekote®, to assist when removing the finished component after cure. To reduce the error rate of ply placement, templates and positioning lines on the tools give a guide for ply location. The surface of the tool must be free from defects and smooth. Any scratches or pits on the surface of the tool will be transferred to the tool-side of the final composite component. As each ply is placed on to the mould tool they form a ‘stack’ of uncured laminate. It is crucial to remove any trapped air, which may hinder the flow of resin or form voids in the final component, from the stack after each ply lay-up operation. This is known as ‘debulking’. The debulking is achieved by applying a vacuum bag (Figure 2.3) and drawing full vacuum pressure on to the component for a short period. This vital procedure adds a significant amount of time to the already time consuming process. Once all the plies that form the tool-side face sheet have been placed on to the stack, the pre-stabilised core is set into the correct position using a template for position if necessary. Film adhesive is placed between the tool-side and bag-side face sheets and the core to provide the skin-core bond. The skin-core bond is co-cured with the face sheet material during the final cure in the autoclave. The plies that form the bag-side face sheet are laid-up over the positioned core, ensuring they drape correctly and avoiding wrinkles. It may be necessary to cut the plies to give better drape, but this must only be done in pre-designated positions to avoid a reduction in final component performance. The finished stack and mould tool are placed into a final vacuum bag (Figure 2.2) ready for cure and transferred to a holding area in preparation to go into the autoclave. The RFI

process is particularly attractive as a replacement for the hand lay-up autoclave cured prepreg, because the lay-up is very similar needing no additional equipment and minimal re-training.

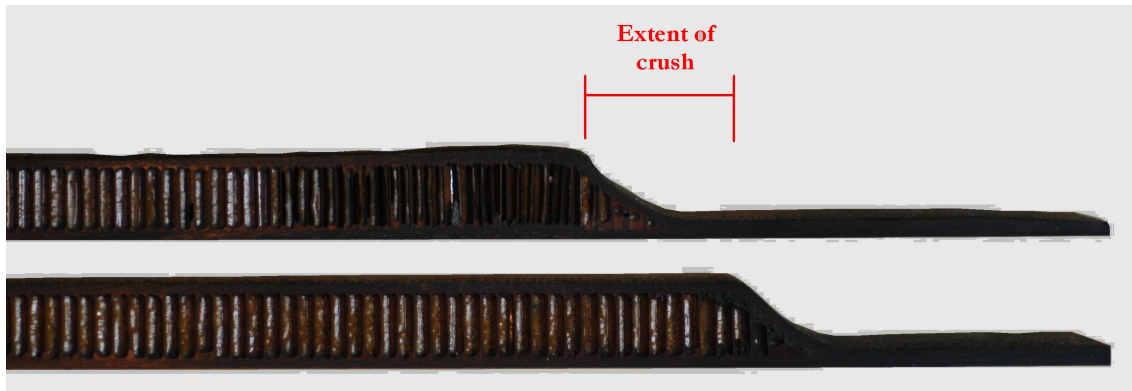


Figure 3.2: Photograph illustrating core crush

3.3.6 Cure Process

It has been identified that to produce composites of sufficient quality for use on aircraft, an autoclave cure is normally required. GE has four large autoclaves for production and a smaller one for research purposes. To make the most efficient use of the autoclaves and minimise running costs, components are queued until enough are ready for cure to fill the vessel. Inside the autoclave the components are subjected to a controlled application of pressure and heat, i.e. a cure cycle (Figure 2.7). The cure cycle and its constituent parts have been explained in chapter 2. After the cure cycle has been completed, and the autoclave has cooled, the bagged tools and components are removed and moved to the debagging area. The cure represents the biggest advantage of the out-of-autoclave technique, but also the largest drawback. The GE site is already set-up for autoclave processing, and as such although ovens incur less capital cost, GE would not see much of this benefit. However, if the autoclave pressurisation was removed GE would still benefit from reduced manufacturing times and running costs.

3.3.7 De-Bag

The consumables are removed and disposed of, and the component is removed from the mould tool with care. Whilst removing the component, care should also be taken to avoid damaging the tool surface, such that it can be re-used. The component is sent to be trimmed to its final shape and size and any necessary holes are drilled, while the tool is cleaned and, if required, a new layer of Frekote® is applied.

3.3.8 Trim/Drill

When manufacturing components using hand lay-up, it is prudent to use over-size plies to guarantee the full laminate thickness across the entire panel once cured. For this reason, it is

necessary to perform some post-cure trimming to provide the net shape and size required. Where possible, the components are trimmed to size using a CNC machine with set cutting programs. The spindle and feed speeds must be carefully controlled to prolong cutting tool life and protect against damage to the laminate. For particular component designs, where tight curvature means the CNC machine is not suitable, it is necessary to trim by hand. The dust from operations on carbon fibre is a hazard and, therefore, operators must wear appropriate health and safety equipment.

3.3.9 Inspection and NDT

The final part is inspected for accuracy of the size and shape, including thickness, and for sub-surface inclusions using NDT techniques. All composite parts manufactured at GE are tested using a mixture of NDT techniques. Initially, parts are visually inspected for obvious defects and measurements are made on flange size and part thickness, for example. All honeycomb cored parts must complete a leak test by submerging in a test tank that contains heated water. Components with a honeycomb core must not leak to ensure moisture is not absorbed in-service that could cause the part to increase in mass. The leak test uses visual inspection to identify signs of bubbles from the surface of the component which will indicate a leak in the part. This constitutes a failure, and a resin wash is required to 'repair' the defect.

GE also operates a policy of 100% testing with ultrasound techniques to identify any subsurface defects that may affect the performance of the component, for example pieces of backing film, or foreign objects such as knife blades. Two types of through transmission scans are utilised, A and C. The A scan is a manual process; the part is moved by hand under the transmitter to search for defects. The advantage of this scan is accuracy and the ability to determine the depth of the defect, however, to completely scan numerous parts in this way would be labour intensive. The C scan automatically scans for defects and, depending on the size of the components, can scan more than one at once. The machine outputs a plan view of the components and varying shades on the screen identifies defects. This depends on the skill of the operator to correctly identify defects from the image.

Both A and C scans send a specified power of ultrasound through the parts and then detect significant losses that indicate inclusions or voids within the part. Ultrasound does not propagate well through air; therefore, a constant jet of water must be maintained between the transmitter and the top surface of the part and the receiver and the bottom surface of the part. To differentiate between signals from a good part and one with defects, it is necessary to compare with those of a

test specimen. A test specimen is required for each type of part and is manufactured from the same materials and has similar lay-up configurations with artificial defects in each layer to give signals indicative of a failure. If a defect has been identified on a part with a C scan, the position can be pinpointed and marked using an A scan. Each part has a specification for NDT that is determined in conjunction with the customer. This contains information on the frequency and probe type to be used as well as the tolerance for defects. If a failure occurs in any of the NDT techniques and it is possible to rectify the fault, GE then have a policy of 100% retesting. When a component passes all levels of inspection, some painting and assembly to other parts may be required. The component is then ready for delivery to the end user.

3.3.10 Observations

The current work focuses on the costs incurred converting the raw material to a cured component, i.e. ‘automated kit cutting’ through to ‘unloading from the autoclave’ as described in Figure 3.3. Each of the stages in the manufacturing process have been observed, and by monitoring the time taken, labour, materials and power usage an estimation of the relative cost of each of the activities shown in Figure 3.3 has been made. Table 3.1 lists the activities identified in Figure 3.3, and provides an indication of the overall contribution to costs by showing the relative cost in terms of capital investment and operation costs. Table 3.1 highlights that both the large labour content in hand lay-up of the face sheets and the capital and running costs of the autoclave incur the largest portion of the cost of producing aircraft sandwich structures. This justifies a thorough investigation into how the process can be changed to reduce the labour costs in the face sheet lay-up procedure, and to remove the autoclave from the process.

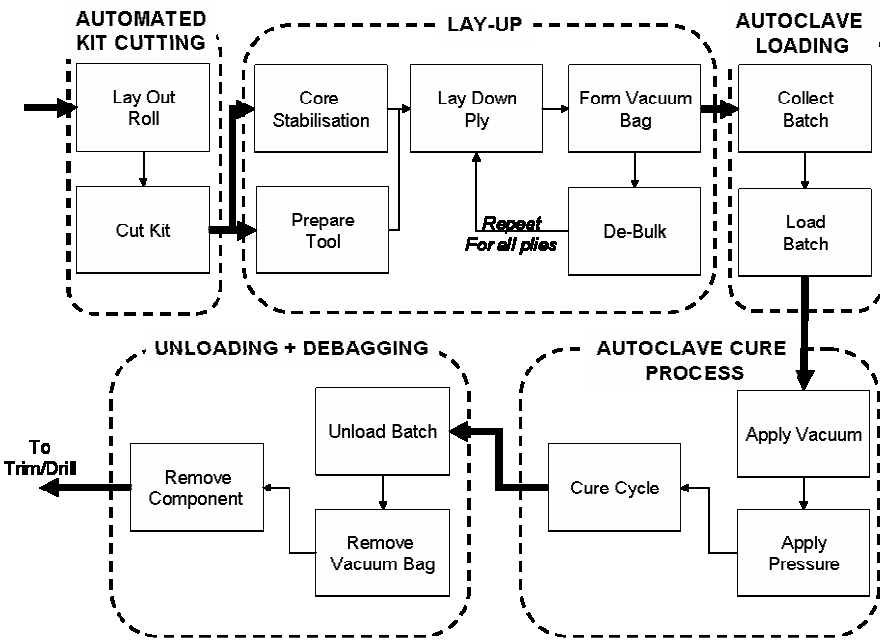


Figure 3.3: Flow diagram of the autoclave based manufacturing process

Table 3.1: Breakdown of costs in autoclave cured prepreg manufacture

Manufacture Area		Capital Costs	Running Costs	
			Labour	Material and Power Usage
Automated Kit Cutting		Medium		
	Layout Roll	-	Low	-
	Cut Kit	-	Low	-
Layup		Low		
	Core Stabilisation	-	Medium	Medium
	Prepare Tool	-	Low	Low
	Layup and Debulks	-	High	Medium
	Form Vacuum Bag	-	Medium	Medium
Loading		Low		
	Collect Batch	-	Low	-
	Load Batch	-	Low	-
Cure Process				
	Autoclave	High	Low	Medium
Unload and Debug		Low		
	Unload	-	Low	-
	Debug	-	Low	-
	Component Removal	-	Low	-

By studying the entire manufacturing process, from receipt of material to full assembly of components, it has also been identified that the autoclave curing process introduces a significant ‘bottleneck’ in production (Figure 3.4). The bottleneck is primarily caused by the need to resort to batch processing of components in the autoclave. This is because the number of autoclaves that a company can purchase and install is restricted by high capital and running costs. To avoid backlogs of components, and increase efficiency, batches are created that require the same curing cycle. Therefore, components often wait in the production line until there are sufficient to fully occupy an autoclave. Another consideration is that the loading and unloading of the autoclave can only be carried out at one end, which also slows the process. Introducing an oven cure, would mean that components could be loaded at one side and removed from the other, creating better production flow, reducing the cost of tooling and unrestricting the size of the batches, because ovens are much less costly to purchase and run than autoclaves. By replacing the autoclave with an oven cure, the production bottleneck would be changed as shown by the dotted lines in Figure 3.4, with lay-up being the main cause of a new, but less severe bottleneck. However it is possible to buy expensive double ended autoclaves, although this would require large capital investment at GE.

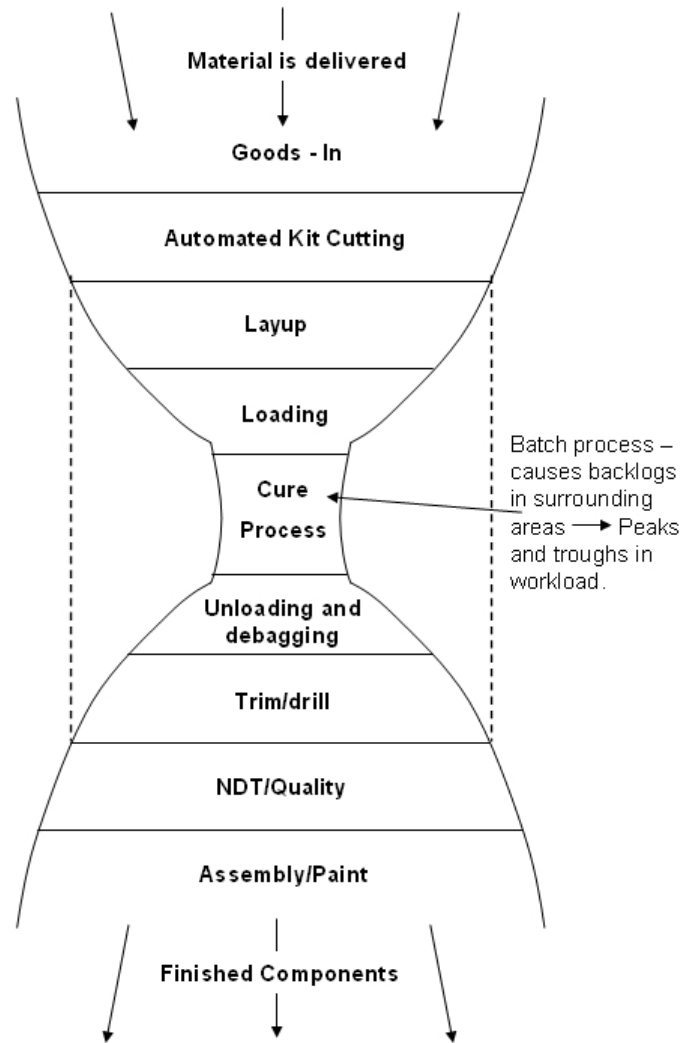


Figure 3.4: Bottleneck caused by autoclave cure

The main cost contributors in the manufacture of composite components have been shown to be the large labour content in manually laying up the laminate and the capital and running costs of the autoclave. Therefore, in this study it is proposed that a process is used that both reduces the high labour content, and removes the autoclave cure in favour of an oven and vacuum only cure. This will have the added advantage of improving the flow of manufacture and removing the bottleneck caused by batch processing used in the autoclave. The conclusions presented here are based upon informed opinions after extensive observation of an industrial process at GE.

3.4 Current costing analysis

At GE two types of costing analysis are in use. Firstly, accounting for the cost of production of components and, secondly, estimating the cost of production when bidding for new contracts. When accounting for the cost of component manufacture, a traditional approach is used as follows:

$$Cost_{Total} = Cost_{Material} + \sum Cost_{Rate} \times Time_{Operation} \quad (3.1)$$

where, $Cost_{Total}$ is total manufacturing cost, $Cost_{Material}$ is the material cost, $Cost_{Rate}$ is a charging rate for a particular operation including overheads and $Time_{operation}$ is the time taken for each of the operations that constitute the process. The use and limitations of such a cost approach, particularly for a complex process such as aircraft composite manufacture, are discussed in Chapter 4.

Engineers at GE use a combination of traditional and analogous cost estimation approaches to estimate the cost of production for new parts when bidding for contracts. For the purposes of the components manufactured at GE, this has been adequate. Although parts may vary slightly in shape and size, all are manufactured using the standard prepreg/autoclave cured process. Therefore, it is possible to provide estimates that can be used to successfully bid for new contracts. However, if a part is to be manufactured using a new method, or material, the current cost estimation techniques used at GE will not provide accurate data. There is a particular difficulty in calculating new charging rates based on an out-of-autoclave cure, such as that considered in this thesis. Therefore, in addition to investigating the use of the out-of-autoclave processing, it is necessary to explore other methods for cost estimation. In the following chapter, the costs incurred by each candidate manufacturing process are summarised. Descriptions of possible cost evaluation routines are given and their relevance to GE.

Chapter 4

4 Cost of manufacture and its analysis

4.1 Introduction

Composites have been used to replace metallic components because of their ability to offer large weight reductions. In [6], it has been suggested it would be possible to reduce the weight of secondary structure of the aircraft by 40% by using composite materials. This ability to save weight, make composites attractive to the aerospace industry, and they are readily selected over metallic components, despite often increased in manufacturing cost [55]. This cost premium has been highlighted in [68], where the estimated cost of the composite parts was approximately 190% of the aluminium parts they were replacing, but this the exact value should be taken as guidance as this paper is 18 years old. In the past the emphasis was always on attaining the correct performance for a particular application [23]. However, there is no longer a concern that composites can be manufactured with adequate performance, although long-term fatigue behaviour and damage tolerance are still a consideration [26]. The focus of research has shifted from performance and weight to achieving a reduction in cost [32] whilst maintaining the required performance.

Gutowski *et al*, [68], identified four major characteristics of composite structure and its manufacture that incur cost in traditional autoclave manufacture: high material costs, high labour costs, design, poor production rates. Gutowski, [69], confirms these findings and suggests solutions. The process can be improved, from a cost perspective, by increasing automation,

changing the material form, and designing for manufacture. An article from the prepreg product manager of a composite materials supplier, Hexcel, [39] provides an excellent discussion of the costs inherent in the current process used for aircraft standard composites and the article highlights strategies to reduce cost. In particular, it is suggested that the removal of the autoclave cure would be advantageous. To address these considerations individually the remainder of this chapter is divided into sections discussing each of the cost contributors: autoclave/out-of autoclave, materials, automation and design.

A final consideration for the cost implication of composite use for aircraft parts is certification. In the aircraft industry all processes that are used for the manufacture of parts are carefully controlled, and must be fully tested before they are certified for use. This caused a restriction when replacing metallic parts with composites [70], and would also mean extensive testing is required to certify a new composite manufacture process or material.

The present chapter considers the manufacturing processes discussed in Chapters 2 and 3 and the costs that are incurred during their use. An important part of this thesis is to analyse ‘new’ process and material combinations for the cost of manufacture. The area of cost estimation has had much attention in the literature recently, in particular to offer designers an estimation of the end cost of parts to be produced ahead of time. Hence, this chapter also investigates the literature on cost estimation models, their advantages and limitations, selection of one type and the reasons for the model’s selection for the current research. GE Aviation currently uses a traditional approach to estimate manufacturing costs for composite parts (Chapter 3). This approach has been approved for use to estimate costs for the baseline manufacturing process currently utilised on site (Chapter 3). However, this research considers manufacturing processes that are new to GE and, therefore, some work may be required to provide a model that is capable of cost estimation. The conclusions from the review in this chapter will allow an informed decision into cost estimation approaches that may be useful both for this research and for further use at GE. Scrap and rework are not considered in this review although this should be considered in future work.

4.2 Cost of composite parts

4.2.1 Autoclave/out-of-autoclave

The sources of expense from the use of autoclaves are well documented [25, 29, 34, 35]. An autoclave represents a large capital investment for a composite manufacturer [30] even a relatively small vessel can cost tens of thousands of pounds, with large production autoclaves (i.e. 3 m diameter and 7 m long) costing £0.5 million upwards, whilst an oven of a similar size would cost

£0.1 million. The size of the autoclave creates a limitation on the maximum part size that can be produced [30] therefore manufacturers will need to purchase expensive, large autoclaves to produce large components. The running costs of an autoclave, i.e. the energy to heat and pressurise the vessel, are also high [42]. In an industrial setting it is necessary to pressurise the vessel with an inert gas, e.g. nitrogen, to prevent internal fires that are a significant risk at high temperatures and pressures. Autoclaves can only support relatively small scale production [30]. However, until recently this has not been a limitation in the aerospace industry, where numbers of parts per year were traditionally low. Finally, the pressure and temperature required inside the autoclave impose added requirements on the mould tools. To ensure the tooling is both temperature and pressure resistant makes the tooling more expensive [35]. Therefore, the benefits of composite manufacture without an autoclave are; no need for such capital expense, reduced energy to cure, potentially lower tooling costs, and no limit on the size of part posed by the autoclave. In [6] it was suggested that out-of-autoclave manufacture is the key to reducing cost in the future. Therefore, it is necessary to remove the autoclave without reducing the mechanical properties of the final laminates or any other elements of quality and yield such as tolerances [30].

An important avenue in out-of-autoclave research is to use a cure in a conventional thermal oven. This would use a similar carefully controlled thermal cure cycle as the autoclave, but with just vacuum pressure to consolidate the part. Soutis [6] suggested that the use of a thermal oven, over an autoclave, could save 90% of the processing time and energy resulting in a cost reduction of approximately 50%. However, there is no detail as to how this conclusion was reached, and it is not indicated whether the total or cure costs are considered.

The Quickstep process (see Section 2.3.3) also benefits from lower initial capital out-lay, lower tooling costs and lower operational expenses [47]. Further, by removing the need for a thermal cure completely, [49] set out a target to reduce the cost of composite manufacture by 40%.

4.2.2 Materials

A significant proportion of the total cost of manufacture for CFRPs is the material cost; Bader and Bibo *et al* [30, 32] estimated that material may account for 25% of the total cost. The current standard for composite manufacture for use on aircraft uses prepreg (see section 2.3.1). The pre-pregging process is lengthy and complex [27], and therefore as a ‘raw’ material prepreg will be more expensive than non pre-processed dry fibres and separate resin [69]. The aircraft industry accepts the expense to ensure composites of the highest quality and lowest void content are achieved [30, 69]. In a freezer, the prepreg will only have a shelf-life of 6-12 months [35]. Due to

the very limited ‘out-life’ of prepreg material (defined as the time a prepreg can be stored out of a freezer), it is necessary for careful auditing of the time spent at ambient temperatures [29]. A further consideration is the waste produced with the use of rolls of prepreg [35]. For many components, complex ply shapes are required in different orientations, and must all be cut from a roll. Therefore, careful nesting of the shapes is important to minimise wastage [29]. Even with careful nesting, greater than 70 % usage of the material is rare. This obviously adds greatly to the material cost for a component when using an already expensive material form such as prepreg.

In its simplest form, and to attain the superior mechanical properties required for the aerospace industry, the prepreg comes as UD tape (see section 2.2.2). The tape is very thin, of the order of 0.125 mm [29], and hence the hand lay-up is time consuming. It will take 8 plies of UD material to make a laminate 1 mm thick. UD tape is not easy to drape over complex shapes [30]. It is particularly difficult to form the material over shapes with double curvature. This adds to the time it takes to lay-up a component and also the skill of the operator required to achieve a good part. A proven method to overcome the disadvantages of UD material is woven preregs [30]. These come in many forms discussed in section 2.2.2. The woven structure provides a much better drapeability for the user, and, because they are thicker (usually 0.25 mm), fewer layers are required to produce the same laminate thickness [30]. Woven preregs have not been used on the most property dependent applications, because the crimp in the weave reduces some of the in-plane properties [30]. They also do not offer the same tailoring advantage as UD materials, because fewer plies are required.

The labour cost for the manufacture of composites from UD materials is estimated to account for more than 50% of the total cost. It has been suggested that by using NCFs to increase the deposition rate it will be possible to reduce the labour, leading to a total saving of approximately 35%. Although these materials show great promise for their use in reducing the cost of aerospace standard composite production, there are a number of disadvantages that must be considered. The main problem remains a reduction in the in-plane properties caused by the slight crimp in the fibres and the corresponding V_f reduction [29]. NCF materials were also more expensive than regular woven dry fabrics when this paper was published [30], however this may not be true today. The biggest strength of NCFs, the ability to greatly increase the deposition rate, reduces the ability of designers to tailor the directional properties ply by ply and incorporating ply drop-offs are problematic [32]. As the requirement for NCFs increases the production rates will allow the manufacturers to demand specific thickness and orientation combinations for each component. Before NCFs can be accepted as a feasible alternative to UD or woven materials, it must be

decided how to treat them from a design perspective to allow models of adequate accuracy to be produced.

Use of materials other than prepregs offer many advantages from a cost reduction perspective. The use of dry fabrics, combined with resin in liquid or film form, will not only reduce the need for cold storage [36], but also reduce the cost of the ‘raw’ materials. However some particular resins designed for specific applications, i.e. RTM, may be more expensive. A final material to be considered in a bid to reduce manufacturing cost is random chopped fibres. The automotive industry is very interested in the use of random chopped fibres to improve the crash-worthiness. Chopped fibres are an inexpensive material form, and the process can be easily automated to produce 3D complex shapes quickly [54]. Direct fibre preforming (DFP), uses an automated spray containing the chopped fibres and a binder to form a preform on to a tool face. It has been proven to have excellent repeatability and, because it is a direct forming process, very little waste (approximately 3% scrap) [54]. It offers a real cost benefit over woven fabrics, but will always have lower V_{fs} due to the inherent structure of such materials.

4.3 Cost analysis

4.3.1 Cost model types

A good cost model must meet certain requirements. It must be accurate, adaptable, able to deal with complex parts, useable at the design stage and transparent as to where the cost comes from [71]. These will, therefore, be the guidelines with which the costing techniques are judged. At the highest level, cost estimation can be split into two branches, qualitative and quantitative (Figure 4.1). Qualitative approaches can be intuitive or analogical and quantitative approaches can be parametric or analytical. Underneath these four types there are many examples listed. Cost estimation is used for many reasons and because of this there are different approaches that may have advantages for some applications and limitations for others. For example, cost estimation may be required to check quotations from suppliers, evaluate product design alternatives, assist long term financial planning, help control manufacturing cost and provide standards for production efficiency [72].

Cost models can be split into three main levels. At the lowest level, these require simple data inputs and will offer a low level of detail, so provide only ballpark figures. At the highest level, models use an in-depth examination of the process and should be highly detailed and, finally, heuristic models use a rule of thumb that depends on expertise of the estimator [73]. For all of these, data must be identified, collected and analysed, but these operations are limited by the

number of cost models required, historical data available, time to develop a model, product or process complexity and process expertise available [73]. Composite manufacture is an inherently complicated process, even for the simplest component, and therefore in the current research process, complexity will be an important factor for the choice of cost model.

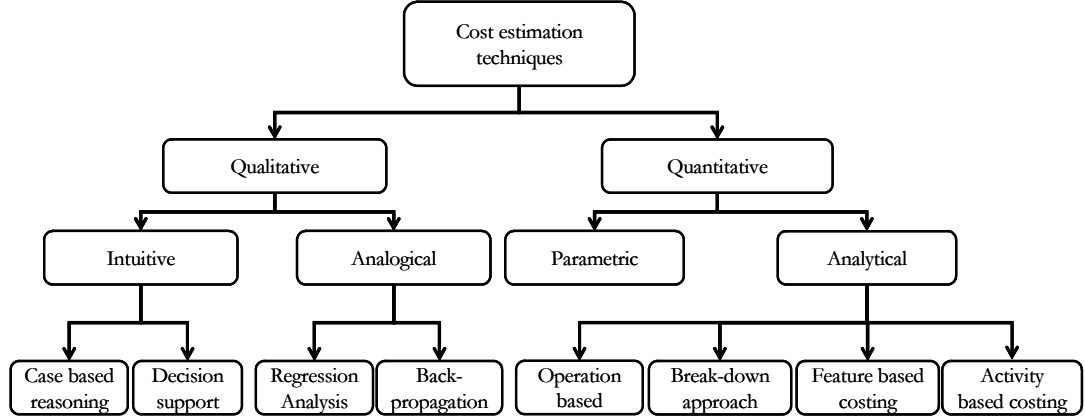


Figure 4.1 : Cost Model Approaches (modified from [74])

4.3.2 Traditional Costing Methods

Traditionally, costs have been apportioned to direct and indirect sources [75]. The direct costs consist of raw material and direct labour costs, whilst the remainder of the costs are considered indirect and labelled overheads [76]. The overheads are allocated to a measure of volume of production as a factor. This ‘volume of production’ can be defined as component weight or volume, or, more commonly, based on labour costs rate per hour [62]. The time to complete a process is estimated through measurement or standard time models and each unit of time is apportioned a labour cost rate. It has been found that such an approach measures the cost adequately for processes that are within the usual operations of the company. However, when a process is significantly altered, the labour rate will no longer accurately represent the overhead costs and, therefore, will distort the total cost [72]. This is of little use to the current research, where the processes considered may be novel and certainly new to GE Aviation.

To accurately produce an estimate with the traditional approach, it is necessary to provide a detailed breakdown of the manufacturing process including the time spent in each operation of the process to complete the final component. Following detailed analysis, a time model can be produced for the complete process. The literature reports such models for drilling [77] and machining [78], but also for composite manufacturing processes. Two examples of such models are the Manufacturing Cost Model for Composites (MCMC) that has been reviewed by Edwards [64], and the Advanced Composite Cost Estimating Model (ACCEM) that was produced by Northrup and reviewed by Gutowski [69]. The ACCEM splits the manufacturing costs of a

composite component, by the conventional aerospace process (Chapter 3), into all the operations that must be performed and applies rules for the time required to complete them.

4.3.3 Case-based reasoning

Case-based reasoning (CBR) can be considered as an analogous technique [79]. An analogous approach considers similar components that have been manufactured previously and, by taking account of the differences with the current component and, more importantly, the similarities between them, makes a cost estimate. The analogous cost estimation technique qualitatively assesses the cost of a component from known products. The process therefore requires previous cost data [74] and an amount of experience of the manufacturing process to make a reliable estimate [62]. For products that are within the usual scope of the component manufacture of a company, the analogical approach will offer reasonable estimates if a number of previous products are known and the estimator fully understands the processes. In this case, it will offer good understanding of the cause and effect of the costs involved [62]. Analogous costing uses a concept of ‘degree of similarity’ to provide an estimate. The difficulty in applying this approach is in assessing the degree of similarity. In Cavalier *et al* [80], a problem in applying a measure to take account of the effect of technological progress was highlighted. The literature review concludes that case-based reasoning would therefore offer inaccurate or unreliable estimates for a component produced by innovative methods, such as those considered in the current research.

4.3.4 Activity Based Costing (ABC)

ABC attributes costs to the completion of activities. Only the raw material is considered an unallocated cost. The method relies on the assumption that a manufacturing process can be made up from many simpler activities. The activities are split into those at unit, batch, product or facility level [76], where the following definitions apply:

- Unit level – activities that must be performed for each product, e.g. inspection;
- Batch level – activities that must be performed for each batch of units;
- Product level – once performed activities at this level benefit all products of the same type;
- Facility level – activities that are performed for the facility, e.g. depreciation. Such costs behave like fixed costs in the traditional approach however there will be fewer in this allocation system [81].

The conventional approach to ABC is to ascertain the activities that are necessary to manufacture a product and then investigate the cost driver for each activity. The implementation of an ABC system is outlined by Tuncel [82] as follows:

1. Identify activities such as drilling, machining, etc;
2. Determine the activity costs;

3. Determine the cost drivers for each activity, e.g. machining hours;
4. Collect the activity cost data;
5. Compute the product cost.

This can be further explained by Figure 4.2, in which a procedure for the implementation of an ABC system has been outlined. Such a model requires a detailed breakdown of a process to determine the activities involved and the factors in each activity that may act as cost drivers. The material flow in the manufacturing process is documented to provide knowledge of the activities and resources used to produce a component. The existing cost information can be used to find the cost of resources. The resources are analysed to investigate the cost driver for each. Simultaneously, the activities are identified and analysed to measure how many of each resource is required for component production. Finally, the cost drivers for each activity are identified. The product cost is found by summing the cost of each resource and activity required to manufacture it.

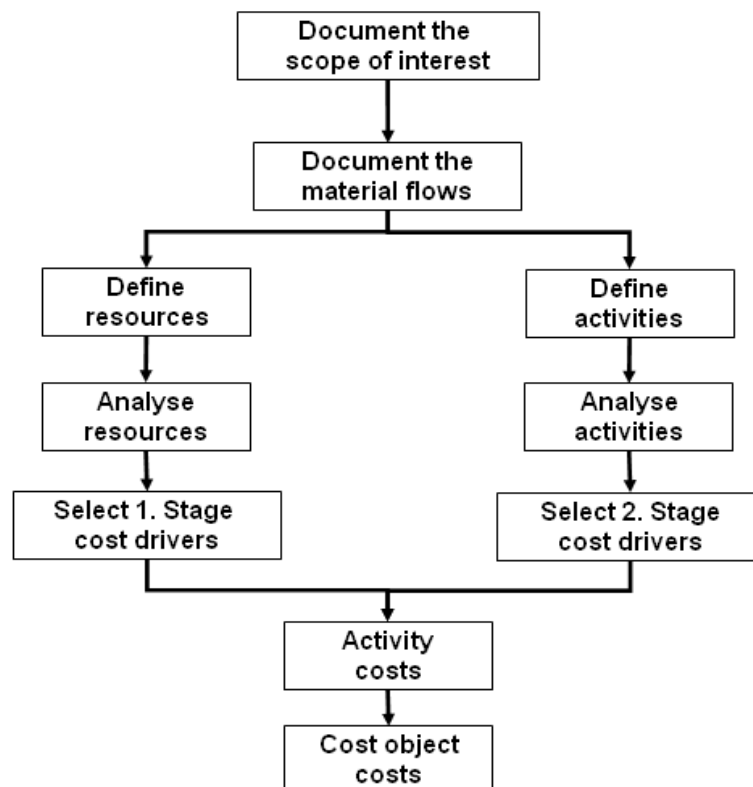


Figure 4.2 :Implementation of an ABC method [83]

Comparisons between traditional methods and the ABC approach have been made for a selection of products [82]. The differences between the estimates were measured as a percentage, where the traditional estimate was 100%. The results showed an S-curve (Figure 4.3). For some products the traditional approach under-estimated the product, most likely because the company was not aware

of hidden costs. For others, the traditional method over-costed the product cost so therefore, was a hidden profit zone. Finally, in a narrow band, the traditional and activity approaches yielded similar estimates [82]. There was no indication of the correct value of the cost, and therefore it is difficult to analyse which model offers the better prediction. The data does indicate some large variations between them however.

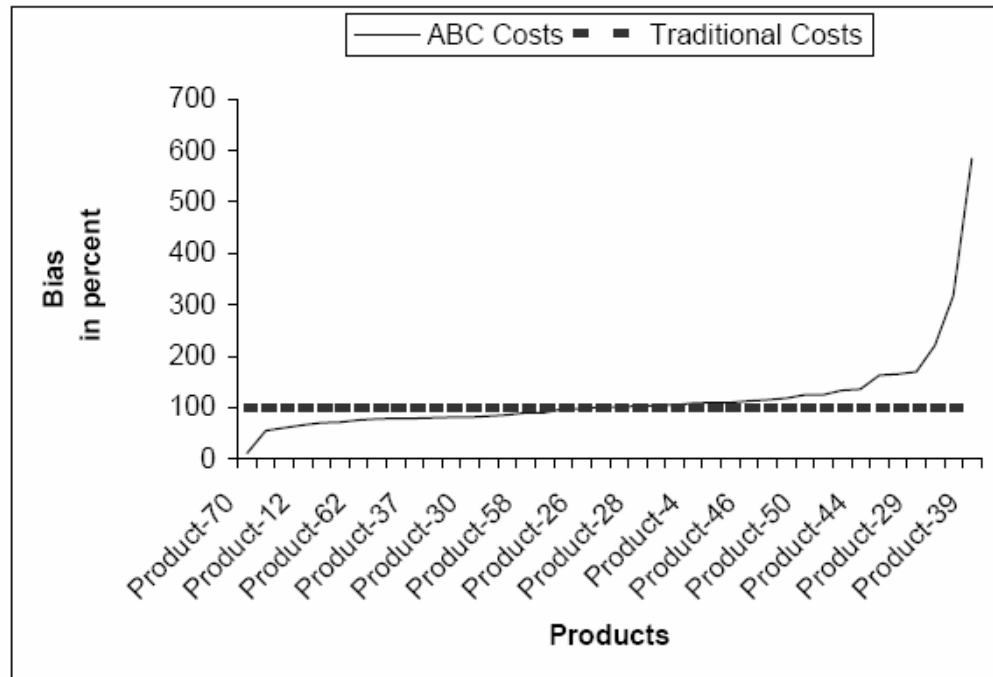


Figure 4.3: Example of results from costing a range of products with ABC and traditional approaches [82]

The ABC approach offers some advantages over the traditional costing method, as ABC has the potential to increase the visibility of costs in a manufacturing process [72]. By considering the activities in turn and analysing those which add value to the process and those which are non-value adding and then, by removing such activities, the manufacturing costs can be reduced. Lere [84] discussed the problems with traditional cost approaches, which are identified as being mainly in the allocation of overheads. It was suggested that changes regarding the handling of these overheads, including changing the factor used in computing overhead rate, dividing the overhead into multiple cost pools and using factors that reflect batch, product level in addition to unit level and therefore, ABC. By allocating the overheads to a number of sources, a more accurate cost and a visible representation of the breakdown of the manufacturing costs is possible. ABC as an approach to compare processes was discussed by Boons [85] when the idea of intermittent variables was introduced. These would allow investigation of processes that had different activities in them with these intermittent variables being used only in the process models that required them. This is of particular interest to the current work that endeavours to compare the cost of different processes to manufacture composite components, each of which may require some similar activities but also some differing ones.

The accuracy of an ABC model depends upon how the process is split down into activities and, therefore, identifies the cost drivers and the cost per unit of the cost driver [81]. Therefore, for complex manufacturing processes, such as composite component production, an in-depth analysis must be performed. In such processes, this may require an unfeasibly extensive analysis and data collection exercise. A modified approach to ABC has been reported that considers the cost of production by monitoring the consumption of resources at particular points within that process called resource centres [86]. The modified approach aims to reduce the amount of data collection and analysis that is necessary to form an estimate; however the accuracy will suffer as a result.

A particular difficulty with the implementation of ABC is identifying the cost drivers for each activity. To overcome this problem, an extra layer to the cost modelling process can be added that attributes time to each activity and then develops time and cost estimating relationships [87]. In this way, time becomes the cost driver for all activities in the manufacturing process. One approach to model the time spent performing an activity [88] was work sampling to investigate the time spent on each activity. This is seen as particularly useful in non-repetitive and irregular activities.

Difficulties have been experienced with the implementation of an ABC scheme, and it will only be successful if it has management commitment, the employees receive education on the approach, and there are incentives for the employees [89]. The literature demonstrates that ABC has been applied to numerous and varied applications, from manufacturing costs to calculating the unit cost of services [90] in the healthcare provider and distribution logistics of a developing country [83].

4.3.5 Parametric cost models

Parametric cost models are a quantitative approach to estimate the cost of a product from data on previous product manufacture. At the simplest level, a parametric cost model considers variables, for example, the weight of a component, and by applying a linear relationship between that variable and the cost, the model is formed. This is known as the method of scales and assumes products are similar but of varying sizes, e.g. cost per kilogram. A more accurate model for complex components uses statistical analysis of product cost data to relate product variables to the cost. Finally, the most complex parametric cost models involve a cost estimating relationship (CER) [80]. CERs relate the cost to parameters via a mathematical relationship. This is generally limited to between two and five parameters. To construct a CER, the parameters must be chosen

along with the structure of the formulae. The coefficients are then computed through multiple regression [79].

The parametric model does have certain advantages. Although it is difficult to develop, it is easy to implement and therefore, a non-expert can use the system and will also allow scope for quantifying the risk of the estimate [62]. It is suggested that a parametric model would be used when there are quite a few similar cases in the past, the attributes that affect the cost are known, there are few cost drivers and it is certain how these drivers influence the cost [91]. The accuracy of the parametric model depends upon identifying the relevant cost driver and therefore, in a complex process, such as composite component manufacture where a number of drivers may be important, parametric cost models will offer inaccurate estimates [74].

The factors in the parametric model must be selected on the basis of available data. Therefore the model will have limitations and should not be used when the process is outside of the database range, or not researched or validated, unless there is appropriate adjustment [62]. A parametric cost model also suffers from a lack of direct cause and effect between a process parameter and the production cost. This means the sources of the cost are not evident and therefore it is difficult to identify areas of a process to reduce cost [62].

Gutowski [92] produced a parametric model for the hand lay-up of composite material using a first order relationship between the process parameters and the time for lay-up. The constants must be found by experimentation and therefore, the model will only estimate the cost of a part made by an established process. For flat and simple components, the model compared favourably with the standard ACCEM time estimation model discussed in section 4.3.2.

To improve the accuracy of parametric cost models, an approach has been suggested [93] to split the parameters into quantitative, such as an area that could be extracted from CATIA models, and qualitative, which are those that are difficult to assign a value and could be found from questionnaires. Statistical analysis is then used to obtain relationships from this data [93]. This study found it was important to understand the design process first. Roy *et al* [93], also stated that when collecting data in the development of CERs it is important to obtain as much as possible, the qualitative data must be cross-checked with more opinions, and the qualitative and quantitative cost drivers should not be mixed. Finally, it is key, to not mix data from dissimilar products [93].

4.3.6 Feature Based cost models

Feature based costing considers a component as being formed from a number of generic features. The identification of the generic features must be understood, and a relationship between the inclusion of such features and the cost incurred to the product is required. The initial step to produce such a model, therefore, is to identify every generic feature that may be included in a component design. This approach depends on correct identification of the features and the costs attributed to them from analysis of data on previous product manufacture. The level of detail of the features that are considered determines the level of detail of the model. Figure 4.4 shows an example component split into its features. It is possible to use feature based costing to analyse a part qualitatively that would simply identify those features that may incur costs and therefore warrant a re-design. It is equally possible to quantitatively estimate the total cost using basic parameter driven relationships.

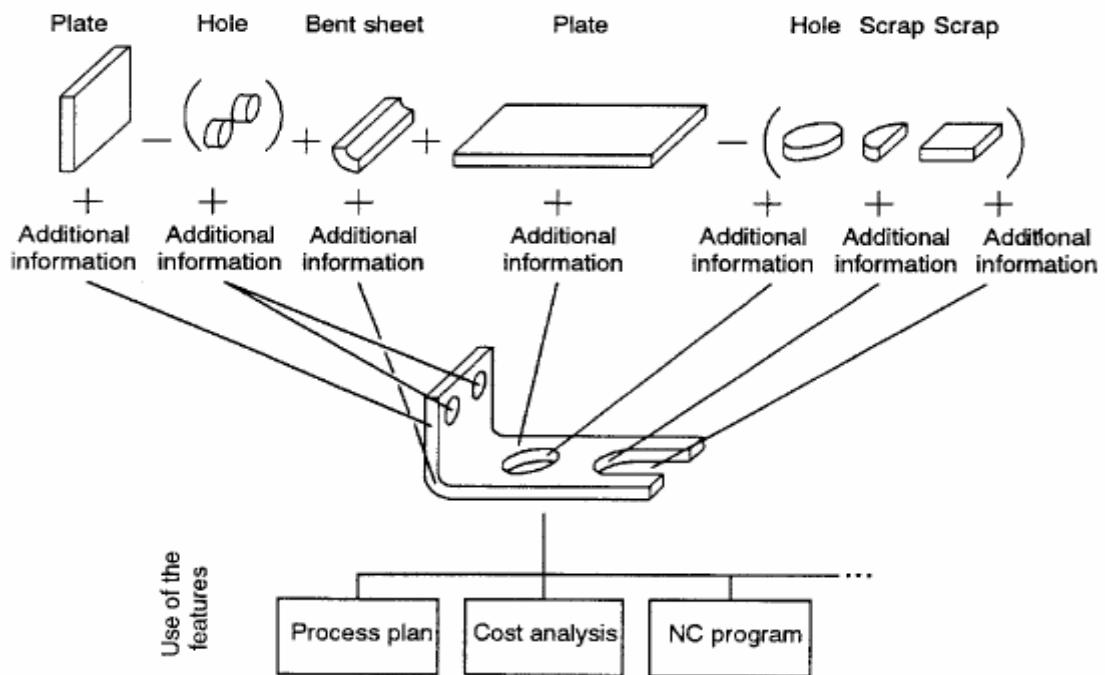


Figure 4.4 :An example of a component split into features [94]

By attributing the costs to particular features, it is possible to identify those that contribute most to component cost. Potentially, designers can use this information to reduce total manufacturing costs by avoiding such features [74]. The accuracy of such a model depends on successfully splitting the part into features whose costs can be identified correctly. Unfortunately, for complex parts it may be difficult to identify the costs of the small and complex features that form the component [74]. Feature based costing splits costs in a similar way to activity based costing. However, it is only possible to attribute material costs of a particular feature if that feature directly contributes positively (material addition) or negatively (material waste) [62]. It has been claimed that using a feature based cost modelling system may lead to a preoccupation of identifying feature

costs and, therefore, may miss opportunities to reduce total product costs [62]. It is also the case that feature based models will produce a relationship between the number of features and the product cost. It has been reported that more features in a component would require more design and manufacture and therefore, increase the cost.

The costing of a machining process is considered that utilises a framework combining cost information of features stored in a product database with a feature based AutoCAD system [95]. The cost is estimated based on the type of feature, e.g. through slot, round corner, as well as the size and precision required. A similar approach was undertaken by [94]. [60] produced a feature based model that was split into material, processing and tooling costs, each of which could be calculated, taking into account certain feature characteristics, e.g. complexity, size. The costs were a combination of qualitative and quantitative costs.

4.4 Linking design and cost optimisation

VICONOPT (Vibration and Instability analysis with CONstraints OPTimisation) is an established optimisation program based on plate theory for buckling and vibration analysis. This was combined with new code [64] to use cost equations that relate manufacturing cost to design variables. The cost model can be defined by the user and can therefore use any cost driver. However, the program does not include optimisation of particular design criteria therefore the program must be used multiple times to confirm the preferred option.

In [96], design decisions are considered as a trade-off between weight, cost, risk and time. The paper presents an example of a multiple objective optimisation. Three approaches are investigated to include cost as a design driver. The standard approach selects an optimal solution from a set of designs that meet the minimum weight criteria. An innovative approach is suggested using a cost parameter (\$/kg) directly in optimisation such that it is a trade-off between cost and weight optimisation stopped when cost penalty becomes too great. Finally, the third approach used a cost increment parameter, $\Delta C/\Delta W$. If the cost increment is large, it was optimising for lower weight, but smaller cost increment would home in on lower cost. The third approach proved successful but, as with other methods described here, it is aimed as a design tool, not a process selection tool.

An optimisation procedure is described in [97] for a particular manufacturing process, i.e. RTM. The procedure optimises the mechanical performance and manufacturing cost by forming the multiple variable problem into a single one using some assumptions. The lay-up is optimised for

performance and fill time (it does not state the form of the cost model, but appears to assume a linear relationship between fill time and cost). The study shows that optimising for mechanical performance often comes at a cost, but the cost can be significantly reduced by a small reduction in performance.

Kaufmann *et al* [12] describes an optimisation framework for composite aircraft structures to minimise the direct operating costs on the part level. The study uses models from previous research and includes NDT. The optimisation is a balance between manufacturing cost, NDT cost and weight (at design stage). The cost of NDT depends on the scan pitch required to measure a predetermined size of flaw. Therefore, the cost and weight of a component is optimised for flaw size. Kaufmann *et al* [12] identified previous models for NDT where costs are based on metallic structures and therefore, NDT in service is a small cost. For composites, laminate quality is highly dependent on process robustness and workman skills, therefore NDT must be rigorous. The cost/weight framework was added to a separate calculation of NDT cost using a feature based cost estimation model. The performance of the laminate was predicted using an FE model formed in ABAQUS investigating buckling and failure criterion. The manufacturing cost estimated using commercially available cost estimation (SEER-DFM) software that again uses a feature based model. The weight of component was predicted from CAD software by measuring the volume and multiplying by density. Finally, the NDT cost was predicted using in-house code that calculates cost dependent on size of panel, etc. Kaufmann *et al* [12] applies the optimisation procedure to a case study on a stringer stiffened panel to find the optimum value of several parameters; skin thickness, stringer thickness, stringer foot, web height and stringer pitch. The study attempts to investigate whether the autoclave process is too conservative, and challenges whether the current predetermined flaw size that must be detected using NDT, 6 mm, is too small. The conclusion is that 6 mm is too small; however this does not include fatigue performance.

Gigliotti *et al* [98] presents results of a study using an in-house optimisation code for stiffened panels. The code optimises for weight and considers buckling and, innovatively, damage resistance. The approach interacts with FE program ANSYS to perform the buckling and damage resistance analysis. The paper optimises composite panels stiffened with both 'I' and 'T' shape stiffeners for both buckling only and buckling and damage resistance combined. The panels produced for damage resistance were between 16 and 18 % heavier than the standard component. Once the optimisation had formed the design of the individual components, a post-process costing code estimated the cost of manufacture and included running costs due to a need for repair to the non-damage resistant panel. With this cost estimation model the paper suggests that the use of the

heavier damage resistant panels will be cheaper over the life of the components. However, the costing procedure takes no account of the life costs of a composite component that is 16 % heavier, and this would undoubtedly have an important effect on the choice a designer would make.

4.5 Summary

Using an autoclave for cure requires a large capital investment, high running costs, high cycle times, and a limit to size of part that can be manufactured imposed by the autoclave size. Prepreg is an expensive form of material due to the pre-processing required, and because it comes in preset sized rolls, high wastage rates are normal. The partially cured resin impregnated into the fibres have a limited shelf-life, particularly at ambient temperatures, therefore cold storage is required to increase the life of the material. Manual lay-up of numerous thin layers of prepreg is time consuming and labour intensive. Literature suggests that the path to reducing the cost of manufacturing composite aircraft parts is to use out-of-autoclave cures on dry fabrics infused with separate resins formed using a reduced labour process. Of particular interest to the aircraft industry are NCFs infiltrated using RFI. Therefore, it is pertinent to select NCFs and RFI for consideration in this thesis.

Table 4.1 summarises the main advantages and disadvantages of the various costing methods considered in this chapter.

Table 4.1: Advantages and disadvantages of the costing approaches

Costing Approach	Advantages	Disadvantages
Traditional	<ul style="list-style-type: none"> Overheads costs are attributed to a charge rate Provides an adequate estimate for a normal process of a company 	<ul style="list-style-type: none"> Distorts the cost for a novel process Requires a detailed time model
Analogous	<ul style="list-style-type: none"> Provides a reasonable estimate for normal processes. 	<ul style="list-style-type: none"> Dependent on expert opinion Will offer an inaccurate estimate for novel

Activity Based Costing (ABC)	<ul style="list-style-type: none"> • Overheads are allocated to individual tasks and therefore is less likely to be distorted • Increases visibility of the causes of cost • Increased accuracy when compared to traditional methods 	<ul style="list-style-type: none"> • Requires a detailed breakdown of the process • Difficult to ascertain the cost drivers for each activity
Parametric	<ul style="list-style-type: none"> • Once developed the model is easy to implement • Will offer a reasonably accurate estimate when there have been many similar cases in the past and few cost drivers that known 	<ul style="list-style-type: none"> • The model can be difficult to develop especially when many cost drivers are involved • Lacks visibility of the causes of cost • Using the parametric model out of the range of the source data will result in inaccurate estimates
Feature Based	<ul style="list-style-type: none"> • Identifies the features that contribute most to the cost 	<ul style="list-style-type: none"> • For complex parts it may be difficult to correctly identify all the features

GE Aviation currently uses a traditional approach to cost estimation and measurement. The time each operation requires for completion is considered, which is multiplied by a charging rate that is dependent on the particular operation. It has been discussed that such an approach will provide a distorted view of the cost for a ‘novel’ process such as those to be investigated in this thesis. For estimating the cost of manufacture at GE the use of case-based reasoning, activity based costing, parametric and feature based cost models have been contemplated. However, each has been rejected, at least for use in the work described in this thesis. Case-based reasoning is already in use at GE, at least in an informal manner, for ‘quick’ estimates when meeting to discuss bidding for a

new contract. However, it has been shown from the literature that this form of cost model does not perform well when used on novel processes. The manufacturing processes considered in this thesis are novel to GE, and therefore case-based reasoning should not be used. Activity based costing requires a detailed breakdown of the process, with the costs applied at each stage investigated. Whilst research on site has provided knowledge of the manufacturing process, it has been difficult to obtain accurate cost values. It would be difficult to apply the model without adequate previous cost data. However, in the future, activity based costing should be considered by GE as an approach to provide good cost estimates. It is known that although the manufacturing processes considered here are novel, many of the activities involved will be similar to the current production. Therefore, with adequate cost data, an excellent cost model could be produced.

A parametric model relies upon a wealth of source data to which a function can be applied. The data should cover many and varied previous components such that the model can cover any eventuality that may occur in the future. The biggest obstacle to the application of a parametric model in this work is the lack of an adequate database of previous data, but it would also be difficult to select a parameter to apply a function to. The parametric model may be the least promising for inclusion by GE in the future. Finally, feature based reasoning was rejected for the work in this thesis because the processes considered are novel and therefore, even with a information on previous panels, it would be difficult to know the cost effect that the addition of a feature would have. The work described in this thesis therefore considers the relative cost of manufacturing the same component by various manufacturing processes. However, feature based costing lends itself more towards the addition of different design features. This cost model could be of interest for use in the design office at GE once a manufacturing process has been established on site. The model could be used to offer a quick estimate to designers when considering the addition of one feature over another.

Once the main types of cost model had been rejected for the current work it was decided that actual cost values were not necessary. The cost analysis would only be required to give a comparison between the use of material and process combinations. Therefore, a combined quantitative and qualitative approach is used. The material cost of each panel is calculated from actual usage and wastage, and the labour cost is estimated by monitoring time to manufacture. However, the other, less tangible costs, such as overheads have been discussed in a qualitative manner. This approach avoids many of the pitfalls of the cost estimation models discussed above that might otherwise have biased the results.

Chapter 5

5 Generic Panel Manufacture

5.1 Introduction

The current practice at GE was reviewed in Chapter 3, and key features of secondary wing structure manufactured on site were highlighted. In this chapter, the information gathered in Chapters 2 and 3 is used to inform the choice of materials and processes being considered, defined as manufacturing options (MOs), and the design of a generic panel. From Chapter 2 it is known that cost savings can be made by removing the autoclave cure, by a conventional oven cure, and reducing the large amount of labour required. The generic panel is representative of panels currently found in secondary wing structure on medium-sized, commercial, passenger aircraft and will be used to measure the relative cost and performance of each MO. This chapter begins by discussing five manufacturing options for the production of aircraft standard secondary structure from composite sandwich. These MOs are incremental steps from a fully hand lay-up of individual layers of unidirectional prepreg cured in an autoclave (the basis of the traditional approach), to RFI using dry fabric and resin film that is cured out-of-autoclave in a conventional oven. These processes will be described in detail with a discussion of some of the advantages and disadvantages of each. The generic panel design is presented, and then a detailed discussion of the manufacture of the test panels using each of the five MOs is provided. Finally, by monitoring the production of the test panels, some detail of the relative cost of each MO is considered.

5.2 Manufacturing Options

In this work, MOs are combinations of material and processing methods that can be used to produce carbon fibre secondary sandwich structure. Five MOs were selected for comparison for cost and performance:

1. Unidirectional prepreg tape cured in an autoclave.
2. Woven prepreg cured in an autoclave.
3. Non-crimped fabric with separate resin film cured in an autoclave.
4. Woven semi-preg and oven cured.
5. Non-crimped fabric with separate resin film using RFI process.

MO 1 forms the basis to which the other MOs are compared and uses the standard GE Aviation approach as described in Chapter 3. MO 1 uses Hexcel's 914C-TS-5-34%, which uses the 914 resin system that has a density of 1.30 g/cm³ and has a content of 34% by weight. The prepreg uses reinforcement in UD form with a fibre density of 1.76 g/cm³ and an areal weight of 131 g/m². MO 2 uses a woven prepreg which, as discussed in Chapter 2, is known to reduce the labour cost for panel production by increasing the thickness of each ply. MO 2 uses Hexcel's 8552S/37%/AGP280/C, which uses the 8552 resin system that has a density of 1.30 g/cm³ and has a content of 37% by weight. The prepreg uses five harness woven carbon with 50% warp and 50% fill by weight as its reinforcement. The fabric has an areal weight of 286 g/m² and uses fibre with density of 1.77 g/cm³. Woven prepreps are already sometimes used in component manufacture at GE. MO 3 introduces the use of NCFs, which can be both thicker than the woven prepreps and suffer from less degradation in mechanical properties due to crimp. MO 3 uses Hexcel's M56 resin film with density of 1.17 g/cm³ and an areal weight of 320 g/m². The quadraxial NCF is used as reinforcement and has four individual plies in a quasi-isotropic configuration and has an areal weight of 568 g/m². NCFs are currently used in aircraft structures, such as the rear pressure bulkhead on the A380, but the material considered in this thesis would require certification before use on aircraft. MO 4 brings in an out-of-autoclave cure using a conventional oven. This will offer the advantages discussed in Chapters 2 and 3 by removing the autoclave. MO 4 uses Hexcel's M56/40%/285T2/AS4C-6K, which uses the same M56 resin used in MO 3 semi-pregged on to 2x2 twill fabric with an areal weight of 285 g/m² and fibre density of 1.79 g/cm³. Finally, MO 5 combines the NCF material infiltrated using an RFI process with an out-of-autoclave cure. MO 5 uses the same materials as MO 3. MO 5 aims to address both the problem of high labour costs, and the costs and limitations that are introduced by the use of an autoclave.

5.3 Generic Panel Design

A generic panel design has been produced that is representative of secondary structure on the wings of commercial passenger aircraft that considers the features reviewed in Chapter 3. As previously stated, the generic panel is to be used to measure the comparative cost and performance of each MO. Therefore, it is important that the generic panel design contains as many of the features described in Chapter 3 as possible, whilst avoiding the introduction of stress concentrations that would detract from straightforward evaluation of the manufacturing processes. The generic panel design (Figure 5.1) is flat and has a plan area of 0.9 m x 0.3 m. The Nomex honeycomb core is 0.6 m x 0.2 m and 12.5 mm thick. A non-core stiffened flange is included as this is a key feature in such panels and is essential for attachment purposes. The flange has a total cured thickness of approximately 3 mm, half formed by the tool-side face sheet and half by the bag-side face sheet. The design has set-aside features such as inserts, attachments, cut-outs and notches, to reduce stress concentrations that are dependent on the ply lay-up and orientation and therefore allows a simple comparison between MOs. The generic panel has been designed to be as simple as possible, and also contains few complex features. In Chapter 4 it was shown that extra design features add to the overall cost to the panel, i.e. feature based costing. Therefore, a complex panel design should not be used to avoid distraction from comparing the cost of the MOs. This is designed to simply be a starting point for performance comparison, and it should be noted that certain features may incur cost at different rates for different MOs.

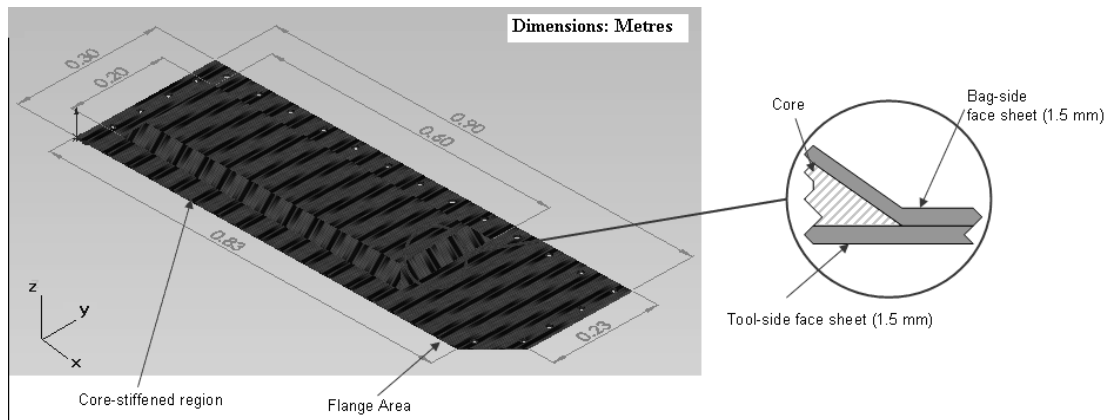


Figure 5.1: Geometry of generic panel design

5.4 Manufacture of Generic Panels

5.4.1 Manufacturing Option 1

MO1 is based on the traditional approach for manufacturing aerospace components, which makes use of unidirectional prepreg tape. The process involves hand lay-up of individual plies that are spliced together from the tape, which provides a cured ply thickness of 0.125 mm. Therefore, for

the generic component shown in Figure 5.1, 12 plies are required to make the 1.5 mm face sheets. A lay-up was defined that would produce quasi-isotropic face sheets. This choice was based on current design guidance outlined in [99]. Therefore a $[0^\circ, 45^\circ, -45^\circ, 90^\circ, 0^\circ, 45^\circ, -45^\circ, 90^\circ, 0^\circ, 45^\circ, -45^\circ, 90^\circ]$ lay-up was used for each face sheet. These were constructed in a symmetrical configuration about a Nomex honeycomb core (Figure 5.2).

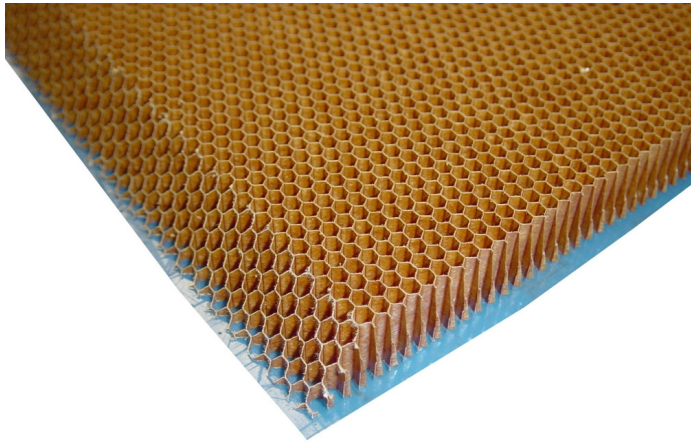


Figure 5.2: Photograph of small section of Nomex honeycomb core

The Nomex core must undergo a stabilisation process prior to the laying-up process so that it does not deform or crush when the curing/vacuum pressure is applied. The stabilisation process was identical to that used in production and used a foam adhesive to strengthen the chamfered edges of the core. A film adhesive is also applied to the flat faces to provide some rigidity. The stabilisation requires that the core undergoes a separate cure before it can be introduced into the sandwich panel lay-up. Table 5.1 lists the operations to stabilise the core before panel lay-up and the breakdown of the times. It should be noted that in this work the time quoted in elapsed time and technically something else could be done during the vacuum debulks. However here it was decided simply to assume that the average employee would not do something else and wait until the debulk had completed.

Table 5.1: Operations in the core stabilisation procedure and their duration

Operation	Time (mins)	Operation	Time (mins)
Layer of lightweight (0.030) glue film	10	Remove bag	5
Peel ply	5	Layer of heavyweight (0.060) glue film	15
Layer of heavyweight (0.060) glue film	10	Replace bag	5
Make consolidation bag	30	Consolidation for 20mins (Reduced vac)	20
Consolidation for 20mins	20	Remove bag	5
Remove bag	5	Peel ply	10
Core down	10	Replace bag	5
Replace bag	5	Consolidation for 20mins (Reduced vac)	20
Consolidation for 20mins (Reduced vac)	20	Remove bag	5
Remove bag	5	Layer of lightweight (0.030) glue film	10
Perimeter of foaming adhesive	20	Layup cure bag	30
Replace bag	5	Consolidation for 20mins (Reduced vac)	20
Consolidation for 20mins (Reduced vac)	20		
Total			305



Figure 5.3: Photograph of an example of the stabilised honeycomb core

Hexcel's 914C-TS-5-34% prepreg tape was used to produce the face sheets. The individual plies were laid-up by hand on a flat mould tool comprising of a sheet of steel. As the stack was constructed, it was vacuum 'debulked' after each ply was introduced in an identical fashion to the production process. The debulk process is essential in production as it removes trapped air from the stack that could cause porosity during the curing process. To perform the debulk, a vacuum bag was constructed on the mould tool that enclosed the stack and a vacuum was applied for approximately 20 minutes. When the tool side face sheet had been laid-up, the Nomex honeycomb core was positioned on the face sheet. The bag side face sheet plies were then laid-up over the core material. A debulk was carried out as each of the 12 plies were added to the stack. The unidirectional tape was difficult to form over the shaped core, and therefore the 12 bag side face sheet plies took longer to lay-up than the 12 tool side plies. Once the component was fully laid up on to the tool, a final vacuum bag was formed around the component that was used during the curing process. The bagged tool and stack were then placed into an autoclave for curing.

When the component was placed into the autoclave, a full vacuum was applied, followed by the application of the autoclave curing pressure. When the autoclave pressure reached approximately 1 bar the vacuum was reduced to a value of 0.2 bar to prevent void formation within the component due to disparity in the vapour pressure. When the curing pressure of 3 bar gauge was achieved, the temperature was increased. The component was heated to 120°C at a rate of 2°C/minute. The ramp rate controls the viscosity of the resin, so that the resin can flow and 'wet out' occurs throughout the component before the resin starts to cure. Initially, the temperature in autoclave was held at 120°C for 60 minutes. The temperature was then ramped at 2°C/minute to the final curing temperature of 175°C. The cure temperature was held for 120 minutes. Once the cure cycle had been completed the autoclave was allowed to cool at 3°C/minute, with the pressure held at 3 bar until the temperature was 60°C or below, ensuring the component was held in position as it cooled to below the glass transition temperature.

During the lay-up procedure, the time spent on each step in the process was noted to allow an estimation of the number of labour hours spent to produce such a panel (see Table 5.2). It was estimated that this component took approximately 14.6 hours to lay-up, with a further 5 hours to perform the core stabilisation (see Table 5.1). These times do not include the length of the two cures.

Table 5.2: Operations in the MO1 manufacturing process and their duration

Operation	Time (mins)	Operation	Time
1st Ply down	5	Consolidate for 20mins	20
Apply Consolidation bag	30	Remove bag	5
Consolidate for 20mins	20	Layer of 319 Film	10
Remove bag	10	Replace bag	5
2nd + 3rd plies down	25	Consolidate for 20mins	20
Replace bag	5	Remove bag	5
Consolidate for 20mins	20	13th ply down	10
Remove bag	5	Replace bag	5
4th + 5th plies down	20	Consolidate for 20mins	20
Replace bag	5	Remove bag	5
Consolidate for 20mins	20	14th ply down	10
Remove bag	5	Replace bag	5
6th + 7th plies down	25	Consolidate for 20mins	20
Replace bag	5	Remove bag	5
Consolidate for 20mins	20	15th + 16th Plies down	30
Remove bag	5	Replace bag	5
8th + 9th plies down	15	Consolidate for 20mins	20
Replace bag	5	Remove bag	5
Consolidate for 20mins	20	17th + 18th plies down	30
Remove bag	5	Replace bag	5
10th and 11th plies down	15	Consolidate for 20mins	20
Replace bag	5	Remove bag	5
Consolidate for 20mins	20	19th + 20th plies down	30
Remove bag	5	Replace bag	5
12th ply down	10	Consolidate for 20mins	20
Replace bag	5	Remove bag	5
Consolidate for 20mins	20	21st + 22nd plies down	30
Remove bag	5	Replace bag	5
Layer of 319 Film	10	Consolidate for 20mins	20
Replace bag	5	Remove bag	5
Consolidate for 20mins	20	23rd + 24th Plies down	30
Remove bag	5	Layup Cure bag	30
Stablised core down	10	Consolidate for 20mins	20
Replace bag	5		
Total			875

The autoclave cure, including time for pressurisation and depressurisation, took approximately 5.7 hours and the core stabilisation cure, 3.5 hours. Therefore, an estimate of the total time to lay-up and cure a component using MO1 is 28.8 hours. This process is time consuming due to the large number of individual plies and therefore the large number (23) of debulks that must be manually

set-up. The nature of the material also means it is not easily draped over shaped objects, such as the core, and this also adds to the time it takes an operator to lay-up an individual ply.

The number of plies required to achieve the thickness leads to a large labour input in the manufacturing process, with the cost of the component reflecting this input. However, an advantage of this method is that the large number of plies required to build the panel face sheets leads to significant flexibility in defining the ply orientations. This has allowed designers to tailor the material properties for the final laminate, but the time taken for lay-up and debulk is excessive, indicating that a material with fewer plies is more desirable.

5.4.2 Manufacturing Option 2

MO2 uses a woven prepreg that incorporates a predefined amount of fibres in both the longitudinal and transverse directions in the same ply. Each ply is equivalent to two plies of the UD tape, laid in a cross-ply (0° , 90°) configuration, and has a cured ply thickness of 0.25 mm. This method reduces the number of plies required in MO1 and hence, lay-up and debulk time, with the 1.5 mm thick face sheets of the generic panel requiring 6 plies of this material. The cross-ply nature of the woven prepreg leads to an alteration in the lay-up of the panels. A $[0^\circ, 45^\circ, 0^\circ, 45^\circ, 0^\circ, 45^\circ]$ lay-up was used for each face sheet, orientated symmetrically about the core material and was comparable to the lay-up in MO1. Prepreg from Hexcel (8552S/37%/AGP280C five harness satin weave) was used to produce the face sheets. The process for lay-up and cure described in section 5.1 was used for panel manufacture. As in MO1, the Nomex honeycomb core underwent the core stabilisation process prior to its inclusion in the generic panel. The time spent on each step in the process was, again, recorded to allow estimation of the labour hours to produce the panel using MO2 (Table 5.3). It was estimated that components manufactured in this way took 8.9 hours, not including the 5 hour core stabilisation (Table 5.1).

These figures also do not include the time for cure, but this is identical to MO1. Therefore, an estimate of the total time for lay-up and cure of a component manufactured using MO2 is 23.1 hours. The lay-up time represents a 19.8% reduction in the number of labour hours, largely attributed to the reduction in plies and debulks. However, the woven prepreg was also easier to drape over the shape of the core, so the time to form the bag side face sheet was also reduced.

Table 5.3: Operations in the MO2 and MO4 manufacturing processes and their duration

Operation	Time (mins)	Operation	Time
1st Ply down	5	Consolidate for 20mins	20
Apply Consolidation bag	30	Remove bag	5
Consolidate for 20mins	20	Layer of 319 Film	10
Remove bag	10	Replace bag	5
2nd + 3rd plies down	25	Consolidate for 20mins	20
Replace bag	5	Remove bag	5
Consolidate for 20mins	20	7th Ply Down	10
Remove bag	5	Replace bag	5
4th + 5th plies down	20	Consolidate for 20mins	20
Replace bag	5	Remove bag	5
Consolidate for 20mins	20	8th and 9th Plies down	15
Remove bag	5	Replace bag	5
6th Ply down	25	Consolidate for 20mins	20
Replace bag	5	Remove bag	5
Consolidate for 20mins	20	10th and 11th Plies down	15
Remove bag	5	Replace bag	5
Layer of 319 Film	10	Consolidate for 20mins	20
Replace bag	5	Remove bag	5
Consolidate for 20mins	20	12th Ply down	10
Remove bag	5	Layup cure bag	30
Stablised core down	10	Consolidate for 20mins	20
Replace bag	5		
Total			535

5.4.3 Manufacturing Option 3

MO3 combines dry, non-crimp fabric and resin film materials proposed for the resin infusion with a traditional autoclave cure. Dry fabric from Hexcel (NC2) was used, which consists of 4 individual layers of UD material that are loosely stitched together to hold their form. Each ply of the NC2 has a lay-up of $[0^\circ, 45^\circ, -45^\circ, 90^\circ]$, with a total fibre weight of 560 gsm. The resin (Hexcel DLS1726 (320 gsm)) is introduced as a layer of resin film between each ply. Each ply of the NC2 consists of 4 layers of UD material, therefore, each 1.5 mm thick face sheet only requires 3 plies of the NC2 fabric. These were laid up as $[0^\circ, 0^\circ, 0^\circ]$, i.e. equivalent to MO1. The layer of resin film was adhered to the underside of the NC2 fabric, before they were both laid up, resin side down, on to a flat mould tool. After each layer was laid-up, a vacuum debulk was required. When the 3 plies that formed the tool side face sheet had been laid-up, the Nomex honeycomb core was positioned. The bag side plies could then be laid-up over the core material, with a debulk after each layer. Once the component was fully laid-up on the tool, a final vacuum bag was then formed around the component that was used during the cure process. The bagged tool and component were placed into the autoclave. A similar cure process as MO1 was used, except that the initial dwell temperature was increased from 120°C to 130°C , and the final post-cure temperature was increased from 175°C to 180°C , as defined by the resin manufacturers. It was estimated that this process took approximately 6.7 hours to lay-up (Table 5.4), with a further 5 hours for the core stabilisation (Table 5.1).

Table 5.4: Operations in the MO3 and MO5 manufacturing processes and their duration

Operation	Time (mins)	Operation	Time
1st Ply resin and fibres down	10	Consolidate for 20mins	20
Apply Consolidation bag	30	Remove bag	5
Consolidate for 20mins	20	Layer of 319 Film	10
Remove bag	5	Replace bag	5
2nd ply resin and fibres down	10	Consolidate for 20mins	20
Replace bag	5	Remove bag	5
Consolidate for 20mins	20	4th ply resin and fibres down	10
Remove bag	5	Replace bag	5
3rd ply resin and fibres down	10	Consolidate for 20mins	20
Replace bag	5	Remove bag	5
Consolidate for 20mins	20	5th ply resin and fibres down	10
Remove bag	5	Replace bag	5
Layer of 319 Film	10	Consolidate for 20mins	20
Replace bag	5	Remove bag	5
Consolidate for 20mins	20	6th ply resin and fibre down	10
Remove bag	5	Layup Cure bag	30
Stabilised core down	5	Consolidate for 20mins	20
Replace bag	5		
Total			400

The time for cure was identical to MO1. Therefore an estimate of the total time to lay-up and cure a component using MO3 is 20.9 hours. This represents a further 9.5% reduction in manufacturing time from MO2. The reduction in labour time is attributed to the reduction in the number of plies and debulks, as well as the material being easy to drape over the shaped core, and, because each ply was laid in the same direction, there was no need for multi-directional alignment.

5.4.4 Manufacturing Option 4

MO4 removes the costly autoclave cure, by combining a woven side-preg with an oven cure. The side-preg 2 x 2 twill woven fabric employed in MO4 (Hexcel DLS1726/40%/285T2/AS4C-6K) uses a similar fibre mat to that described in MO2, and the same resin system as that in MO3. This resin system has been specifically formulated for use in vacuum-only cure. The lay-up for this component is identical to that of MO2, so 6 plies are required for each face sheet. The lay-up procedure was identical to the method described in section 4.3.2, for MO2. When the final vacuum bag had been made, the bagged tool and component were placed in an oven, where a full vacuum was applied. The component was then heated to 130°C at a rate of 2°C/minute. The oven was held at 130°C for 60 minutes, before a second ramp at 2°C/minute up to 180°C was initiated. The oven was held at 180°C for 120 minutes, before the component was allowed to cool at 3°C per minute.

Estimations of the time to lay-up were approximately the same as MO2, i.e. 8.9 hours to lay-up (Table 5.3) and 5 hours to core stabilise (Table 5.1). The component cure time has, however, been reduced from 5.7 hours to 5 hours, by replacing the autoclave with an oven cure, and removing the

pressurisation and depressurisation stages. An estimate of the total time to lay-up and cure a component through MO4 is 22.4 hours, which represents a 3% reduction in manufacturing time from MO2.

5.4.5 Manufacturing Option 5

MO5 uses the same fabric and resin as that of MO3 (Hexcel NC2 dry fabric with DLS1726 resin film). These are laid-up in an identical approach as that described for MO3. Once the component had been placed in the final vacuum bag, the bagged tool and component were put in the oven for cure. The oven cure was identical to that for MO4.

The time estimate for this component is 6.7 hours for lay-up (Table 5.4), 5 hours for core stabilisation (Table 5.1), 5 hours for component cure and 3.5 hours for core stabilisation cure. A total manufacture time for this component is 20.2 hours, which represents a 12.6% reduction in manufacturing time from MO2. MO5 benefits from significantly reduced lay-up and cure times over the other manufacturing options. However, the performance of the material needs to be assessed prior to making any claims that this approach can replace MO1 or MO2 and reduce cost of manufacture.

5.4.6 Relative Cost of each MO

Table 5.5 presents the time to manufacture of each MO in hours. The baseline, MO1, is estimated to require 28.8 hours to manufacture. A large proportion of this time is on the lay-up of the individual plies of the UD material, which provides the majority of the labour costs. By using the heavier woven fabric in MO2, this time is reduced to 23.1 hours, and by using the even heavier non-crimp fabric in MO3, this is further reduced to 20.9 hours. A total reduction in time of approximately 27% is achieved by using a heavier material and hence reducing the large labour content of the lay-up stage of the manufacturing process.

By removing the autoclave cure in favour of an oven (vacuum only) cure, in MO5, the total time to manufacture is 20.2 hours. This represents a further reduction of approximately 3% of the total manufacture time. However, this does not take into account the reduction in cost provided by removing the autoclave from the process, or the manufacture flow process advantage discussed in section 2. Furthermore, MO3 and MO5 do not require freezer storage of the dry mat and therefore, further reduce the running cost of the processes and the production time by removing the need to defrost.

Table 5.5: Time to manufacture panels for each MO and the relative cost of each process

MO	Time Lay-up (hrs)	Cure time (hrs)	Total time to manufacture (hrs)	Relative Labour Costs	Relative Running Costs	Relative Capital Costs
1	19.6	9.2	28.8	5	5	5
2	13.9	9.2	23.1	3	5	5
3	11.7	9.2	20.9	2	4	4
4	13.9	8.5	22.4	3	3	2
5	11.7	8.5	20.2	2	3	2

Table 5.5 contains an assessment of the relative labour, running and capital cost involved in each MO in the form of a value between 1 and 5 for each. The scales represent relative cost values, and are the author's opinion based upon observation of the processes during manufacture. MO 1 is considered to score 5 for all three cost indicators, due to the labour intensive lay-up and expensive autoclave cure. MO 2 and 4 show a reduction in labour to score 3 while MO 3 and 5 show a further reduction to score 2. The removal of some of the need for freezer storage in MO 3 reduces its running and capital cost scores to 4, while the total out-of-autoclave processes (MOs 4, 5) reduce the running and capital costs further. It is thought that a reduction in the labour could offer an 'easier' reduction in cost for these processes in many cases, where autoclaves are already installed and in use. Therefore, any reduction in capital costs is only relevant when considering investment in new plant.

An estimation of material cost is given in Table 5.6. The estimation was based on material usage during panel manufacture and the price per square metre of each material. It should be noted that the actual material usage may be reduced during production with the use of nesting, and the cost of material is highly dependent on volume purchased. However, it is clear that the material cost for MO 3 and 5 is significantly less than that for MO 1 and marginally less than that for MO 2 and 4. The material costs quoted are for the development size samples used during this research, and therefore any conclusions should be taken with some reserve. It should also be noted that whilst every effort was taken to choose five materials that are comparable from the point of view of fibre weight and type, it is not possible to use identical off-the-shelf materials.

Table 5.6: Estimation of material costs of manufacture of a panel using each MO

MO	Price per m ² (\$)	Material used (m ²)	Cost per material (\$)	Total cost (\$)
1	33	11.5	380	380
2	45	5.9	264	264
3	a) Resin 32	2.4	77	232
	b) Fibres 65	2.4	156	
4	39	6.2	242	242
5	a) Resin 32	2.4	77	232
	b) Fibres 65	2.4	156	

5.5 *Test panels manufactured*

A total of 24 full-scale panels were manufactured during this research. Each test panel was given a code, to ensure accurate identification (Table 5.7). Initially, three test panels were manufactured from each MO, to provide a comparison between generic panels produced using each of the five MOs, and to measure of consistency within each MO. In section 4.3.1, the procedure for stabilising the honeycomb core is described. The stabilisation process has been shown to be time consuming and therefore, of added expense. However, after manufacture of panels MO1G1NO1, MO1G1NO2 and MO2G1NO1 it was clear that the stabilisation process was necessary. Once three panels of each MO had been manufactured to offer comparison between them, and give an indication of process consistency, it was decided to produce panels with ply drop-offs over the core and to replace the honeycomb with a foam core (see Figure 5.4). Rohacell foam core 71IG was used, with a density of 75 kg/m³. Ply drop-offs are used for in-service design to reduce unnecessary weight over the core stiffened regions, and will also provide a more even stress distribution across the whole panel. Replacing the honeycomb with a foam core will remove the need for the time-consuming stabilisation process. The panels including ply drop-offs and foam cores will be compared directly with the others to investigate the optimum design solution for the application considered in this work. Finally, after initial tests on the generic panel design, and comparison to FE models, (in Chapter 8) a further panel with face sheets of cross-ply construction was deemed necessary.

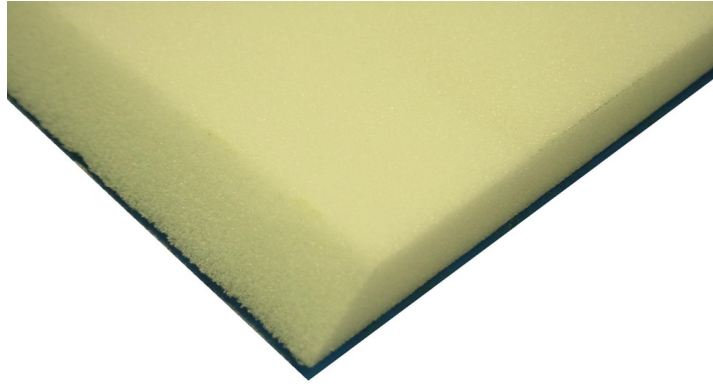


Figure 5.4: Photograph of Rohacell foam core

Table 5.7: List of generic test panels

Panel Name	Manufacturing Options	Description
MO1G1NO1	1	Standard panel, with honeycomb core (unstabilised) repeat 1
MO1G1NO2	1	Standard panel, with honeycomb core (unstabilised) repeat 2
MO1G1NO3	1	Standard panel, with honeycomb core (stabilised) repeat 1
MO1G1NO4	1	Standard panel, with honeycomb core (stabilised) repeat 2
MO1G1NO5	1	Standard panel, with honeycomb core (stabilised) repeat 3
MO2G1NO1	2	Standard panel, with honeycomb core (unstabilised) repeat 1
MO2G1NO2	2	Standard panel, with honeycomb core (stabilised) repeat 2
MO2G1NO3	2	Standard panel, with honeycomb core (stabilised) repeat 3
MO3G1NO1	3	Standard panel, with honeycomb core (stabilised) repeat 1
MO3G1NO2	3	Standard panel, with honeycomb core (stabilised) repeat 2
MO3G1NO3	3	Standard panel, with honeycomb core (stabilised) repeat 3
MO4G1NO1	4	Standard panel, with honeycomb core (stabilised) repeat 1
MO4G1NO2	4	Standard panel, with honeycomb core (stabilised) repeat 2
MO4G1NO3	4	Standard panel, with honeycomb core (stabilised) repeat 3
MO4G2NO1	4	Honeycomb core, with ply drop-offs over core
MO4G2NO2	4	Replaced honeycomb with foam core
MO4G2NO3	4	Foam core with ply drop-offs over core
MO5G1NO1	5	Standard panel, with honeycomb core (stabilised) repeat 1
MO5G1NO2	5	Standard panel, with honeycomb core (stabilised) repeat 2
MO5G1NO3	5	Standard panel, with honeycomb core (stabilised) repeat 3
MO5G2NO1	5	Honeycomb core, with ply drop-offs over core
MO5G2NO2	5	Replaced honeycomb with foam core
MO5G2NO3	5	Foam core with ply drop-offs over core
MO1Crossply	1	Honeycomb core, cross ply face sheets

5.6 NDT of generic panels

Under current manufacturing practice (Chapter 3), all panels produced at GE must undergo NDT to ensure they are free from sub-surface defects that may cause premature failure during service. The generic test panels produced for this research were tested using ultrasound C-scan. The C-scan maps the total signal attenuation due to all causes over the panel after an ultrasound signal has been passed through it. The scan provides an image of the panel, and operators set the upper and lower threshold by experience, such that a ‘clean’ panel will pass while a defect will appear as out of range. The ultrasound C-scan confirmed that all generic panels manufactured for this research were initially structurally sound, and the skin/core bonds are complete. Therefore, when testing the generic panels manufactured using the five different MOs for comparison, any differences are known to originate from differences in materials and not from initial sub-surface defects. The ultrasound also proved that the use of the ‘novel’ MOs did not introduce manufacturing defects.

Figure 5.5 shows the C-scan images of the panels produced using MO 1. In each image the flange regions of the panel register as white, where the ultrasound has an easy path through the well consolidated carbon fibre, whilst the core stiffened region registers as a dark grey. Blue regions surround some of the perimeter of the panels, where the signal is below the minimum of the range set by the operator as there is no obstruction to the ultrasound. Panels MO1G1NO1 and MO1G1NO2 had the attachment holes drilled before C-scanning and therefore the holes are apparent as blue dots on the white flange region. These two panels also suffered from core crush during cure, this is noticeable when C-scanning, and therefore the grey area of the cores are distorted when compared to the rectangular shape of the non-crushed cores on the other three panels.

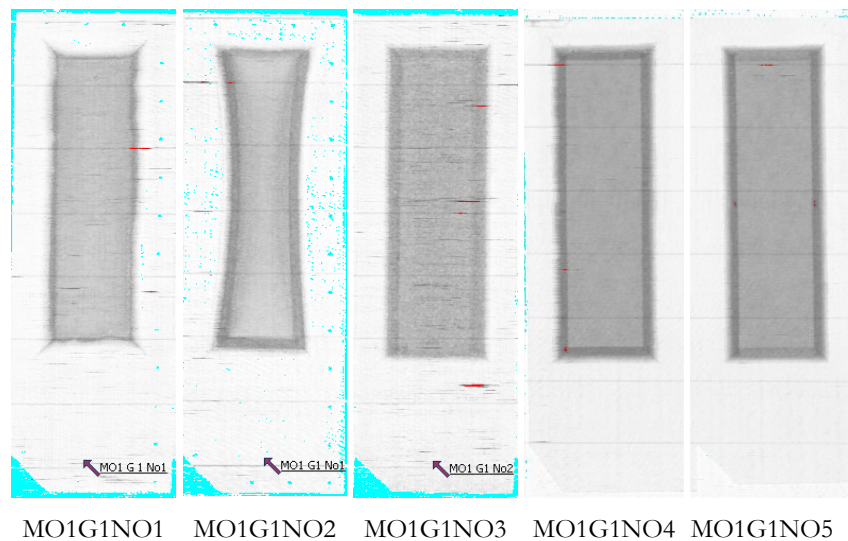


Figure 5.5: Ultrasound C-scan images of MO1 panels

Figure 5.6 presents the C-scans of the generic panels produced using MO 2. As before, the white region represents the flange area and the grey regions are the core stiffened area. Panel MO2G1NO1 suffered core crush as MO1G1NO1 and MO1G1NO2 and this is evident on the image. Also of importance in Figure 5.6, is the difference in colour of images of panels MO2G1NO2 and MO2G1NO3. The difference in colour is due to the thresholds for response set by the operators, and not any problems with the panels.

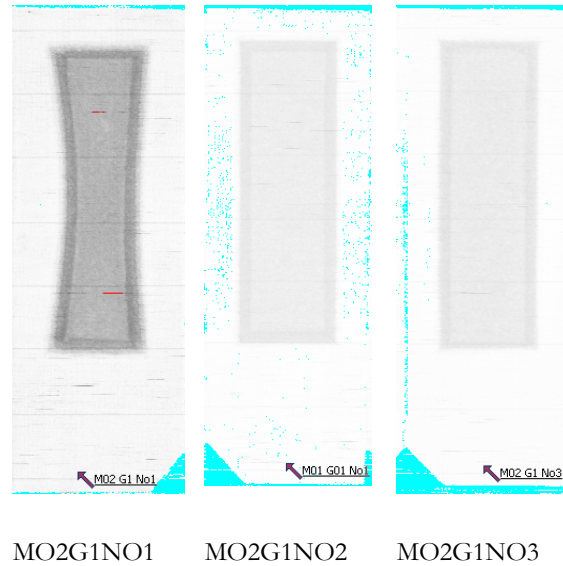


Figure 5.6: Ultrasound C-scan images of MO2 panels

Figure 5.7 contains C-scans of generic panels produced using MO 3. The images were produced using the same response thresholds as those for panels MO2G1NO2 and MO2G1NO3, and therefore the colours are similar.

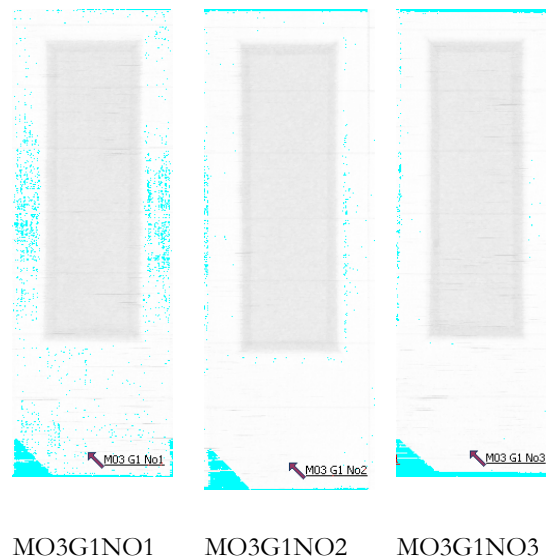


Figure 5.7: Ultrasound C-scan images of MO3 panels

Figure 5.8 and Figure 5.9 show the C-scans for the panels produced using MO 4 and 5 respectively.

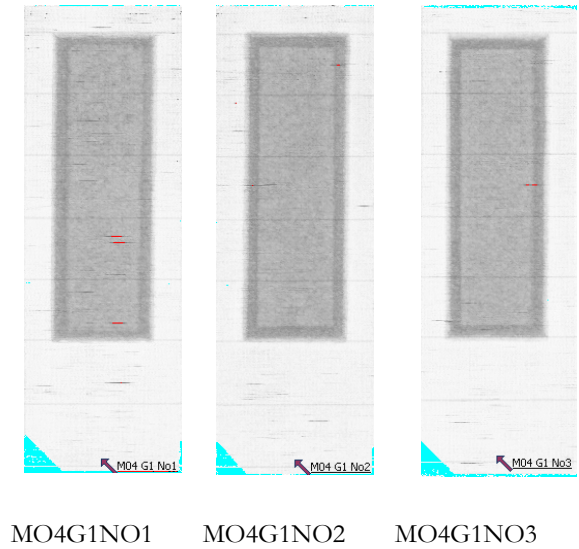


Figure 5.8: Ultrasound C-scans images of MO4 panels

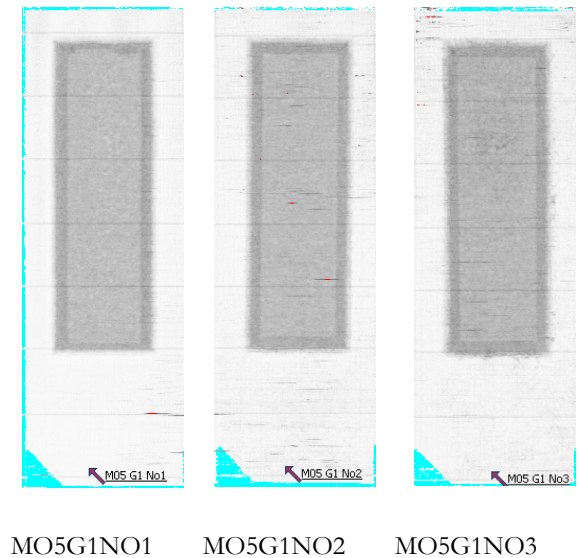
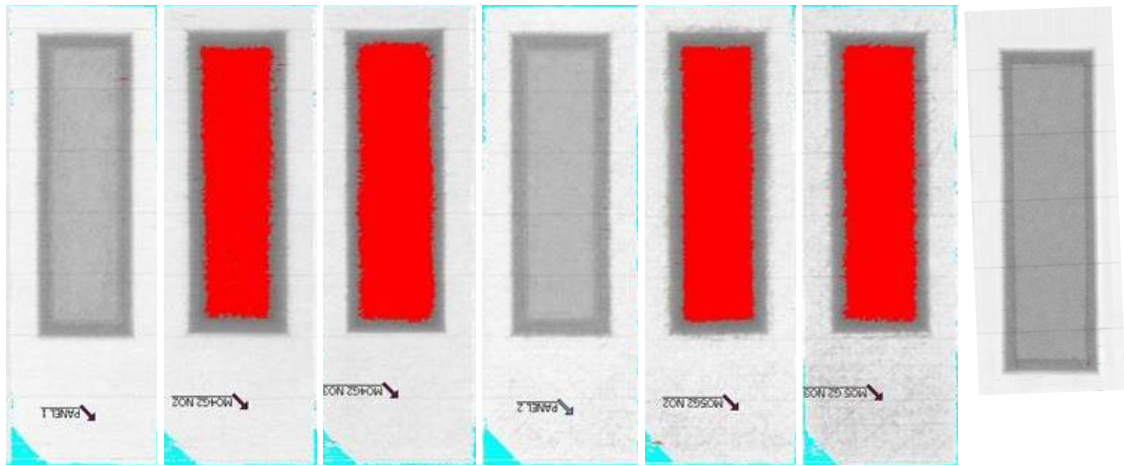


Figure 5.9: Ultrasound C-scans images of MO5 panels

Finally, the C-scans for the generic panels with ply drop-offs, foam cores and the cross-ply face sheets can be seen in Figure 5.10. The scans for the panels that have a honeycomb core, i.e. MO4G2NO1, MO5G2NO1 and MO1 crossply, show a similar response to the other figures and therefore it is clear there are no subsurface defects. However the scans for the panels that use a foam core have a red region on top of the core. This indicates an above threshold response from the panels, and would normally be a cause for concern. However it is known that the ultrasound signal struggles to propagate through the closed cell foam core material and therefore the response

differs to that expected from a honeycomb core. If a foam core was to be employed as a replacement core material the C-scan would need to be developed to accommodate this.



MO4G1NO1 MO4G1NO2 MO4G1NO3 MO5G2NO1 MO5G2NO2 MO5G2NO3 MO1Cross-Ply

Figure 5.10: Ultrasound C-scans images of other panels

5.7 Summary

Chapter 5 contains details of the manufacture of the generic test panels. This began with the definition of five MOs that are to be compared during this work. The five MOs are incremental steps from a UD prepreg autoclave cure to a NCF with separate resin film cured in a conventional oven. The features found to be common in current secondary wing structure in Chapter 3 were used to inform the design of three generic panels to be representative of those current components. The generic panel used in the current work has a plan area of 0.9 m x 0.3 m with a core stiffened area of 0.6 m x 0.2 m and a non-stiffened flange region. The total face sheet thickness is 3 mm, whilst the honeycomb core thickness is 12.5 mm.

Once the design of the panel was established, the manufacture was monitored using each MO. The method and time spent were described. It was found that MO 1 took 28.8 hrs to manufacture a panel, and the process had high relative labour, running and capital costs. However, MO 5 took 20.2 hrs to manufacture a panel and, when compared to MO 1, had much lower labour, running and capital costs. In total 24 test panels were manufactured, including three of each MO and a number with ply drop-offs and foam cores in place of the standard honeycomb.

Finally the chapter was rounded off with the results from NDT on the 24 generic panels. The NDT was performed at GE by a trained ultrasound C-scan technician. The ultrasound has shown

all the panels to be structurally sound prior to the mechanical testing undertaken in this work, and has confirmed the core and skin bond is good in all panels with a honeycomb core. The ultrasound tests on the foam cored panels are inconclusive.

The cost evaluation has clearly shown it is beneficial to manufacture secondary aircraft sandwich structure face sheets using MO5. The next step is to demonstrate that changing the manufacturing process does not result in a reduction in quality or performance of the face sheet materials. Hence, the following chapter describes the material characterisation of the face sheet materials.

Whilst manufacturing of generic panels using the five MOs, separate flat panels of the face sheet material were produced. The flat sheets have the same lay-up as that in the generic panel face sheet and were cut into specimens for standard testing to measure the in-plane and flexural material properties and to produce micrographs to investigate the consolidation and quality of the material. The results from these tests provide an initial comparison of the MOs and provide the properties for the finite element models and are presented in Chapter 6.

Chapter 6

6 Face sheet material characterisation

6.1 Introduction

In Chapter 5 five manufacturing options (MOs) for the production of carbon fibre sandwich structure suitable for use as secondary structure on passenger aircraft wings were presented. The MOs were used to produce a range of generic panels. The generic panel production was monitored and this allowed an assessment of the relative cost of manufacture of each MO. The cost of manufacture was significantly reduced by use of out-of-autoclave processing (MO 5), in comparison to standard production (MO 1). The purpose of the work described in this chapter is to evaluate the performance of the face sheet materials. A series of material characterisation tests were performed on the face sheet material manufactured using each MO. During generic panel manufacture, separate flat panels with the same lay-up and thickness as the sandwich face sheets were laid-up. These panels are used to make the specimens for the material characterisation. The panels follow the same cure cycle conditions as the generic panels as they are laid up on the same tool and under the same vacuum bag. Specimens cut from these panels are used to establish in-plane (tensile) and out-of-plane (flexural) material properties and to assess the material quality by fibre volume fraction calculations and microscopy.

The material property data derived from the characterisation tests given in this chapter will also be used for input into finite element (FE) models of the generic panel (see Chapters 7 and 9). Two types of FE model are to be used. The first will treat the face sheets as homogenous, orthotropic

blocks with material properties equivalent to the global face sheets response; this is the approach used by GE in their design office. The second will model the face sheets as made up from individual plies with material properties of an individual lamina. For this reason, further tensile specimens, with all the plies aligned longitudinally, were produced for MO1, 2 and 4 where the individual lamina properties can be obtained. The individual lamina of materials produced by MO3 and 5 are stitched together, and it would not be feasible to unstitch and produce laminates from them.

6.2 Fibre volume fraction

This section of the chapter describes the work undertaken to analyse the quality of the face sheet material produced by the five MOs by assessing the consolidation. This was done by estimating the fibre volume fraction (V_f) using thickness measurements and through visual analysis of microscopy images. V_f was chosen as the quality indicator as it provides a measure of the effectiveness of the curing process. The micrographs will provide an indication of the void content and hence wet out. Furthermore, the V_f also indicates how much resin has been lost during the curing process. For aerospace laminates V_f s > 50% are required [36, 100]; in the case of the five MOs it is expected that the V_f would be in the range 50 to 60%. The quality assessment is essential as out-of-autoclave processes traditionally provide laminates that are less well wetted and consolidated than a full autoclave cure.

A common means of estimating V_f of laminates is carried out by measuring the average thickness of the laminate using the following equation:

$$V_f = \frac{nA_w}{\rho_f t} \quad (6.1)$$

where V_f is fibre volume fraction, n is number of plies, A_w is areal fibre weight, ρ_f is fibre density and t is thickness.

The thickness of each laminate was obtained in 10 positions using Vernier callipers; the average thickness, t , is provided in Table 6.1 along with the V_f value calculated from Equation (6.1). The values of n and A_w , used in the calculation are also listed in Table 6.1, whilst ρ_f was assumed to be 1.77 g/cm³ for all. This is known to be accurate for MO1 and MO2 and it is therefore reasonable to use this for the other MOs, as the density of carbon fibre can be assumed to be constant for each of them. The laminates manufactured by MOs 1 and 2 (autoclaved prepreg) have identical V_f values of 55%. The laminates manufactured by MOs 3 and 5 (new material, one autoclaved, one oven cured) also have identical V_f s of 53%. However the V_f of MOs 3 and 5 are approximately

4% lower than that of MOs 1 and 2. The similarity of the V_f of MOs 3 and 5 indicated that removing the autoclave cure has little effect on the quality of the consolidation. MO4 has a V_f of 52%, which is approximately a 7% reduction from MOs 1 and 2. This may be due to the open weave structure of the 2 x 2 twill used in this MO. The important outcome from this work is that in all cases the volume fraction of the material is greater than 50%. However, the measure of V_f derived from Equation (6.1) provides no indication of the void content or distribution of the resin within the laminate; this assessment must be made by visual inspection using micrographs of each MO. Image analysis of microscopy images was also used to estimate the V_f of the laminate.

Laminates produced by each MO were cut transversely and divided into small sections. These were potted into resin and polished so that they could be viewed in an optical microscope. 16 sections were taken from each material. The polished sections were assessed firstly at five times magnification to investigate the overall quality. Then each section was assessed to estimate the V_f by applying a greyscale threshold in an image analysis process and counting the number of pixels above this threshold.

Table 6.1: Volume fraction of the face sheets produced by each MO obtained from thickness measurements and image analysis

MO	n	A_w (g/cm ²)	t_{avg} (mm)	V_f % (Thickness)	V_f % (Image analysis)
1	24	131.8	3.21	56	56
2	12	280	3.41	56	57
3	6	560	3.57	53	54
4	12	285	3.74	52	53
5	6	560	3.56	53	56

Figures 6.1 to 6.5 show two images from each MO at five times magnification. Figure 6.1 shows microscopy images of laminates produced by MO1. As expected from prepreg tape manufactured in an autoclave, the laminate is well consolidated with resin and fibres evenly distributed. Images from MO2 (Figure 6.2) show pockets of resin in between the tows of the woven structure, however the fibres are closer packed in the tows than in MO1. Figure 6.3 is images from laminates manufactured by MO3. The laminate is well consolidated as in MO1, but there are some resin pockets around the discontinuity caused by the polyester stitching that loosely binds the dry NC2 fabric prior to layup. Although MO3 is cured in an autoclave there is also some evidence of small voids across the laminate; these areas are darker than the resin. Figure 6.4 show images of MO4, a woven fabric cured in the oven. These images have a similar structure to that for MO2, but the

fibres are less closely packed and there is some evidence of very small voids. The other oven cured laminate MO5 is shown in Figure 6.5 and has a similar structure to that of MO3. The out-of-autoclave cure appears to have had no apparent negative impact on the consolidation of the laminate. In fact there appears to be smaller resin pockets and less voids.

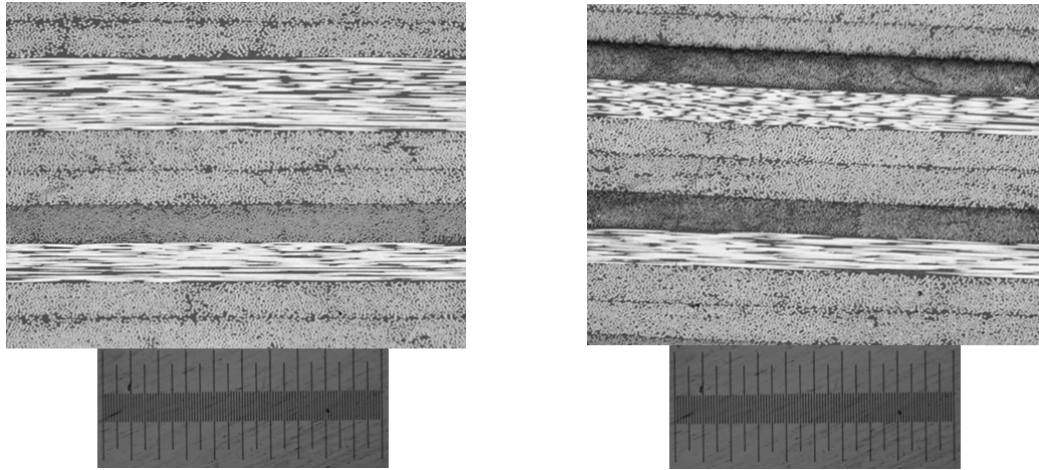


Figure 6.1: Microscopy images of consolidated laminates from MO 1(each division represents 0.5 mm)

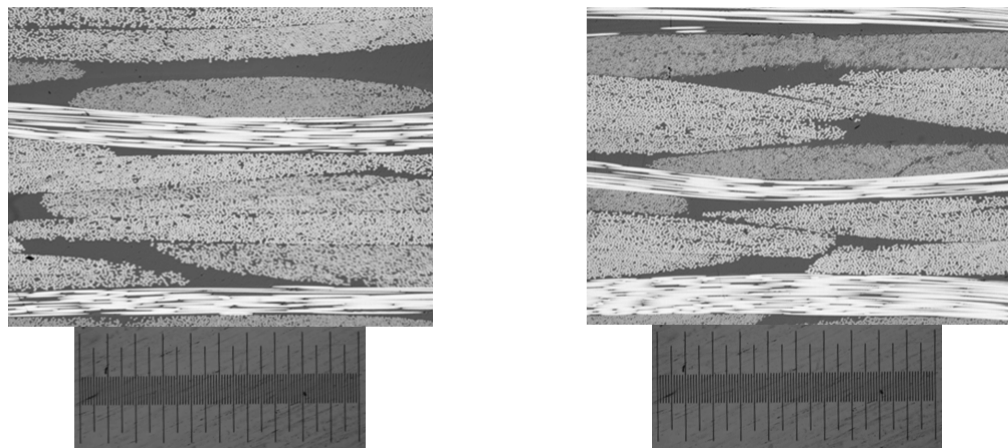


Figure 6.2: Microscopy images of consolidated laminates from MO 2 (each division represents 0.5 mm)

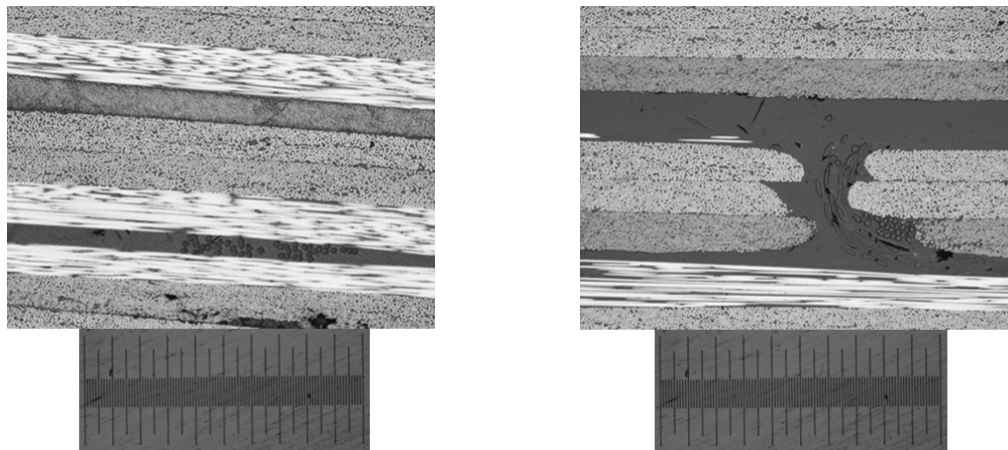


Figure 6.3: Microscopy images of consolidated laminates of MO 3 (each division represents 0.5 mm)

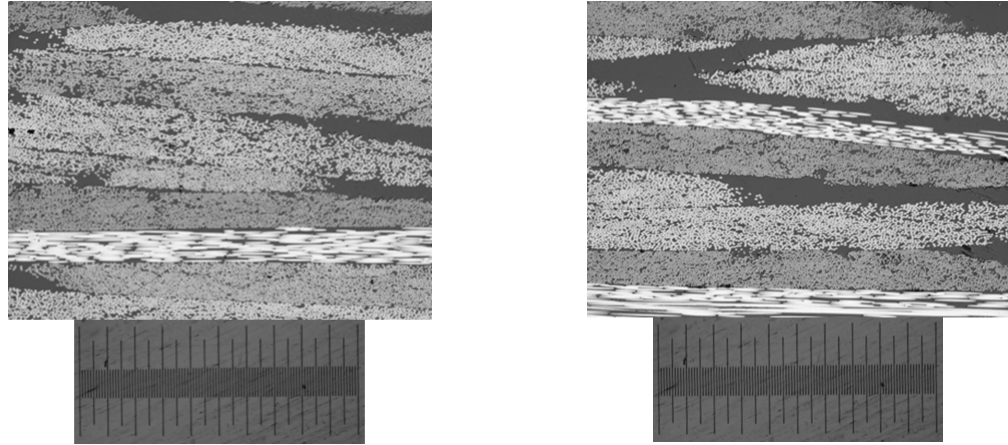


Figure 6.4: Microscopy images of consolidated laminates of MO 4 (each division represents 0.5 mm)

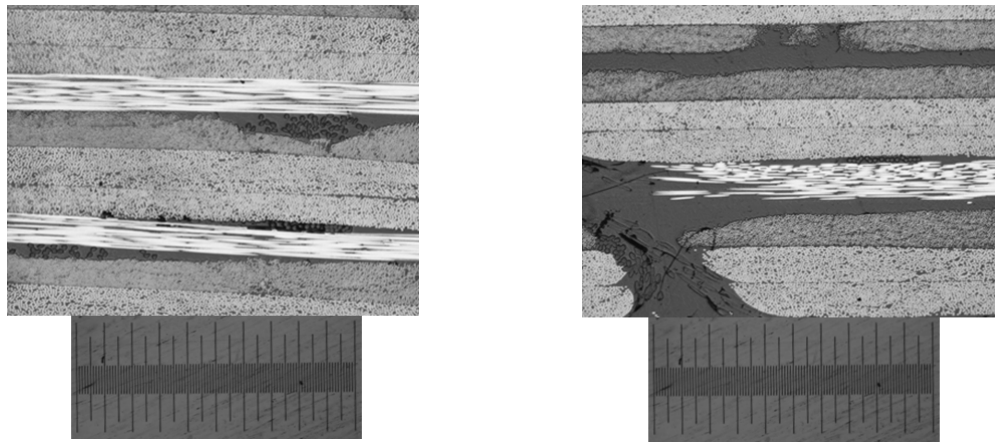


Figure 6.5: Microscopy images of consolidated laminates from MO 5 (each division represents 0.5 mm)

Table 6.1 contains V_f values estimated from analysis of microscopy images. These values compare favourably with those estimated through the thickness method for MO1-3, and confirm the accuracy of Equation (6.1) for autoclave cure. However, there is a significant difference in the V_f obtained from the micrographs and that from Equation (6.1) for MO4 and 5. The V_f of MO5 (at 56%) through this method compares identically with V_f given for MO1. The only explanation for this is that as the NCF produces a thicker laminate in the oven consolidation the resin is infused through the stack and some drawn to the surface, but in the autoclave consolidation (MO3) the resin is forced to remain within the stack.

In general the micrograph analysis has produced results that confirm that in all cases the MOs produce aerospace quality laminate face sheet. It is shown that the actual volume fraction of the MO5 is identical to that produced in the autoclave and in this sense the quality of the face sheet material is not changed by the new less expensive process. However, the micrographs show voids and localised large resin pockets that occur as a result of stitching. The effect of these on mechanical performance must be assessed in order to confirm that the MO5 can be used instead of MO1 with confidence.

6.3 In-plane tests

The in-plane properties were measured using tensile tests on specimens manufactured from laminates with the plies all aligned in the longitudinal direction. These will provide material properties for individual lamina that can be used in the FE models (E_1 , E_2 , ν_{12} , ν_{21}). Tensile tests were also carried out on laminates with the plies in the same configuration as the face sheets in the generic panel to assess the global performance of each face sheet material (σ_{FL} , σ_{FT}) and obtain global material properties (E_L , E_T , ν_{LT} , ν_{TL}). The test specimens were manufactured to the geometry specified in ASTM D3039 and loaded according to the standard in an Instron 5569 servo-mechanical test machine; the longitudinal strains were obtained using a 50 mm gauge length extensometer whilst the transverse strains were measured using a 12.5 mm gauge length extensometer. Five specimens of each orientation and MO were tested. The specimens were orientated so that the longitudinal direction was in the x-direction shown, in Figure 5.1 and the transverse was in the y-direction.

Table 6.2 provides the tensile properties for the lamina used in MOs 1, 2 and 4; it was not possible produce these kinds of specimen for the stitched NCF dry mat used in MOs 3 and 5. It is clear from these results that, as expected, the MO1 produces highly orthotropic lamina and the woven material of MO2 and 4 lamina with similar properties to a cross-ply lay-up.

Table 6.3 provides the global tensile properties for each MO and Figure 6.6 shows a histogram with values of strength and Young's modulus normalised to MO 1 values. For the longitudinal modulus, E_L , there is practically no difference between the two autoclaved, prepreg products. Using MO5 results in a 7% reduction in E_L with an 8% reduction for MO3 and 13% loss for MO4 compared to MO1. There is practically no difference between the autoclave cured material in MO3 and the oven cured material in MO5. The resin system used for MO3 and MO5 is identical, and has been formulated for out-of-autoclave cure and will therefore wet-out the fibres better during an oven cure; this can explain the slight improvement in modulus. The reduction in properties for MO4 can be attributed to the woven form of the material in MO4. A similar pattern is observed for the transverse modulus. It is interesting to note, the Poisson's ratio values vary enormously, with MO1 being significantly different from MO3 and MO5 which are all made from NCF materials. Therefore, classical laminate theory was used to estimate the value for Poisson's ratio for the laminate produced using MO 1. It was estimated that both values of Poisson's ratio should be equal and be approximately 0.3, and therefore the values measured appear to be spurious. The material manufactured using MO1 has a longitudinal failure stress of 565 MPa and transverse failure stress of 597 MPa, while the material manufactured using MO5 shows an

improved longitudinal failure stress of 640 MPa and a transverse failure stress of 667 MPa. This represents an increase in strength of approximately 12% by using the out-of-autoclave MO. This is an unexpected result as it is generally accepted that the autoclave will produce a higher quality product. The increase in strength may be attributed to the resin used and possible improved wet-out, although the indication from the micrographs is that there are significant resin pockets around the stitching in MO5 and therefore a much less uniform distribution of the resin. Figure 6.7 shows typical strain to failure curves for the two materials. This data was taken without an extensometer using only the cross head displacement. The compliance of the test machine causes a false reading and hence an increase in the strain; these should be used for comparison only. The extensometer data for both tests is also shown to demonstrate the level of inaccuracy. However, it can be seen for both MO1 and MO5 that the failure is immediate and progressive failure is not the reason for the increased strength values. The simple explanation is that the NCF oven cured approach produces a stronger material. From these results it can be concluded that the out-of-autoclave product shows no significant changes in mechanical properties, although the differences in Poisson's ratios will have an effect on the behaviour of the generic panels when loaded in bending.

Table 6.2: Elastic properties of the face sheet lamina material for MO1, MO2 and MO4

MO	$E_L(\text{GPa})$	$E_T(\text{GPa})$	ν_{12}	ν_{21}
1	134.3 ± 9.3	9.0 ± 0.4	0.32 ± 0.02	0.05 ± 0.01
2	80.9 ± 5.6	75.6 ± 1.4	0.06 ± 0.02	0.04 ± 0.02
4	64.4 ± 10.5	66.1 ± 3.1	0.10 ± 0.05	0.09 ± 0.05

Table 6.3: Tensile properties of the face sheet materials produced from each MO

MO	$E_L(\text{GPa})$	$E_T(\text{GPa})$	ν_{LT}	ν_{TL}	$\sigma_{FL}(\text{MPa})$	$\sigma_{FT}(\text{MPa})$
1	48.7 ± 3.5	50.4 ± 4.0	0.09 ± 0.02	0.15 ± 0.03	565 ± 5.5	597 ± 22.3
2	47.1 ± 1.1	49.3 ± 0.6	0.26 ± 0.03	0.25 ± 0.02	534 ± 8.4	568 ± 15.8
3	44.5 ± 2.1	44.3 ± 1.1	0.32 ± 0.04	0.27 ± 0.01	595 ± 21.5	579 ± 42.4
4	42.2 ± 0.6	41 ± 0.5	0.24 ± 0.03	0.25 ± 0.04	532 ± 10.5	549 ± 17.5
5	45.2 ± 0.6	46.7 ± 1.1	0.32 ± 0.02	0.26 ± 0.02	640 ± 24.5	667 ± 37.1

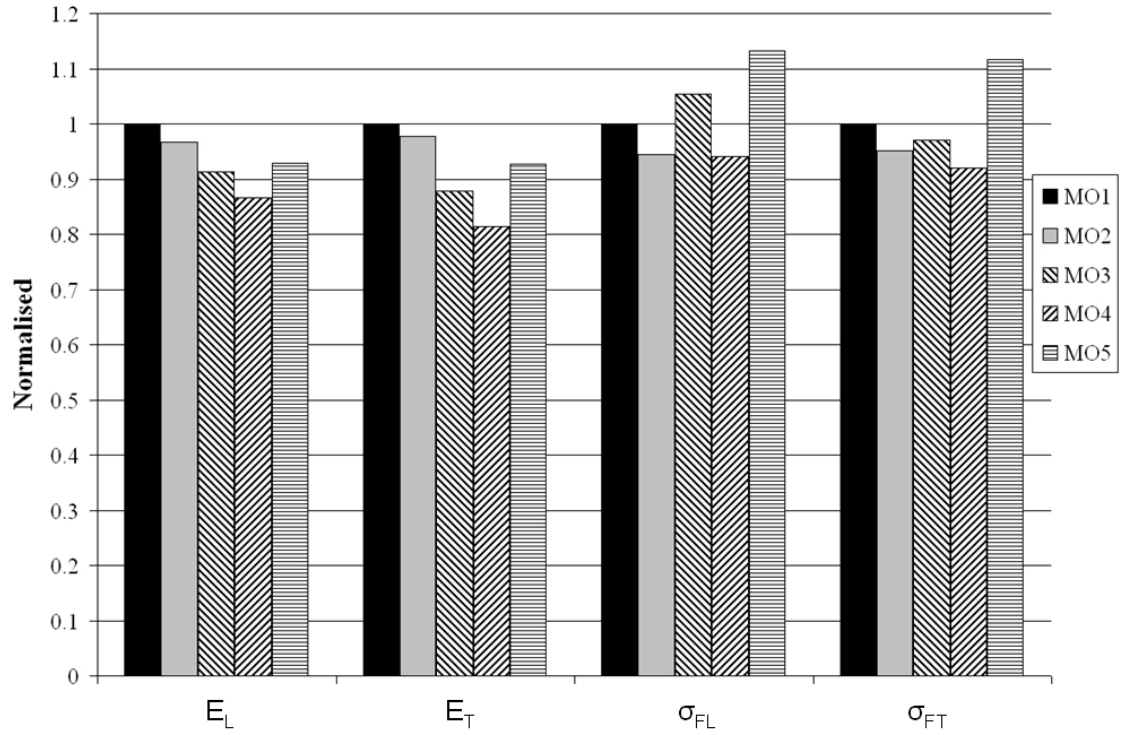


Figure 6.6: Bar chart showing Young's modulus and strength data normalised against MO1

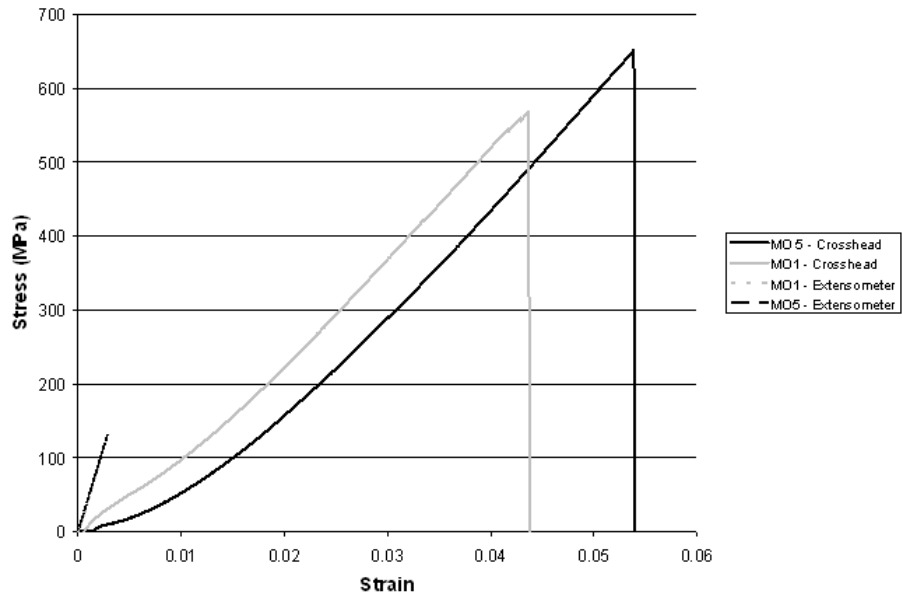


Figure 6.7: Typical stress-strain curves of specimens manufactured from MO1 and MO5

6.4 Flexural tests

The flexural properties of a laminate may be greater affected by poor quality material or process than in-plane properties. Therefore the interlaminar shear strength (ILSS) and flexural properties of laminates of the five MOs is also investigated. The test specimens were manufactured and tested as specified in ASTM D2344 for interlaminar shear strength and ASTM D4762 for the flexural properties. These tests were conducted using an Instron 8872 servo-hydraulic test

machine. At least five specimens of each MO were tested for each out-of-plane property. Table 6.4 lists the out-of-plane properties of QI laminates produced by the five MOs, namely ILSS, flexural strength and flexural modulus and Figure 6.8 shows a normalised plot of the flexural data.

The laminate produced by MO1 has an ILSS of 56.8 MPa, the laminate produced using MO3 (new material, autoclaved cure) has an ILSS of 43.3 MPa. This represents a reduction of 24%. However, the laminate produced by MO5 has an ILSS of 52.8 MPa, a reduction of only 7% compared to MO1. It is considered that because the resin system has been formulated for out-of-autoclave cure, the best consolidation results are provided by a vacuum only cure. It is known from literature that the ILSS reduces by 7-10% per 1% void content [101]. The micrographs in Figure 6.7 show that there are more voids in MO5 than in MO1 and furthermore, there are many more voids in MO3 than in MO5. The flexural properties of the laminate produced by the out-of-autoclave procedure (MO5) compare favourably with the original method (MO1). The MO1 laminate has flexural strength (σ_{Ff}) of 827.7 MPa and flexural modulus (E_f) of 47.4 GPa, while the MO5 laminate has a flexural strength and modulus of 795.1 MPa and 46.4 GPa, respectively. This represents a reduction of 4 and 2 % in the flexural properties by curing out-of-autoclave.

Table 6.4: Out of plane properties of the face sheet material produced from each MO

MO	ILSS(MPa)	σ_{Ff} (MPa)	E_f (GPa)
1	56.8 \pm 0.5	827.7 \pm 26.7	47.4 \pm 1.4
2	59.6 \pm 3.0	760.9 \pm 38.7	48.1 \pm 0.9
3	43.3 \pm 2.6	763.9 \pm 52.7	45.0 \pm 2.1
4	52.0 \pm 1.9	689.7 \pm 5.9	40.0 \pm 0.8
5	52.8 \pm 2.6	795.1 \pm 35.4	46.4 \pm 2.4

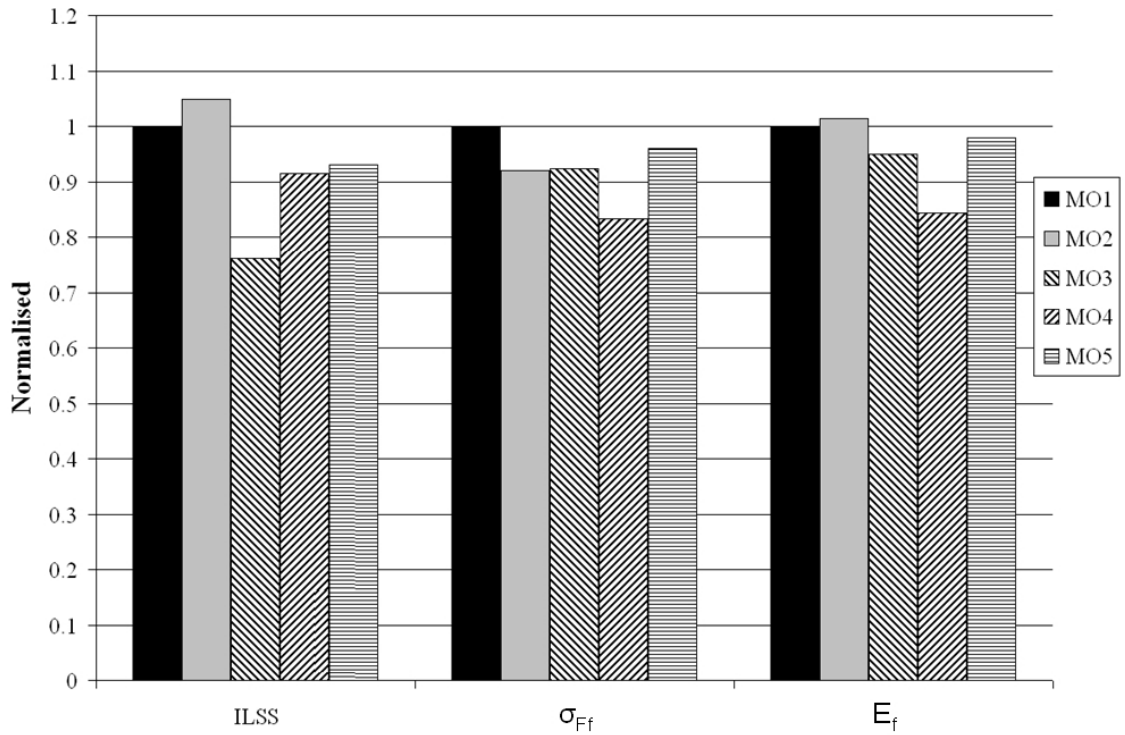


Figure 6.8: Bar chart showing flexural data normalised against MO1

6.5 Summary

Material consolidation was tested by estimating the fibre volume fraction by measuring the thickness of the consolidated material and analysis of microscopy images of material sections. These showed that the volume fraction of the laminates produced by the new process is of similar quality to the current process. A visual check of the microscopy images also revealed features in the NCF that may cause detrimental effects on the mechanical performance. In general, the mechanical testing showed that the new material performed equally well to the autoclaved material in tension, with only a 7% reduction in stiffness and a 12% increase in failure strength. Similarly, the out-of-plane properties, namely interlaminar shear strength and flexural stiffness and strength, were reduced by only between 2 and 7 %. In summary, it has been shown that the most cost effective manufacturing process, MO5, produces face sheet materials that can perform to aircraft specification. The work in this chapter provides an encouraging confirmation that the out-of-autoclave face sheet material (MO5) can perform as well as the autoclaved material (MO1). However, it is essential that the performance of the face sheet material is assessed when assembled into the sandwich panels. Therefore, the following chapters will further evaluate the construction and performance of the panels in full-scale tests.

Chapter 7

7 Design and commissioning of a full scale test rig

7.1 Introduction

The work described in Chapter 6 of the mechanical characterisations of the face sheet materials, produced using the five MOs, provided an initial comparison of the performance of the materials. The material properties were concluded to have not been degraded by removing the autoclave cure or changing material from UD to non-crimp fabrics. Therefore, the next stage in the material performance evaluation will be to test the face sheet performance in a full sandwich panel. The purpose of the work in this chapter is to design and commission a full scale test rig to apply a pressure load to the generic panel designed in Chapter 5. The rig will be used to test generic panels manufactured from the five MOs.

It might be considered prudent at this stage to conduct some tests on sandwich beams, perhaps in three and four point bending. These types of tests require contact between the face sheet and the loading points. Deformation at the contact points needs to be controlled and this can lead to spurious results. Furthermore, it is difficult (although not impossible [102]) to gain optical access to the face sheet to apply optical techniques. Moreover beams and ‘plates’ behave in different ways and it is not always possible to link the behaviour of the two. Therefore, it was decided to omit this stage in characterisation and move directly to panel testing.

The chapter starts with an FE model of the generic panel to provide information for the design of the rig. The rig was designed to allow unobstructed visual access to the generic panel to permit the use of optical measurement techniques, such as digital image correlation (DIC) and thermoelastic stress analysis (TSA). Therefore, the predicted strains and stresses in the initial finite element (FE) model are used to establish if the resolution of DIC and TSA is sufficient to obtain meaningful data from these techniques. The concept of the test rig is fully described, and then a detailed discussion of the design is given. The chapter concludes with some results from initial tests performed to validate the operation of the rig.

7.2 Initial FE analysis of generic panel

Before considering the test rig design, the effect of the pressure load on the composite sandwich generic panels must be estimated. Without this information, it would be impossible to establish if there was sufficient space around the rig to accommodate the deformation of the panels. For this reason, an FE model of the generic panel made from MO 1 was produced to provide an estimation of the deformations and stresses to be expected during loading. The FE model was constructed using ANSYS 11 (*ANSYS Inc, Canonsburg, USA*). Firstly, the flange region of the panel was constructed to include the plies of both the mould side and bag side face sheets. Then the core was constructed by setting the size of the core that is touching the mould side face sheet and extruding in the z-direction (as shown in Figure 5.1). The chamfer on the core was produced by tapering in the x and y direction. The model was completed by adding the mould side face sheet plies to the base of the core volume and the bag-side face sheet plies to the areas on the top of the core.

The core was assumed to be a single anisotropic solid volume with material properties as given in Table 7.1, from Chapter 6 and Hexcel datasheets [103]; it was modelled using eight-noded brick elements (Solid185) of 0.01 x 0.01 x 0.01 m. The carbon fibre face sheets were modelled using Shell181; a four-noded element suitable for producing layered FE models. The element can accommodate large linear rotations and large nonlinear strains, hence enabling the out-of-plane displacement of the panel to be derived. The ability of the element to allow a layered construction is also essential as this enabled the generation of a ply-by-ply model of the face sheets. The flange of the model comprised both the mould and the bag side face sheet and contained 24 layers, whilst the face sheets surrounding the core had 12 plies each. This construction follows identically the construction of the generic panels using the autoclave and prepreg manufacturing process, MO 1. Therefore, the material properties, given in Table 7.1, for the autoclave cured material were used in the model. The fibre orientation was maintained on the angled edges of the core by altering the individual element coordinate systems such that z remained perpendicular to the surface.

Table 7.1: Material properties used for initial FE model

Property	Carbon fibre	Honeycomb
E_x (Pa)	134×10^9	400×10^6
E_y (Pa)	9×10^9	400×10^6
E_z (Pa)	9×10^9	400×10^6
ν_{12}	0.32	0.3
ν_{21}	0.09	0.3
ν_{23}	0.09	0.3
E_{12} (Pa)	6.6×10^9	59.3×10^6
E_{21} (Pa)	6.6×10^9	32.4×10^6
E_{23} (Pa)	6.6×10^9	32.4×10^6

The fixings in the flange of the generic panel generate the added complexity of contact and stress concentration. It was considered at this stage in the design process that these should be omitted from the model. Therefore, the service constraints were represented by imposing zero deflection on three edges of the model; i.e. the two short edges and one of the longer edges. With such boundary conditions, the model is constrained in all degrees of freedom along three edges, whilst the free edge has six degrees of freedom. The pressure load of 0.0210 MPa was applied to the model by applying a force perpendicular to each of the 2150 surface nodes. The pressure equates to a load of 1.92 N per node. The model is relatively thin in comparison to its length and width, and is subjected to an out-of-plane pressure load that would induce relatively large deflections. For this reason, the model was solved using a geometrically nonlinear solver. The size of elements was altered from a starting point of 0.1 m and reduced, estimating the maximum displacement each time. As the element size was altered, the maximum displacement converges on one value as shown in Figure 7.1, hence demonstrating that the model is estimating correctly. From this convergence curve it was decided to use an element size of 0.01 m. This choice was a compromise between processing time and accuracy, as using smaller elements would have increased the spatial resolution, but at a cost of much longer run times.

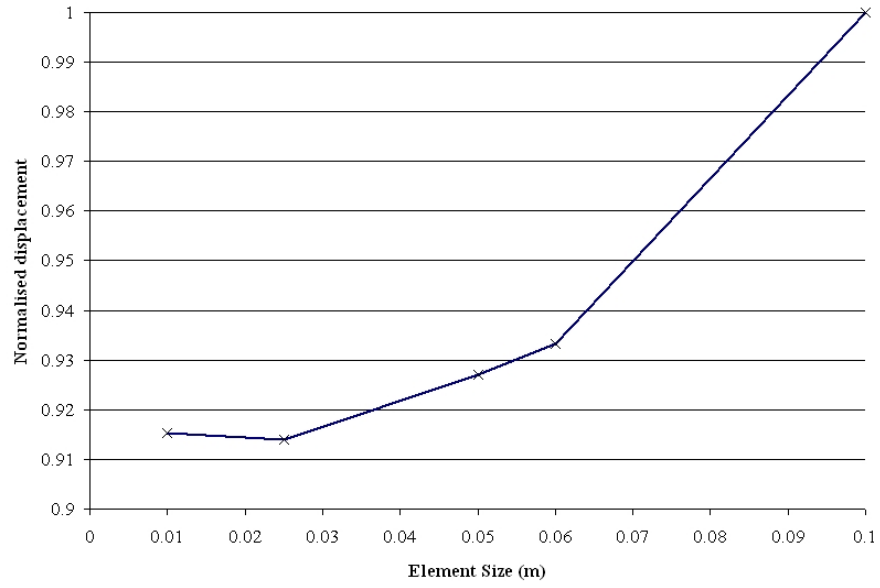


Figure 7.1: Graph demonstrating convergence of FE model with element size

The results from the FE model provide an insight into the expected response of the generic panel under the pressure load. Figure 7.2 shows the FE mesh along with the forces and boundary conditions. The red crosses represent an out-of-plane force applied to a node, by applying 1.92 N per node a pressure load of 0.0210 MPa was applied across the surface of the panel. The orange and yellow crosses represent the lines of the boundary conditions. Figure 7.3 shows the out-of-plane deformation. The model generated a maximum deflection, on the free edge, of about 10 mm. The rig would therefore be designed to accommodate the panel deformation estimation, allowing a safety factor for inaccuracies in the model and ‘over-loading’. The model also provides an estimate of the stresses and in-plane strains (see Figure 7.4) in the panel under pressure loading. The stress is expected to peak at a value of around 200 MPa, and the longitudinal in-plane strains range between -2000 and 3000 μ strain. If the use of full-field optical measurement techniques is to be successful for these tests, the expected response from the panel must be greater than the resolution of each technique. The resolution of TSA is heavily dependent upon the infra-red detector. The Cedip Silver 480M system, to be used in this work (see Chapter 9), has a thermal resolution of between 6 and 10 mK and can detect temperature changes of less if using the lock-in features required for TSA. For carbon fibre/epoxy composites this means a stress resolution of about 2 MPa for the transverse direction. The LaVision DIC system is capable of measuring in-plane strains of 220 μ strain. Therefore, the suggested geometry and construction of the generic panels is suitable for analysis with the TSA and DIC techniques.

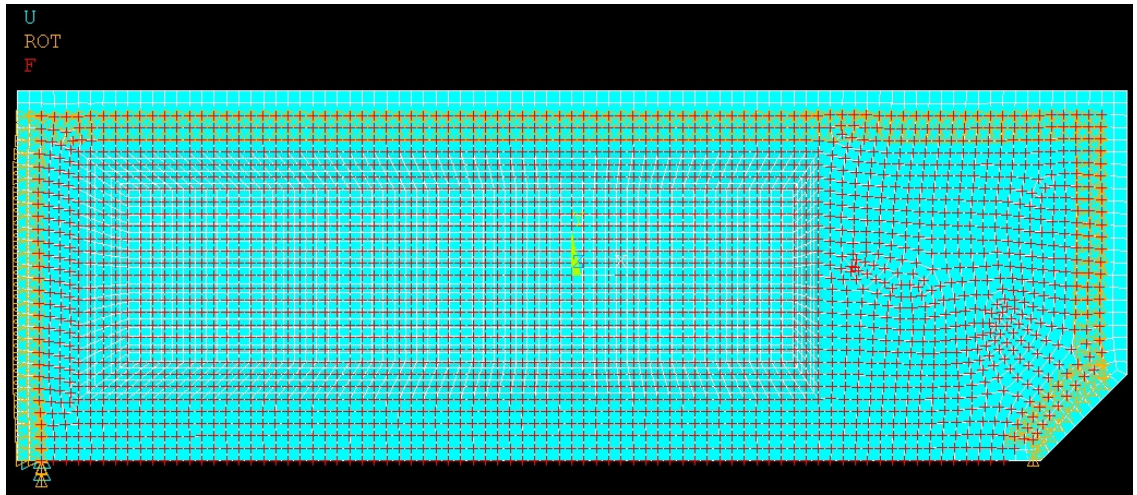


Figure 7.2: FE model mesh with loads and boundary conditions

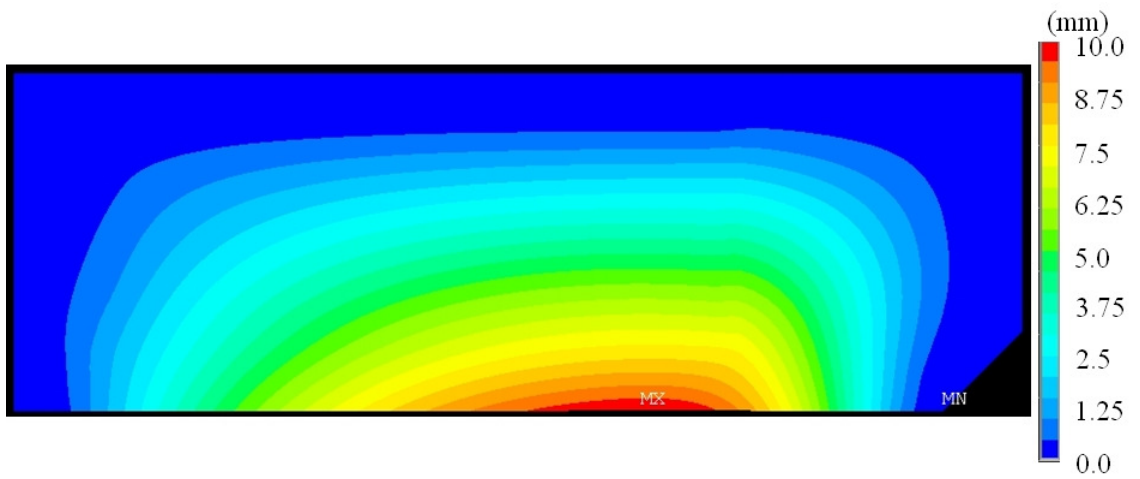


Figure 7.3: Predicted out of plane deformation from FE model

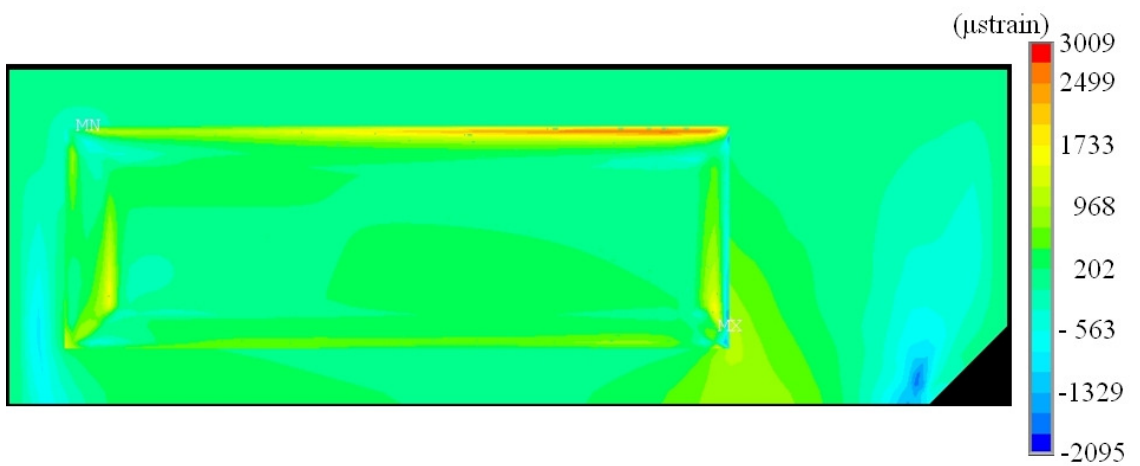


Figure 7.4: Predicted ϵ_x strain field from FE model

7.3 Concept Design of Test Rig

To replicate the in-service loading conditions on the secondary structure panels it was necessary to construct a test rig. As the behaviour of the generic panels will be complex, with non-uniform stress and strain, it was decided that rather than just obtaining simple load deflection data from the loaded panels it would be much more informative to generate full-field strain data. The proposed techniques for full-field analysis are TSA and DIC, which are both optical techniques. Therefore, the test rig must allow an uninterrupted view of the surface of the generic panels for the optical techniques to be applied successfully.

To facilitate the necessary cyclic load for the use of TSA a standard Instron servo-hydraulic test machine 8802 (*Instron, High Wycombe, UK*) was used as the basis for the loading rig. The Instron 8802 load frame is free-standing and floor mounted and has a working volume of up to approximately 640 mm wide by 1500 mm tall and 300 mm deep, although this can be increased if the specimen is allowed to extend over the base of the machine. The hydraulic system is capable of applying a load of 100 kN, and its frame, which is rated to 200 kN, forms a rigid bed for mounting the rig. To replicate the in-service loading, the test rig must be capable of imparting a pressure load across the mould side surface of the generic panels. To obtain the pressure load, a fully constrained, fluid filled, flexible cushion was employed. The pressure load is imparted by clamping the panels on three edges and pulling the clamped panel over the pressure cushion. The concept is shown in Figure 7.5 in both the unloaded and loaded conditions. By fully constraining the cushion it is possible for a pressure load, equal to that inside the cushion, to be imparted into the test panels. To minimise compressibility, and for safety reasons, the cushion working fluid is water. Previous work has demonstrated that a water bag can be used to apply a pressure load across the surface of a composite sandwich panel [104] and enabled a static load to be applied. However, in this study it is envisaged that by attaching the rig to a servo-hydraulic test machine it would be possible to apply a cyclic pressure load to a panel, facilitating the use of TSA.

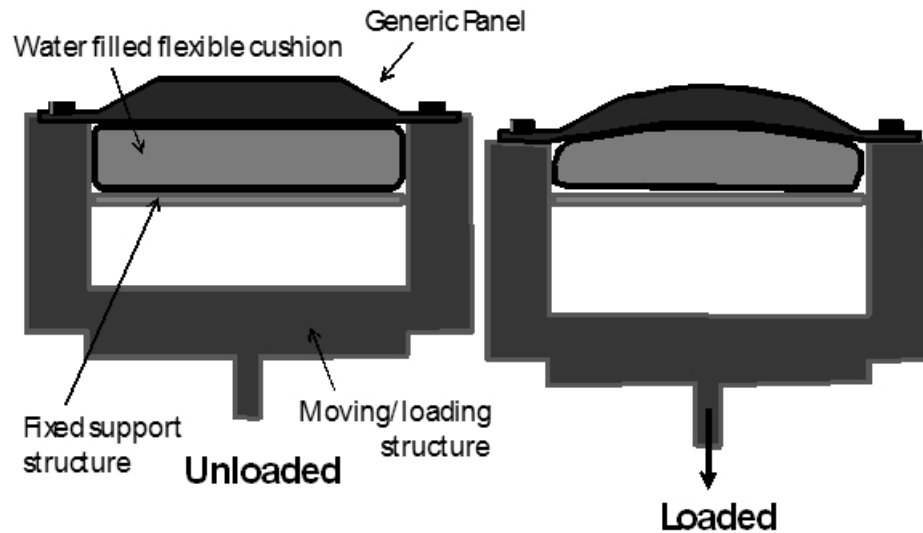


Figure 7.5: Concept of pressure test rig

The initial concept for the loading rig is shown in Figure 7.6. It comprises essentially of four components:

- The servo-hydraulic test machine, shown in light grey
- The fixed support structure, shown in dark grey
- The moving loading structure, shown in white
- The generic panel, shown in black

The fixed structure houses the flexible cushion and must have negligible deformation during loading to ensure full load transfer between the flexible cushion and test panel. It was decided that the fixed structure should be constructed of steel box section that would support a steel plate, upon which the flexible cushion is mounted (see Figure 7.5). The fixed construction is attached to both the pillars and the feet of the test machine. The generic panel is bolted to the moving section. The moving section is mounted in the lower grips of the test machine that are attached to the actuator. The actuator moves down and the panel is pulled over the flexible cushion imparting a pressure load to the cushion that is transferred to the test panel. The optical devices are positioned directly above the panel to provide a plan view of the stress/strain field in the panel. The design has the benefit that there are no loading shackles acting as detractors in the field of view. However, there is not a load cell in the loading chain, hence it is necessary to monitor the applied load or pressure using a pressure transducer attached to the flexible cushion; the cushion and pressure transducer are therefore effectively acting as a load cell.

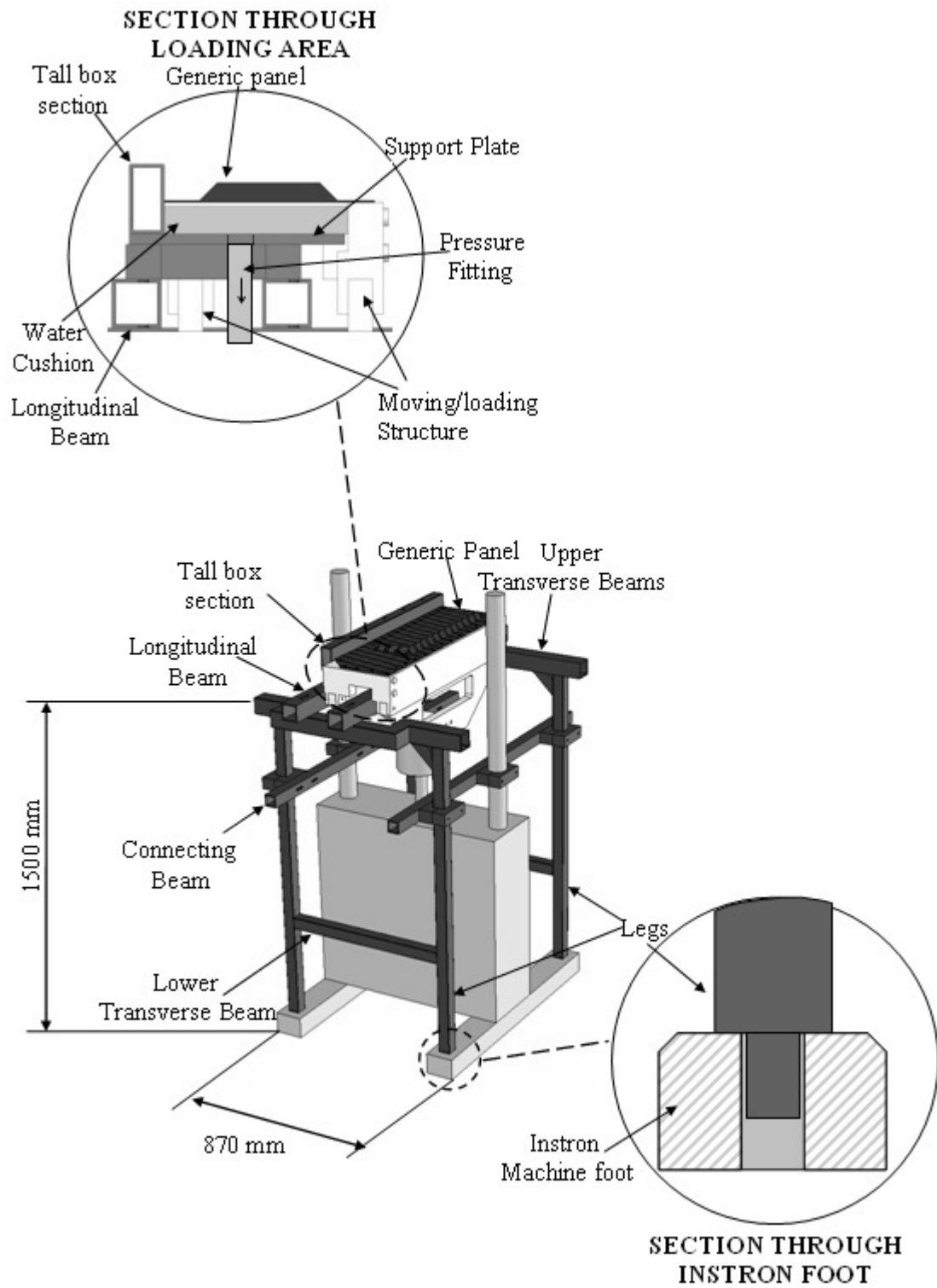


Figure 7.6: Initial design of pressure test rig

7.4 Detailed Design of Rig

7.4.1 Flexible pressure cushion:

The pressurised part of the pressure rig design concerns the flexible cushion, and methods to pressurise and monitor the pressure within the cushion. The water cushion was specified to withstand internal pressures of 0.345 MPa and was manufactured by Flexitec (*Flexitec Structures Ltd, Fareham, UK*). The cushion is made from polyurethane, and must be fully constrained when pressurised. It was designed so that it fits neatly into the rig, taking the geometry of the space between the support plate and the panel (see Figure 7.6). The pressure cushion has a similar shape to the generic panel (see Figure 7.7), and is designed to be block shaped with a thickness of 40 mm. The block shape allows the pressure cushion to correctly fill the space between the support plate and generic panel, hence transferring the pressure right to the edge of the panel. A hand pump is attached to enable initial pressurisation to a mean level and hence, allowing a greater range of pressures to be imparted by the water cushion. The cushion also has two push fittings; one to pressurise, using the hand pump, and the second connected to a pressure transducer. The pressure transducer, model 07356-02 from Cole Parmer (*Cole Parmer Instrument Company Ltd, London, UK*), has a full range of 60 psi gauge pressure with an accuracy of 1 % and provides an electrical output of 1-5 Vdc. The end of the transducer containing the measurement diaphragm is screwed into a flexible pipe directly connected to the base of the water cushion. The other end of the transducer has a 9-pin D connector and is plugged into a high-level card on a Vishay Strainsmart 6200A scanner which calibrates the electrical signal and records the pressure values.



Figure 7.7: Design of pressure cushion

7.4.2 Fixed structure:

The fixed support structure takes the form of a table, and fits around the Instron test machine without interfering with the operation of the moving part of the rig. The construction is mainly of steel box section. The legs of the fixed part were designed to connect to the feet of the test machine. As the load through the structure is always compressive, it was possible to use a simple pin configuration for the attachment without the need for mechanical fasteners, as shown in Figure 7.6. The structure consists of two separate sections each with two legs that are topped by the upper transverse beams, see Figure 7.6, that are welded to the two legs. The leg sections are additionally stiffened by transverse members closer to the feet. The two sections are connected by the 'connecting beams' (see Figure 7.6). The connecting beams are also fixed to the pillars of the test machine. The longitudinal beams that support the steel plate upon which the pressurised cushion is mounted are attached using bolts once the rest of the fixed structure is assembled on the test machine. The pressure bag must be fully enclosed while pressurised, and therefore the fourth edge that is not enclosed by the moving part must be closed. The final section of the fixed part is a tall box section that is mounted on one side of the steel plate as shown in Figure 7.6.

Once the design of the fixed part had been finalised it was important to investigate if it would remain rigid under operation. For this reason the fixed part was modelled using FE software ANSYS 11. The model was constructed with solid elements using a cross-section with the same second moment of area as a box section to simplify the model. A load of 0.345 MPa, i.e. ten times greater than that used in the testing, was applied to the model to provide an adequate safety factor. The table structure was assumed to be constrained at the base of each leg in all degrees of freedom and the load imparted on the top surface of the metal support plate as a pressure load. The maximum deformation was calculated as 2.55 mm, at an unsupported edge of the water cushion support plate, under the 0.345 MPa pressure loading which is approximately 10 times more than will be applied in the experiment. This was not considered to be significant when considering the scale of the rig, so it was concluded that this part of the rig design was of suitable construction to carry the loads developed during testing.

7.4.3 Moving structure

The second section of the test rig is the moving part. This was connected to the actuator of the test machine at one end, and bolted to the test panel at the other. The movement of the actuator pulls the test panel over the fully supported pressurised cushion and imparts the load. The top of the moving part was formed from three sections of solid steel. One section is the length of the moving part, while the other two form the front and rear of the top part. These three sections were bolted together during manufacture and were not designed to be dismantled. The top section

of the moving part is mounted on the two vertical sides formed from solid steel sections, which contained lightening holes. The sides were attached to the top with pins, which, again, were not designed to be dismantled. Finally, a solid section sits between the vertical sides at their base with a pin protruding from its base for attachment to the test machine. The standard hydraulic grips supplied with the test machine were used to secure the moving structure to the test machine. The moving part had a circular cross section pin of diameter 17 mm machined into it to accommodate this fixing. In the upper part of the moving structure, 19 tapped holes were machined so that the test panel can be fixed to the structure. It was considered that loading through tapped holes was not ideal but it was not practical to achieve the loading in any other way. To spread the load more evenly in the flange, penny washers were used under each bolt head.

The moving part was modelled using ANSYS 11 to confirm that it was practically rigid under operational loads. The model of the moving part was constrained along the top perimeter where the generic panel is held and a tension load applied to the base of the circular section that is accommodated in the grips attached to the actuator of the test machine. The maximum deformation was calculated as 0.68 mm, on the fourth side to which the generic panel is not bolted, under the maximum load. Again this was not deemed to be significant, and under the expected 'service' loads the rig can be considered 'rigid'. The pressure fittings, water inlet and transducers, are attached to the bottom of the water cushion and therefore must pass through the steel supporting plate. Two holes were drilled into the supporting plate to allow this. Pipes connecting to these pressure fittings then pass between the two vertical sides of the moving part of the rig (see Figure 7.6). These pipes are flexible hydraulic hoses, and therefore were routed around the rigid sections of the rig.

The results of the FE model of both structural parts of the test rig demonstrated that under load the rig will not deform significantly. Therefore, the pressure within the water cushion will be completely transferred to the generic panel. The results of the FE model also provided the stress data that allowed the selection of the grade of steel to be used to manufacture the rig. The steel chosen for the manufacture was EN8 medium carbon steel that has a yield stress of 530 MPa. This is higher than the maximum stresses predicted by the FE.

Detailed drawings of all the sections of the test rig are included in Appendix A.

7.5 Commissioning of the test rig

Figure 7.8 shows two photographs of the rig installed on the test machine; the moving structure has been painted red and the fixed structure has been painted yellow. The first image shows the entire fixed support structure and the second shows a close-up of the generic panel viewed from the same projection as shown in Figure 7.6.

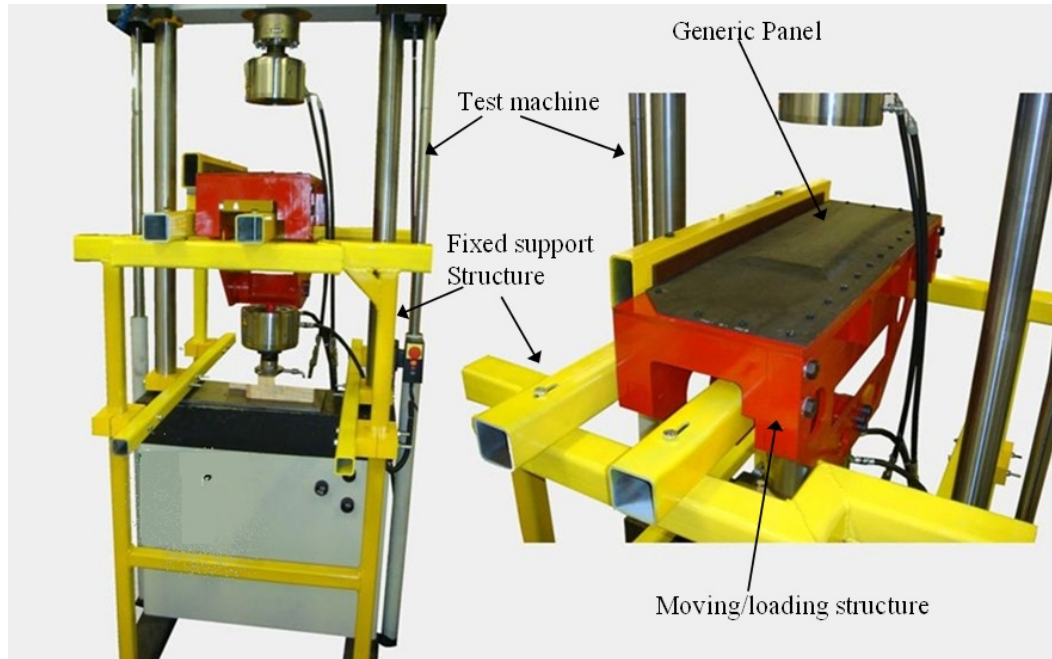


Figure 7.8: Photographs of the rig installed on the test machine

7.5.1 Static Testing

The commissioning began with static tests that applied a variety of pressures to the panel and ensured the rig could reach and maintain the required pressures. The water cushion is filled with water such that it has a pressure of 0 MPa gauge. The test machine actuator was manually moved downward and therefore applied an increasing pressure. The applied pressure was monitored using the Vishay strainsmart 6200A system. During these tests the out-of-plane displacement was independently measured using a linear variable differential transformer (LVDT) displacement transducer located on the free edge of the generic panel approximately 160 mm from the front. This coincides with the point that is expected to undergo the maximum out-of-plane deformation. Three static tests were performed, increasing the maximum applied pressure in each. The pressure was initially ramped to 0.0138 MPa (2 psi), then to 0.0207 (3 psi) MPa and finally, to 0.0276 MPa (4 psi). Figure 7.9(a) plots the maximum out-of-plane displacement against the applied pressure for each of the three tests. The plot shows that for all three loading cases the displacement of the panel is virtually linearly related to the applied pressure. Importantly, the plots from the three tests show the same slope and therefore, the rig is capable of consistent panel loading. This demonstrates the viability of the rig for static loading and application of DIC. For the rig to be

correctly controlled using position control of the test machine, it is vital to understand the relationship between the position value and the applied pressure. Therefore, during the static tests the position of the test machine loading ram was also recorded at each pressure value, as shown in Figure 7.9(b). The pressure increases linearly with test machine position, except for pressure values below 0.00345 MPa (0.5 psi). It is thought that this initial nonlinear relationship between the actuator position and pressure is due to initial ‘slack’ in the loading rig due to clearances in fittings and some flexibility in the rig. The results of these tests show to increase the applied pressure by 0.0069 MPa (1 psi) requires an actuator movement of approximately 4 mm. However, there is some disparity between the gradients of the displacement and position against pressure curves. From Figure 7.9 (a) an application of 1 MPa to the panel will produce a displacement of approximately 600 mm. Whereas, from Figure 7.9 (b) an actuator movement of 650 mm is required to apply a pressure of 1 MPa. This is considered to be due to the compressibility of the water and possibly the actuator oil.

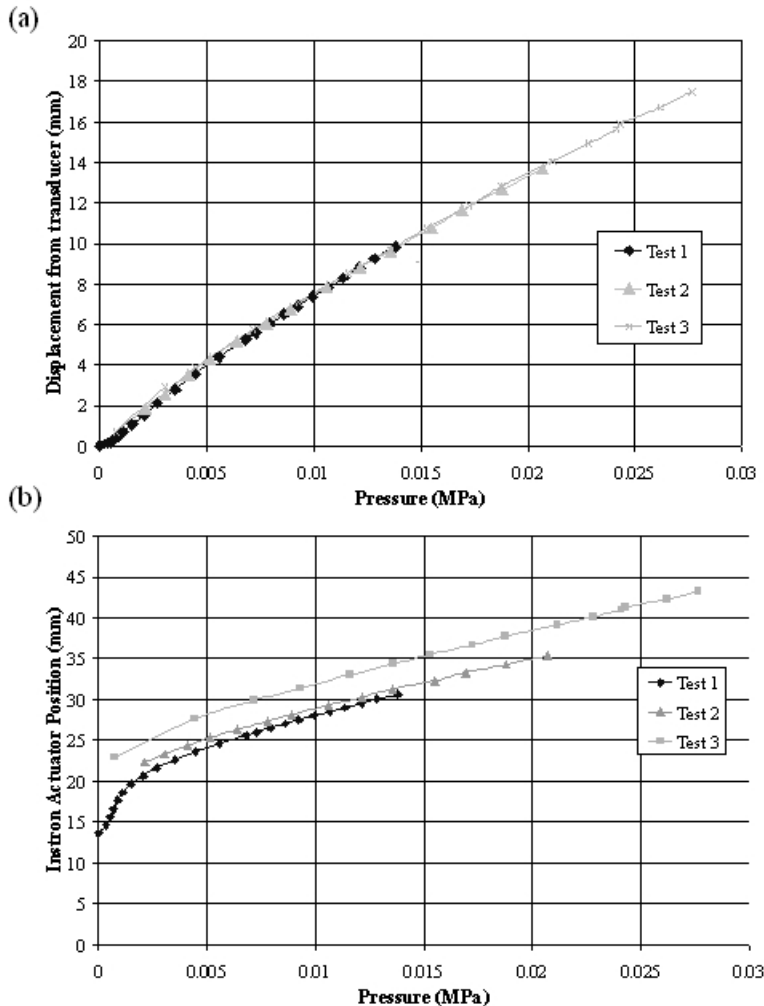


Figure 7.9: Plots of static tests

7.5.2 Cyclic Testing

As TSA requires a cyclic load, it was also necessary to demonstrate the viability of the rig to impart a consistent cyclic pressure into the panels. In cyclic loading, the pressure must be controlled by the servo-hydraulic machine position control facilities. Therefore the information produced in the static tests was used to determine the applied displacement range necessary to achieve a certain pressure range in the panel. The Instron actuator was moved manually by controlling the position until the applied pressure recorded 0.002 MPa. A 3 mm displacement range was applied around the mean pressure of 0.002 MPa at frequencies of 1 and 2 Hz. According to Figure 7.9 this should result in an applied pressure range of 0.0052 MPa (0.75 psi). Figure 7.10 shows the profile of the cyclic pressure for both loading frequencies. It can be seen that at 1 Hz the cyclic pressure range is 0.0052 MPa and at 2 Hz the cyclic pressure range is 0.005 MPa. For both loading frequencies the plots in Figure 7.10 show the pressure range is well maintained repeatedly cycle after cycle. It should be noted that the small reduction in the pressure range achieved for the higher frequency is entirely consistent with what is expected from a standard machine. The important feature here is that the pressure cushion set-up can apply and maintain a viable cyclic sinusoidal load that is suitable for TSA.

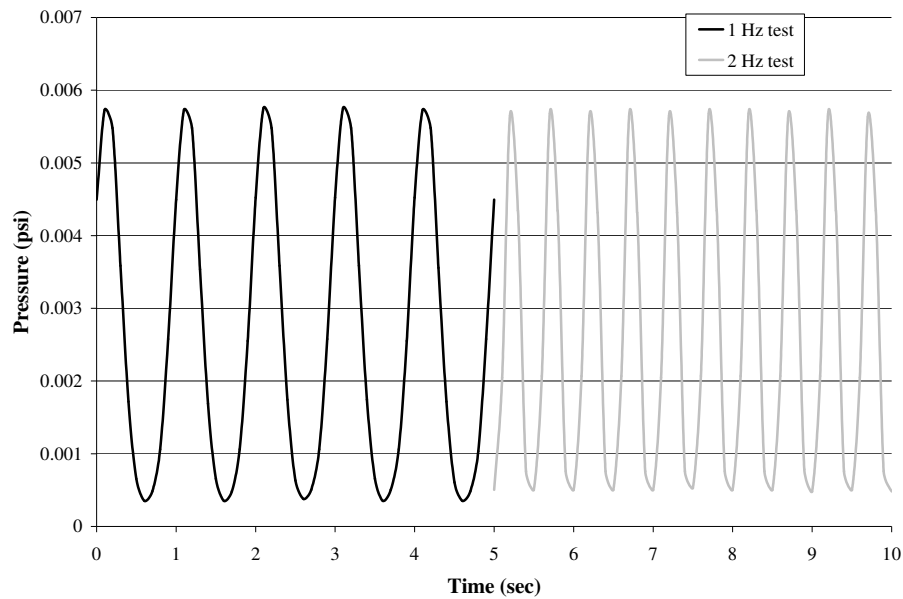


Figure 7.10: Cyclic tests

7.6 Summary

A full scale test rig has been designed to accurately impart a representative pressure load to obtain the mechanical performance of the generic panels, described in Chapter 5, using optical strain measurement techniques. In order to inform the design of the rig, an initial FE model has been constructed of the generic panel to offer an insight into the expected response that must be

accommodated by the test rig. Predicting the stresses and in-plane strains also proved the responses would be of an adequate range to allow the use of TSA and DIC techniques. The rig is based on the use of a standard servo-hydraulic test machine that loads the generic panels via a fully constrained water filled cushion. The pressure inside the cushion is completely transferred to the surface of the test panel. The test rig has been commissioned and through preliminary tests its operation has been tested. The ability of the test rig to apply a consistent static pressure has been tested, and in the process it has been shown that the pressure is linear to the movement of the actuator of the Instron machine. The maximum deformation was also measured using a displacement transducer, and was proven to be linear to the applied pressure. Finally, the ability of the test rig to maintain sinusoidal cyclic loading at both 1 and 2 Hz has been demonstrated. This is vital for the use of TSA, but also demonstrates the feasibility of the use of the rig for the application of fatigue loading.

Chapter 8

8 Digital Image Correlation (DIC)

8.1 Introduction

Digital Image Correlation (DIC) tracks the movement of a random surface pattern to monitor deformation or displacement. The random surface pattern is usually achieved by covering the surface of a component with a painted speckle pattern. Images of the deformation process are recorded using either one (2D DIC) or two (3D DIC) charge coupled device (CCD) cameras. The images are divided into discrete interrogation windows (or cells) and the displacement is obtained by tracking features within each cell [16]. Strain measurements are obtained by taking the measured displacement and dividing by the size of the undeformed cell. DIC is therefore a full-field, non-contact technique to measure the strain distribution across the surface of a deformed component. Strain resolutions quoted as being as low as 40 μ strain [105], although this is highly dependent upon application and test conditions, such as lighting and orientation. The DIC technique has been successfully used to analyse the strains in heterogeneous engineering materials such as composites [17].

The application of DIC to the generic panels will allow a full-field measurement of the strains across the entire panel. Obtaining this with traditional techniques, such as strain gauges, would be infeasible. The full-field data is particularly important when considering the response of a complex material, such as the composites used in this work, under a complex loading configuration such as the pressure load applied in this work. DIC has been used before on composite materials, e.g. [17],

but not as a full scale application. In this chapter the results of some initial work performed on tensile strips manufactured for the material characterisation described in Chapter 6 will be used to define the performance of the DIC and assess its suitability in this application. This will include an assessment of correlation speckle patterns used on the surface of the material, as the application of a paint speckle pattern is time consuming and it would be beneficial if, instead, the natural pattern of the composite surface could be used. Finally, DIC is applied, full-field, to the generic panels.

In this chapter, the feasibility of the use of the LaVision system on the composite materials considered in this research is presented and discussed. Tests were initially performed on tensile specimens produced from both MO 1 and MO 2 to investigate if it is possible to measure the level of strain that may be expected in these materials. These simple tensile tests were also used to investigate if it is possible to find an optimum cell size and configuration. Finally, these tensile tests were to be used to analyse different surface patterns for their ability to be used as correlation patterns. These tensile tests are followed by results from the use of DIC on a generic panel produced using MO 1 loaded on the pressure rig described in Chapter 7. The strain distribution and values measured using DIC are compared to an FE model of the panel. The chapter concludes with a discussion of the feasibility of the use of this technique for full-field strain measurements with particular attention given to the current application.

8.2 Brief overview of application of DIC

In work described in this thesis, the LaVision system (Imager pro S) was used for DIC. The system comprised of two digital cameras with 2 Mpixel resolution CCDs (14 bit digital) and therefore, allowed 3D deformation analysis and measurement of the in-plane strains. The cameras were fitted with 50 mm lenses with a focal ratio of 1.8. The images were recorded and processed using DaVis 7.2 (produced by LaVision) (see Figure 8.1).

All that is required for DIC analysis is an unstrained (reference) image and a strained (deformed) image that can be compared to the reference image [106]. The reference image is divided into ‘cells’ of a given number of pixels from 2×2 to 1024×1024 . This value is known as the cell size; for the LaVision system this can only be defined in powers of two. A further processing parameter is the percentage of overlap between cells, which for the LaVision system can set between 0 and 87 %. By altering the combination of cell size and cell overlap when processing DIC data, it is possible to correlate the strains for a large range of loading and structural applications. Figure 8.2(a) shows an example cell configuration with 2×2 cells and no overlap. It can be seen that the undeformed image has a grey scale pattern within the 2×2 cell before

deformation. After deformation the grey scale pattern is retained, but its spatial position has moved. By recognition of the grey scale pattern from the undeformed to the deformed condition, the deformation of the specimen can be obtained.

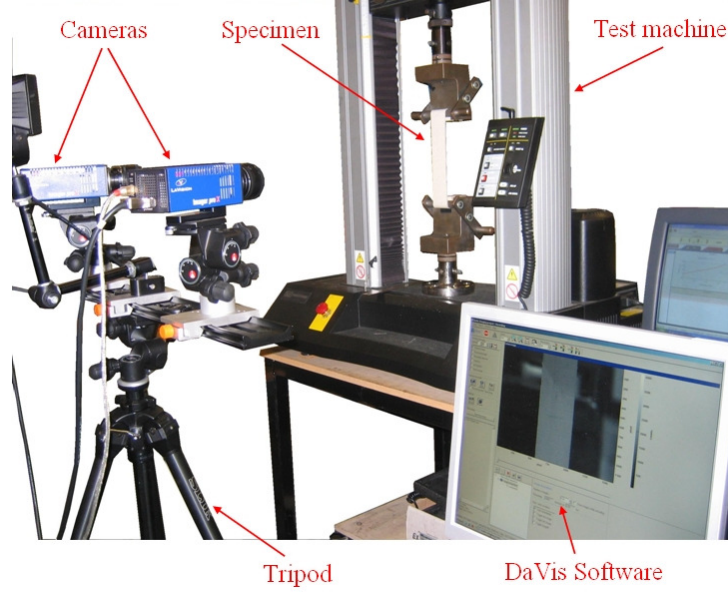


Figure 8.1: Photos of LaVision system set-up for a test

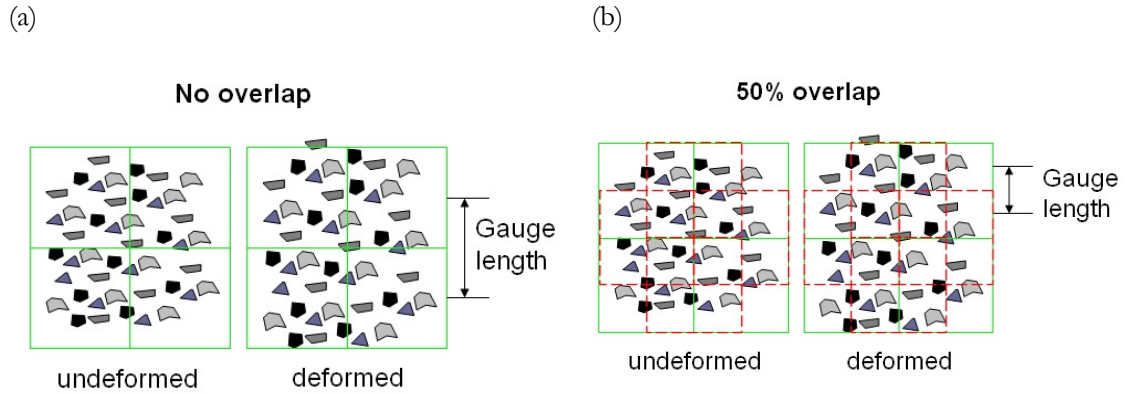


Figure 8.2: Demonstration of cell size and cell overlap and its application to correlation

The choice of cell size is a compromise between accuracy and spatial resolution; the larger the cell size, the more values there are to find an average over. A second factor to be considered in the compromise is cell overlap, as shown in Figure 8.2(b). The strain is calculated from the deformation vectors in each cell or in the case of overlapping data each sub-cell. This is indicated by the gauge length shown in Figure 8.2(a) and (b) where the overlap shortens the gauge length. Therefore, the increase in spatial resolution shortens the distance over which the strain is measured. This will inevitably create more scatter as the measurement region decreases.

When using DIC to measure 3D deformation, it is necessary to undertake an extra step in the image processing. This step is known as calibration and calculates a ‘working volume’ for the analysis (see Figure 8.3). The working volume contains the calibration plane and the two cameras, whilst the calibration file contains information on the relative position and orientation of the two cameras with respect to the calibration plane. The calibration is conducted by placing a ‘calibration’ plate, with a regular prescribed pattern of points on it, in front of the specimen to be deformed (see Figure 8.4). The calibration plate used with this system has points on two levels and this reduces the total number of calibration images required. A number of images (in this case, usually three from each camera) are taken whilst the calibration plate is rotated around the vertical such that it moves out-of-plane with respect to the surface of the specimen. The user manually picks three known points from the calibration plate in each of the calibration images when prompted by the DaVis software. The software then searches each image to find the rest of the points from the plate. The more points, the more accurate the calibration, with a good measure of success being the RMS fit error. A value of less than 0.2 is considered a successful calibration. The use of 3D DIC requires an extra level of image processing and as such, the errors in calculation are increased. These inaccuracies are compounded as each extra level of processing incurs some error. Therefore for 3D DIC, LaVision quotes a best local minimum strain resolution of 220 μ strain.

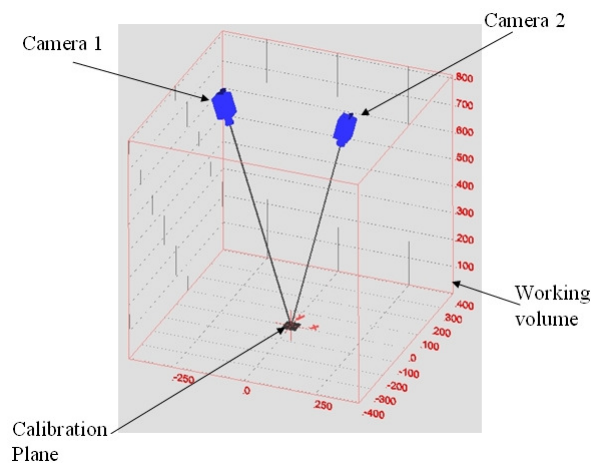


Figure 8.3: Example of working volume calculated using calibration step

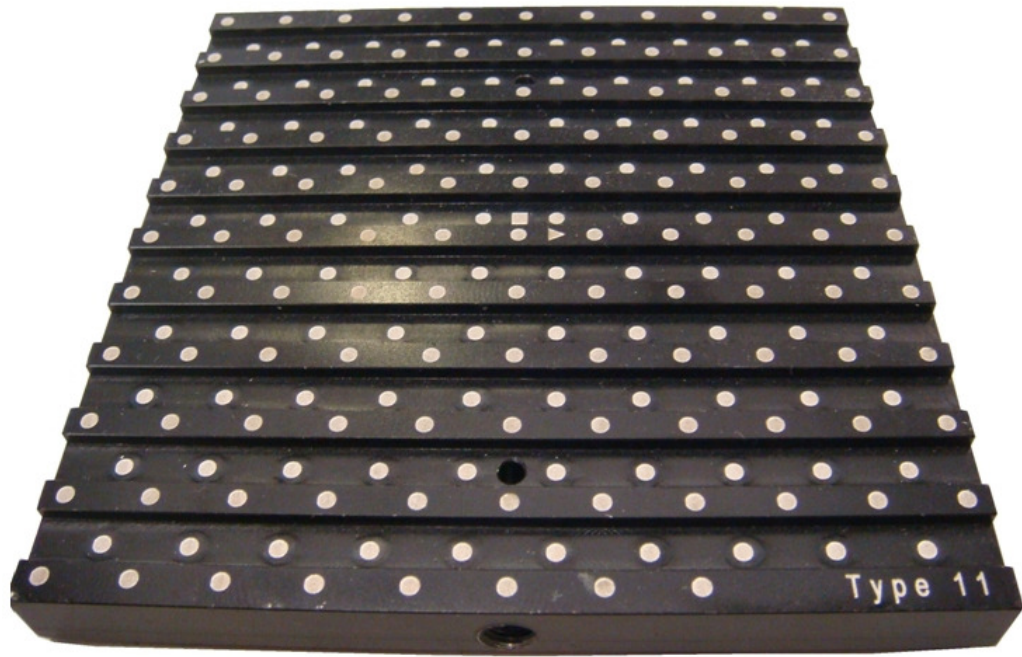


Figure 8.4: Example of a calibration plate used with the LaVision system

Before conducting any experiments with DIC it is important to realise that it is an optical technique, and as such the results will only be as good as the data collected, in this case the quality and contrast of the images. Care must be taken in achieving good focus and maintaining lighting conditions. The lighting must be diffuse and avoid reflections, such that any difference between the images is due only to the structural deformation. The DIC works by measuring the greyscale value of each pixel and searching each image for the best match.

8.3 Correlation cell size

Tensile tests were performed on specimens produced using MO 1 and MO 2, identical to those in Chapter 6, which were approximately 15 mm wide and 150 mm in length. The specimens were strained by approximately 0.1 % in an Instron 5569 servo-mechanical test machine, whilst the load was recorded by the machine and the strain independently monitored by a long gauge extensometer (gauge length of 50 mm) attached to the rear of the specimen. The extensometer strain measurement is used to compare to the DIC reading averaged over the whole surface. The DIC was used in its 3D format, i.e. with two cameras, as this is expected to be required when dealing with real components and the full scale tests in this work where significant out-of-plane deformation will occur. A pair of images was taken before deformation and a second set at the end of the test. The DaVis software was used to correlate between these two sets of images.

Initially, the test on the specimen made using MO 1 with a recommended ‘paint speckle’ pattern (see Figure 8.5) was used to compare the ability of the system to measure strains with varying cell size and cell overlap combinations. Ten combinations of cell size and overlap were used; the cell size was either 128 x 128 or 64 x 64, whilst the cell overlap was 0 %, 25 %, 50 %, 75 % or 87 %. The test was run three times to ensure the repeatability of DIC strain measurements, however the processing parameter variation was conducted on each of the three tests. For comparison with the extensometer strain value, an average of the strain over the whole surface of the specimen is taken. Figure 8.6 plots the averaged strain from the DIC obtained in the longitudinal direction for each processing combination normalised against the extensometer value. There is significant variation between not only the accuracy of the strain reading between processing parameter combination, but also in some cases between the three tests. In particular, some processing parameter combinations seem completely unsuccessful, for example 128 x 128 with 0 % overlap and 128 x 128 with 50 % overlap. However, one combination stands out as both accurate and consistent across the three tests. 64 x 64 with 50 % overlap consistently measures an accurate strain value. This offers less than 5 % error on all three tests. Although the quoted minimum strain resolution locally is 220 μ strain, and therefore anything within 20 % of the measured 1000 μ strain would be considered ‘accurate’, the strain resolution is greatly improved when averaging over a large area as in these tests. The minimum strain resolution is reduced to 60 μ strain for 128 x 128 cell size and 100 μ strain for 64 x 64 globally. It is therefore expected that an error of only 10% can be achieved when using 64 x 64.

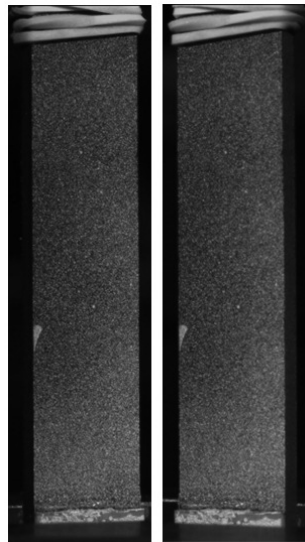


Figure 8.5: Recommended paint speckle pattern on the tensile specimen

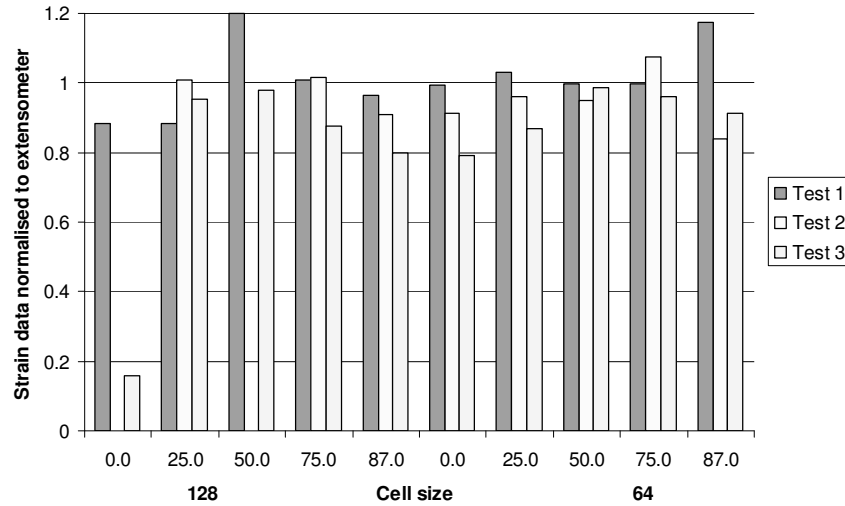


Figure 8.6: DIC strain data normalised to the extensometer for each of the processing parameter combinations

Figure 8.7 shows the full-field strain map of the longitudinal strain (ϵ_L) in the specimen using 64 x 64 and 50 % overlap. Even though this is the most accurate configuration when the strain is measured globally, there is a significant amount of strain variation across the specimen surface. To quantify this variation, the values along the centreline were taken and the coefficient of variation from the global average was calculated for each processing parameter combination. Figure 8.8 plots the value of coefficient of variation along the centreline for each processing combination. As the cell overlap percentage is increased the variation also increases. There is also a step change in variation when 64 x 64 is used instead of 128 x 128. These increases in variation are symptomatic of not only of an increase in error, but also simply because there are more strain values over which variation can occur.

These simple tensile tests, where an average, or global strain, is the only value of interest, have shown that it would be best to apply a cell size of 64 x 64 with 50% overlap. However, the increased strain variation of approximately 25% when using this combination may have deleterious effects when considering a more complex strain field where higher spatial resolution will be more important. It is for this reason, that currently the search for an optimum processing combination is inconclusive and instead a similar process may be required for each application. This will not only be time consuming and laborious, but it would also be difficult to have confidence in the results when considering a strain field that cannot be confirmed independently, such as using an extensometer.

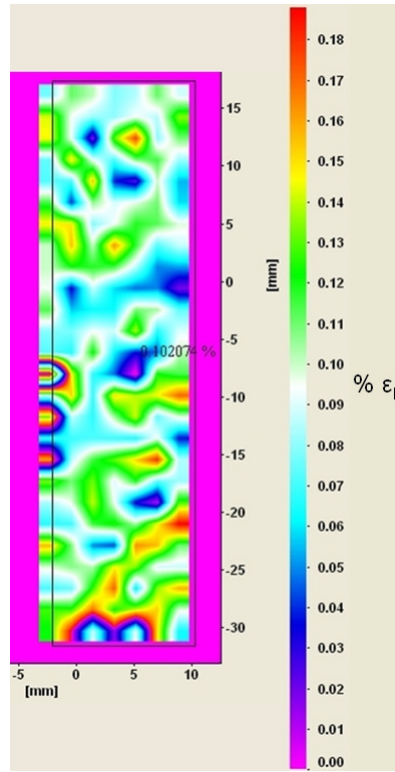


Figure 8.7: Longitudinal DIC strain map of tensile specimen using 64 x 64 pixels with 50 % overlap

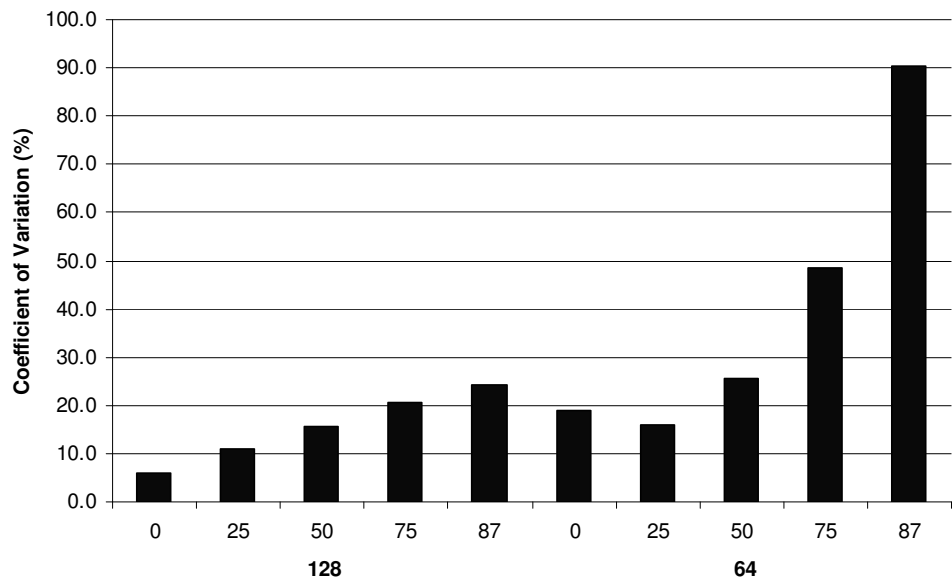


Figure 8.8: Coefficient of variation of DIC strain along the centreline of the tensile specimen for each of the processing parameter combinations

8.4 Correlation pattern

With a preferred processing parameter combination selected for use on the tensile specimens, it was decided to investigate the effect of changing correlation pattern. Five different correlation

patterns were tested on specimens manufactured from both MO 1 and MO 2. Figure 8.9 shows a small representative square of each correlation pattern on each specimen: first, the natural pattern formed by the application of the textured peel ply during composite manufacture; second, the recommended paint speckle; and the other three were different sized paint dots with different densities. The larger paint dots would allow a fast, and easy, method of stamping the required correlation pattern on to the surface of a specimen. A white square of the approximate size of the correlation cells is included in Figure 8.9 to offer an indication of the size of the correlation pattern in relation to correlation cell size. As in the previous, test the DIC readings were taken in conjunction with an extensometer to allow a comparison. When using the composite natural pattern it was considered that the nature of the base material, i.e. UD or woven, may have a role in the results and hence, specimens from MO 1 and MO 2 were used.

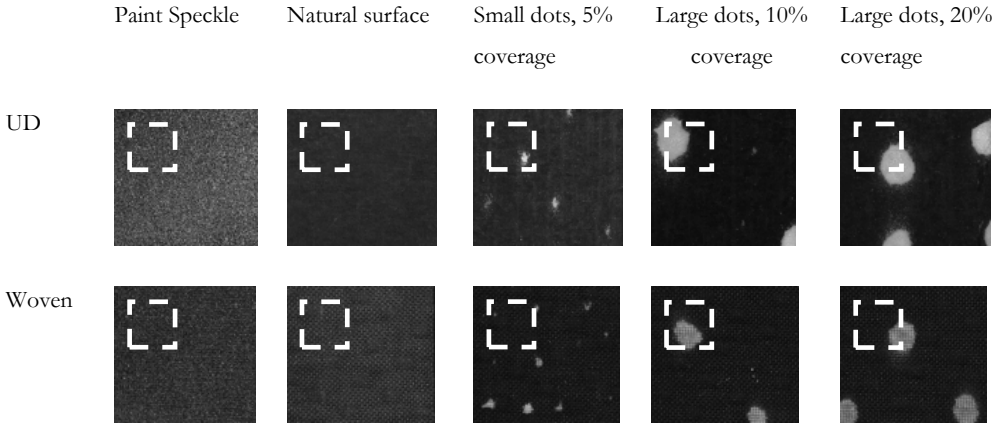


Figure 8.9: Representative plots of surface patterns on specimens MO 1 and MO 2

Figure 8.10 plots the DIC strain values normalised against the extensometer for each of the correlation patterns and materials. It is immediately clear that the patterns involving larger paint dots were unsuccessful and would be incapable of providing accurate strain readings. The failure of these patterns is largely due to the dots being too large and ‘crossing’ between interrogation cells and therefore calculation of deformation or strain is impossible. This is confirmed when considering the strain plots of the tests with large dot correlation patterns in more detail. The regions around one of these large dots register as nothing. A surprising result, however, is the success of the use of the natural pattern as a correlation base. In fact, these results suggest that the natural pattern can offer better correlation than even the recommended paint speckle. This is a promising result for the use of DIC on the much larger generic panel, where application of a paint speckle pattern would be time consuming.

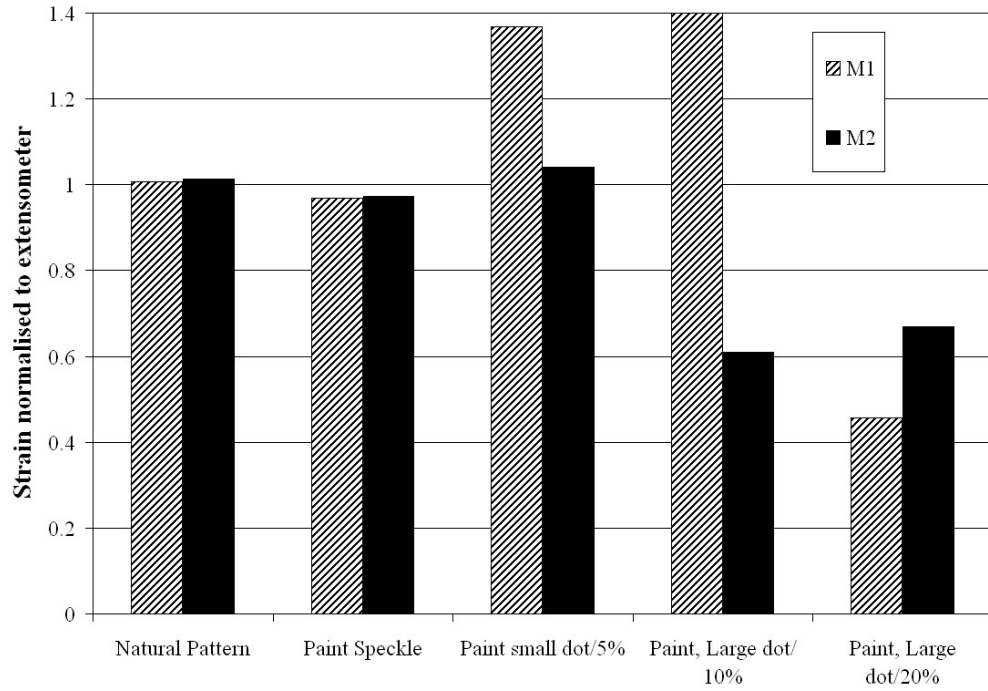


Figure 8.10: Normalised DIC strain values for the different correlation patterns and materials

A final conclusion that can be drawn from these simple tensile tests is that the use of DIC on the types of composite used in this work is feasible and it is possible to discern strains of the order that may be expected in the generic panel, i.e. in the range of 0 to 1000 or 2000 μ strain.

8.5 Full-scale test

8.5.1 Experimental approach

It is known, from experience and the initial tensile tests that it is not be possible to image the entire generic panel for DIC in one shot. To offer a field of view of 900 mm by 300 mm the cameras would need to be far from the surface of the panel, which cannot be accommodated, either by the space around the test machine or the camera stand available. With such a large field of view, the spatial resolution of the strain maps calculated would also be too low to encompass all of the important features. Instead only an area on the panel of approximately 120 mm by 100 mm can be imaged. Hence, for initial tests to ascertain the effectiveness of this technique for this application it was decided to concentrate on one region of the panel. This region should have a reasonable strain range and some strain distribution. From the strain plot of the FE model described in Figure 7.4, it is clear that the area around the corner of the core towards the extended flange would be a suitable location.

The generic panel MO1G1NO5 was loaded using the custom design test rig described in Chapter 7, up to a maximum applied pressure of 0.00138 MPa (2 psi). By incrementing this pressure application into ten regular steps it was possible to record ten pairs of images for DIC. This allows the correlation to be performed as integration over these ten steps to reduce the error. During the tests the DIC cameras were suspended directly over the generic panel on a large stand (see Figure 8.11). This allowed the cameras to be held vertically and therefore perpendicular to the surface of the generic panel. The area of focus is also confirmed in Figure 8.11. The images were taken using the background illumination from the laboratory overhead lights. This was considered sufficient, particularly as the generic panel is horizontal and therefore the surface is in direct line of sight of the lights.

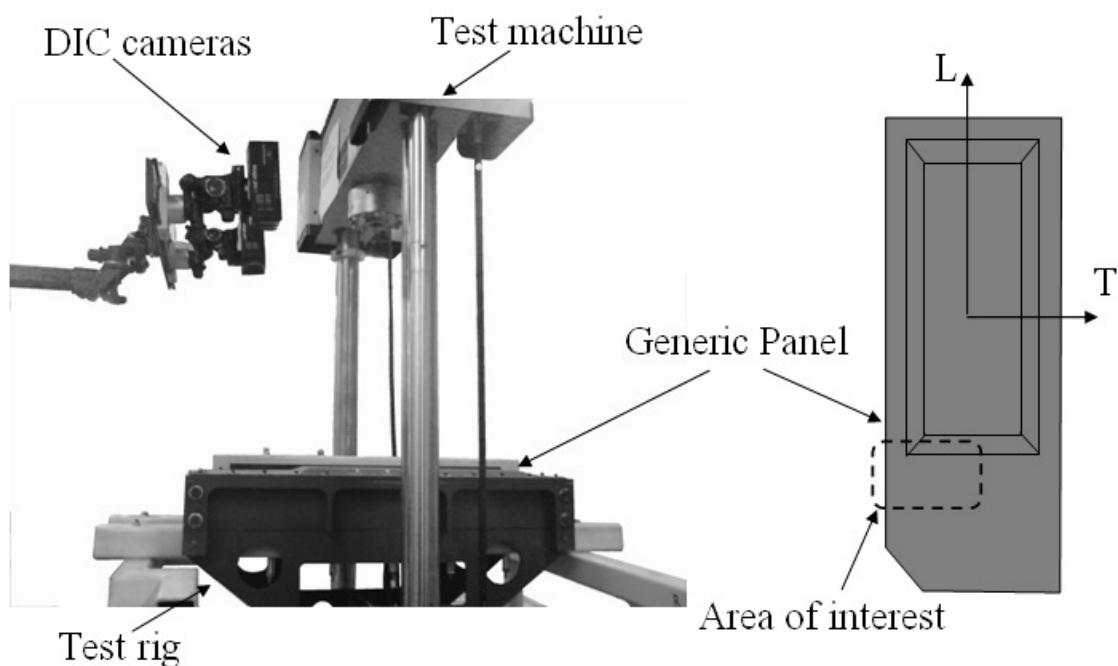


Figure 8.11: Photograph of DIC cameras supported over the generic panel

8.5.2 FE for comparison

The FE model described in Chapter 7 was altered to simulate the 0.0138 MPa applied during the DIC full scale feasibility tests. These tests concentrated on the area of focus highlighted in Figure 8.11. Figure 8.12 plots the predicted out-of-plane deformation with the colour scale ranging from 0 to 10 mm, and Figure 8.13 plots the in-plane strain in the longitudinal direction with the colour scale ranging from 0 to 1500 μ strain. The FE model predicts an increasing deformation from bottom right (at 3 mm) to top left (at 6.5 mm), with a difference of approximately 3.5 mm. The strain plot shows a similar trend to the out-of-plane deformation, except for the important feature around the corner of the core where the strain reaches a peak. The strain ranges from approximately zero towards the base of the image, to 1500 μ strain at the corner of the core.

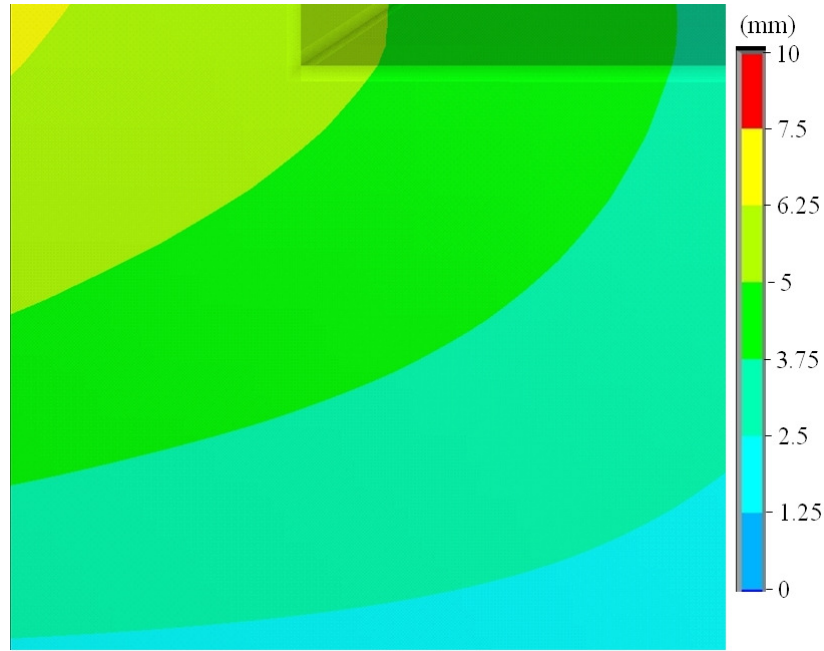


Figure 8.12: FE predicted out-of-plane deformation in the area of interest

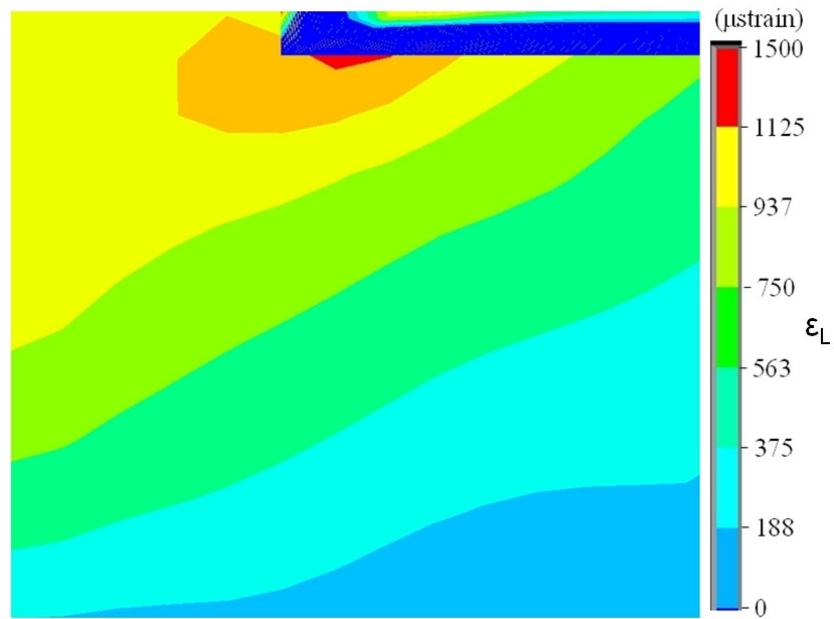


Figure 8.13: FE predicted in-plane strain in the area of interest

8.5.3 Full-scale – Natural pattern

Following the investigations into correlation patterns (described in section 8.4), the test was initially undertaken using the natural surface of the generic panel as the correlation pattern. The cameras were positioned approximately 740 mm above surface of the panel, and were focused to give a field of view of 130 mm by 105 mm. Figure 8.14 shows the pair of reference images. The corner of the core is clearly visible towards the top of each image. The calibration plate was placed

flat on the panel abutting the core. The calibration produced an RMS fit error of 0.126, i.e. much less than the 0.2 threshold for a successful calibration.

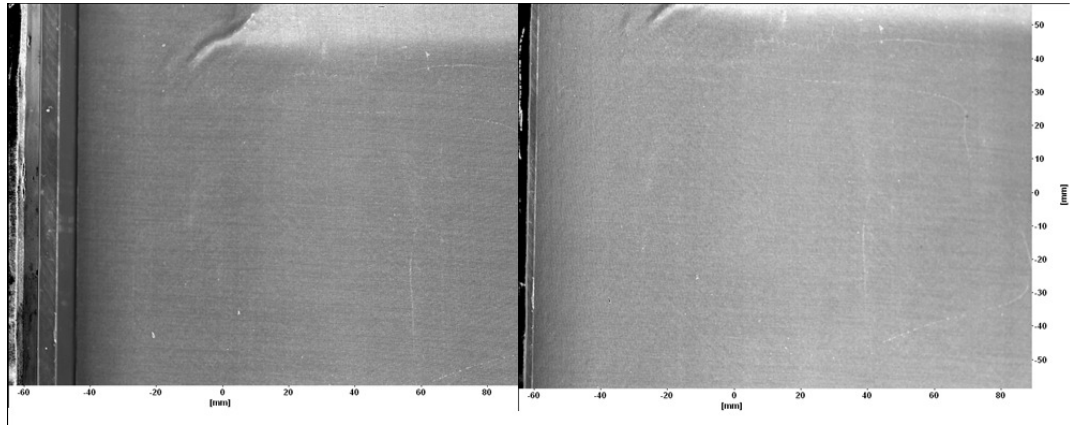


Figure 8.14: Raw reference images of the first feasibility test with a natural correlation pattern

Figure 8.15 shows the ‘surface height’ or out-of-plane deformation, which is measured from the initial calibrated plane.

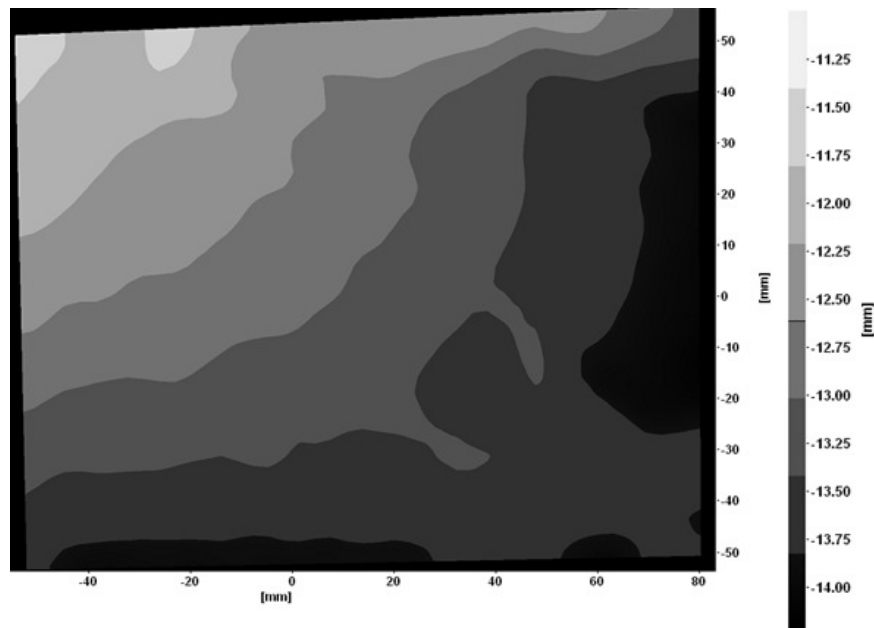


Figure 8.15: Surface height correlated with natural surface pattern

The DaVis software can also present this information as a 3D interpretation of the out-of-plane deformation of the original raw data (see Figure 8.16). Both these figures show an out-of-plane deformation, with an increasing amount from the bottom right to the top left. The scale of the surface height plot in Figure 8.15 ranges from -11 mm, in white, to -14 mm, in black. The actual value of surface height measured in this plot represents the distance the interrogation cell has moved from the initial plane defined during the calibration phase. In the current test this includes the movement of the rig that imparts the pressure. Therefore, ascertaining actual deformation

values is difficult and may be inaccurate. Instead, it is possible to measure the difference in surface height across the image, and hence infer the deformation of the panel. In the bottom right corner the panel is 14 mm below the original calibration plane, whilst the top left is only 11 below the plane. Therefore, across the span of the image the DIC has measured 3 mm deformation.

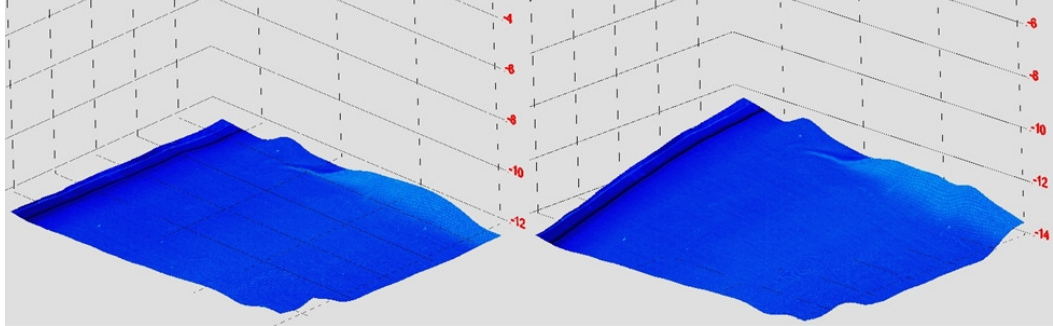


Figure 8.16: 3D representation of the measured panel's deformation

The shape and value of the deformation region is consistent with that predicted by the FE model. However, when processing for in-plane strain the software failed to correlate and strain values could not be obtained. Therefore, it was decided to apply a recommended paint speckle pattern to the surface of the panel in the region of interest.

8.5.4 Full-scale – Recommended pattern

The second full-scale feasibility test used the recommended paint speckle pattern in the same region as that investigated in the previous test. Aerosol spray paint, both black and white, was used to apply the speckle pattern manually. Figure 8.17 shows the raw images from both cameras of the reference image. Applying the paint pattern means that the images have a larger contrast range, which is important for the use of DIC. The same incremental pressure, up to 0.00138 MPa, was applied. Figure 8.18 shows the out-of-plane deformation plot, and Figure 8.19 shows a 3D representation of this deformation.

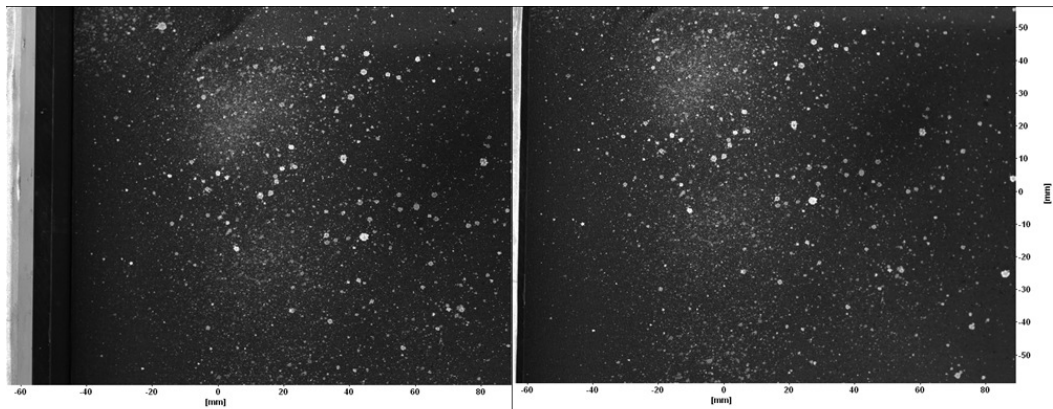


Figure 8.17: Raw reference images of the second feasibility test with a recommended correlation pattern

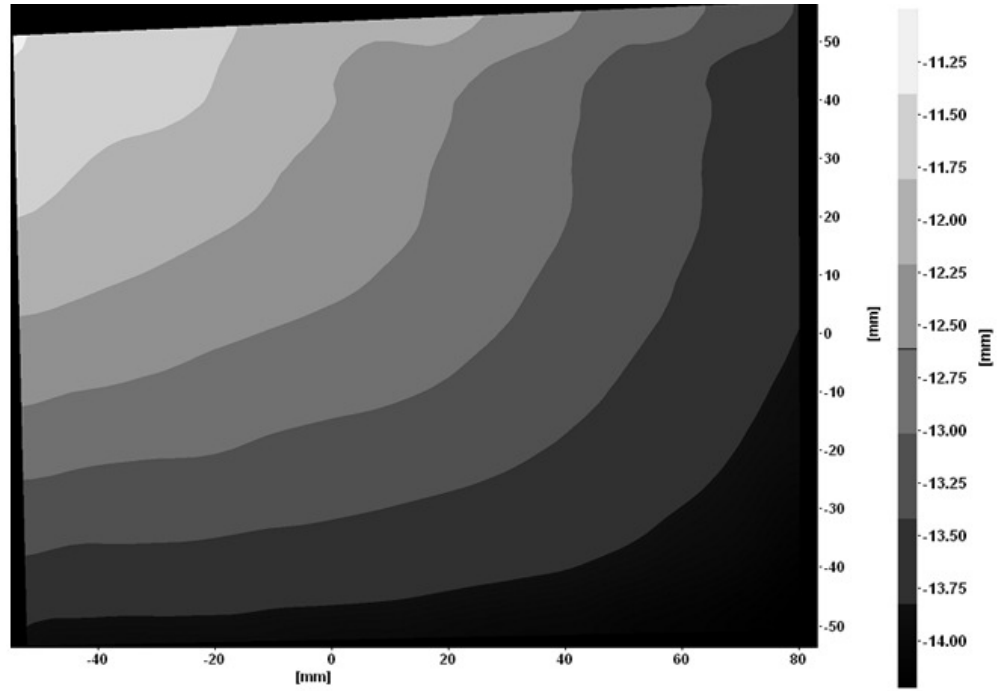


Figure 8.18: Surface height correlated with recommended surface pattern

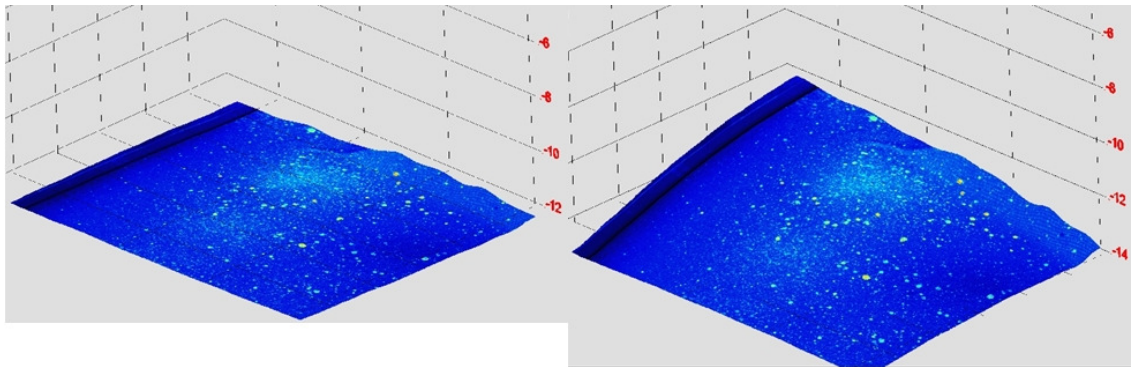


Figure 8.19: 3D representation of the measured panel's deformation with recommended pattern

The manner and magnitude of the deformation is similar to that measured by the natural pattern test and that predicted by the FE model. However, the investigation of the 2D plot of deformation demonstrates that it is smoother and better matches the shape of the FE deformation than the previous measurement.

With a different correlation pattern the possibility of correlating to obtain in-plane strain information was explored. Therefore, the images were processed using all combinations of cell size and cell overlap. With a single processing step it was again impossible to obtain any strain data. However, in this test it was found that by using a multi-pass process of 256×256 pixels with 50 %, followed by either 128×128 with 25 % or 64×64 with 25 % it was possible to obtain strain values. Figure 8.20(a) shows the longitudinal in-plane strain correlated using a second step of 128

x 128 with 25 %, and Figure 8.20 (b) shows the strain correlated using a second step of 64 x 64 with 25 %. Both plots look noisy, especially towards the bottom and right-hand side of the images. This corresponds to regions that the FE model predicted low levels of strain. When the DaVis software cannot detect a strain it outputs a noisy, often large, response which confuses the image of strain distribution. However, in both plots there is a trend of increasing strain towards the top left of the images as predicted by the FE model. The strain values peak at around 700 μ strain, which is significantly lower than that predicted by the FE analysis. Therefore, although the strain shows the same correct distribution it does not provide accurate strain values. The strain map provided by the DIC has a relatively low spatial resolution, with each 128 x 128 cell being equivalent to 9 mm². To improve the spatial resolution it was decided to reduce the field of view, by moving the cameras closer to the surface of the generic panel.

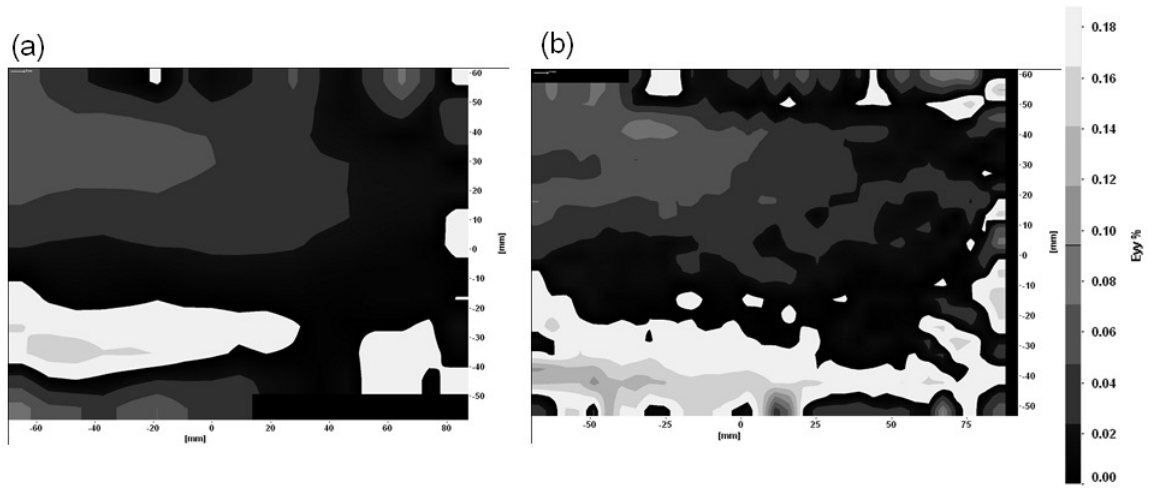


Figure 8.20: DIC strain map using recommended pattern using (a) 128 x 128, (b) 64 x 64

8.5.5 Full-scale – Recommended pattern/reduced area of interest

To improve the spatial resolution of the strain data measured by the DIC the cameras were moved to within approximately 430 mm of the surface of the generic panel. In doing so, the area of interest is reduced to approximately 80 mm by 60 mm. The raw images are shown in Figure 8.21. The much reduced area of interest requires the use of a smaller calibration plate. This plate has the same form as that in Figure 8.4, but on a smaller scale. The RMS fit error using this setup was 0.151, which is still well below the threshold for a successful calibration. Processing for surface height and out-of-plane deformation gives Figure 8.22 and Figure 8.23.

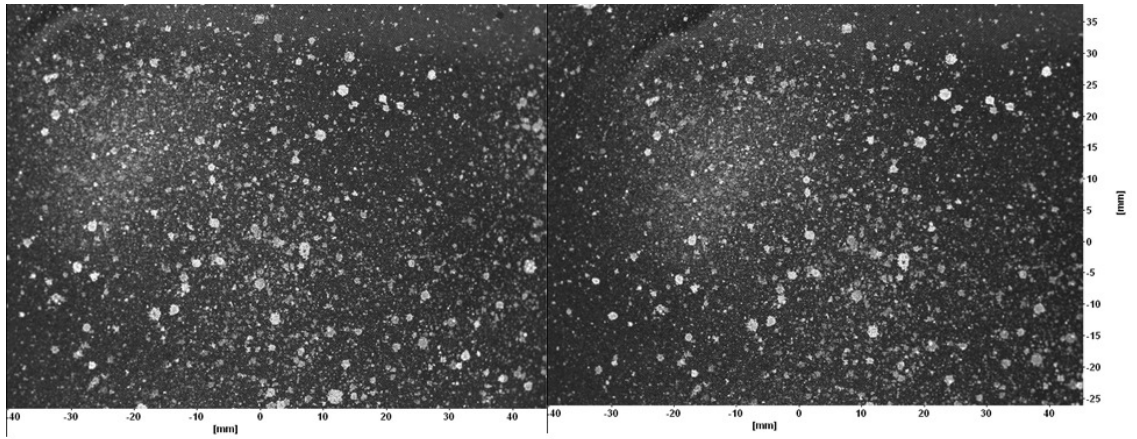


Figure 8.21: Raw reference images of the second feasibility test with a recommended correlation pattern and reduced area of interest

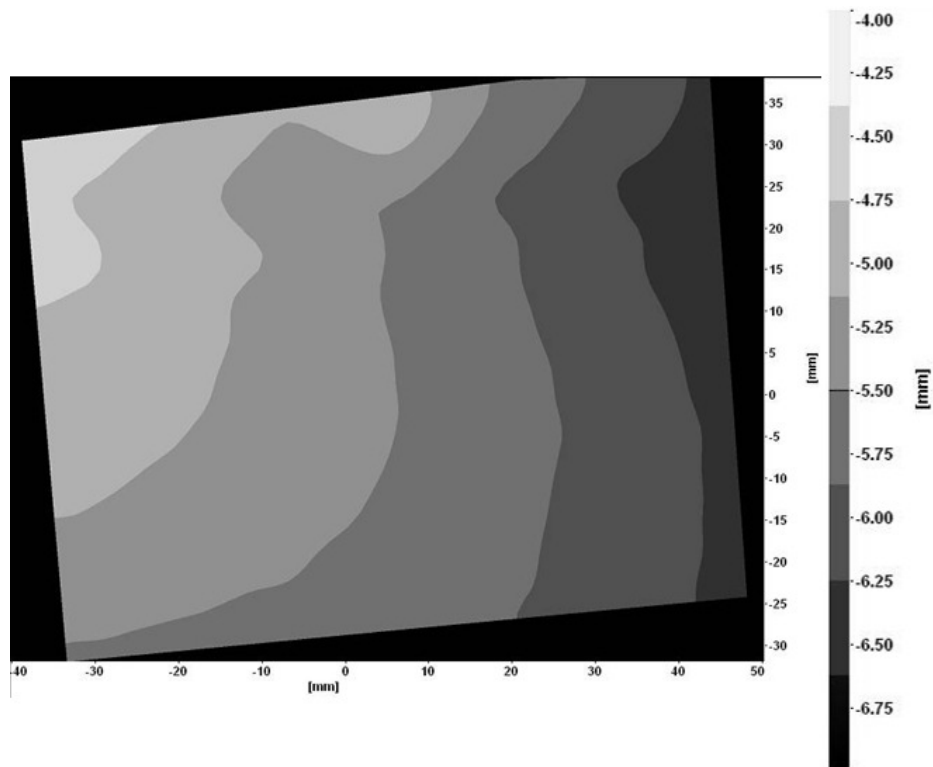


Figure 8.22: Surface height correlated with recommended surface pattern and reduced area of interest

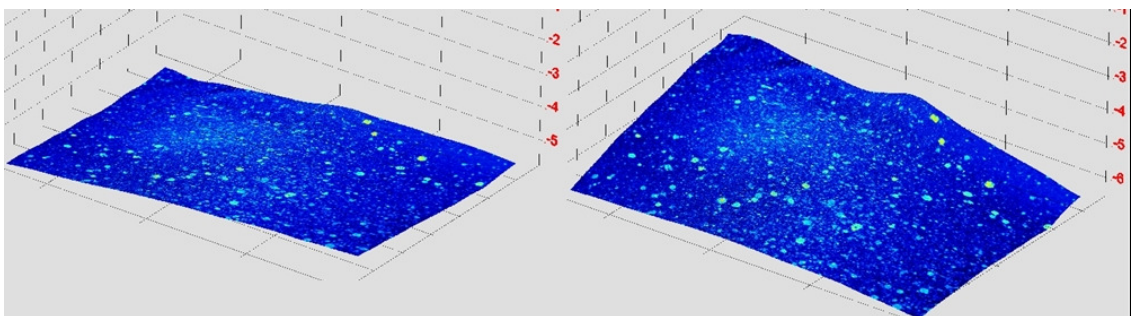


Figure 8.23: 3D representation of the measured panel's deformation with recommended pattern and reduced area of interest

This test used the same correlation pattern as the previous test, and as such there was not expected to be any significant differences in the measured out-of-plane deformations. Hence, the out-of-plane deformations are only included for completeness. The in-plane strains were correlated with the same two step process as in the previous test, with the same processing parameter combinations. Figure 8.24(a) shows the longitudinal strain correlated using a second process of 128×128 pixels with an overlap of 25 %, whilst Figure 8.24 shows the strain using 64×64 with 25 %. Both images show the same strain distribution as that predicted by the FE model, with a peak strain around the corner of the core. It was decided that the plot in Figure 8.24(b) was too noisy and, therefore, the strain calculated using 128×128 with 25 % was used to compare in more detail with the FE strain data. To provide a direct comparison between the DIC and FE data both were imported into Matlab and plotted on to regular mesh (see Appendix B for code). Initially the FE data was plotted on to a rough mesh of 10 by 15 points to compare to the number of data points measured using the DIC. The images at the top of Figure 8.25 show the raw DIC data and rough FE data with the same strain scale. The data from both DIC and FE were then interpolated on to a finer grid to offer a better indication of the strain distribution (see the bottom of Figure 8.25).

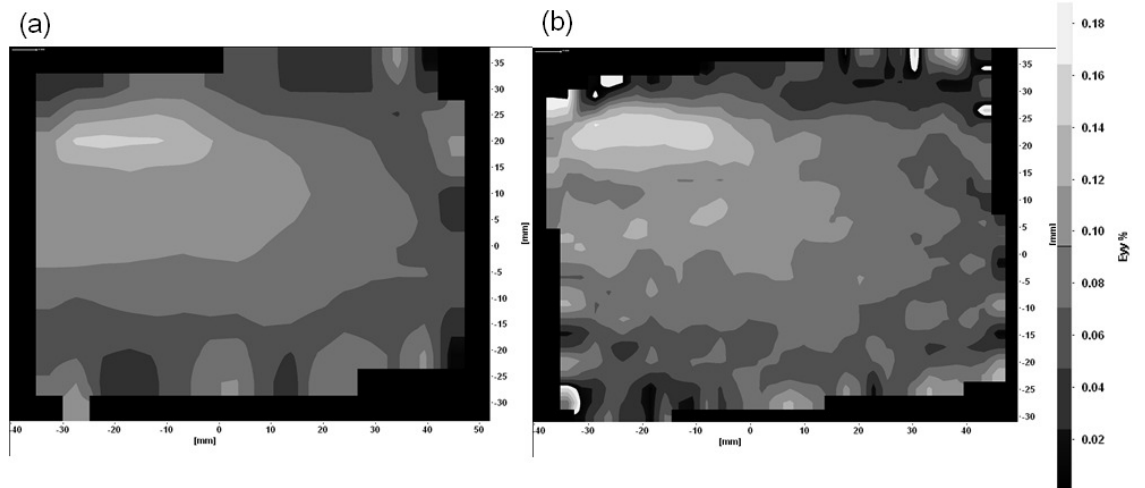


Figure 8.24: DIC strain map using recommended pattern and reduced area of interest using (a) 128×128 , (b) 64×64

The black lines on each of the images in Figure 8.25 show the same points. It is also important to note that the DIC image represents a smaller region than that of the FE image. From these images it is possible to see a good correlation between the FE and DIC data, however for closer inspection the strains along the black line is plotted for both data sets in Figure 8.26.

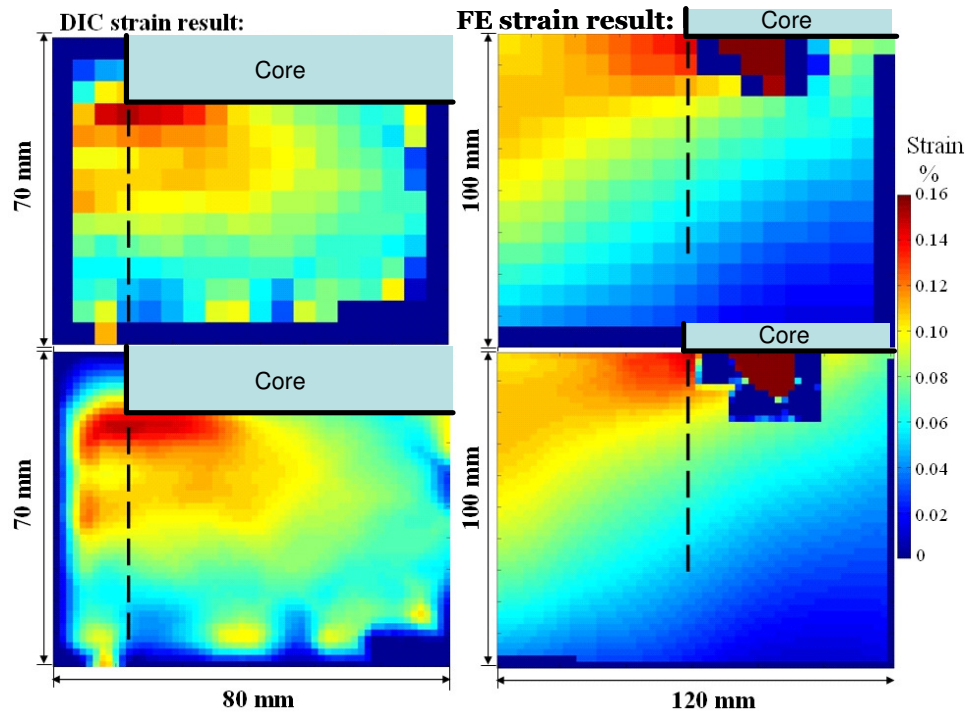


Figure 8.25: FE and DIC strain maps interpolated on to a regular grid for comparison

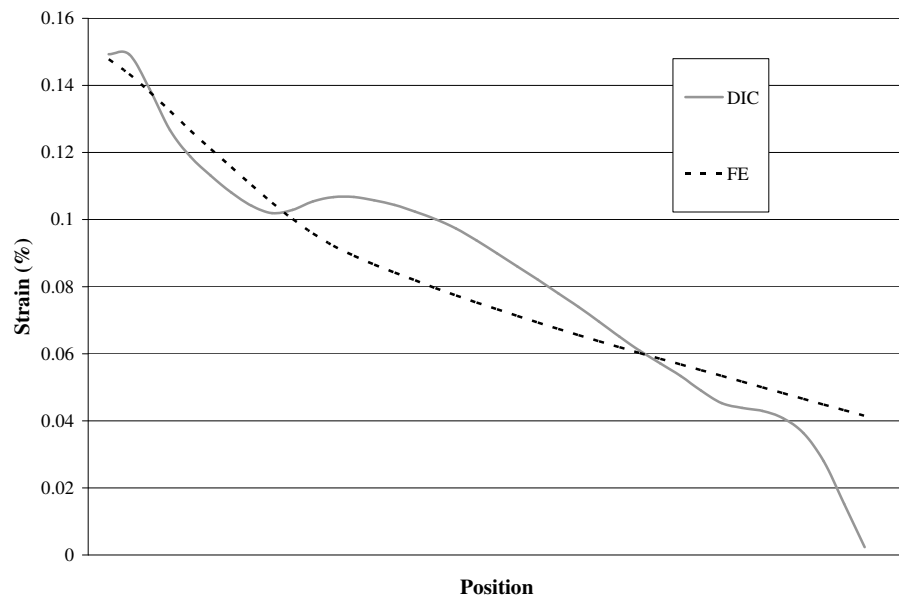


Figure 8.26: Line plot of FE and DIC strain along line in Figure 8.25 for comparison

Figure 8.26 shows good agreement between the DIC measurement and FE data. The DIC measures a peak strain of 1510 μ strain, whilst the FE predicts 1440 μ strain. Differences between these figures may be accounted for by either the spatial resolution of the DIC, or a slight offset of the position of the line taken for comparison.

8.6 Summary

DIC has been successfully applied to measure the response of a generic panel to a pressure load applied by the custom designed rig (see Chapter 7). Attempting a range of correlation routines, size of correlation cells and processing parameters has enabled the measurement of both the out-of-plane deformation and in-plane strain using DIC. The FE mode generated in Chapter 7 was used to obtain strain values in the same form as the DIC output. The FE prediction and the DIC output showed very good correlation. However, to obtain the necessary strain accuracy and resolution the DIC was only applied to a small region of the whole panel (approximately 80 mm by 60 mm) and during the feasibility test a number of challenges have been discovered for its use to provide full-field data of the larger structure. With a field of view of only 80 mm by 60 mm a minimum of 60 images will be required to measure the strain in the whole panel. Capturing and processing this large number of images would prove an onerous task and would be very time consuming. This would be exacerbated by the need to calibrate the system for every image as a calibration must be performed whenever the cameras are moved. With 60 image sets and 60 calibrations, full-field analysis of the generic panel could take in excess of 15 hours. It may be possible to improve the field of view, thereby reducing the required number of images, by the use of higher resolution cameras. However, the effect of the use of such cameras has not been investigated in this work.

A further issue with the LaVision system is the size of the interrogation cell required to obtain accurate strain. In this study cells of size 128 x 128 pixels were required, therefore across an image only 16 strain values were measured. This gives poor spatial resolution, and around complex features important detail may be missed. The choice of processing parameters is not intuitive, and hence for each new test, every combination must be tested to obtain the best results. This adds time to the processing of the tests and reduces the confidence in the results. Finally, when there is zero strain, the software does not register it as zero strain. Instead the software plots noisy data with regions of high and low strain. The FE plot of the full-field strain data (Figure 7.4) showed that large portions of the panel will have zero strain, which would not be validated by the DIC. When such noisy data is returned from the DIC it is difficult to infer whether this due to a lack of strain to be measured, or a bad correlation. This again reduces confidence in the results.

The results from the feasibility tests on tensile specimens and on the generic panel have shown promise, but a number of limitations of its use (particularly the LaVision system) have hindered its selection to measure the response from all the generic panels in this research. Therefore, another

full-field measurement technique, in the form of thermoelastic stress analysis (TSA), is to be tested for its feasibility in Chapter 9 and applied to the generic panels.

Chapter 9

9. Thermoelastic stress analysis (TSA)

9.1 Introduction

Thermoelastic stress analysis (TSA) [18] is a well-established, non-contacting technique for the evaluation of stresses in engineering components, e.g. [107] where an infra-red detector is used to measure the small temperature change associated with the thermoelastic effect. An important requirement for the successful application to a structure is the need for cyclic loading at a suitable frequency to ensure adiabatic conditions. The technique relies on the surface of the structure being free from reflection, especially in the infra-red part of the spectrum, and it must have an emissivity that is constant and relatively high [108]. The polymer composites considered in this thesis have a high emissivity, above 0.9, [109] and, therefore, this is not a concern. TSA has been successfully applied to composite structure in the past, e.g. to large wind turbine blades [110] and to a marine T-joint [111].

This chapter presents the full scale tests on the generic panels using each of the five MOs, the manufacture of which was discussed in Chapter 5. The panels were tested on the full scale test rig described in Chapter 7 and the response was measured using both a point measurement from a displacement transducer and using TSA as a full-field stress measurement technique. The results are used to validate a series of FE models produced by altering the initial model presented as part of the test rig design in Chapter 7. The first part of the Chapter discusses the TSA approach and its application to composite structure as a full-field stress measurement technique. The

experimental approach is followed by a presentation of feasibility tests of the use of the TSA technique to the composite materials considered in this thesis. This is done on simple tensile strips. The work then progresses to provide an approach for obtaining full-field data from an entire generic panel. This includes joining of separate images using Matlab code, and processing into a form that can be directly compared to the stress data from an FE model.

Once the TSA approach has been proven for use on composites and the generic panels, the FE models and their results are validated. The FE section presents models of each MO using two methods; first with the face sheets treated as quasi-isotropic homogenous orthotropic blocks and second by modelling the behaviour ply-by-ply. A panel that has face sheets of a cross-ply configuration is used to better understand the difference in deflection prediction between the homogeneous model and the ply-by-ply FE models for validation. The full-field data and displacement transducer measurements from each of the generic panels are compared with each other and the FE models. This provides the basis for the comparison of the performance of components manufactured using each of the MOs.

9.2 Brief overview of application of TSA

In current work a Cedip Silver 480M infra-red system (*Cedip Infrared Systems*) was used for application of TSA. The system comprises of an infrared camera with an InSb detector with 320 x 256 pixels at a pitch of 30 μm and allows frame rates between 5 and 380 Hz. The images are recorded and processed using AltairLi software (produced by Cedip). This system is radiometrically calibrated so it is possible to obtain the temperature changes directly that occur as a result of the thermoelastic effect and correct for any changes in the specimen temperature as described in [107]. A 'lock-in' signal from the test machine is used to synchronise the TSA measurement, and in this way the response of the structure from the loading can be averaged over a number of cycles and the accuracy improved (see Figure 9.1). The cyclic loading also provides pseudo adiabatic conditions.

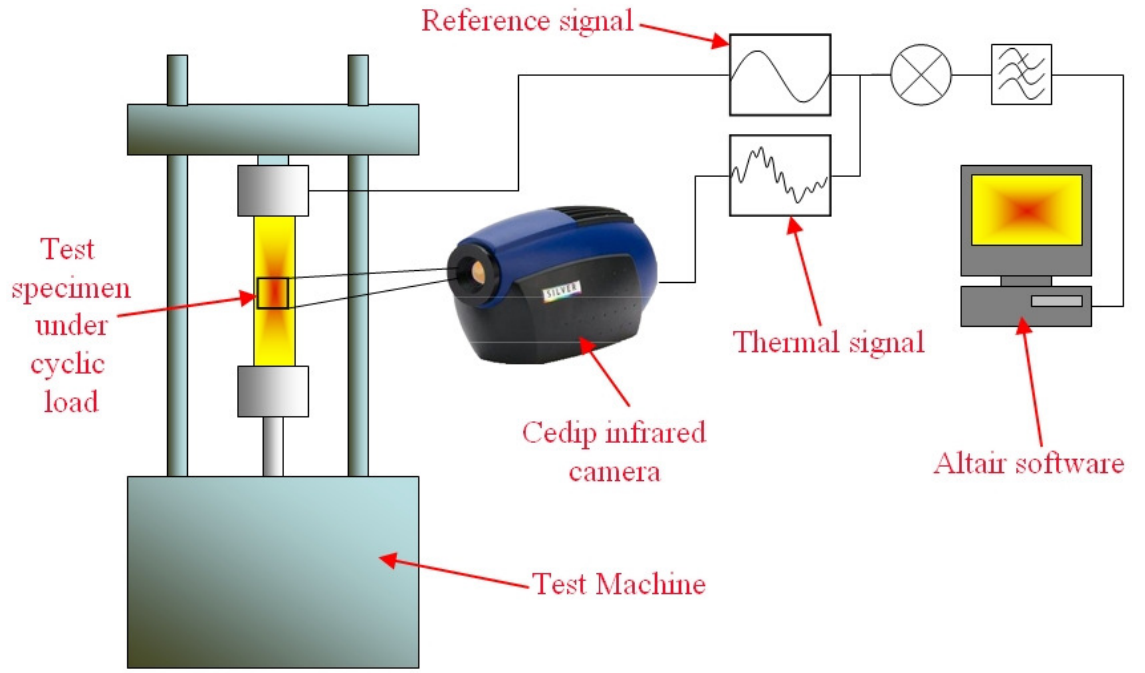


Figure 9.1: Schematic of application of TSA to test specimen

The output from the detector provides the change in surface temperature, ΔT , resulting from the change in the sum of the principal stresses on the surface of the material. For an orthotropic material, such as the composites considered in this thesis, ΔT can be related to the stresses in the material, σ_L and σ_T , as follows [111]:

$$\Delta T = -\frac{T}{\rho C_p} (\alpha_L \sigma_L + \alpha_T \sigma_T) \quad (9.1)$$

where α_L and α_T are the coefficients of linear thermal expansion in the longitudinal and transverse material directions, σ_L and σ_T are the stresses in these directions, ΔT is the change in temperature, T is the ambient temperature, ρ is the density and C_p is the specific heat at constant pressure. It is possible to combine the materials constants in this equation, i.e. α_L , α_T , ρ and C_p into two calibration constants K_L and K_T as follows [112]:

$$\Delta T = T (K_L \sigma_L + K_T \sigma_T) \quad (9.2)$$

where $K_L = \frac{\alpha_L}{\rho C_p}$ and $K_T = \frac{\alpha_T}{\rho C_p}$.

The advantage of the form of the relationship in Equation (9.2) is that it is not necessary to obtain the thermal and mechanical properties, but instead the values of thermoelastic constants, K_L and K_T , can be measured experimentally. The simple unidirectional stress state in tensile test specimens provides the ideal situation to measure the thermoelastic constants of a material. For the work described in this chapter, tensile strips with surface plies at 0° for K_L and at 90° for K_T are used.

9.3 Tensile feasibility tests

9.3.1 Strain measurement

Feasibility tests on tensile specimens were used to confirm the use of TSA on the composites considered in this thesis, in particular to confirm the suitability of the surface finish for the application of TSA. The composites were manufactured with peel ply between the panel and the release film, which provides a matt surface finish that will minimise reflections during testing. Tensile strips manufactured for the mechanical characterisation tests in Chapter 6 were used for each of the five MOs with a lay-up identical to the generic panel face sheets. The tensile strips were loaded using a servo-hydraulic Instron test machine under a mean load of 3.5 kN and cycled with an amplitude of 3 kN. Hence, the specimens were subjected to a range of load of 6 kN. It is known that a larger loading frequency would offer a more adiabatic condition, and it is recommended that a frequency of at least 10 Hz is applied [113, 114]. Initially, all the specimens were loaded at 10 Hz. Figure 9.2 shows the TSA image of each specimen, at 10 Hz. The first point to note is the response offered by the woven materials (i.e. MO 2 and 4) shown in Figure 9.2 (c) and (e). The individual tows provide significantly different changes in temperature with the transverse tow consistently offering a larger change than the longitudinal. This is either indicative of a non-uniform strain distribution or an artefact of the different material constants for the different tows. However, with this interesting response it was decided to include a TSA sample of the UD MO 1 material with its surface ply at 90° for comparison to the response of the transverse tows of the woven materials. The TSA image for MO 1 at 0° is practically uniform with a ΔT of 0.0351 °C. Figure 9.2 (b) shows the image of MO 1 with the surface ply at 90° and is also uniform, but has a significantly larger response of 0.1253 °C. Figure 9.2 (c) and (e) from the woven composites MO 2 and 4, respectively, show that the tows at 0° show a similar response to Figure 9.2 (a) and the tows at 90° are similar to Figure 9.2 (b). Figure 9.2 (d) and (f) are from the NCF of MO 3 and 5. These have uniform responses similar to the specimen MO 1 in Figure 9.2 (a), which is to be expected, but the stitching holding the individual plies together is evident in the image. This may be because resin has accumulated in the trough caused by the stitching (as seen in the microscope images in Chapter 6) or due to the different material used for the stitching.

It should be noted that the specimens were subjected to a constant applied stress of the same value. However, this is a global measure and the TSA provides values that are related to the stress in the surface ply. For a tensile specimen the ΔT can also be related to the strains in the principal material directions, i.e. ϵ_L and ϵ_T , as follows [115]:

$$\Delta T = -\frac{T}{\rho C_p} [(\alpha_1 Q_{11} + \alpha_2 Q_{12})\epsilon_L + (\alpha_1 Q_{12} + \alpha_2 Q_{22})\epsilon_T] \quad (9.3)$$

where a_1 and a_2 are the coefficients of linear thermal expansion in the surface ply principal material directions, Q_{11} , Q_{12} , and Q_{22} are the surface ply lamina stiffnesses, $Q_{11} = \frac{E_1}{1 - \nu_{12}\nu_{21}}$, $Q_{12} = \frac{\nu_{21}E_1}{1 - \nu_{12}\nu_{21}}$, $Q_{22} = \frac{E_2}{1 - \nu_{12}\nu_{21}}$, T is the ambient temperature, ρ is the density and C_p is the specific heat at constant pressure.

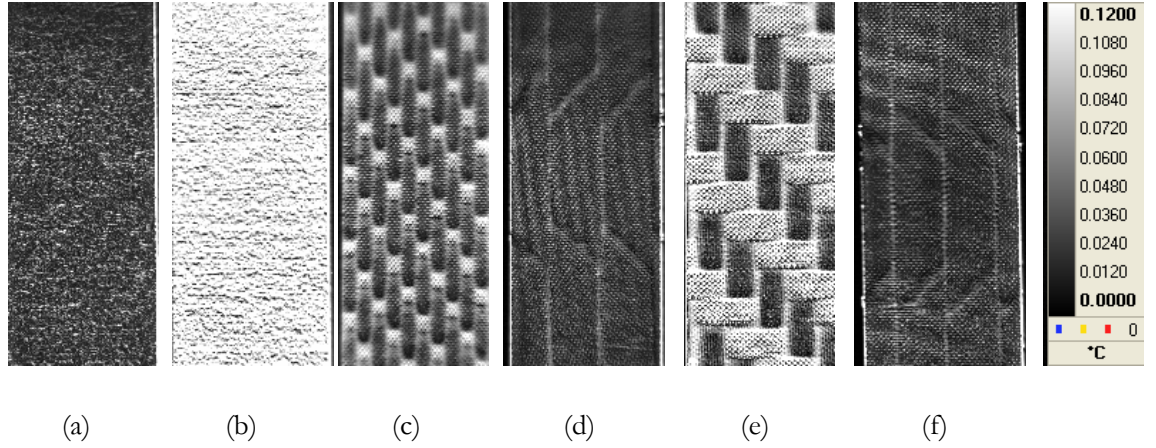


Figure 9.2: TSA images of tensile specimens; (a) M1 with surface ply at 0° , (b) M1 with surface ply at 90° , (c) M2, (d) M3, (e) M4, (f) M5

This approach relies upon complete and accurate knowledge of the thermal and mechanical properties of the materials being measured. To compare the response it was decided to obtain the strain sum in each specimen, which should be constant through the thickness and apply equation (9.3) to obtain a theoretical ΔT for each of the MOs. The cyclic stress applied to each specimen is known, therefore using a measured global Young's modulus, E_L , (from Chapter 6) for each material it was possible to calculate ε_L . The ε_T value was calculated by a measured value of ν_{LT} , again from Chapter 6. To calculate Q_{11} , Q_{12} and Q_{22} it was necessary to assume the individual tows had the same UD properties as the UD specimen for MO 1. From Chapter 6, the UD specimen of MO 1 had an E_1 of 134 GPa, E_2 of 8.99 GPa, ν_{12} of 0.316 and ν_{21} of 0.048. Hence, Q_{11} was calculated to be 136 GPa, Q_{12} as 6.53 GPa and Q_{22} as 9.13 GPa. Finally, the thermal constants were found from the literature; C_p of 1130 J/K °C [116], α_1 of $-0.9 \times 10^{-6}/^\circ\text{C}$ and α_2 of $27 \times 10^{-6}/^\circ\text{C}$ [1]. The values of coefficient of thermal expansion were selected to be representative of a carbon fibre with similar stiffness and strength. Table 9.1 shows the measured (m) and calculated (c) surface temperature changes for each specimen at a loading frequency of 10 Hz.

The measured change in temperature for MO 1 with 0° surface ply compares well with the calculated value, even though such low values are at the limits of the thermal resolution of the Cedip system. Similarly, the temperature change for MO 1 with 90° surface ply has excellent

agreement. In these two cases the material elastic properties in Equation (9.1) have been obtained using identical material, whilst the constants were estimated from the literature. For the woven materials MO 2 and 4 the temperature change ΔT_L differs by 23% and 36% respectively with the calculated value greater in both cases. ΔT_T for MO 2 and 4 are in much closer agreement, which suggests the estimation of the stiffness parameters based on UD material does not sufficiently model the longitudinal weave. The non-crimp fabrics MO 3 and 5 have a larger error in measured and calculated temperature change of almost 40%. It is noteworthy that in all cases the experimental values of ΔT_T , the greater temperature, are within 16% of each other.

Table 9.1: Comparison of the measured temperature change at 10 Hz against calculated

Spec	$\Delta\sigma$	E_L	ν_{LT}	ε_L	ε_T	$\varepsilon_L + \varepsilon_T$	ΔT_L		ΔT_T	
	MPa	GPa					m	c	m	c
MO1 0°	122.8	48.7	0.086	0.0025	0.00022	0.00274	0.0335	0.0307	n/a	n/a
MO1 90°	124.4	50.4	0.149	0.0024	0.00037	0.00284	n/a	n/a	0.1388	0.1002
MO2 QI	116.5	47.1	0.262	0.0024	0.00065	0.00312	0.0426	0.0472	0.1169	0.1028
MO3 QI	113.2	44.5	0.317	0.0025	0.00081	0.00335	0.0327	0.0540	n/a	n/a
MO4 QI	105.7	42.2	0.241	0.0025	0.00060	0.00310	0.0355	0.0457	0.1119	0.1037
MO5 QI	112.8	45.2	0.32	0.0025	0.0008	0.0033	0.0326	0.0533	n/a	n/a

It was considered that the difference in longitudinal values could be caused by non-adiabatic conditions. To investigate this, the loading frequency was varied. Tests were performed at frequencies of 1, 2, 5, 15, 20 and 30 Hz. These were considered for MO 1, with surface plies at both 0° and 90°, and the two woven materials MO 2 and 4, i.e. where data was available for longitudinal and transverse ply directions. Figure 9.3 shows plots of the longitudinal and transverse experimental data from the three specimens along with the ΔT calculated from Equation (9.3). In all cases the longitudinal experimental data decreases over a range of 0-20 Hz and similarly the transverse data increases over the frequency range 0-20 Hz and then becomes constant. This is clearly showing that at low frequencies the response from the materials cannot be considered to be adiabatic. It is interesting that only in MO 1 in the longitudinal direction the agreement between the adiabatic data and the calculated data is close. The discrepancy in the transverse value points, perhaps, to error in the value of α_2 obtained from the literature. In Figure 9.3(b) the longitudinal direction values agree at 10 Hz only. In the transverse direction the data does not agree at all. A similar trend is seen for MO 4 in Figure 9.3(c). This indicates that not only are the material properties incorrect for the calculated values but the simple model given by

Equation (9.3) is not valid and the woven nature of the material is providing additional mechanical and thermal effects. It is thought that because MO 2 has a tight weave even at 20 Hz some heat transfer occurs between the tows. For MO 4, the large weave means reduced heat transfer and therefore the measured values become constant from 15 Hz and above.

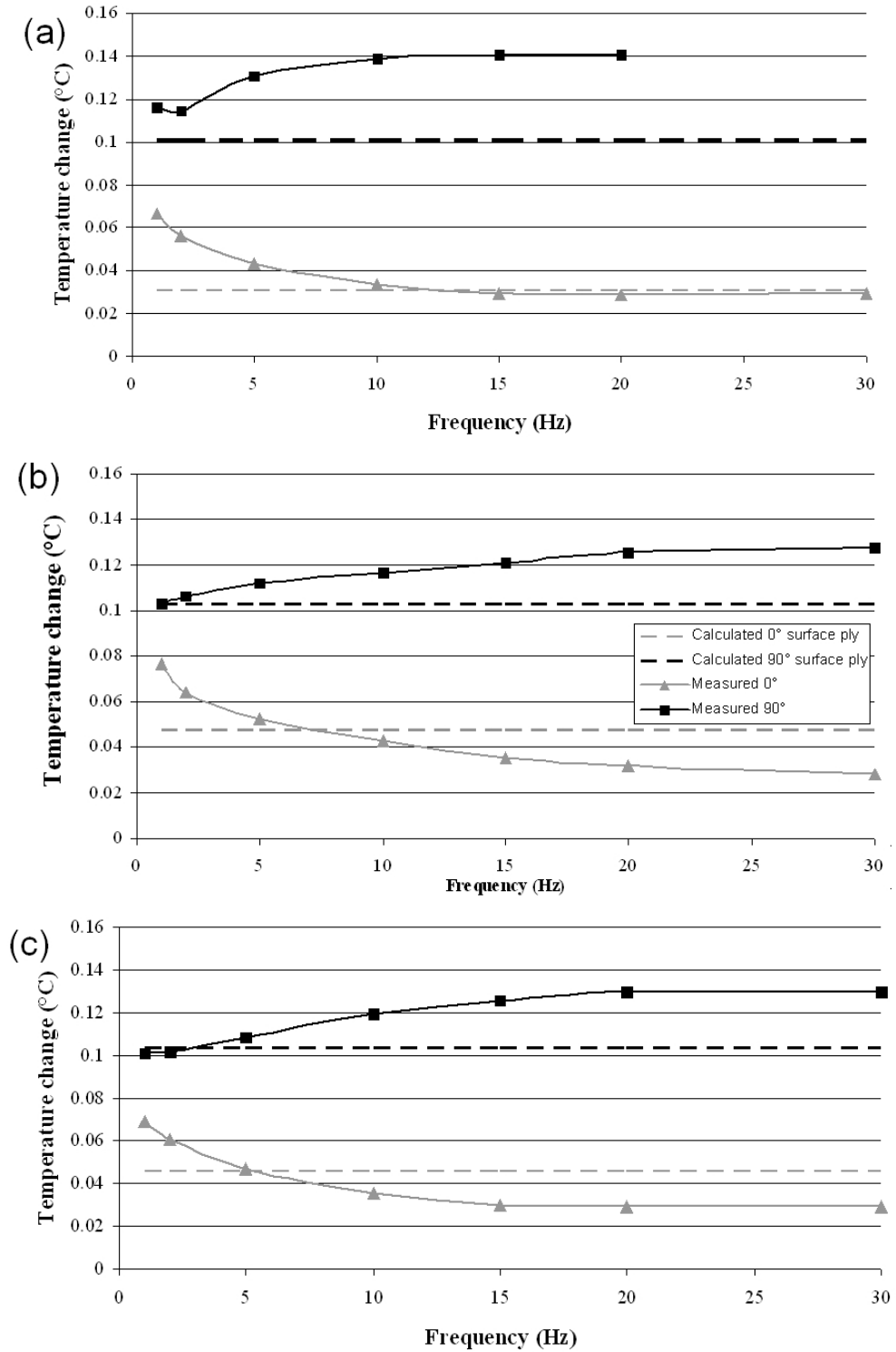


Figure 9.3: Graphs of measured and calculated temperature changes for (a) MO 1, (b) MO 2, (c) MO 4

The results of initial feasibility of obtaining the strains on the material surface by use of Equation (9.3) have demonstrated the difficulty of the application to orthotropic materials. This method of relating the temperature change to strains relies upon complete and accurate thermal and mechanical properties for the material to be tested. It is particularly difficult to measure properties for the woven composites, and this is confirmed by the comparison between measured and calculated temperature change.

9.3.2 Experimental calibration

To overcome the need for extensive and accurate measurement of thermal and mechanical properties it was decided to utilise Equations (9.2) and (9.3). By using the same tensile testing technique, it is possible to use the unidirectional stress state in the laminate to measure K_L and K_T independently. The calibration constants should be measured during tests at the same loading frequency expected to be used in the final full field test. The results in the previous section show that adiabatic conditions cannot be achieved at less than 15 Hz. However, it would be impossible to load at this rate using the test rig. Therefore, it was decided to use the 1 Hz loading frequency for the TSA work in the rig. As epoxy has a low thermal conductivity it was considered that this might be practical and the applied pressure range of 0.01 MPa (1.5 psi) could be achieved at this frequency.

The calibration constants were measured from tensile strips manufactured from all five MOs. The mean applied load was 3.5 kN with an amplitude of 3 kN. To provide the calibration constants for the full scale tests the tensile strips were cycled at 1 Hz, and to offer an idea of the quality of this data the strips were also cycled at 10 Hz. Figure 9.4 shows the TSA images of all materials with surface plies at 0° (defined as longitudinal) and 90° (defined as transverse) and under loading frequencies of 1 and 10 Hz. The response from MO 1, 3 and 5 materials types are similar and, therefore, it is clear that both materials are responding in a similar manner when subjected to the same load. It is important to note the difference in response between the longitudinal specimens and the transverse specimens. The longitudinal specimens show an average change in temperature of between 0.03 and 0.05 °C and the transverse specimens show a change of temperature between 0.12 and 0.14 °C. It is also of interest that in the TSA images from MO 3 and 5 the loose stitches, which hold the non-crimp fibres together before infiltration, can be discerned. It is considered that the stitches are visible because they are produced from a different material than the rest of the specimen or because of the resin build up. The average of the change in temperature from each specimen was used to calculate the thermoelastic constants shown in Table 9.2. On average the thermoelastic ‘constants’ change by between 30 and 40 % when the loading frequency is changed from 1 to 10 Hz. The longitudinal responses decrease when the loading frequency is increased, and the transverse response increases. This is a clear indicator that the response of the material at

1 Hz is not adiabatic and there is influence from the stress induced temperature change from the subsurface plies. Nevertheless, it was decided to use the thermoelastic constant derived at 1 Hz to calibrate the response from the panels. There is a further complication when considering the calibration of woven materials MO 2 and 4; the woven pattern also allows an opportunity for in-plane non-adiabatic behaviour. The stresses in the longitudinal and transverse components of the weave will be different, hence ΔT will be different, providing the mechanism for the in-plane heat transfer. This is particularly noticeable at 1 Hz, where the response from both components of the weave is similar. At 10 Hz the response is clearly different and close to that seen in the UD material at 10 Hz and clearly indicates a non-adiabatic response. However, the weave patterns are small in comparison to the size of the generic panel and, therefore, it was decided to use the average signal across the tensile strip. The overall thermoelastic constants for the woven materials show a smaller difference between the longitudinal and transverse constants than the UD and non-crimp fabrics. The five harness satin in MO 2 does not have equal tows in the longitudinal and transverse directions and this explains the difference in K_L and K_T . However, MO 4 has a similar fibre count longitudinally and transversely and hence $K_L \approx K_T$.

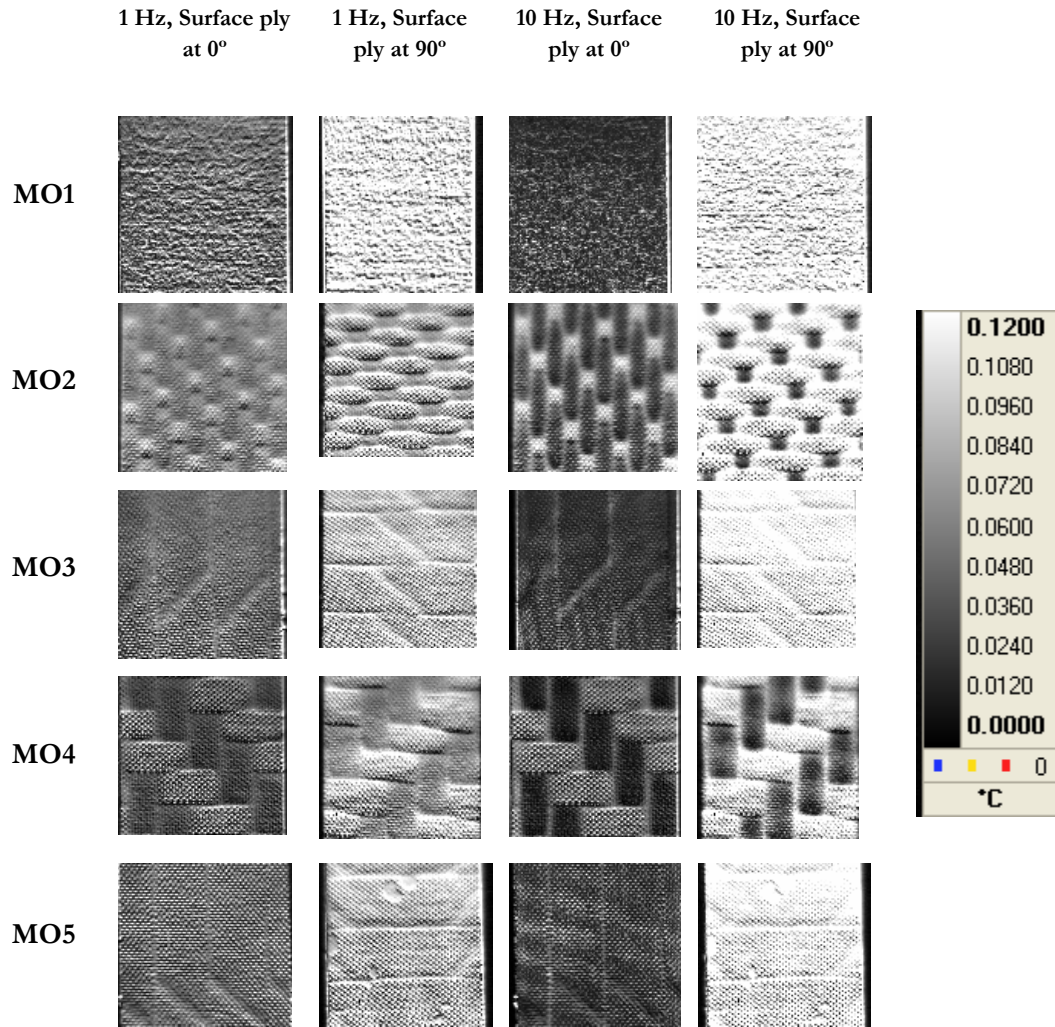


Figure 9.4: TSA images to measure the calibration constants for each of the MOs

Table 9.2: TSA calibrations constant K_L and K_T for the five Mos

Material	K_L at 1 Hz ($\times 10^{-6}$) MPa $^{-1}$	K_T at 1 Hz ($\times 10^{-6}$) MPa $^{-1}$	K_L at 10 Hz ($\times 10^{-6}$) MPa $^{-1}$	K_T at 10 Hz ($\times 10^{-6}$) MPa $^{-1}$
MO1	1.592	3.112	0.969	3.5
MO2	1.85	2.511	1.56	3.168
MO3	1.44	2.909	0.982	4.188
MO4	2.59	2.412	2.64	2.598
MO5	1.58	2.837	0.981	3.914

The calibration constants measured in the work described in this section will be used to process both the TSA and FE data into a form that can be directly compared. This process will be described in the next section.

9.3.3 Full scale experimental approach

The generic panels were loaded on the test rig designed in Chapter 7. The response to the pressure applied to each of the generic panels was measured at a single point using a displacement transducer (because the DIC was shown to be infeasible for total scanning) and with the TSA. The point measurement is made using a LVDT displacement transducer at the region where the maximum out-of-plane deformation was predicted by the FE model (see Chapter 7 and the next section). This corresponds to a point on the unconstrained edge approximately 160 mm from the front of the panel (here the front is the extended flange area). The displacement is recorded as the panel is loaded up to 0.02 MPa (3 psi).

Once displacement measurement was recorded, TSA was used to image the entire surface of the panel. The cyclic tests in Chapter 7 confirmed the test rig was capable of producing the type of consistent cycle that is necessary to perform TSA. The panels were subjected to a mean load of 0.01 MPa (1.5 psi) and then loaded in displacement control with 3 mm amplitude. This imparts a range of pressure of approximately 0.01 MPa (1.5 psi) to the panel; the loading frequency was 1 Hz.

The Cedip camera was attached to the same large stand used in the DIC work (Chapter 8). The stand allowed the vertical position of the camera to be held while movement of the arm in the horizontal plane allows easy scanning of the surface of the panel. Each TSA image was 320 x 256 pixels and to obtain adequate resolution of the stresses within the panel it was necessary to obtain

32 separate images by scanning across the surface. With this many images a pixel represented between 0.3 and 0.5 mm on the panel. Reference points were applied to each panel using a pencil, as the graphite lead provides a different response to the panel in the infra-red. These reference points act as a guide to match the images while joining them together. The images are analysed manually to find the joining lines. Then the images are imported into Matlab (see Appendix B) as an array of temperature change values, one for each pixel. The arrays are then joined along the predefined joining lines using Matlab code developed for this purpose (see Appendix B).

The full field TSA data was processed into a form that can be compared with the FE. This is done by rearranging Equation (9.3) as follows:

$$\frac{\Delta T}{TK_L} = \Delta \sigma_L + \frac{K_T}{K_L} \Delta \sigma_T \quad (9.4)$$

TSA **FE**

The TSA data is calibrated using K_L and then it is necessary to obtain σ_L and σ_T separately from the FE model. The stresses from the FE model are summed with a factor applied to the σ_T of K_T/K_L .

9.4 FE Models

Further to the initial FE model described in Chapter 7, individual models were constructed to accommodate the mechanical properties and final cured thickness of each MO. The models were produced, initially, with the face sheets treated as homogeneous orthotropic blocks and mechanical properties of a quasi-isotropic (QI) lay-up measured by the mechanical characterisation test in Chapter 6. Then a second model was produced for MO 1, 2 and 4 with the face sheets formed from the individual plies with lamina properties from Chapter 6. The models used honeycomb properties from Chapter 7. The models are loaded with a pressure of 0.01 MPa (1.5 psi) to match the pressure range applied during TSA measurement. Table 9.3 shows the thickness used for the model of each MO, and the maximum deflection predicted by each.

For a complete comparison between the predicted deflections it is necessary to use the results from the homogenous models. The FE model predicts the generic panel manufactured using MO 1 deflects the most, with a value of 7.7 mm, and MO 4 deflects the least, at 6.77 mm. The panels modelled using MO 3 and 5 also show significant reduction in maximum deflection, to 6.89 mm. However, it is noteworthy that the panels made using MO 3, 4 and 5 are also thicker than MO 1. In fact, the percentage of reduction in maximum deflection matches the percentage of increase in thickness. There is also a large difference between the predicted deflections between the models

using homogenous face sheets and those given by the ply-by-ply model. The difference is approximately a 30% reduction in deflection from the homogenous model to the ply-by-ply model.

Table 9.3: Predicted maximum deflection for each MO

Face sheet material	Total face sheet thickness (mm)	Max deflection (mm) homogeneous model	Max deflection (mm) ply-by-ply
MO 1	3.2	7.7	5.7
MO 2	3.4	7.1	4.8
MO 3	3.56	6.89	n/a
MO 4	3.73	6.77	4.7
MO 5	3.53	6.89	n/a

It was concluded that the homogenous model is not correctly modelling the coupling that is present in the actual laminate configuration. To investigate this further, it was decided to analyse the simplest case (i.e. MO 1) to avoid complications of weave. The full lay-up including core was calculated for stiffness matrices A, B and D using classical laminate theory (CLT) [1]. The stiffness matrices relate the stresses and strains as follows:

$$[\sigma] = \begin{bmatrix} A & B \\ B & D \end{bmatrix} \times [\epsilon] \quad (9.5)$$

The stiffness matrices for the homogenous model, are as follows:

$$\begin{aligned} A &= \begin{bmatrix} 1.4879 \times 10^{11} & 1.8961 \times 10^9 & 0 \\ 1.8961 \times 10^9 & 1.539 \times 10^{11} & 0 \\ 0 & 0 & 2.0169 \times 10^{10} \end{bmatrix} \\ B &= \begin{bmatrix} 0 & 0 & 0 \\ 0 & 0 & 0 \\ 0 & 0 & 0 \end{bmatrix} \\ D &= \begin{bmatrix} 6.6956 \times 10^{12} & 8.246 \times 10^{10} & 0 \\ 8.246 \times 10^{10} & 6.9285 \times 10^{12} & 0 \\ 0 & 0 & 9.0667 \times 10^{11} \end{bmatrix} \end{aligned} \quad (9.6)$$

The stiffness matrices for the ply-by-ply model are as follows:

$$\begin{aligned}
 A &= \begin{bmatrix} 1.7102 \times 10^{11} & 4.7052 \times 10^{10} & 0 \\ 4.7052 \times 10^{10} & 1.7102 \times 10^{11} & 0 \\ 0 & 0 & 6.1141 \times 10^{10} \end{bmatrix} \\
 B &= \begin{bmatrix} 0 & 0 & 0 \\ 0 & 0 & 0 \\ 0 & 0 & 0 \end{bmatrix} \\
 D &= \begin{bmatrix} 8.1086 \times 10^{12} & 2.1401 \times 10^{12} & 6.6238 \times 10^{10} \\ 2.1401 \times 10^{12} & 7.3137 \times 10^{12} & 6.6238 \times 10^{10} \\ 6.6238 \times 10^{10} & 6.6238 \times 10^{10} & 2.7735 \times 10^{12} \end{bmatrix}
 \end{aligned} \tag{9.7}$$

The A matrix contains extensional stiffnesses (in-plane laminate moduli) that relate to in-plane loads and in-plane strains. Therefore, differences found in the A matrix will be insignificant for the bending dominant load situation considered in this work. The B matrix contains coupling stiffnesses, which relate to curvatures and moments to in-plane strains. Therefore, if non-zero values are found in the B matrix, in-plane forces produce flexural and twisting deformations. However, because the lay-ups are symmetrical, the B matrices are all zero as expected. Finally, the D matrix contains bending and flexural laminate stiffnesses relating moments to curvature. The D matrix shows the major difference between the two types of FE model. The D matrix for the homogeneous model has zero values for torsion coupling stiffness, whilst for the ply-by-ply model these stiffnesses have significant values. This accounts for the lower deflection evident in the individual ply model. To confirm this conclusion the FE models were repeated with a cross ply lay-up that is known to have no coupling. In a cross-ply material the value of torsion coupling stiffness in matrix D for both homogeneous and ply-by-ply models is zero. For the homogeneous model the stiffness matrices are:

$$\begin{aligned}
 A &= \begin{bmatrix} 2.1795 \times 10^{11} & 6.963 \times 10^8 & 0 \\ 6.963 \times 10^8 & 2.1795 \times 10^{11} & 0 \\ 0 & 0 & 2.0169 \times 10^{10} \end{bmatrix} \\
 B &= \begin{bmatrix} 0 & 0 & 0 \\ 0 & 0 & 0 \\ 0 & 0 & 0 \end{bmatrix} \\
 D &= \begin{bmatrix} 9.8498 \times 10^{12} & 2.7737 \times 10^{10} & 0 \\ 2.7737 \times 10^{10} & 9.8498 \times 10^{12} & 0 \\ 0 & 0 & 9.0667 \times 10^{11} \end{bmatrix}
 \end{aligned} \tag{9.8}$$

For the ply-by-ply model of the cross-ply the stiffness matrices are:

$$\begin{aligned}
 A &= \begin{bmatrix} 1.0779 \times 10^{11} & 3.1841 \times 10^9 & 0 \\ 3.1841 \times 10^9 & 1.0779 \times 10^{11} & 0 \\ 0 & 0 & 9.9 \times 10^9 \end{bmatrix} \\
 B &= \begin{bmatrix} 0 & 0 & 0 \\ 0 & 0 & 0 \\ 0 & 0 & 0 \end{bmatrix} \\
 D &= \begin{bmatrix} 4.9297 \times 10^{12} & 0.1452 \times 10^{12} & 0 \\ 0.1452 \times 10^{12} & 4.9032 \times 10^{12} & 0 \\ 0 & 0 & 4.5153 \times 10^{11} \end{bmatrix}
 \end{aligned} \tag{9.9}$$

As can be seen from Equations (9.8) and (9.9) the torsional stiffness terms are zero in both models. FE models of the cross ply laminate were built and provided a prediction of the maximum out-of-plane deflection of 7.112 mm for the homogeneous model and 7.126 mm for the ply-by-ply model. This goes some way to explaining the difference in the predicted deflections for the two different model types and demonstrates that it is essential to build a ply-by-ply model to avoid conservative prediction of deflection. It is for this reason that in all of the following work the ply-by-ply model will be validated using a deflection measurement. FE models will be validated by the point displacement measurement and the full-field stress sum derived from TSA data. The results from the cross ply model will also be confirmed using a generic panel test.

The second part of the panel analysis and FE validation depends upon a comparison of measured stresses from TSA and predicted stresses from FE models, as described in section 9.3.3. The stress state predicted by a typical FE model (using MO 1) is presented for both the longitudinal and transverse directions in Figure 9.5. Apart from the stresses imparted by the boundary, the major stresses predicted by the FE model are around the top left corner of the core in the images. This stress concentration is dominated by the longitudinal stress, although it is still slightly evident in the transverse plot, and is tensile up to a peak of approximately 75 MPa. The stresses around at the boundary are generally compressive and towards the left and right of the panel are dominated by longitudinal stress, whilst at the bottom edge they are dominated by transverse stress. At the boundary the stress peaks at a compressive value of approximately 100 MPa. The majority of the panel, particularly that stiffened by the core, has small stresses, between 25 MPa compressive and tensile, in both the longitudinal and transverse directions. The TSA will be used to validate the overall stress distribution predicted by the FE model, and will then concentrate on confirming the value of stress around the core corner.

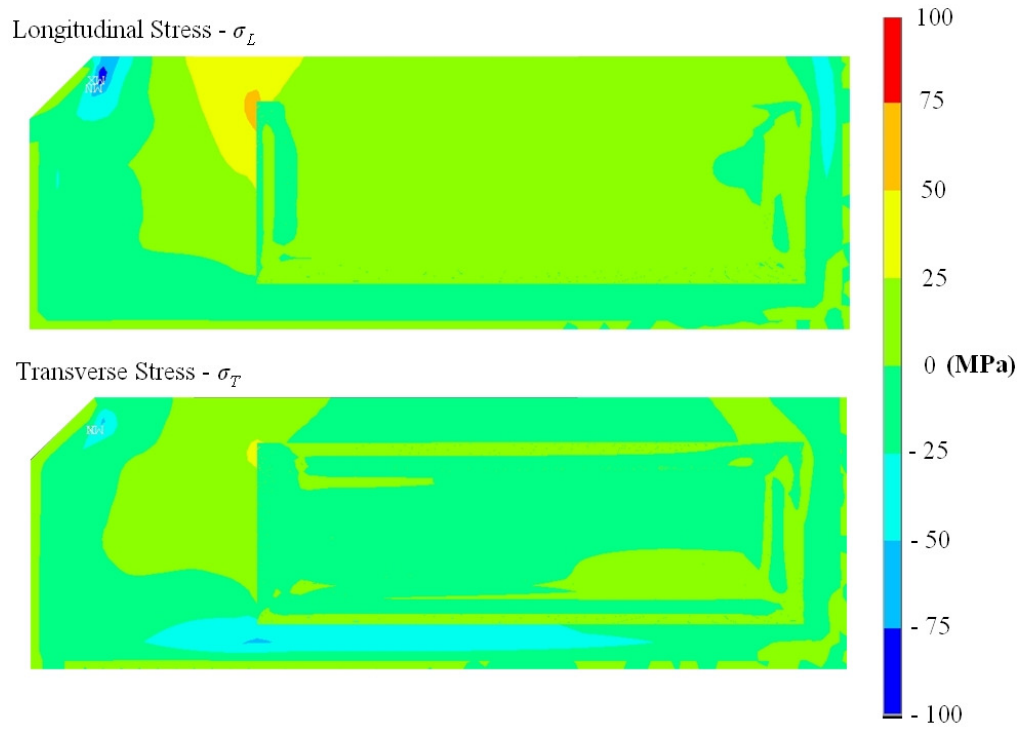


Figure 9.5: Predicted longitudinal and transverse stresses from FE model

The FE model data was processed into the form given by Equation (9.4) using calibration constants obtained in section 9.3.2 for comparison to the experimental data presented in the next section. Figure 9.6 shows the processed stress data for both the homogeneous and ply-by-ply models of MO 1.

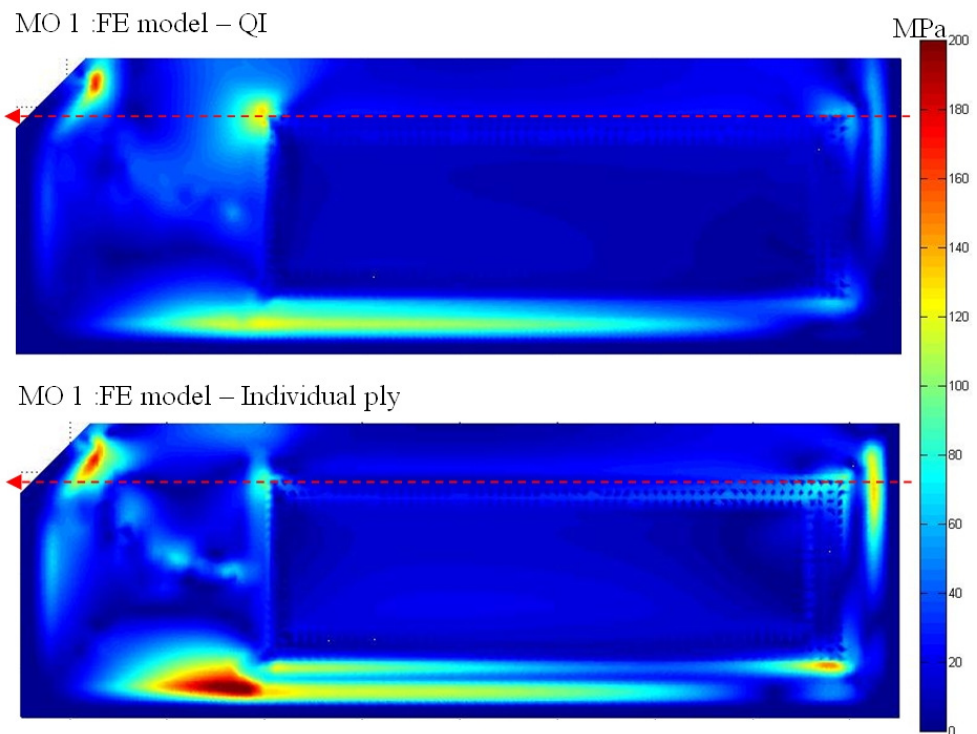


Figure 9.6: Processed stress data from FE models using both homogeneous and ply-by-ply face sheet models

The stress data from the two different types of FE model show similar differences between the homogeneous and ply-by-ply approach for the deflection predictions. A line of stress data has been taken along the dashed red line on both the plots in Figure 9.6. These plots are shown Figure 9.7. The ply-by-ply model has a different stress distribution to the homogeneous model, and appears to be more effected by the boundary.

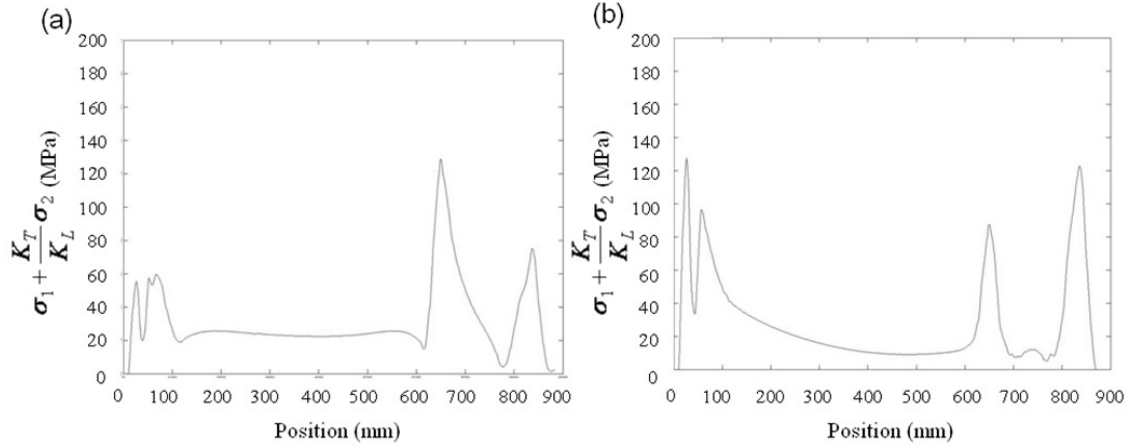


Figure 9.7: Lines of stress from (a) homogenous model (b) ply-by-ply model

As the calibration constants were obtained for the global response of the material, i.e. taking stress in the entire laminate as a basis, the homogeneous model will provide values that are comparable with the calibrated TSA data. The following images show the processed FE stress data from the rest of the models. Figure 9.8 shows the processed, predicted stress data from MO 2, Figure 9.9 shows the processed, predicted stress data from MO 4 and Figure 9.10 shows the processed, predicted data from MO 3 and 5 (where an individual ply model was not possible). From qualitative observations of the QI FE model predictions it appears the response under pressure for panels manufactured from MO 1, 3 and 5 are similar. The stress concentration around the corner of the core appears to be reduced by the model of materials MO 2 and 4. However, it is unclear if this is an effect of the material or an artefact of the calibration method applied to the woven structure in section 9.3.2. It will still be possible to validate the model of MO 2 and 4 with the TSA data, as the same calibration approach is applied to the TSA plot. This does raise complications with the use of the TSA full-field technique when applied to materials with varying surface properties, such as woven composites. In Section 9.5 full-field TSA data will be used to validate the processed stress sum plots from the homogeneous FE models and also provide a comparison between the different MOs.

MO 2 :FE model – QI

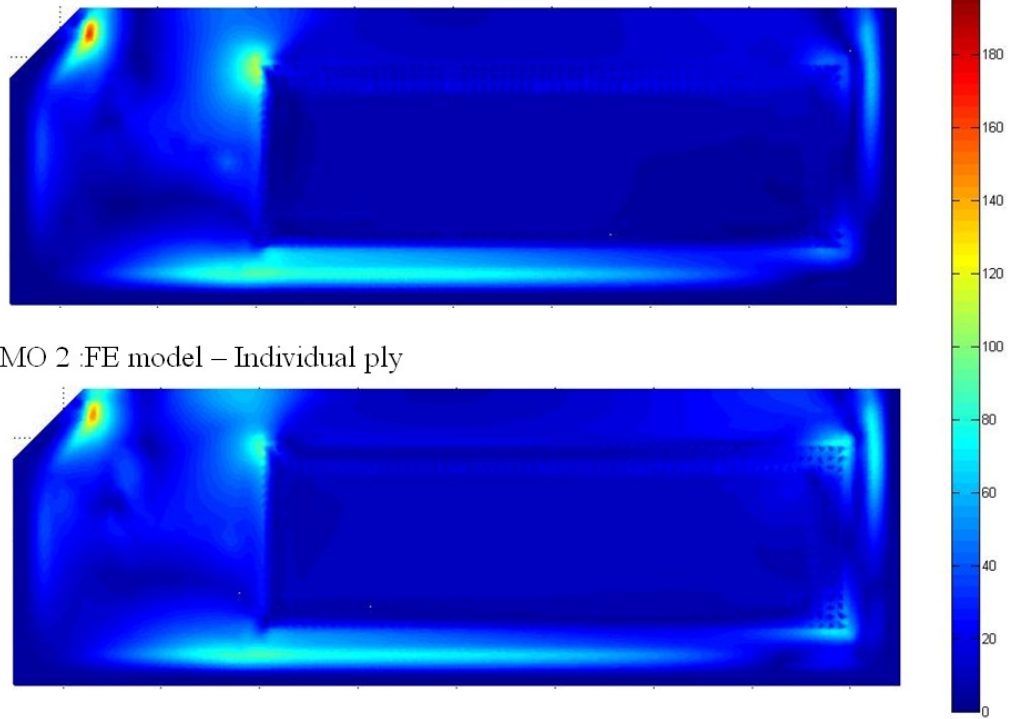


Figure 9.8: Processed stress data for MO2 from FE models using both homogenous and ply-by-ply face sheets

MO 4 :FE model – QI

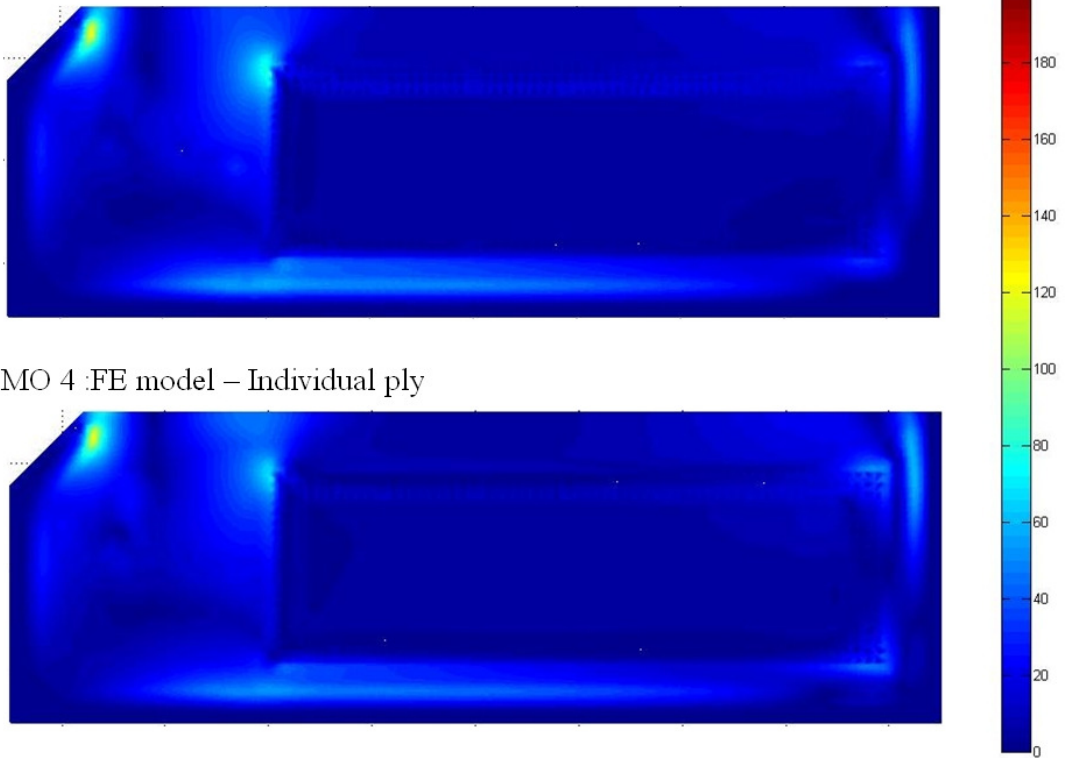
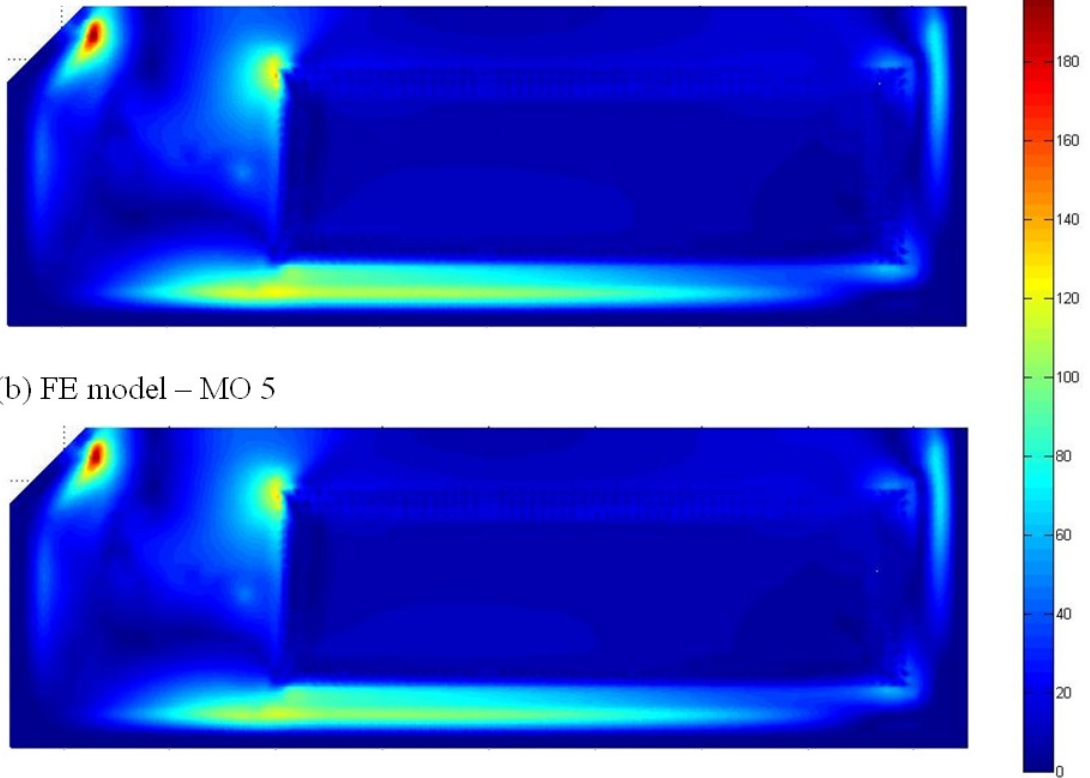


Figure 9.9: Processed stress data for MO4 from FE models using both homogeneous and ply-by-ply face sheets

(a) FE model – MO 3



(b) FE model – MO 5

Figure 9.10: Processed stress data for (a) MO3 and (b) MO5, from homogeneous FE models

9.5 Comparison of generic panels

9.5.1 Maximum deflection results

The initial comparison between panels and validation of FE models is performed on point measurements of out-of-plane deflections. These were measured as described in Section 9.3.3. Measuring the maximum deflection of the crossply panel provided a maximum deflection of 7.032 mm at 0.01 MPa (see Figure 9.11) which agrees well with the homogeneous model, 7.112 mm, and the ply-by-ply model, 7.126 mm. Therefore, it has been shown that both models can provide accurate deflection predictions when the ply configuration provides no coupling in the stiffness matrices. Therefore, it was expected that the experimental results from the other panels should validate the ply-by-ply deflection data.

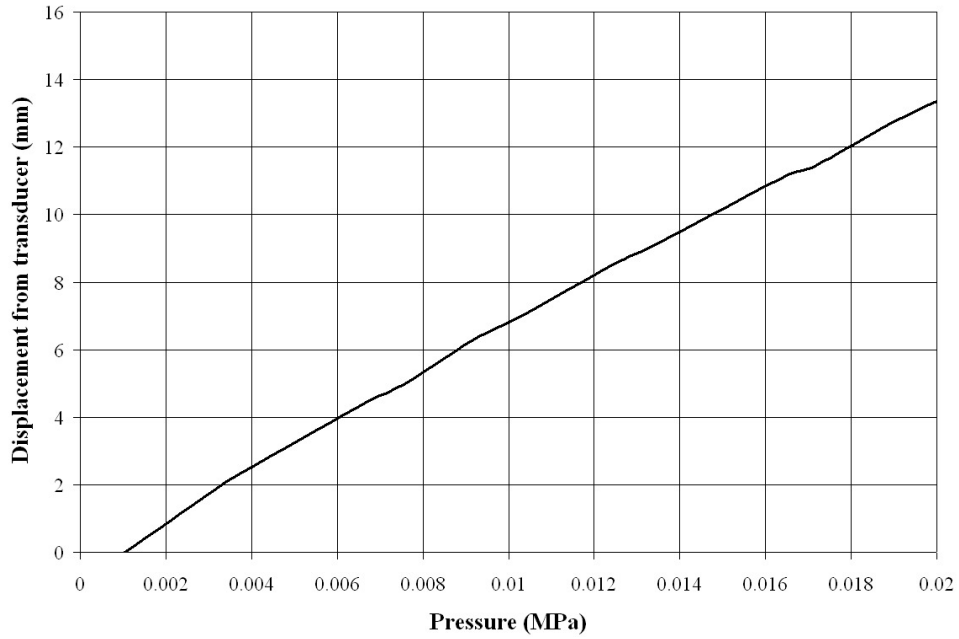


Figure 9.11: Maximum displacement from transducer for crossply panel

Figure 9.12 shows the deflection data for panels manufactured using MO 1 up to an applied pressure value 0.02 MPa (3 psi). The lines for each of the five panels produced in this way show a consistent maximum deflection, and at 0.01 MPa (the applied pressure in the FE models) there is less than 0.7 mm between them, and show an average value of 6.34 mm with a standard deviation of 0.3 mm. The individual ply model for MO 1 estimated a maximum deflection of 5.7 mm; this proves to be an underestimate of almost 10%, whilst the QI model overestimates by a more significant 20%.

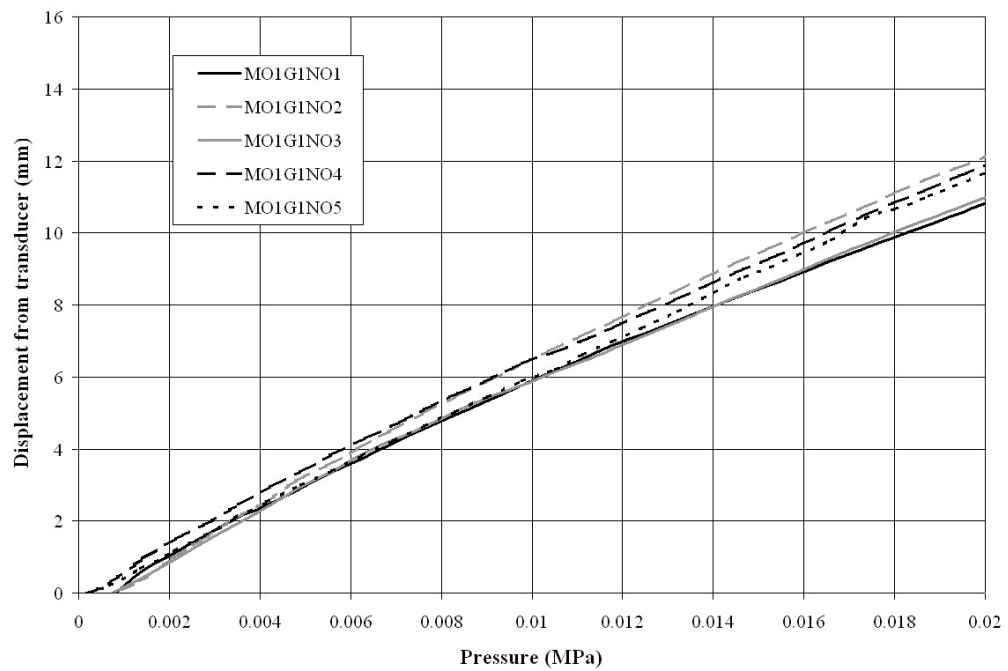


Figure 9.12: Maximum displacement from transducer for panels made from MO 1

Figure 9.13 shows the deflection data for panels produced using MO 2. Only the two without core crush were tested, but both offered deflection values that are consistent with each other. At 0.01 MPa the panels produced using MO 2 show an average maximum deflection of 5.41 mm (no standard deviation is given as this would be meaningless when considering just two values). The ply-by-ply FE model underestimates the deflection, again, by 10%. The homogeneous model overestimates by almost 25%. When compared to the deflection of MO 1 panels we find a reduction of bending by 15%. This is a significant result, even when taking into account the 5% increase in thickness of laminate when changing the material from MO 1 to MO 2, and may be explained by an out-of-plane effect of the weave in MO 2.

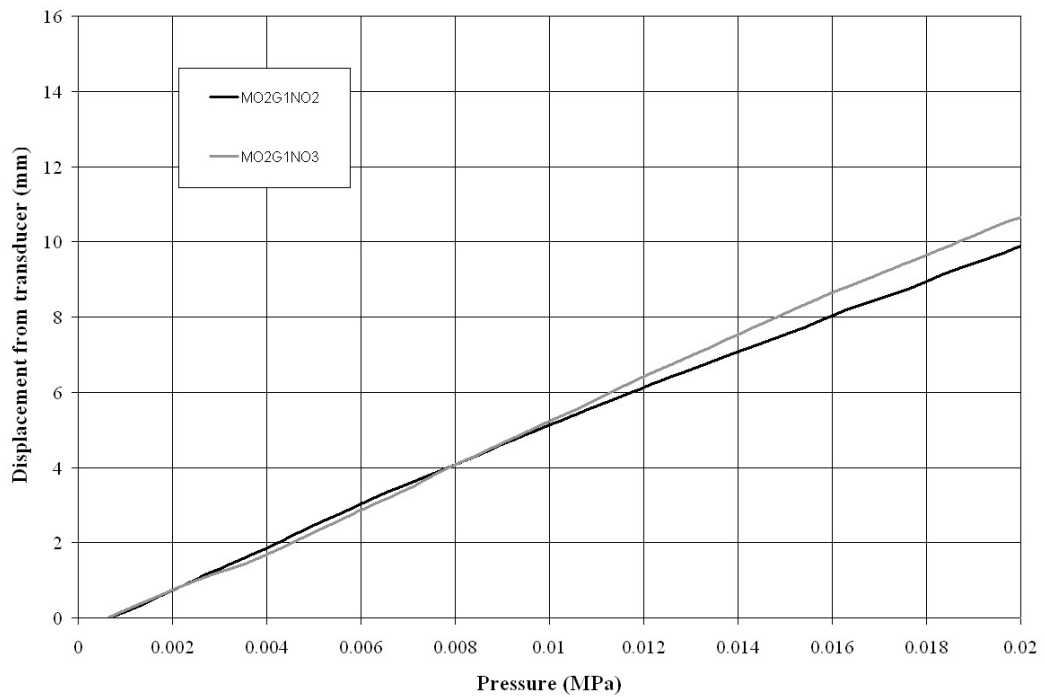


Figure 9.13: Maximum displacement from transducer for panels made from MO 2

Figure 9.14 shows maximum deflections from generic panels manufactured from MO 3. The consistency of the manufacturing approach is again proven, and at 0.01 MPa the average value of deflection is 5.13 mm, with a standard deviation of 0.4 mm. Due to the nature of the non-crimp fabric it was not possible to produce an individual ply FE model, but the QI FE model over estimates the deflection by more than 25%. Comparing the deflections of panels manufactured by MO 3 to the baseline process, MO 1, we find a reduction of almost 20%. It should be noted that there is some increase in the thickness of the panels produced using MO 3, however this not of the same order as the apparent increase in flexural stiffness.

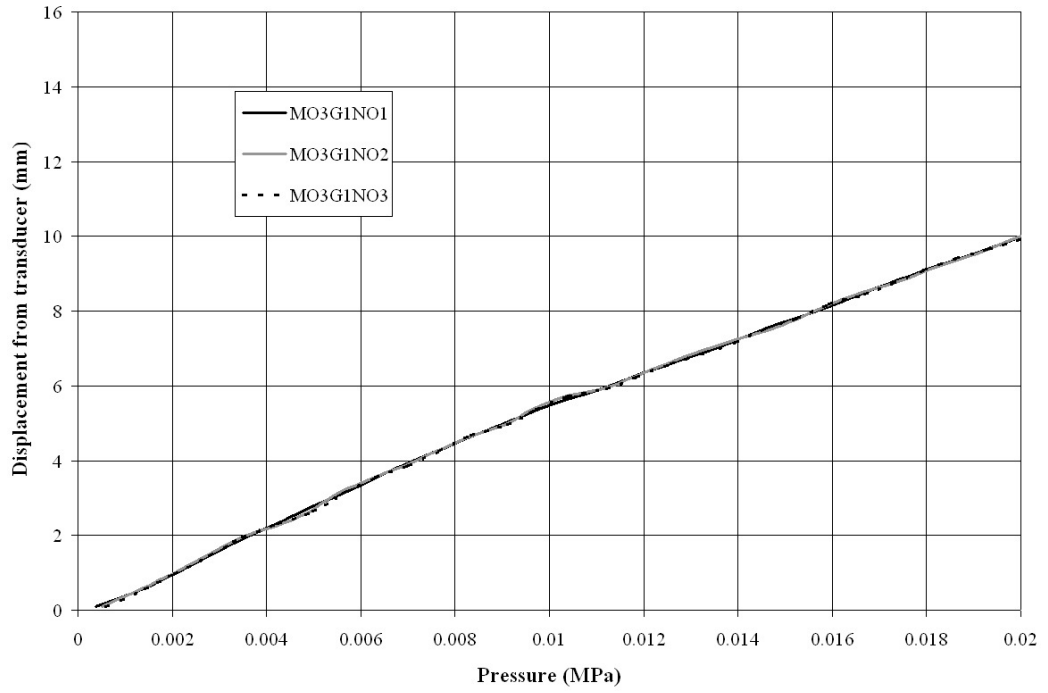


Figure 9.14: Maximum displacement from transducer for panels made from MO 3

Figure 9.15 presents the deflection data for MO 4. An applied pressure of 0.01 MPa provides an average deflection of 4.84 mm, with a standard deviation of 0.26. This is surprisingly well predicted by the individual ply FE model with an under estimation of only 3%. It is a surprising result that the FE model of a woven composite, with no account taken for the effect of weave, produces the most accurate prediction of panel deformation.

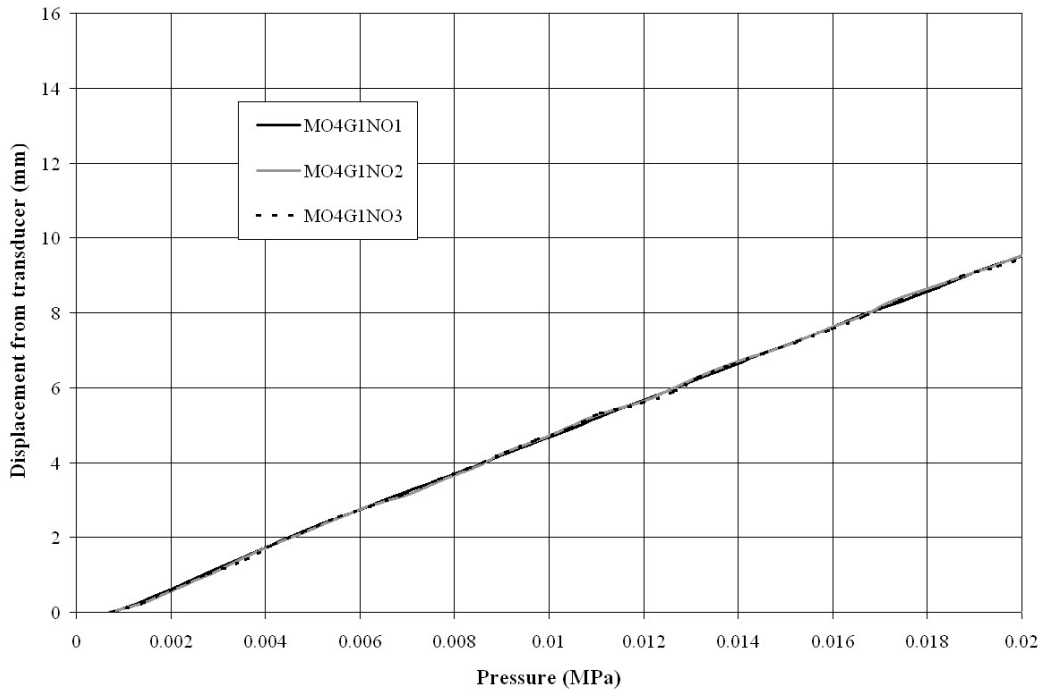


Figure 9.15: Maximum displacement from transducer for panels made from MO 4

Finally, the deflection results from panels produced using MO 5 are shown in Figure 9.16. At 0.01 MPa the maximum deflection from the three panels is 4.6 mm, with a standard deviation of 0.36 mm. By using the non-crimp fabric infiltrated using RFI in a conventional oven the maximum deflection was reduced by 27% over the baseline process, MO 1. Such a large reduction in deformation is significant, and could be due to the stitching in the NCF. Table 9.4 summarises the deflection results from the panels manufactured using the five MOs and the predicted deflections from both the homogeneous and ply-by-ply models. It is evident that the agreement between the crossply (CP) data is almost exact, it is also clear that the ply-by-ply model provides the best match. Furthermore, it can be seen that the NCF and out-of-autoclave process produces the least deflection. The next step is to compare the stress responses from panels produced by the five MOs to investigate if the promising result from the deflection data is mirrored in the stress fields.

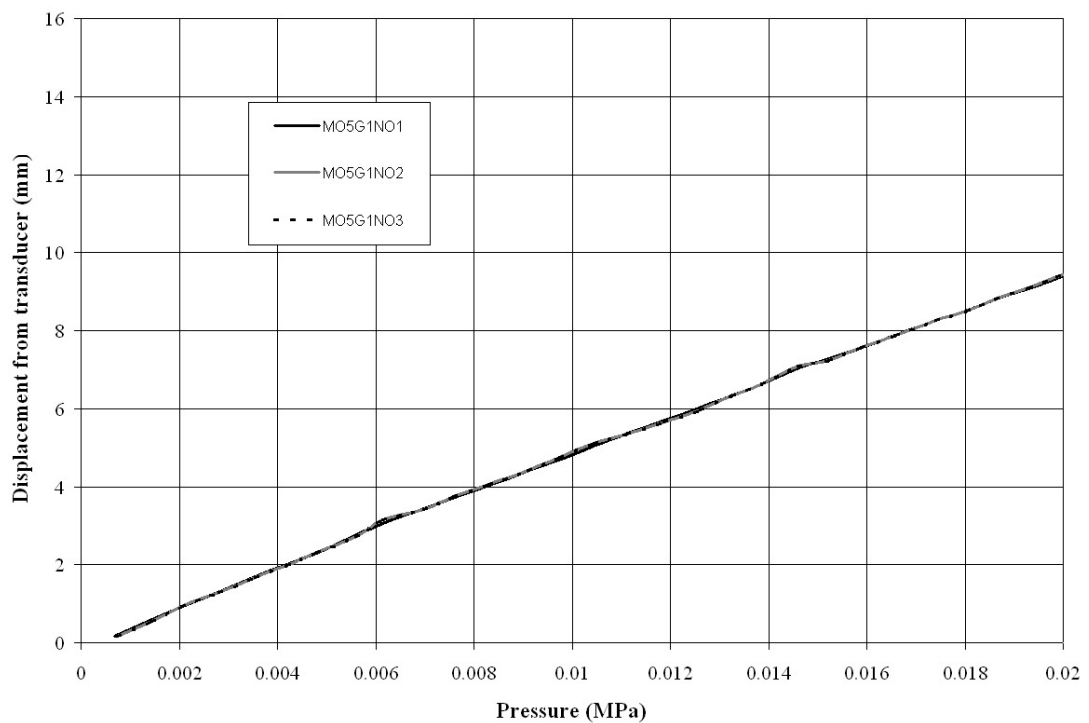


Figure 9.16: Maximum displacement from transducer for panels made from MO 5

Table 9.4: Experimental and FE deflections of panels produced using the five MOs

MO	Maximum deflection (mm)	Maximum deflection (mm)	Experimental (mm)
	Homogeneous model	Ply-by-ply model	
CP	7.112	7.126	7.032
1	7.7	5.7	6.34 ± 0.3
2	7.1	4.8	5.41
3	6.89	n/a	5.13 ± 0.4
4	6.77	4.7	4.84 ± 0.26
5	6.89	n/a	4.6 ± 0.36

9.5.2 Full-field TSA results

To further assess the response of the different panels to the pressure load, TSA was applied as described in Section 9.3.3. The processed TSA was manipulated into a form that can be directly compared to FE models, described in Section 9.4. Figure 9.17 contains an example of processed TSA images of panels MO1, Figure 9.18 contains an example of processed TSA images of MO 2, Figure 9.19 contains an example from MO 3, Figure 9.20 contains an example from MO 4 and finally, Figure 9.21 contains an example of MO5. From a qualitative appraisal of these images, it is clear that MO 1 offers the ‘best’, noise free, plot whilst the others suffer from some artefacts of the form of material. MO 2 and 4 show fluctuations due to the weave of the composite, whilst the stitches in MO 3 and 5 are evident as expected from the tensile tests described in Section 9.3.2. In all images, the brighter circles around the perimeter of the panels are the metal penny washers used to counteract the stress raiser around the attachment holes. On top of the core the two rows of rectangular patches at regular intervals are used to assist in the image joining process described in Section 9.3.2.

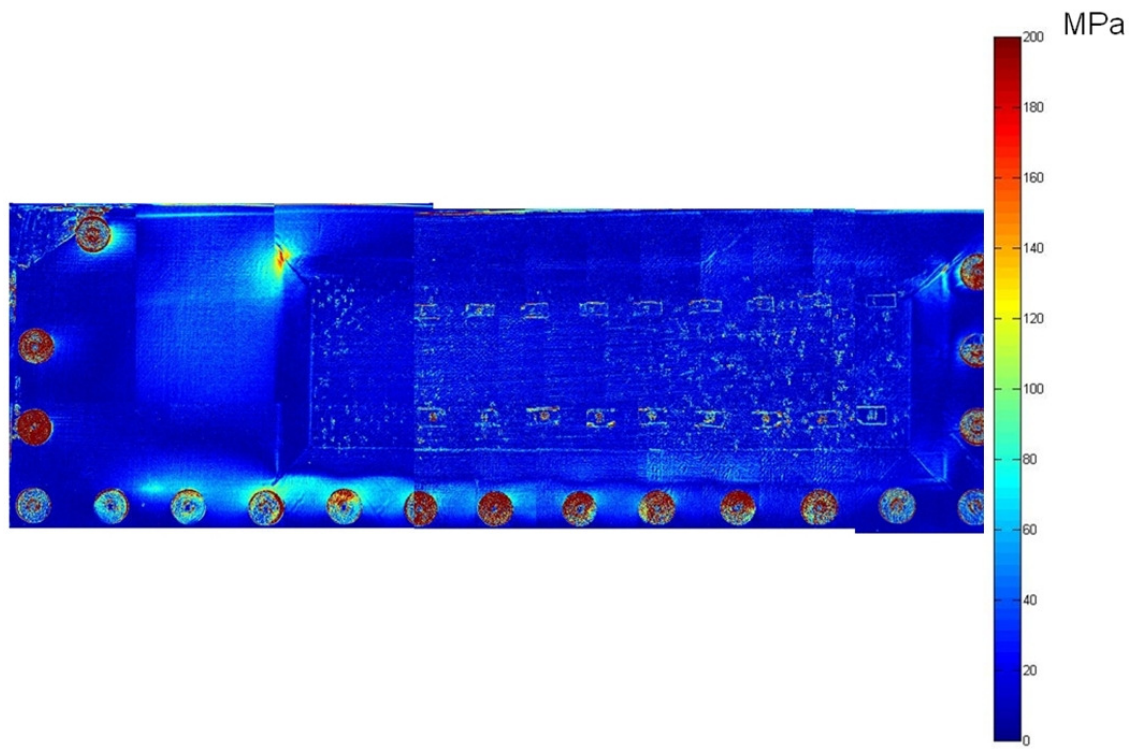


Figure 9.17: Example of full-field data from MO1

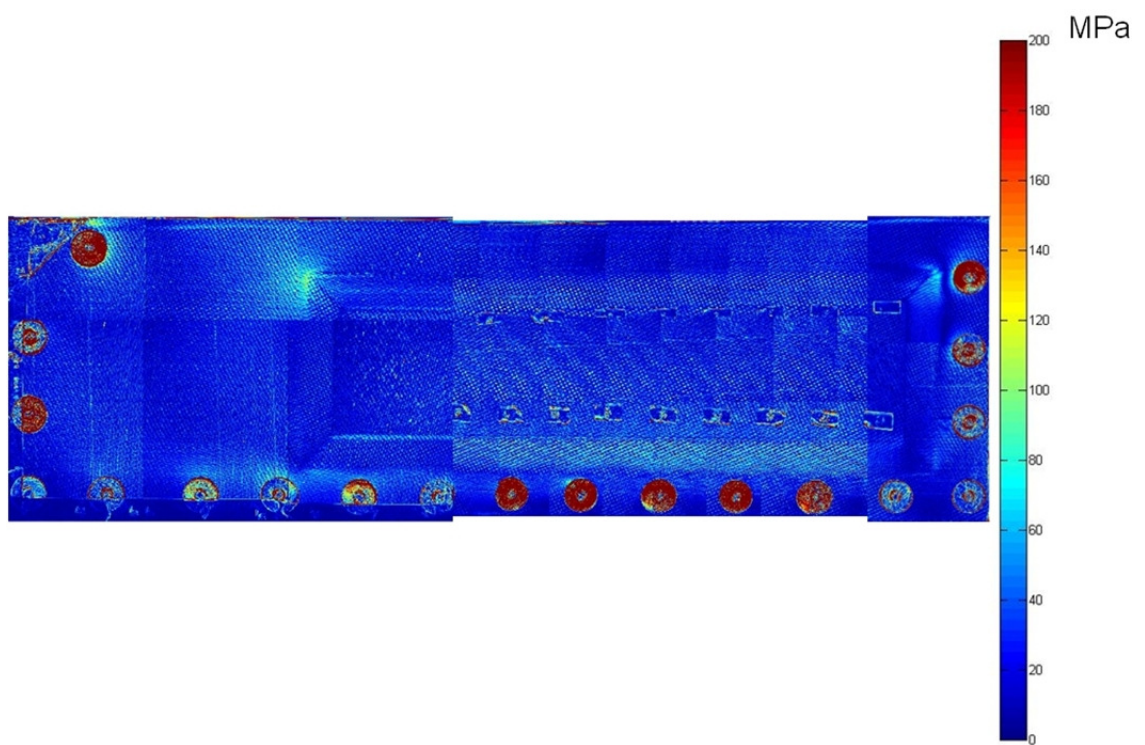


Figure 9.18: Example of full-field data from MO 2

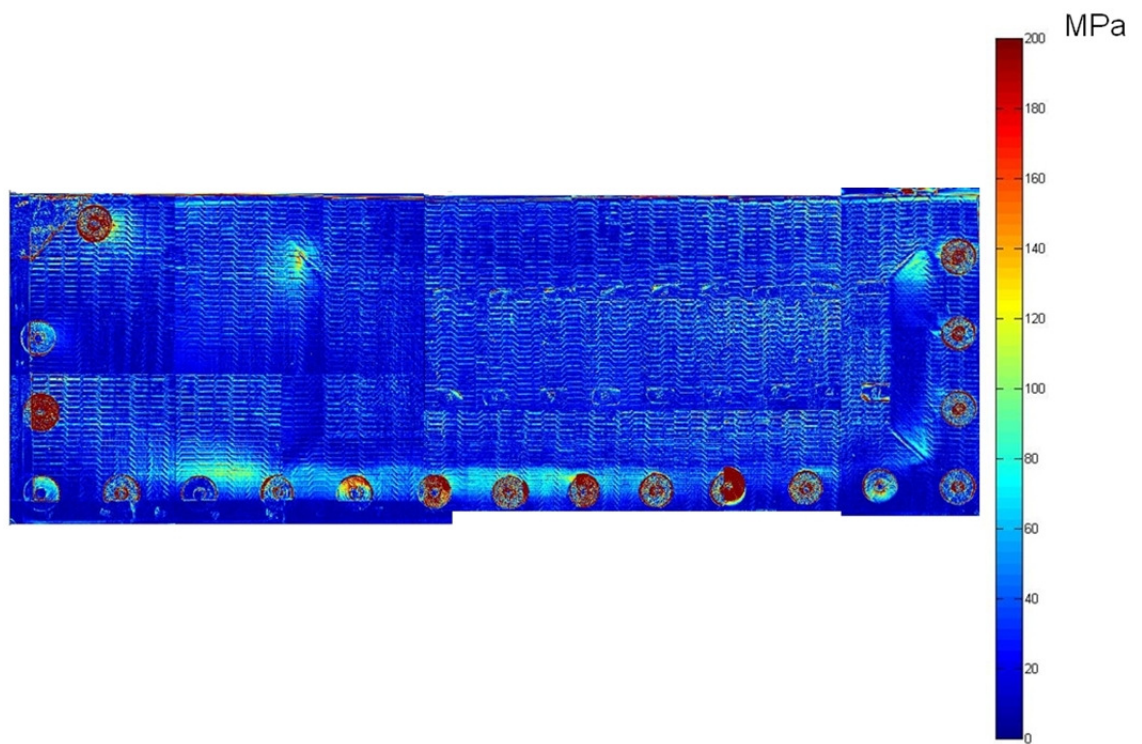


Figure 9.19: Example of full-field data from MO 3

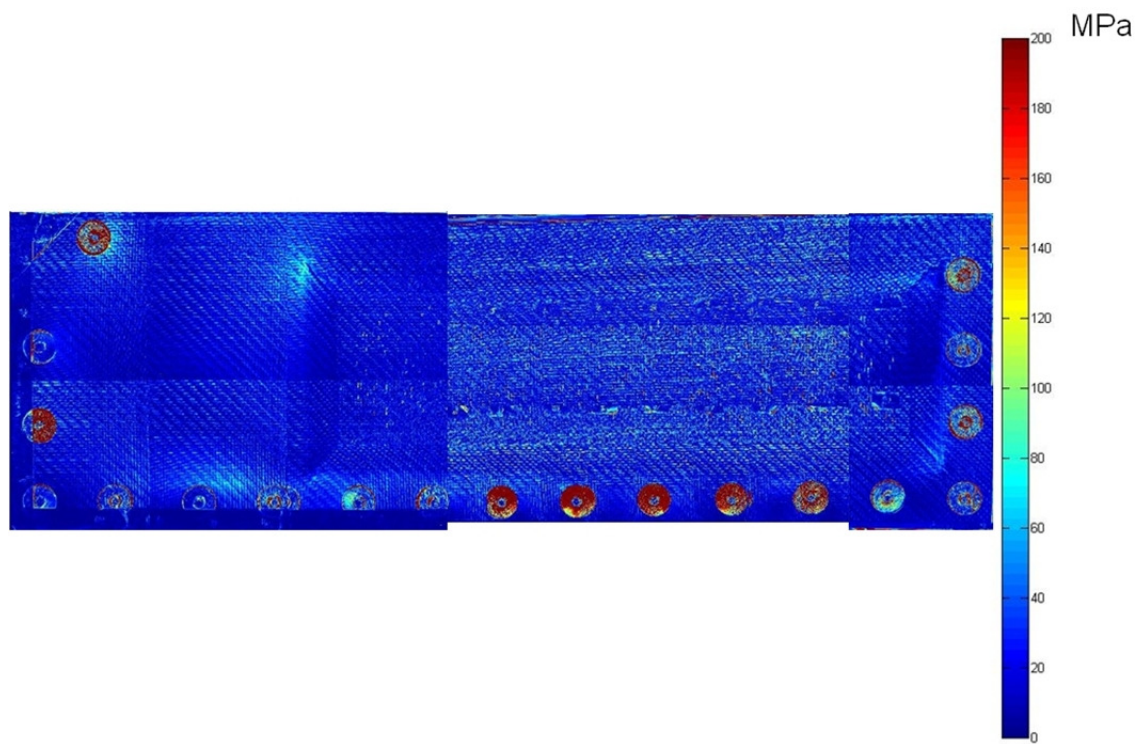


Figure 9.20: Example of full-field data from MO 4

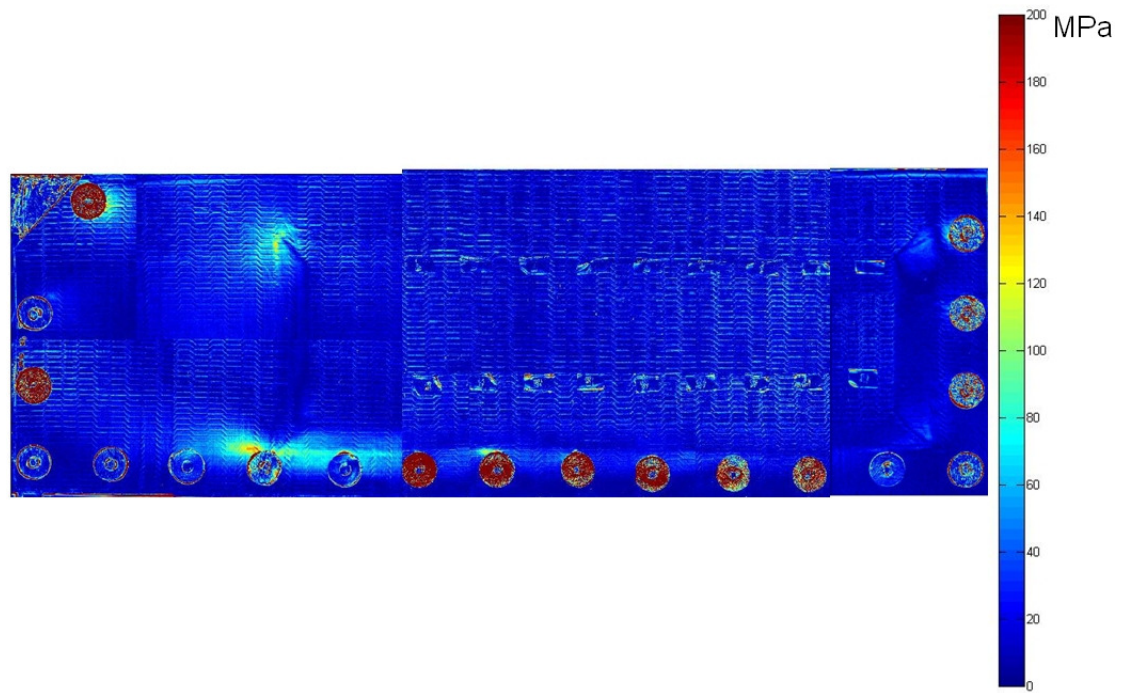


Figure 9.21: Example of full-field data from MO 5

Using a visual inspection of the images from each MO and their respective predicted image from the homogeneous FE model, it is possible to see good agreement between them. The experimental results validate the processed FE model stress fields, confirming the distribution of stresses in the panel. There is a comparatively small level of stress in the majority of the panel, and the position of stresses caused by the boundary conditions is verified. More interestingly, the position and magnitude of the stress concentration around the corner of the core predicted by the FE model is validated by the experimental data. To provide an appreciation of the agreement between FE model and TSA results, a line of stress sum is taken horizontally across the image from left to right through the stress concentration at the corner of the core. Figure 9.22 plots the stress through the corner of the core for a panel produced using MO 1 on the same axes as a plot from the homogeneous FE model. There is excellent agreement in the position of the stress peak, and the shape of the curve of the stress immediately around the peak. The stress gradually builds up across approximately 100 mm of the non-stiffened flange region and peaks at the junction between non-stiffened and stiffened areas. The stress rapidly reduces across the core stiffened region until it settles to a low, background level. This is intuitively correct, as the sudden increase in the flexural rigidity of the panel with the inclusion of the core would immediately reduce the stress. Although there is some noise in the TSA data it closely follows the FE data, and peaks at exactly the same position. The FE predicts a peak stress sum of approximately 130 MPa, but the TSA records a stress of around 160 MPa. This difference may be accounted for by the number of nodes in the FE model around the core corner, or also by some noise in the TSA. However, this plot validates the FE model for use in stress prediction in this material.

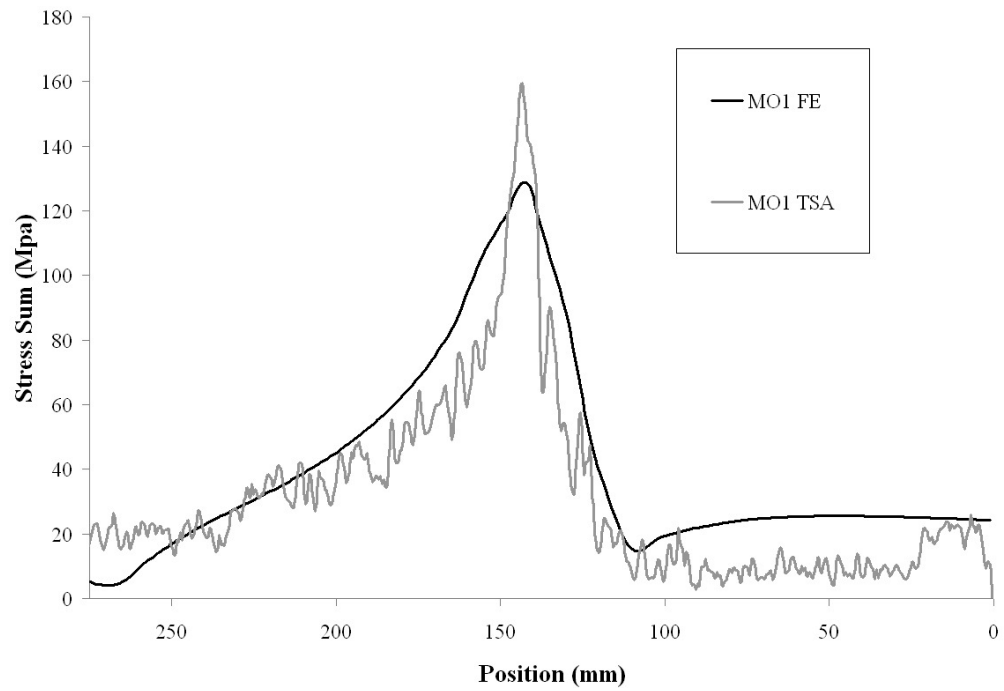


Figure 9.22: FE and TSA comparison for MO 1

A line plot of the processed stress sum for MO 2 from the homogeneous FE model and the TSA data through the corner of the core is provided in Figure 9.23. The TSA data shows the same trend as the FE, although unlike the plot for MO 1 there is a regular variation in the TSA data. It is considered that this regular ‘noise’ is produced by the weave pattern of the material. The FE and TSA data provide a peak in stress of approximately 110 MPa. This shows that the FE model provides a good representation of this MO.

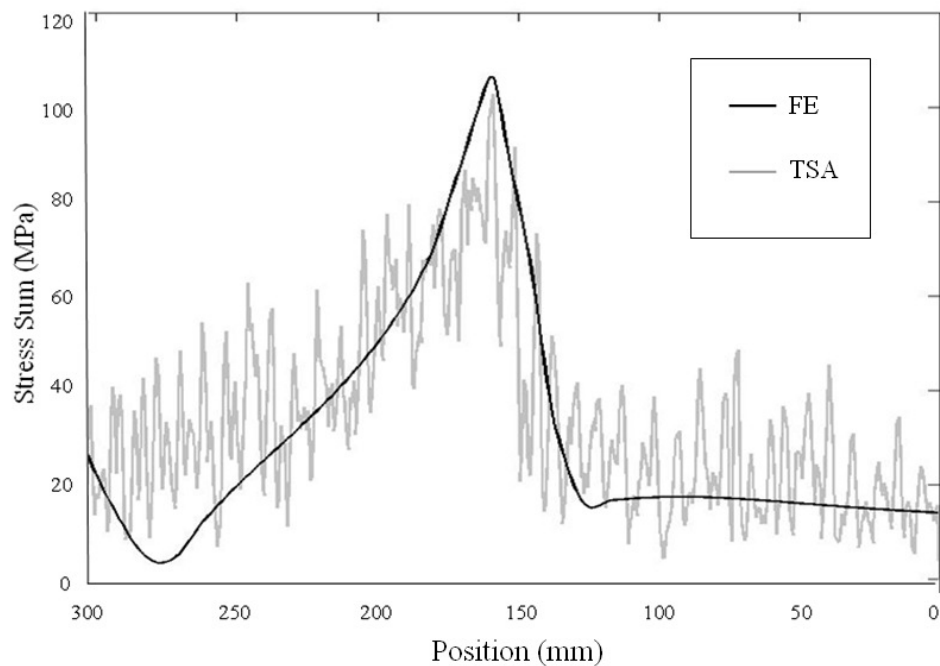


Figure 9.23: FE and TSA comparison for MO2

The stress through the corner of the core from the FE and TSA for MO 3 is shown in Figure 9.24. There is significant noise in the TSA data as a result of the stitching, although the size of the variation appears to increase in line with the increase in stress sum expected from the FE model. For the panel produced using MO 3 the stress sum peaks at approximately 120 MPa. Once again the trend is shown, but the validation is not as conclusive.

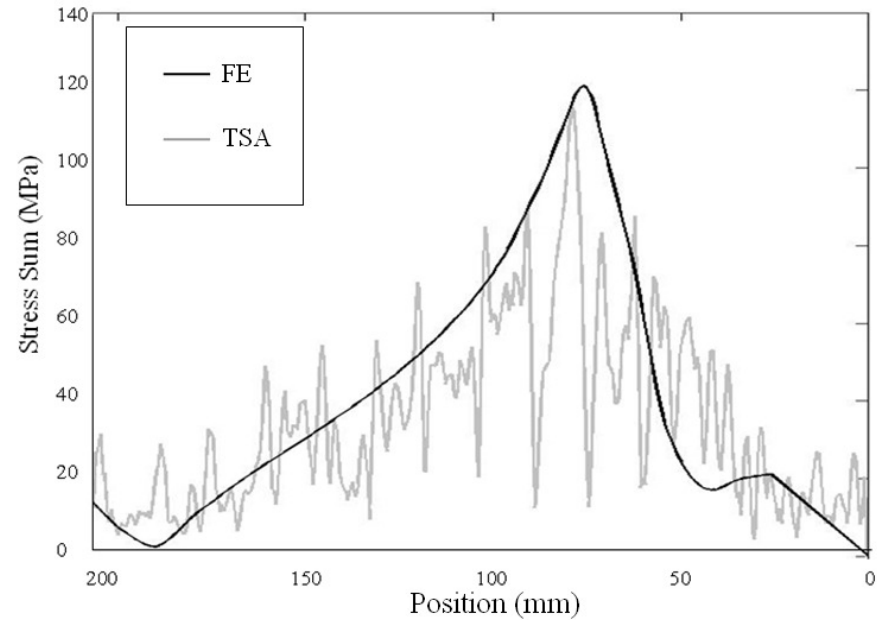


Figure 9.24: FE and TSA comparison for MO3

Figure 9.25 contains the line of stress sums through the core corner for MO 4.

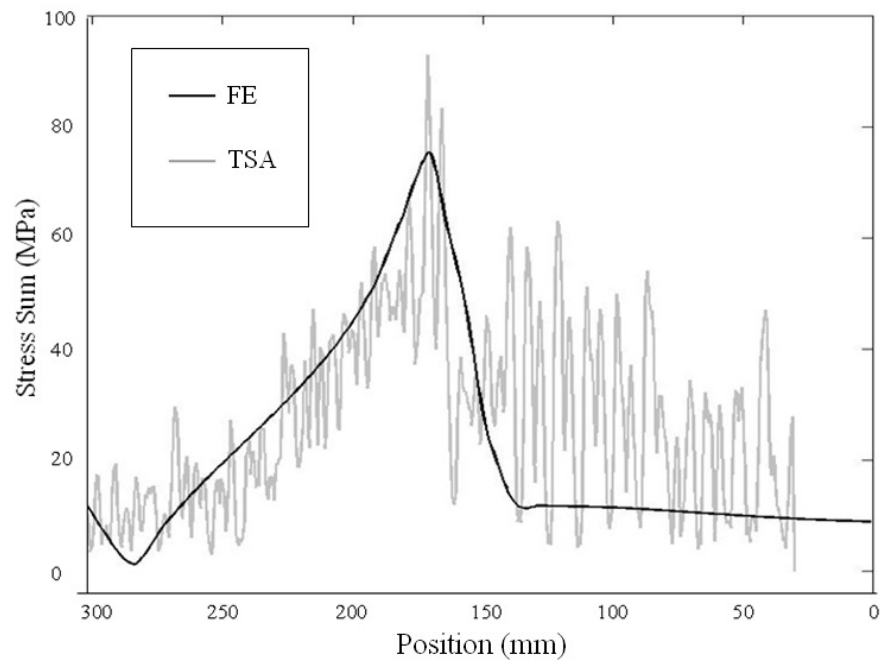


Figure 9.25: FE and TSA comparison for MO4

The FE data peaks at just under 80 MPa, but the TSA data shows a peak of between 80 and 90 MPa. The TSA data also shows the same variation in values that follows the weave pattern as that seen in the plot for MO 2 and a continuing validation of the model.

Finally, the plot of stress sum for MO 5 is shown in Figure 9.26. The peak stress from the TSA is approximately 105 MPa, which is slightly lower than the peak of 120 MPa predicted by the FE model. There is also some disagreement with the stress distribution, indicating that the FE model is not predicting the stress distribution adequately.

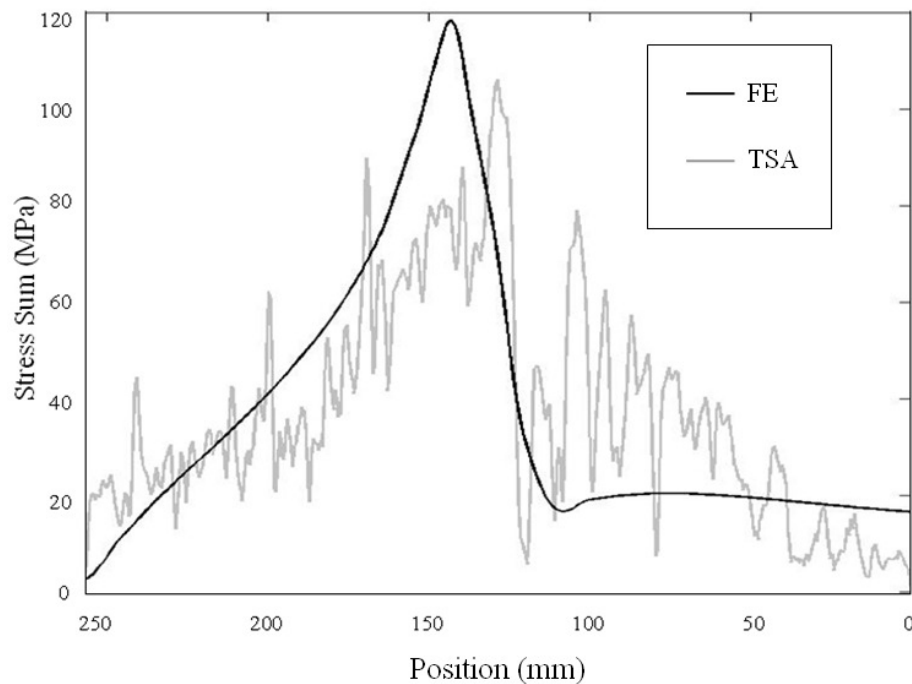


Figure 9.26: FE and TSA comparison for MO5

To investigate the effect of the noise in TSA data has on the result, ten lines of data are plotted that go through the stress concentration on the corner of the core, as considered in the previous plots. These ten lines represent a width of 6 mm on the generic panel, and therefore should be spatially coincident enough that they should give consistent values. By plotting these lines for each of the panels tested for each MO it is also possible to measure the consistency of the peak stress sum from one to the next. It is known from the displacement results that the panels are all consistent within each MO and therefore the variation in peak stress can be considered an effect of the TSA measurement. Figure 9.27 shows ten lines of stress sum MO1G1NO4 and shows a peak stress sum of 190 MPa. The plot shows a low level of noise, which is considered to be low enough to allow an adequate measurement of stress.

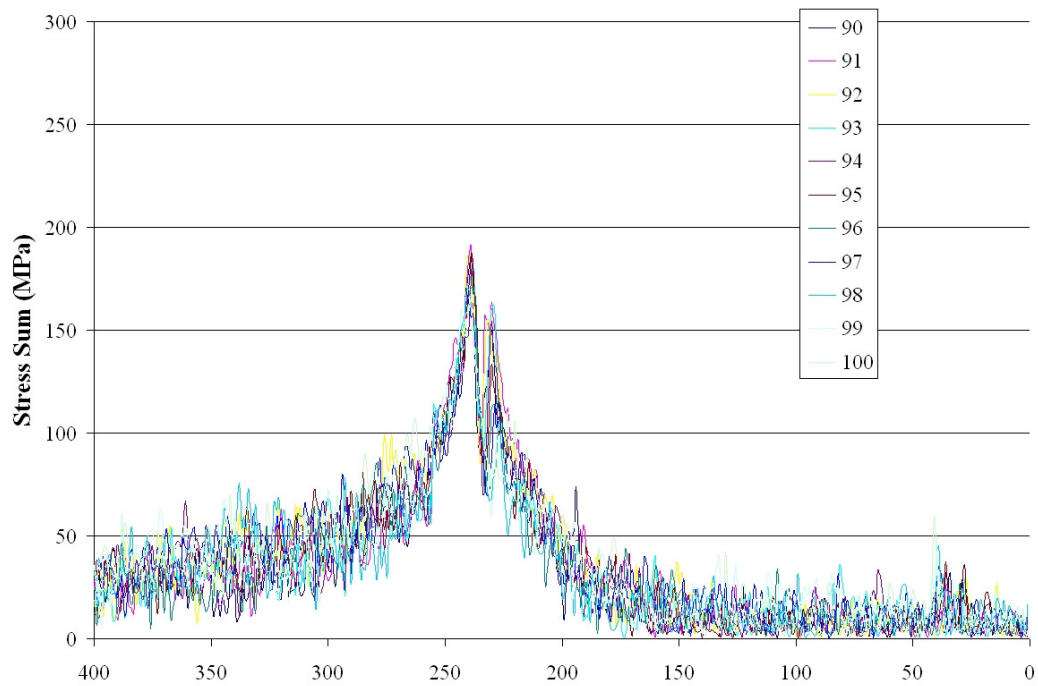


Figure 9.27: Example line plot through stress concentration at the corner of the core for MO 1

Figure 9.28 shows ten plots of stress sum for a panel manufactured using MO 2. The stress peak can be seen at a position of approximately 250 mm from the plot, and peaks at around 150 MPa. However, unlike the plots for MO1, the noise considered to be from the weave pattern is significant in comparison to the stresses that are to be measured.

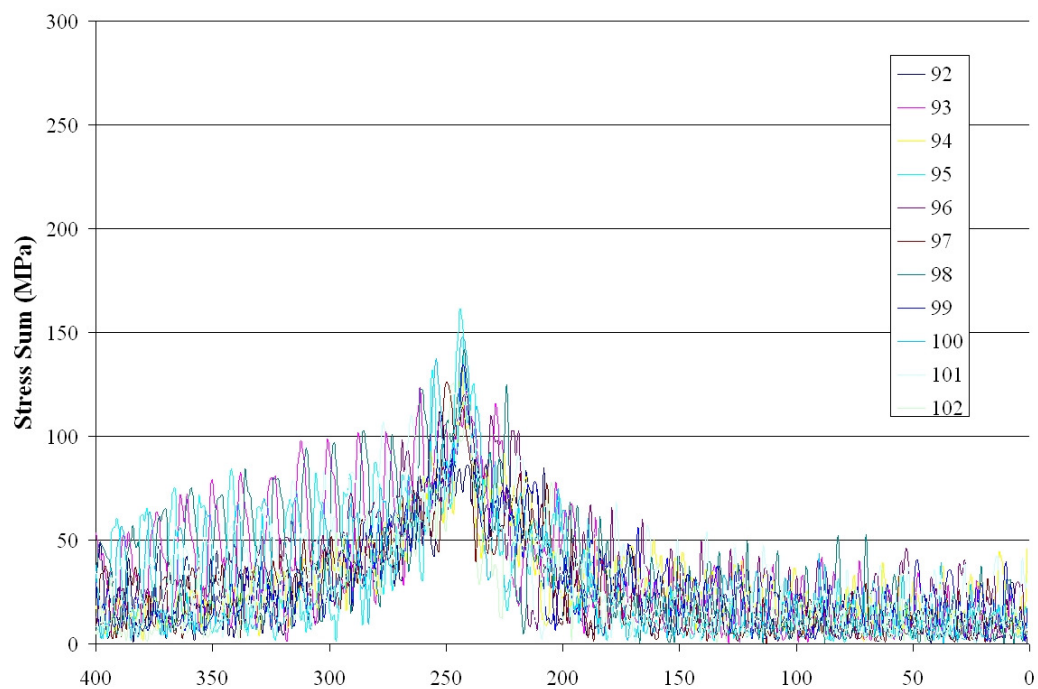


Figure 9.28: Example line plot through stress concentration at the corner of the core for MO 2

The plot of variation in the panel produced using MO 3 (see Figure 9.29) shows the peak stress somewhere between 150 and 200 MPa. It is difficult to ascertain a value more accurate than that due to the level of noise, and the lower levels of stress are totally overwhelmed by the noise. The stitching is making accurate measurement of stress values difficult. However, it is possible to infer a reduction in stress peak when compared to the panels produced using MO 1.

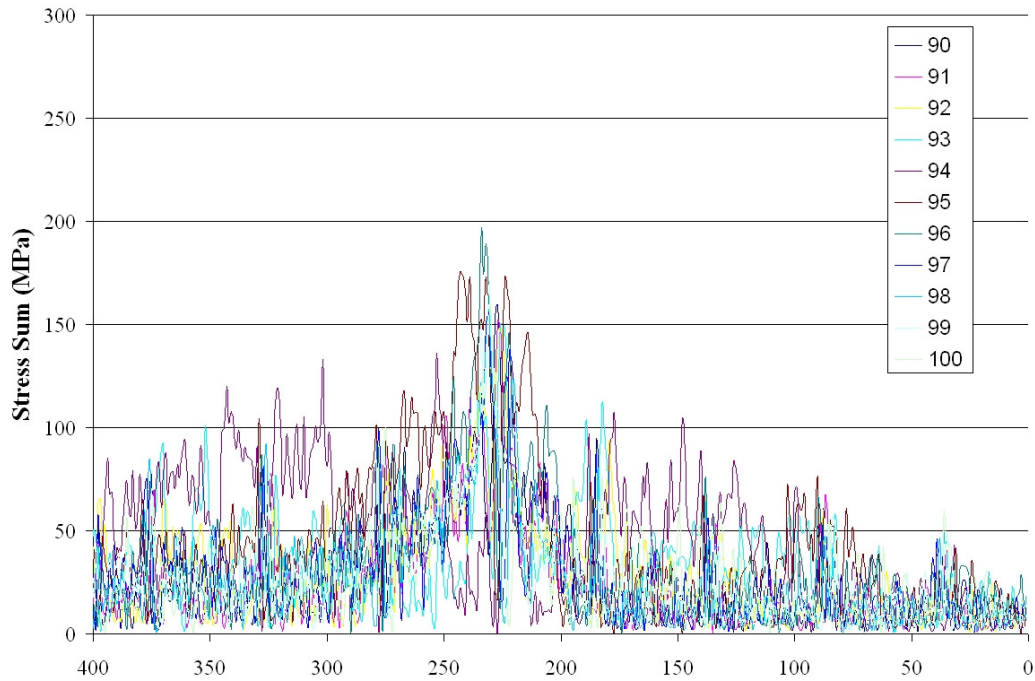


Figure 9.29: Example line plot through stress concentration at the corner of the core for MO 3

Figure 9.30 shows the plot for MO 4. The peaks are clearly much lower than that for MO 1 and MO 3, somewhere around 100 MPa. However, there are also some spurious peaks that by inspection of the panel are considered to be the result of dry patches which appear shiny in comparison to the matt surface of the rest of the panel and therefore give a false high response. The noise in the data is consistent, and can therefore be considered a result of the weave pattern.

The variation plot for MO 5 (Figure 9.31) is similar to the other non-crimp fabric material MO 3. The noise from the stitches hides some of the details of the stress sum plot. The result of these plots illustrating noise scatter in TSA data show that the use of the approach can be successfully applied to the UD material used in MO 1 when the panel is cyclically loaded with a pressure range of the order of 0.01 MPa. It is also evident that the stress sums measured using TSA can be used to validate an FE model of the panel. When applying TSA to panels produced using MO 3 and MO 5, i.e. non-crimp fabrics, the stitching used to hold the loose fibres together before processing represents a significant difficulty; this was also noted in [102]. It has been shown that it may be difficult to accurately measure a point stress sum due to noise. However, this may not be as great a

difficulty as it appears. If the TSA data is considered as whole, and not as line plots through it, it is clear from Figure 9.21 that the approach can provide a good representation of the stress distribution in a panel, and also indicate whether the peak stresses are higher or lower than other plots.

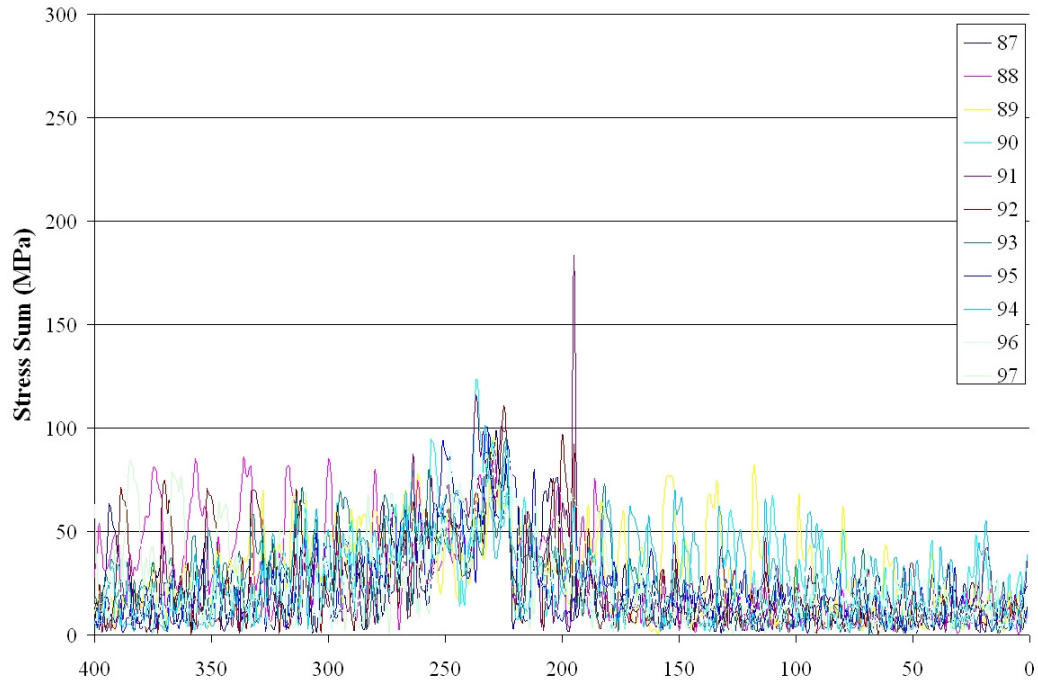


Figure 9.30: Example line plot through stress concentration at the corner of the core for MO 4

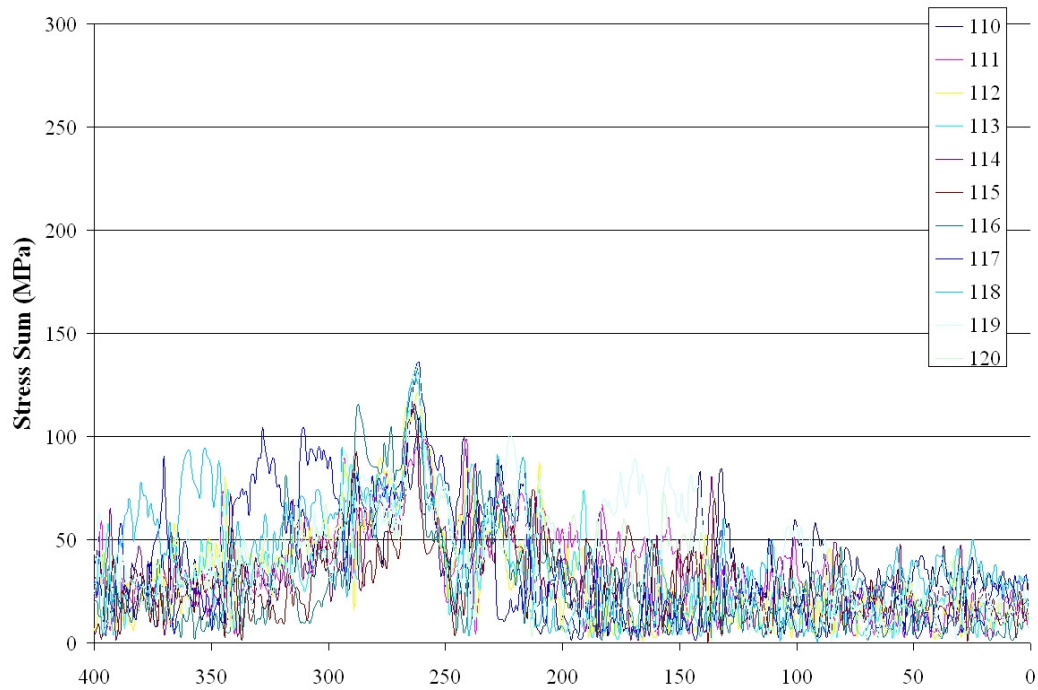


Figure 9.31: Example line plot through stress concentration at the corner of the core for MO 5

Further challenges appear when using TSA on the woven composites used in MO 2 and 4. Similar variation in the data exists, although this time, as a result of the weave of the composite, it is of a level that stress difference can still be discerned. The greater concern though is the manner in which the data had to be calibrated. By averaging across the entire woven specimen when finding the calibration constants, the peak stresses may be truncated. Therefore, whilst in the work described here it is possible to validate the FE model for the panels produced using MO 2 and 4 it is not considered possible to compare the stress states from panels manufactured from MO 2 and 4 to those manufactured using MO 1, 3 and 5.

Table 9.5 shows the average stress in the, relatively, constant region to the left of the peak (between position values of 250 and 400) which is averaged across the ten lines plotted. The table also shows a similar average stress to the right of the stress peak (between position values of 0 and 150), and finally, the average peak stress across the ten lines with the maximum given in square brackets. It is evident that all MOs offer similar stresses in the two regions of constant stress, although the scatter is relatively high in comparison to the value of the stress. This is to be expected, as the stresses recorded in these regions are towards the resolution of the measurement technique. More interestingly, the peak stresses confirm the qualitative analysis, offered above, and MO 1 has the highest peak stress at 178 MPa, whilst the out-of-autoclave process (MO 5) shows a stress of only 122 MPa. This is an apparent stress reduction of approximately 30%.

Table 9.5: Values of variation in stress sum in each MO

MO	Average left of stress peak (between 350- 400) (MPa)	Average Peak [Max] (MPa)	Average right of stress peak (between 0-150) (MPa)
1	32.1 ± 9.2	178 ± 10 [191]	10.5 ± 10
2	24.3 ± 13.9	129 ± 18 [161]	14.4 ± 14
3	29.4 ± 15.9	159 ± 18 [196]	16.9 ± 16
4	21.2 ± 12.9	99 ± 13 [123]	14.7 ± 14
5	29.2 ± 12.4	122 ± 12 [136]	21.3 ± 19

Combining the results from the deflection data and the TSA it is possible to infer some improvement in performance when MO 1 is replaced by the out-of-autoclave MO 5. It is possible that this may be a result of the stitching in the NCF providing some out-of-plane reinforcement.

9.6 Summary

This chapter has described the successful use of TSA to measure the response of the generic panels loaded on the pressure test rig. TSA was initially applied to tensile strips and using an equation to link the ΔT with the strains in the specimen the use of the technique on the materials considered in this thesis was investigated. The use of this simplified equation proved ineffective, particularly on the more complex woven materials of MO 2 and 4. These tests also highlighted the difficulty of obtaining accurate values without a full set of correct thermal and mechanical properties. To apply the TSA technique full-field to the generic panel calibration, constants were measured experimentally from the tensile strips. The generic panels were loaded at a frequency of 1 Hz on the test rig and therefore, although there was evidence of issues with adiabatic behaviour, the calibration constants were measured by loading the tensile strips also at 1 Hz.

The chapter then considers full scale tests on the generic panels to assess the mechanical performance of the five MOs. The performance was measured using first point measurements of the out-of-plane deflections from a displacement transducer, and then the application of TSA as full-field technique to measure the stresses in the panels. These measurements were also used to validate FE models. Two types of FE model were used to predict the response of the generic panels subjected to the pressure load: first the face sheets are considered as homogeneous orthotropic blocks, and second the individual plies are considered in a ply-by-ply model. The two types of model predicted significantly different deflections and stresses, and by the use of a cross ply panel, and deflection data, it was possible to confirm that the homogeneous panel did not adequately model torsional coupling. Therefore, the experimental deflection data was compared to the ply-by-ply model. However, the TSA was calibrated using thermoelastic constants from the global response of the laminates in the tensile strips, and therefore the homogeneous models were validated by the TSA data. To allow a direct comparison between the FE and TSA data it was necessary to process them into a similar form.

The deflection results from the full scale tests showed a significant reduction in deformation when using MO 5 in preference to MO 1 of almost 27%. The ply-by-ply model produced the best prediction of deflection, expectedly, although under-estimated by around 10%. Qualitatively, the full-field experimental images from TSA compared favourably with the FE data, and therefore

appears to validate the models. When plotting a line of data through the largest stress concentration around the corner of the core it was possible to closer compare the FE and TSA data. For panels produced using MO 1 the data showed close agreement between FE and TSA, and both confirm the position of value of the peak stress. For the woven materials MO 2 and MO 4 the TSA data shows the same trend as the FE, but there is natural variation in the experimental data from the weave pattern. A similar response is seen from the TSA data of the non-crimp stitched materials MO 3 and 5. Analysing the relative values of stress peak recorded by the TSA there is a clear reduction between MO 1 and MO 5. MO 1 has an average maximum stress of 178 MPa, whilst MO5 has an average of 121 MPa, a reduction of 30%. The deflection and TSA data appear to confirm that MO 5 offers mechanical performance improvement over MO 1.

Chapter 10 will consider the mechanical performance analysis discussed in this chapter and Chapter 6, and the cost analysis from Chapter 5 to provide an optimisation of the generic panel.

Chapter 10

10. Optimisation of panel

10.1 Introduction

The work described in this thesis investigates the optimisation of a generic component representative of secondary structure on the wings of medium size commercial passenger aircraft. In Chapter 5 the manufacture of generic panels using the five MOs was discussed with some analysis of the relative cost of manufacture of each. The cost of material was estimated and the time of manufacture, including cure time, was monitored. In Chapter 6 some mechanical characterisation tests on the face sheet materials manufactured using each MO provided an initial comparison between their performance. To fully assess the mechanical performance of the sandwich construction, generic panels were manufactured using each MO and were loaded on the full scale pressure test rig. The response to the pressure load has been recorded using point measurements from a displacement transducer and full-field stress assessment using the TSA technique.

In this chapter all the components of cost and performance analysis of the different MOs are considered concurrently and the use of the out-of-autoclave (MO5) process for panel manufacture is discussed. A summary of the conclusions from previous chapters is provided, and then the weight of each panel is reported. The application of the ‘novel’ process to the manufacture of

components on-site at GE is examined. This is followed by the production of a capital cost analysis of two greenfield sites; one setup for conventional autoclave cured composite manufacture and the second for the manufacture of out-of-autoclave composites.

10.2 Summary of previous chapters

10.2.1 Manufacturing and material costs

In Chapter 5 the manufacture of generic panels using each of the five MOs was analysed for relative production costs. MO 1, the UD prepreg autoclave cured, required 28.8 labour hours to produce a panel and cost \$380 worth of material. By replacing the UD prepreg for a woven prepreg (MO 2) the production time was reduced to 23.1 hours (a reduction of more than 19%) and the material cost was reduced to \$264 (30% lower). This is significant, and it is for this reason that many secondary panels are currently manufactured using this material and process combination. However, by exchanging the woven prepreg for the heavier NCF (MO 3), which required many less layers, the time for manufacture was further reduced to 20.9 hours (a further reduction of 10%). The material cost for the NCF and resin film was approximately \$232, which represents a 38% reduction from MO 1 and a 12% reduction from MO2. Finally, replacing the autoclave cure for a conventional oven cure (MO 5) requires 20.2 hours for production. This is a further improvement from MO 3 of 3%. Hence, by exchanging MO 1 for MO 5 it was possible to reduce the time to produce a panel by approximately 30% and reduce the material cost by 38%, thus providing a significant cost advantage.

The costing analysis also highlighted the time, and hence cost, penalty that is caused by the need for a core stabilisation to protect the honeycomb core from crush. It is therefore possible that replacing the honeycomb for a foam core, which does not require stabilisation, would offer an additional cost benefit.

10.2.2 Mechanical characterisation

In Chapter 6 mechanical characterisation tests were performed on the face sheet materials from each of the MOs, and provided an initial comparison of the mechanical performance of each. First, the V_f of each laminate was estimated to offer an indication of the consolidation from each process/material combination. All MOs produced laminates with a V_f greater than 50%, although there was an indication that a slight V_f reduction was present between MO 1 and MO 5.

The results of the in-plane stiffness and strength tests offered some interesting conclusions. There was a small reduction of 7 and 8 % for the stiffness when using MO 5 in favour of MO 1, and this

was largely attributed to the slight crimp present in the NCF material. MO 4, with its woven structure and therefore larger crimp, had a reduction of 13% in stiffness. However, the out-of-autoclave process (MO 5) provided laminates with improved strength over the autoclaved MO 1. The strength was higher by 12%, a not insignificant amount.

Finally, tests were also performed to measure the out-of-plane properties of the laminates. MO 5 suffers a reduction of 7% in ILSS, which is considered to be due to an increase in void content that was evident in the micrograph images. However, the flexural strength and stiffness had approximately a 2-4% drop from MO 1 although this is inside the data scatter and therefore not statistically significant. MO 4, the other out-of-autoclave process, suffers more detrimental effects and the flexural strength and modulus is 10 and 17% lower than MO 2 (the other woven composite). The out-of-plane properties were considered important for the current material application, as the generic panels undergo a pressure load which will cause considerable out-of-plane deformation. Therefore, it was encouraging that MO 5 offered similar properties to MO 1.

10.2.3 Generic panel comparison

In Chapter 9 the results of full scale tests on the generic panels were reported. A note of caution should be applied to the conclusions drawn from the results of these tests. Although every attempt was made to choose materials that would offer the same laminate thickness and weight of fibre, there is some variation in the cured thickness from each MO and hence, the generic panel weight. Table 10.1 lists the average weight per unit area of the generic panels produced using the five MOs. Interestingly the panel made using MO 1 had a lower average weight than any of the other panels that all had similar areal weights. MO 5 produces panels with an average areal weight of 6280 g/m² whilst MO 1 panels are 5689 g/m², which is an increase of approximately 10%. This should be taken into account when considering any performance differences found in the full scale tests.

Table 10.1: Average mass per unit area of generic panels

MO	Mass per unit area (g/m ²)
1	5689
2	6115
3	6327
4	6404
5	6280

From the deflection measurements in Chapter 9 it was found that MO 5 provided a 27% decrease in maximum deflection compared to the MO 1 panels. This seems like an important result even taking into account the 10% increase in weight. The stress results from the TSA and, therefore, the validated FE model showed panels produced using MO 1 had a peak stress of approximately 190 MPa, whilst MO 5 panels had between 100 and 120 MPa. This appears to agree with the deflection data, although the measured stress for MO 5 has noise in the data due to the stitching in the NCF.

Some consideration should also be given to panels produced using MO 4, because the woven out-of-autoclave material has recently become the process of choice for the future [117]. Panels manufactured with MO 4 are on average 12% heavier than MO 1. However, the MO 4 panels show 24% less deflection, which is a promising result. Due to the woven nature of MO 4 it was difficult to offer a comparison from the stress field found using TSA. Further work is required to investigate the effect of calibrating the woven data. When performing visual inspection of the panels produced using MO 4, patches of dry fabric were identified on the perimeter of the core and between the tows.

To offer a further optimisation of the generic panel, the inclusion of ply drop-offs and replacement of the honeycomb for a foam core have been considered on panels using MO 4 and 5. These tests were performed on a separate occasion to the previous panels, and the water cushion was emptied in between. Upon re-filling, the cushion must have been filled to a different level as the rig was more responsive and therefore the 3 mm actuator amplitude provided a load range of 0.02 MPa (3 psi) and not the required 0.01 MPa (1.5 psi). Therefore, the results from the full-scale results from these panels were divided by two so that some comparison could be made. Figure 10.1 shows the maximum deflection, measured using the displacement transducer, for the panels manufactured using MO 5. The panels with a honeycomb core and ply drop-offs (designated MO5G2NO1) and the foam core (designated MO5G2NO2) show similar deflections at 0.01 MPa of 4.89 mm and 4.86 mm. These are marginally larger than the value of deflection for the standard MO 5 panel at 4.6 mm. However, the panel using foam core and ply drop-offs (designated MO5G2NO3) has a deflection of 5.3 mm. This is 15% greater than that of the standard panel. Therefore the use of drop-offs and a foam core will degrade the performance of the generic panel.

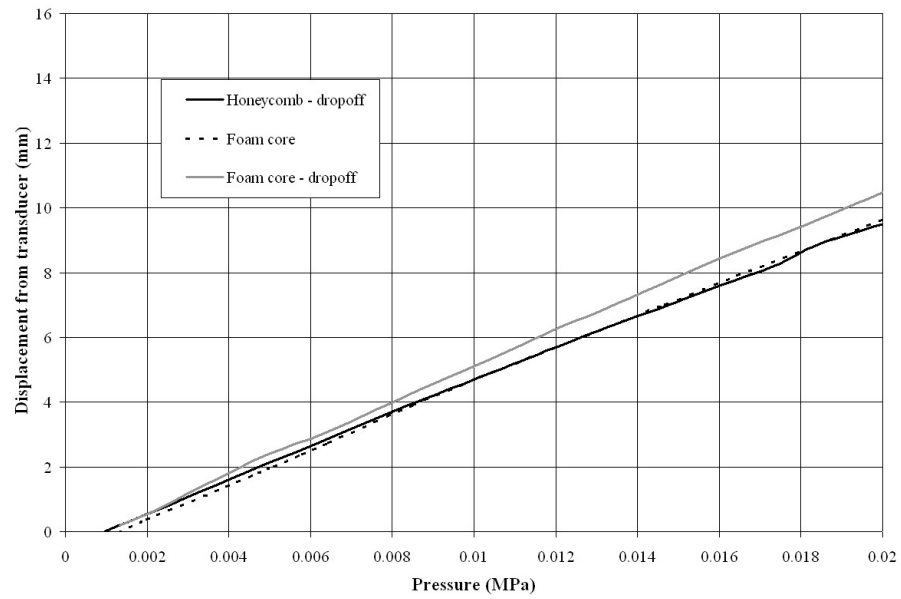


Figure 10.1: Maximum displacement using transducer of MO 5 other panels

Figure 10.2 shows the deflection plots for the three other designs of panel manufactured from MO 4. Panel MO5G2NO1 and panel MO5G2NO2 provided similar deflections at 0.01 MPa of 4.84 mm and 4.97 mm. These compare favourably with the standard MO 4 panel, at 4.84 mm. However, the panel MO5G2NO3 had a deflection of 4.28 mm demonstrating a reduction in deformation from the standard panel. These results are the reverse of those seen from MO 5, and it is possible that the woven structure of MO 4 may provide a design that is more stable to alterations.

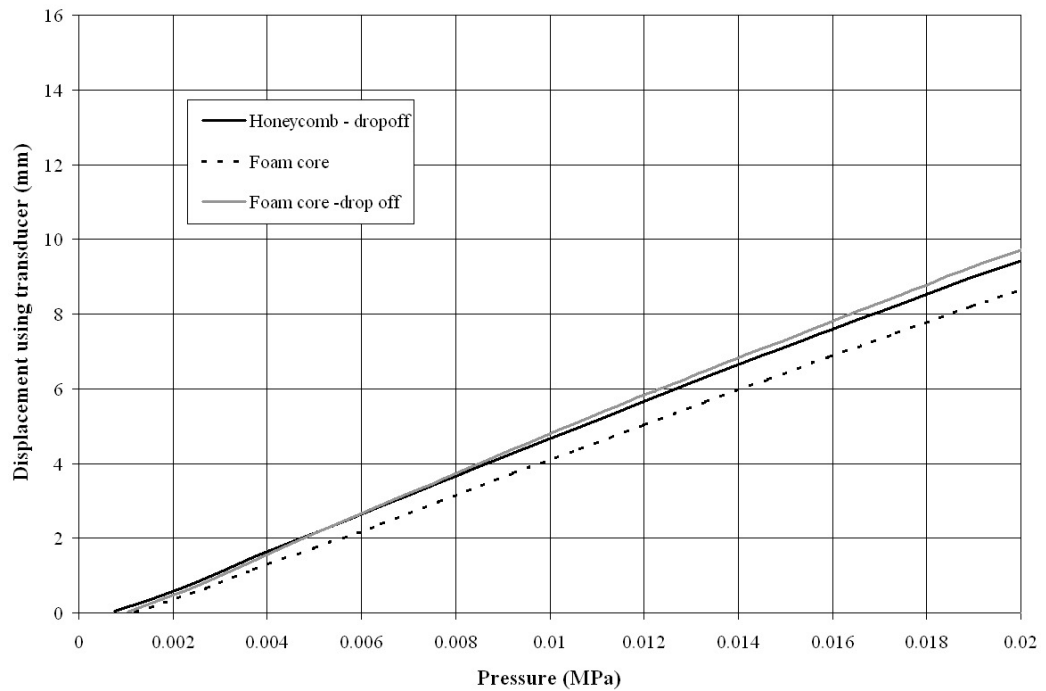
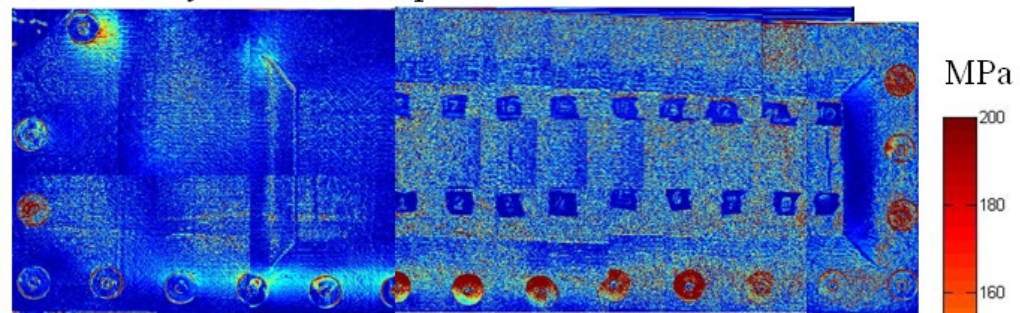


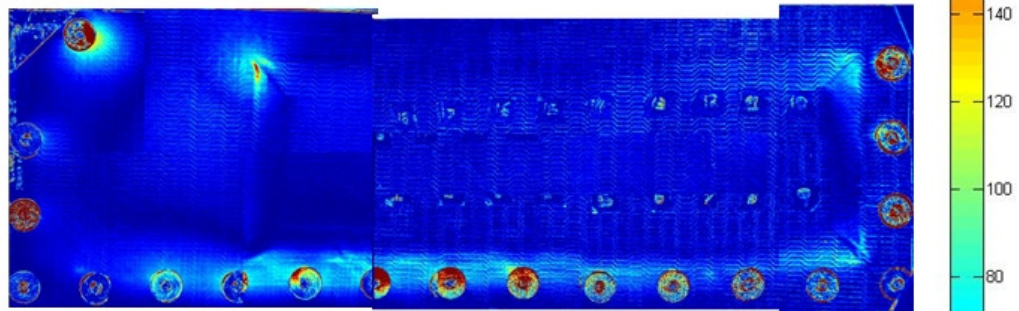
Figure 10.2: Maximum displacement using transducer of MO 4 other panels

Figure 10.3 shows the TSA images of the three panels from MO 5 with the ‘new’ designs. Qualitatively, it appears that the two panels with foam cores have similar stress distributions, but the panel MO5G2NO1 has a lower stress concentration. However, the stresses at the corner of the core in MO5G2NO1 have an average of 170 MPa and a maximum of 212 MPa. This is a large increase compared to the standard MO 5 panel. The two foam cored panels, MO5G2NO2 and MO5G2NO3, show even larger average peak stresses of 193 and 191 MPa. The use of drop-offs and the foam core appear to provide a larger stress concentration and this will require further investigation in the future. Similar stress distributions can be seen in the panels manufactured using MO 4.

MO5 – Honeycomb with drop-offs



MO5 – Foam core



MO5 – Foam core with drop-offs

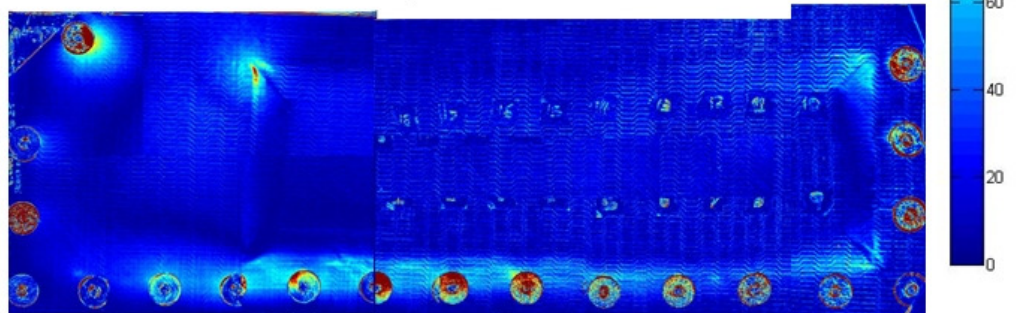


Figure 10.3: Full-field TSA on MO 5 of other panels

10.3 Application of out-of-autoclave manufacture to GE

From the work described in this thesis on cost and performance analysis of composite processing techniques the most promising approach is MO 5, i.e. NCF infiltrated with RFI and cured in an

oven. It would be feasible to apply this process successfully at GE with modest changes to equipment and current operating procedures. The RFI process described in this thesis has a similar hand layup approach to the baseline UD prepreg, and therefore minimal re-training would be necessary for production staff. To avoid the need for expensive capital outlay, the autoclaves could be used, without pressurisation, as conventional ovens. In doing so, some of the advantages discussed from the removal of the autoclave, such as through processing to reduce the effect of batch processing, would be reduced. Despite this, the heavy NCF will vastly reduce the production time, and material cost, and removal of the pressurisation would reduce energy costs.

Challenges that must be overcome for the uptake of the 'novel' process, in particular the NCF material, consist of certification issues and convincing the major aircraft producers of the advantages of the material to gain their support. All materials and processes for use in the aircraft industry are required to undergo an extensive certification procedure before being classed as safe for flight. One limitation of the NCF for certification will be the ability to adequately model the material for design purposes, the literature reports some progress on this [31, 118], but further work is necessary. The FE work performed in this thesis offers an initial approach to modelling the materials in a full scale component. Once these challenges have been surpassed, the process described by MO 5 should offer significant cost savings for composite manufacture at GE.

10.4 Greenfield site analysis

Applying the out-of-autoclave process at the current GE site reduces its benefit. In particular, GE has already made the capital outlay for the expensive equipment involved in autoclave composite manufacture. Therefore, the final part of this chapter investigates the most advantageous use of the 'novel' process to obtain all of its benefits. If an imagined greenfield site was to be equipped for the use of MO 5, the capital cost of the autoclave can be removed completely. However, it would also remove the need for ancillaries for autoclave use, such as autoclave pit, pressurisation system and loading system. Using some standard costs for the equipment used in composite manufacture (see Table 10.2) an estimate of the capital outlay for both an autoclave (see Table 10.3) and out-of-autoclave site (see Table 10.4) is given. The autoclave site is estimated to need an outlay of almost £9 million, with just over £5 million of this being apportioned to the autoclaves and the related equipment. The out-of-autoclave site has an estimated capital cost of £4.6 million. Whilst the actual values cannot be confirmed the potential saving is clear. This greenfield analysis is simplistic and speculative to offer an indication of levels of capital investment required for the two types of process.

Table 10.2: Cost of individual items [117]

Item	Cost (£)	Cost Format
Class 100,000 cleanroom to fed std 209e (UK)	250	per cubic metre
Automated prepreg/preform cutting machine	120000	Unit
Honeycomb cutting machine	600000	Unit
Freezer to -20°C	250	per cubic metre
Mould tool cleaning and extracted area	100000	Unit
Autoclave	15000	per cubic metre
Autoclave loading system	50000	Unit
Autoclave pit	50000	Unit
Nitrogen generation system with pressure receivers	200000	Unit
Oven (part thermocouple controlled + int vac system	4000	per cubic metre
Routing machine X 3.6 m Y 3.6 m Z 1.2m +extraction	750000	Unit
Hand trim finishing bay	150000	Unit
Test piece cutting diamond saw	50000	Unit
C scan device	500000	Unit
Paint, prep	200000	Unit
Infrastructure i.e. trolleys, lay-up tables etc	200000	Unit

Table 10.3: Capital cost of greenfield autoclave site

Item	Quantity	Cost per unit (£)	Cost of item (£)
Automated cutting	1	120000	120000
Honeycomb cutting	1	600000	600000
Mould tool cleaning and extracted area	1	100000	100000
Autoclave loading system	1	50000	50000
Autoclave pit	2	50000	100000
Nitrogen generation system	1	200000	200000
Routing machine	1	750000	750000
Hand trim finishing bay	1	150000	150000
Test piece diamond saw	1	50000	50000
C scan device	1	500000	500000
Paint, prep	1	200000	200000
Infrastructure	1	200000	200000
Cleanroom	2700	250	675000
Freezer	400	250	100000
Autoclave	316	15000	4740000
Oven	100	4000	400000
Total			8935000

Table 10.4: Capital cost of greenfield out-of-autoclave site

Item	Quantity	Cost per unit (£)	Cost of item (£)
Automated cutting	1	120000	120000
Honeycomb cutting	1	600000	600000
Mould tool cleaning and extracted area	1	100000	100000
Routing machine	1	750000	750000
Hand trim finishing bay	1	150000	150000
Test piece diamond saw	1	50000	50000
C scan device	1	500000	500000
Paint, prep	1	200000	200000
Infrastructure	1	200000	200000
Cleanroom	2700	250	675000
Freezer	200	250	50000
Oven	300	4000	1200000
Total			4595000

Further, in Chapter 3 the effect of the autoclave on the manufacturing flow was discussed. It was identified that the need for batch processing, to ensure the autoclave operates with a full load, and that the autoclave had to be loaded and unloaded at the same end caused a large bottleneck in production. Parts may be stored awaiting others to be formed before a cure is initiated and once cure is complete the debagging area will be flooded. It is envisaged that by using ovens with doors at both the front and back, and with vastly reduced running costs, it would be feasible to minimise waiting and loading/unloading times. The ideal approach would use a flow oven, where the components moved through as cured therefore continuing the process flow. Such an oven has been described [119], although investigation would be required to ensure the component continued to see a controlled temperature profile during cure. There would also need to be a rail system to allow the vacuum fittings to follow the components as they moved through the oven. Component layup would be staggered to ensure that each would have its place in the oven. Such an extreme approach would only be cost-effective, and necessary, when considering high production rates. For aerospace manufacture this may not be necessary, but may be of interest to future automotive applications.

10.5 Summary

This chapter summarised and combined the conclusions from Chapters 5, 6 and 9 to provide an optimisation of the generic panel considering cost and performance. The weights of the generic panel produced using the five MOs was obtained and it was evident that MOs 2-4 provided panels that were approximately 10% heavier than MO 1. However the performance of the panel

produced using MO 5 was consistently much higher than that from MO 1 by approximately 30%. Therefore, it will be possible to optimise the design of the panel produced using MO 5 to offer a similar weight to that of MO 1 and should still provide adequate, possibly improved performance. An attempt to further optimise the panel was undertaken by including ply drop-offs and replacing the honeycomb core with a foam core. However, the full scale tests on these panels proved inconclusive and appeared to reduce the performance significantly.

The application of the out-of-autoclave (MO 5) process at the GE site was discussed and, although some changes would be required, it was decided that the use of such a process would offer them worthwhile cost benefits whilst maintaining panel performance. However, GE is already fully-equipped with autoclaves and therefore would not benefit from the capital cost reduction by using an out-of-autoclave process. Therefore, to investigate the savings that could be available through capital costs, an analysis of equipping greenfield sites was performed. Although the actual cost values are estimates, the greenfield analysis predicted savings of up to 50%. Further analysis would be required to investigate the total cost reduction, in particular the overheads, scrap, rework, repair and concession costs. However in this work the lack of real cost data has proved a limitation to offer a total cost comparison.

Chapter 11

11. Conclusions and future work

There is an increasing use of composite structure in aircraft to reduce weight and hence improve fuel efficiency, for example, for the previous generation Airbus A320 or Boeing 777 between 10 and 20% of the total airframe was manufactured from composites by weight [3], whilst the Airbus A380 has 22% and Boeing 787 is expected to have 50% [4]. The current standard for manufacturing aircraft secondary structure uses hand layup of prepreg cured in an autoclave, which is an expensive process with the sources of cost well documented [8, 9]. Therefore, the major limitation for composite use in the aircraft industry is material and manufacturing cost in comparison with metallic structure. In an increasingly competitive composite manufacturing market, GE Aviation Systems are keen to reduce their cost of manufacture, so a method to assess the ‘new’ process/material combinations for cost and performance was required to measure the suitability of ‘new’ procedures.

The work in this thesis investigated the alternatives for composite manufacture, considering the advantages and limitations of each, paying particular attention to the sources of cost (fulfilling objective 1 given in the introduction). With input from GE, the most attractive alternatives were identified for cost and performance analysis. Five manufacturing options (MOs) consisting of material and process combinations were considered. The five MOs were incremental steps from

the baseline unidirectional prepreg cured in an autoclave to the ‘new’ non-crimp fabrics (NCF) infiltrated using RFI and cured in a conventional oven. It is known from the literature that the baseline suffered from expensive raw materials, high labour content and an expensive autoclave cure. A generic panel was designed for this work and is representative of secondary wing structure (Chapter 1, objective 2) so that the cost and performance could be analysed for each MO.

The manufacture of the generic panels using the five MOs was monitored to investigate the time of manufacture and material cost (hence fulfilling objective 3). MO 1, the UD prepreg autoclave cured, required 28.8 labour hours to produce a panel and cost \$380 worth of material. By replacing the UD prepreg for a woven one (MO 2) the production time was reduced to 23.1 hours (a reduction of more than 19%) and the material cost was reduced to \$264 (30% lower). This is significant, and it is for this reason that many secondary panels are currently manufactured using this material and process combination. However, by exchanging the woven prepreg for the heavier NCF (MO 3), which required many less layers, the time for manufacture was further reduced to 20.9 hours (a further reduction of 10%). The material cost for the NCF and resin film was approximately \$232, which represents a 38% reduction from MO 1 and a 12% reduction from MO2. Finally, replacing the autoclave cure for one in a conventional oven (MO 5) requires 20.2 hours for production. This is a further improvement from MO 3 of 3%. Hence, by exchanging MO 1 for MO 5 it was possible to reduce the time to produce a panel by approximately 30% and reduce the material cost by 38%, thus providing a significant cost advantage. Further analysis of the current process highlights the issues that inclusion of an autoclave brings. To ensure efficient use of the autoclave, it is necessary to wait until the vessel is full before curing, and therefore the production becomes a batch process. This forms a bottleneck because the autoclave can only be loaded/unloaded at one end. To investigate the use capital cost benefit of out-of-autoclave processing, a greenfield site was envisaged, first being equipped for autoclave production and second for oven-only cure. Significant capital cost savings were estimated, and it was possible to visualise a site where composite manufacture could be in the form of a flow process.

With the significant cost benefits of removing the autoclave and use of NCFs proven, the focus of the thesis turned to concentrate on measuring the performance of panels produced using each MO. It is important that the ‘new’ process can at least match the performance of the baseline. The performance has been measured using both mechanical characterisation and full scale tests on generic panels. The mechanical characterisation tests were performed on the face sheet materials from each of the MOs, and provided an initial comparison of the mechanical performance of each one (objective 4a). First, the V_f of each laminate was estimated to offer an indication of the

consolidation from each process/material combination. All MOs produced laminates with a V_f greater than 50%, although there was an indication that a slight V_f reduction was present between MO 1 and MO 5. The results of the in-plane stiffness and strength tests offered some interesting conclusions. There was a small reduction of 7 and 8 % for the stiffness when using MO 5 in favour of MO 1, and this was largely attributed to the slight crimp present in the NCF material. MO 4, with its woven structure and therefore larger crimp, had a reduction of 13% in stiffness. However, the out-of-autoclave process (MO 5) provided laminates with improved strength over the autoclaved MO 1. The strength was 12% greater, a not insignificant amount. Finally, tests were also performed to measure the out-of-plane properties of the laminates. MO 5 suffers a reduction of 7% in interlaminar shear strength (ILSS), which is considered to be due to an increase in void content that was evident in the micrograph images. However, the flexural strength and stiffness had approximately a 2-4% reduction from MO 1, although this is inside the data scatter and therefore not statistically significant. MO 4, the other out-of-autoclave process, suffers more detrimental effects and the flexural strength and modulus is 10 and 17% lower than MO 2 (the other woven composite). The out-of-plane properties were considered important for the current material application, as the generic panels undergo a pressure load which will cause considerable out-of-plane deformation. Therefore, it was encouraging that MO 5 offered similar properties to MO 1.

The mechanical characterisation provided an initial assessment of the performance of MO 5, however the performance of full scale sandwich components was also considered important. Therefore, a test rig was designed to fit around a standard servo-hydraulic test machine (hence fulfilling objective 4c). The rig applies a pressure load across the surface of the generic panel by pulling it over a water filled cushion. It was decided that traditional measurement techniques, such as strain gauges, would not provide sufficient information to measure the complex response of the generic panel subjected to the pressure load. Hence, the rig was designed to allow access to the surface of the panel, enabling the use of optical measurement techniques, i.e. digital image correlation (DIC) and thermoelastic stress analysis (TSA). The test rig was tested to ensure it could provide both a consistent static and cyclic load. The optical techniques were both tested for their feasibility on the composites considered in this thesis at the stress and strain levels expected from the full scale tests (hence fulfilling objective 4b).

The DIC was initially applied to tensile strips of carbon fibre. These tests determined that the optimum processing parameters used to calculate the strains were an interrogation cell size of 64 x 64 with 50 % overlap, and that the best correlation pattern to apply to the surface of the test

specimen to ensure accurate correlation was the natural surface. The test also confirmed that the DIC system used was capable of measuring the level of strain applied under load. The feasibility of applying DIC as a full-field measurement technique for the generic panel was investigated. Initially, DIC was applied to an area of approximately 120 mm by 100 mm that a finite element (FE) model predicted would have relatively high levels of strain. It was discovered that the optimum processing parameters and the best correlation pattern for use on the tensile strips were not suitable for use on the full scale test. This proved the sensitivity of the DIC technique, and it was realised that an optimum operating procedure was not possible, and instead each application would require optimisation. Eventually, by reducing the area of application to 80 mm by 60 mm, applying a paint speckle pattern to the surface and using a multi-pass processing technique, it was possible to measure strains in the generic panel that validated the FE model. However, during the course of the feasibility study a number of issues for the use of full-field DIC on the generic panel were discovered. The relatively small area of interest for each DIC image means a total of 60 images would be required with a new calibration between each set. It was estimated that one generic panel would require in excess of 15 hours testing which is unfeasible.

A similar feasibility investigation was applied to TSA. TSA requires the application of a cyclic load to the test specimen to ensure pseudo-adiabatic conditions; the higher the loading frequency, the closer to adiabatic condition. However, it was not possible to maintain a frequency above 1 Hz in the full scale rig. Nevertheless, it was decided to apply full-field TSA to the generic panels. To image the entire generic panel it was necessary to take 32 separate images and it was possible to scan the surface in approximately 30 minutes. The images were then 'stitched' together using some Matlab code. The joined data was calibrated using constants experimentally measured from tensile specimens loaded at 1 Hz. The TSA data validated the processed FE data. The TSA technique was found to be more feasible than DIC and was therefore applied to all the generic panels for MO comparison.

The comparison of the performance of the MOs was continued on the generic panels, using full scale testing on the pressure test rig (hence fulfilling objectives 4d and e). Point measurements of the out-of-plane deflection were taken using a displacement transducer and full-field stress measurements using TSA. The deflection measurements in Chapter 9 determined that MO 5 provided a 27% decrease in maximum deflection compared to the MO 1 panels. This was an important result, even taking into account the 10% increase in weight. The stress results from the TSA and, therefore, the validated FE model showed panels produced using MO 1 had a peak stress of approximately 190 MPa, whilst MO 5 panels had between 100 and 120 MPa. This is in

agreement with the deflection data, although the measured stress for MO 5 has noise in the data due to the stitching in the NCF. Some consideration should also be given to panels produced using MO 4, because the woven out-of-autoclave material has recently become the process of choice for the future [117]. Panels manufactured with MO 4 are on average 12% heavier than MO 1. However, the MO 4 panels show 24% less deflection, which is a promising result. Due to the woven nature of MO 4 it was difficult to offer a comparison from the stress field found using TSA. Further work is required to investigate the effect of calibrating the woven data. When performing visual inspection of the panels produced using MO 4, patches of dry fabric were identified on the perimeter of the core and between the tows.

Performance analysis of the panels produced using MO 5 has measured an improvement of in performance of approximately 30%, although this should be tempered against the excess weight in the design of 10%. The cost analysis showed a reduction in material and labour cost when applied on site at GE, but also further advantages when considering a greenfield site. Therefore, it has been concluded that by using the NCF infiltrated with RFI and cured out-of-autoclave it is possible to produce aerospace standard components at a significant reduction in manufacturing cost (fulfilling objective 5).

In the future, impact and fatigue tests would provide a complete investigation of the performance of MO 5 for manufacture of secondary structure. Further analysis of the NCF material from the microscopic to panel level will be important, and the consideration of an improvement of the FE model discussed in this thesis. This model should take account of the individual plies within the NCF and the effect of the loose stitching. Further work is also required on the use of TSA for the analysis of the stresses in panels manufactured from woven composites. This would be necessary to confirm or disprove the use of global calibration to average over the individual tows or the weave. Also of interest is the analysis of more complex features for inclusion in the design of the generic panel (Appendix C shows two more generic panel designs). Finally, with adequate cost data from previous panel production it would be of interest to attempt to develop a cost model using feature or activity based costing described in this thesis.

References

1. Daniel, I.M., Ishai, O., *Engineering Mechanics of Composite Materials*. 1994: Oxford University Press.
2. Dow, M.B., *The ACEE program and basic composites research at Langley Research Center (1975 to 1986)*, N.A.A.S. Administration, Editor. 1987: Hampton, V A.
3. *The research requirements of the transport sectors to facilitate an increased usage of composite materials Part 1: The composite material research requirements of the aerospace industry*. 2004, EADS Deutschland GmbH, Coporate Research Centre.
4. Network, N.C. www.ncn-uk.co.uk. 04/2008].
5. Breuer, U.P., *Composite technology at Airbus Germany past, present and future*. 2002, Composite Technology Germany.
6. Soutis, C., *Fibre reinforced composites in aircraft construction*. Progress in Aerospace Sciences, 2005. **41**: p. 143-151.
7. Jones, R.M., *Mechanics of Composite Materials Second Edition*. 1999: Brunner-Routledge.
8. Chestney, J.A., Sarhadi, M. *A Prototype Manufacturing Cell for Automated Assembly of Fibre Reinforced Composite Preforms*. in *4th International Conference on Automated Composites*. 1995. Nottingham UK Institute of Materials.
9. Crump, D.A., Dulieu-Barton, J.M., Savage, J., *The manufacturing procedure for aerospace secondary structreu panels*. Journal of Sandwich Structures and Materials, 2009. **In press**: p. 1-28.
10. Abraham, D., McIlhagger, R, *Investigations into Various Methods of Liquid Injection to Achieve Mouldings with Minimum Void Contents and Full Wet Out*. Composites Part A: Applied science and manufacturing, 1998. **29**: p. 533-539.
11. Hinrichsen, J., Bautista, C., *The challenge of reducing both airframe weight and manufacturing cost*. Air and Space Europe, 2001. **3**: p. 119-121.
12. Kaufmann, K., Zenkert, D., Mattei, C., *Cost optimisation of composite aircraft structures including variable laminate qualities*. Composites Science and Technology, 2008. **68**: p. 2748-2754.
13. McCarthy, M., *BOJCAS: Bolted joints in composite aircraft structures*. Air and Space Europe, 2001. **3**: p. 1-4.
14. Stockton, D.J., R. Forster, and B. Messner, *Developing time estimating models for advanced composite manufacturing processes*. Aircraft Engineering and Aerospace Technology, 1998. **70**(6): p. 445-+.
15. Sheno, R.A., Groves, A., Rajapakse, Y. D. S., *Theory and Applications of Sandwich Structures*. 2005: Dorset Press.
16. Brillaud, J., Lagattu, F., *Limits and possibilities of laser speckle and white-light image-correlation methods: theory and experiments*. Applied Optics, 2002. **41**(31): p. 6603-6613.
17. Godara, A., Raabe, D., *Influence of fiber orientation on global mechanical behavior and mesoscale strain localization in a short glass-fiber-reinforced epoxy polymer composite during tensile deformation investigated using digital image correlation*. Composites Science and Technology, 2007. **67**: p. 2417-2427.
18. Stanley, P., Chan, W.K., *Quantitative stress analysis by means of the thermoelastic effect*. The Journal of Strain Analysis for Engineering Design, 1985. **20**(3): p. 129-137.
19. Woods, J.A., Modin, A. E., Hawkins, R. D., and Hanks, D. J., *Controlled atmospheric pressure resin infusion process*, U.P. Office, Editor. 2008, The Boeing Company: USA.

20. Miller, A.G., Lovell, D., Seferis, J.C., *The Evolution of an Aerospace Material: Influence of Design, Manufacturing and In-Service Performance*. Composite Structures, 1994. **27**: p. 193-206.
21. Mairtin, P.O., McDonnell, P., Connor, M.T., Eder, R., Bradaigh, C.M., *Process Investigation of a Liquid PA-12/Carbon Fibre Moulding System*. Composites Part A, 2001. **32**: p. 915-923.
22. Diaz, J. and L. Rubio, *Developments to manufacture structural aeronautical parts in carbon fibre reinforced thermoplastic materials*. Journal of Materials Processing Technology, 2003. **143-144**: p. 342-346.
23. Manson, J.A.E., Wakeman, M.D., Bernet, N., *Composite processing and manufacturing-an overview*, in *Comprehensive Composite Materials*, A. Kelly, Zweben, C., Editor. 2000. p. 577-607.
24. Rozant, O., Bourban, P.E., Manson, J.A.E., *Manufacturing of three dimensional sandwich parts by direct thermoforming*. Composites: Part A, 2001. **32**: p. 1593-1601.
25. Deo, R.B., Starnes I. H., Holzwart, R. C. *Low-cost composite materials and structures for aircraft application*. in *NATO RTO AVT Panel spring symposium and specialist's meeting*. 2001. Leon, Norway.
26. Karlsson, K.F., Astrom, B.T., *Manufacturing and applications of structural sandwich components*. Composites Part A: Applied science and manufacturing, 1997. **28A**: p. 97-111.
27. Laricheva, V.P., Korotkii, A.F., *Manufacture of High-Strength Composite Materials from Prepregs Prepared by Radiation Processing*. High Energy Chemistry, 2008. **42**(1): p. 23-28.
28. Carter, J.T., Emmerson, G.T., Lo Faro, C., McGrail, P.T., Moore, D.R., *The Development of a Low Temperature Cure Modified Epoxy Resin System for Aerospace Composites*. Composites Part A: Applied science and manufacturing, 2003. **80**(83-91).
29. Bibo, G.A., P.J. Hogg, and M. Kemp, *Mechanical characterisation of glass- and carbon-fibre-reinforced composites made with non-crimp fabrics*. Composites Science and Technology, 1997. **57**(9-10): p. 1221-1241.
30. Bader, M.G., *Selection of Composite Material and Manufacturing Routes for cost effective Performance*. Composites Part A: Applied science and manufacturing, 2002. **33**: p. 913-934.
31. González, A., E. Graciani, and F. París, *Prediction of in-plane stiffness properties of non-crimp fabric laminates by means of 3D finite element analysis*. Composites Science and Technology, 2008. **68**(1): p. 121-131.
32. Bibo, G.A., et al., *Carbon-fibre non-crimp fabric laminates for cost-effective damage-tolerant structures*. Composites Science and Technology, 1998. **58**(1): p. 129-143.
33. Aceves, C.M., A.A. Skordos, and M.P.F. Sutcliffe, *Design selection methodology for composite structures*. Materials & Design, 2008. **29**(2): p. 418-426.
34. Newell, G.C., R.O. Buckingham, and K. Khodabandehloo, *The automated manufacture of prepreg broadgoods components - A review of literature*. Composites Part a-Applied Science and Manufacturing, 1996. **27**(3): p. 211-217.
35. Edwards, K.L., *Exploiting new materials and processes for higher productivity: use of advanced composite technologies*. Materials and Design, 2004. **25**: p. 565-571.
36. Dexter, H.B. *Development of Textile Reinforced Composites for Aircraft Structures*. in *4th International Symposium for Textile Composites* 1998. Kyoto, Japan.
37. Henne, M., Ermanni, P., Deleglise, M., Kraeczak, P., *Heat Transfer of Fibre Beds in Resin Transfer Moulding: an experimental approach*. Composites Science and Technology, 2004. **64**: p. 1191-1202.
38. Pearce, N.R.L., Summerscales, J., Guild, F.J., *Improving the Resin Transfer Moulding Process for Fabric Reinforced Composites by Modification of the Fabric Architecture*. Composites Part A, 2000. **31**: p. 1433-1441.
39. Howard, N., *Cost effective composites for aerospace applications*. Reinforced Plastics, 2001. **45**(1): p. 40-42.
40. Gotch, T.M. *Improved production process for manufacture of GRP on British Rail*. in *Eleventh Reinforced Plastics Conference*. 1978. Brighton.
41. Sevostianov, I.B., Verijenko, V.E., Von Klemperer, C.J., Chevallereau, B., *Mathematical Model of Stress Formation During Vacuum Resin Infusion Process*. Composites Part B: Engineering, 1999. **30**: p. 513-521.
42. Antonucci, V., Giordano, M., Nicolais, L., Calabrò, A., Cusano, A., and A. Cutolo, Inserra, S., *Resin flow monitoring in resin film infusion process*. Journal of Materials Processing Technology, 2003. **143-144**: p. 687-692.

43. Park, J., Kang, M.K, *A numerical simulation of the resin film process*. Composite Structures, 2003. **60**: p. 431-437.
44. Edwards, K.L., *A risk-based approach to manufacturing process control: use in autoclave moulded composite sandwich panels*. Materials and Design, 2005. **26**: p. 690-699.
45. Margueres, P., Torres J.L., Perie, J.L., and K.S. Muhammad, Collombet, F., *Combined Approach for the Characterization of Composites Manufactured by RFI and Industrial Application*. Journal of Composite Materials, 2008. **42**(2): p. 189-209.
46. Abraham, D., S. Matthews, and R. McIlhagger, *A comparison of physical properties of glass fibre epoxy composites produced by wet lay-up with autoclave consolidation and resin transfer moulding*. Composites Part a-Applied Science and Manufacturing, 1998. **29**(7): p. 795-801.
47. Silcock, M.D., Garschke, C., Hall, W., Fox, B.L., *Rapid Composite Tube Manufacture Utilizing the Quickstep™ Process*. Journal of Composite Materials, 2007. **41**(8): p. 965-978.
48. Yoda, M.m.S., S., Yokoe, Y., Aijima, M., Shakudo, T., Imuta, M. *Electron Beam Processing for Aircraft Structures*. in *16th International Conference on Composite Materials (ICCM)*. 2007. Kyoto, Japan.
49. Imuta, M., Enomoto, K. *Development of Radiation Curing Technology of Polymer Matrix Composites by Japanese National Project on Advanced Materials and Process Development for Next Generation Aircraft Structures*. in *16th International Conference on Composite Materials (ICCM)*. 2007. Kyoto, Japan.
50. Honda, Y., Ogisu, T., Yoneda, H., Arai, N., Natsume, N., Ishikawa, T., Imuta, M. *Development of Composite Curing Process by Visible Light*. in *16th International Conference on Composite Materials (ICCM)*. 2007. Kyoto, Japan.
51. Mizuno, H., Hayashi, N., Enomoto, K. *Development of the UV-Cured RTM Process*. in *16th International Conference on Composite Materials (ICCM)*. 2007. Kyoto, Japan.
52. www.futurecomposites.org.uk. [cited 2009 March].
53. Zhang, Z. and M. Sarhadi, *An integrated CAD/CAM system for automated composite manufacture*. Journal of Materials Processing Technology, 1996. **61**(1-2): p. 104-109.
54. Harper, L.T., Turner, T.A., Warrior, N.A., Rudd, C.D. , *Characterisation of random carbon fibre composites from a directed fibre preforming process: The effect of tow filamentisation*. Composites: Part A, 2007. **38**: p. 755-770.
55. Mills, A., *Automation of Carbon Fibre Preform Manufacture for Affordable Aerospace Applications*. Composites Part A: Applied science and manufacturing, 2001. **32**: p. 955-962.
56. Buckingham, R.O. and G.C. Newell, *Automating the manufacture of composite broadgoods*. Composites Part A: Applied Science and Manufacturing, 1996. **27**(3): p. 191-200.
57. Groppe, D., *Robotic "layup" of composite materials*. Assembly Automation, 2003. **23**(2): p. 153-158.
58. Prasad, P.A. and J. Atkinson, *Automated manufacture of composites: handling, measurement of properties and lay-up simulations*. Composites Part a-Applied Science and Manufacturing, 2003. **34**(6): p. 493-501.
59. Hicks, B.J., S.J. Culley, and G. Mullineux, *Cost estimation for standard components and systems in the early phases of the design process*. Journal of Engineering Design, 2002. **13**(4): p. 271-292.
60. Tang, D.B., W. Eversheim, and G. Schuh, *Qualitative and quantitative cost analysis for sheet metal stamping*. International Journal of Computer Integrated Manufacturing, 2004. **17**(5): p. 394-412.
61. Weustink, I.F., et al., *A generic framework for cost estimation and cost control in product design*. Journal of Materials Processing Technology, 2000. **103**(1): p. 141-148.
62. Curran, R., Raghunathan, S., Price, M, *Review of Aerospace Engineering Cost Modelling: The Genetic Causal Approach*. Progress in Aerospace Sciences. **40**: p. 487-534.
63. Ulrich, K., et al., *Including the Value of Time in Design-for-Manufacturing Decision-Making*. Management Science, 1993. **39**(4): p. 429-447.
64. Edwards, D.A., F.W. Williams, and D. Kennedy, *Cost optimization of stiffened panels using VICONOPT*. Aiaa Journal, 1998. **36**(2): p. 267-272.
65. Kassapoglou, C., *Simultaneous cost and weight minimisation of composite-stiffened panels under compression and shear*. Composites Part A, 1997. **28A**: p. 419-435.
66. Kassapoglou, C., *Minimum cost and weight design of fuselage frames Part A: design constraints and manufacturing process characteristics*. Composites Part A, 1999. **30**: p. 887-894.

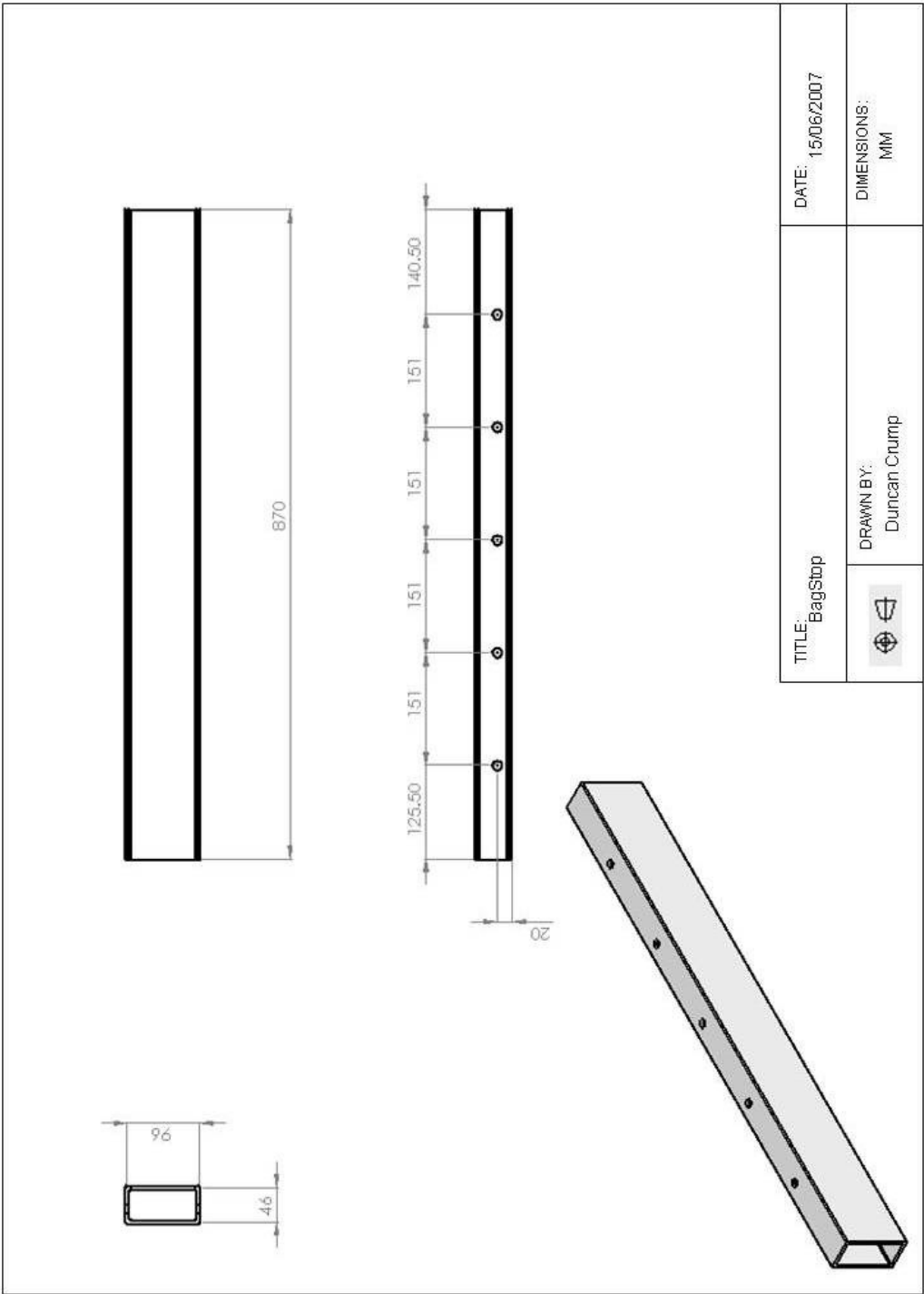
67. Kassapoglou, C., *Minimum cost and weight design of fuselage frames Part B: cost considerations, optimisation and results*. Composites Part A, 1999. **30**: p. 895-904.
68. Gutowski, T., Henderson, R., Shipp, C., *Manufacturing Costs for Advanced Composites Aerospace Parts*. SAMPE Journal, 1991. **27**: p. 37-43.
69. Gutowski, T.G., *Advanced Composite Manufacturing First Edition*. 1997: New York : Wiley.
70. Baker, A.A., et al., *An affordable methodology for replacing metallic aircraft panels with advanced composites*. Composites Part a-Applied Science and Manufacturing, 2002. **33**(5): p. 687-696.
71. Layer, A., et al., *Recent and future trends in cost estimation*. International Journal of Computer Integrated Manufacturing, 2002. **15**(6): p. 499-510.
72. Ben-Arieh, D. and L. Qian, *Activity-based cost management for design and development stage*. International Journal of Production Economics, 2003. **83**(2): p. 169-183.
73. Qing, W., Stockton, D., *Cost Model Development Using Artificial Neural Networks*. Aircraft Engineering and Aerospace Technology, 2001. **73**: p. 536-541.
74. Niazi, A., et al., *Product cost estimation: Technique classification and methodology review*. Journal of Manufacturing Science and Engineering-Transactions of the Asme, 2006. **128**(2): p. 563-575.
75. Haslehurst, M., *Manufacturing Technology Third Edition*. 1981: Hodder and Stoughton.
76. Boyd, L.H. and J.F. Cox, *Optimal decision making using cost accounting information*. International Journal of Production Research, 2002. **40**(8): p. 1879-1898.
77. Wang, Q., D.J. Stockton, and P. Baguley, *Process cost modelling using neural networks*. International Journal of Production Research, 2000. **38**(16): p. 3811-3821.
78. Niemi, E., *Machining Cost Optimization Involving Shift and Overtime Work*. Journal of Manufacturing Science and Engineering. **122**: p. 790-794.
79. Duverlie, P. and J.M. Castelain, *Cost estimation during design step: Parametric method versus case based reasoning method*. International Journal of Advanced Manufacturing Technology, 1999. **15**(12): p. 895-906.
80. Cavalier, S., P. Maccarrone, and R. Pinto, *Parametric vs. neural network models for the estimation of production costs: A case study in the automotive industry*. International Journal of Production Economics, 2004. **91**(2): p. 165-177.
81. Lere, J.C., *Activity-Based Costing: A Powerful Tool for Pricing*. Journal of Business and Industrial Marketing, 2000. **15**: p. 23-33.
82. Tuncel, G., et al., *Application of activity-based costing in a manufacturing company: A comparison with traditional costing*, in *Computational Science - Iccs 2005, Pt 3*. 2005. p. 562-569.
83. Pirttila, T. and P. Hautaniemi, *Activity-based costing and distribution logistics management*. International Journal of Production Economics, 1995. **41**(1-3): p. 327-333.
84. Lere, J.C., *Your product-costing system seems to be broken: Now what?* Industrial Marketing Management, 2001. **30**(7): p. 587-598.
85. Boons, A., *Product costing for complex manufacturing systems*. International Journal of Production Economics, 1998. **55**(3): p. 241-255.
86. Ozbayrak, M., M. Akgun, and A.K. Turker, *Activity-based cost estimation in a push/pull advanced manufacturing system*. International Journal of Production Economics, 2004. **87**(1): p. 49-65.
87. Jiao, J.X. and M.M. Tseng, *A pragmatic approach to product costing based on standard time estimation*. International Journal of Operations & Production Management, 1999. **19**(7): p. 738-755.
88. Tsai, W.H., *A technical note on using work sampling to estimate the effort on activities under activity-based costing*. International Journal of Production Economics, 1996. **43**(1): p. 11-16.
89. Gunasekaran, A. and M. Sarhadi, *Implementation of activity-based costing in manufacturing*. International Journal of Production Economics, 1998. **56-7**: p. 231-242.
90. Waters, H., H. Abdallah, and D. Santillan, *Application of activity-based costing (ABC) for a Peruvian NGO healthcare provider*. International Journal of Health Planning and Management, 2001. **16**(1): p. 3-18.
91. Bode, J., *Neural networks for cost estimation: simulations and pilot application*. International Journal of Production Research, 2000. **38**(6): p. 1231-1254.
92. Gutowski, T., et al, *Development of a Theoretical Cost Model for Advanced Composite Fabrication*. Composites Manufacturing, 1994. **5**: p. 231-239.

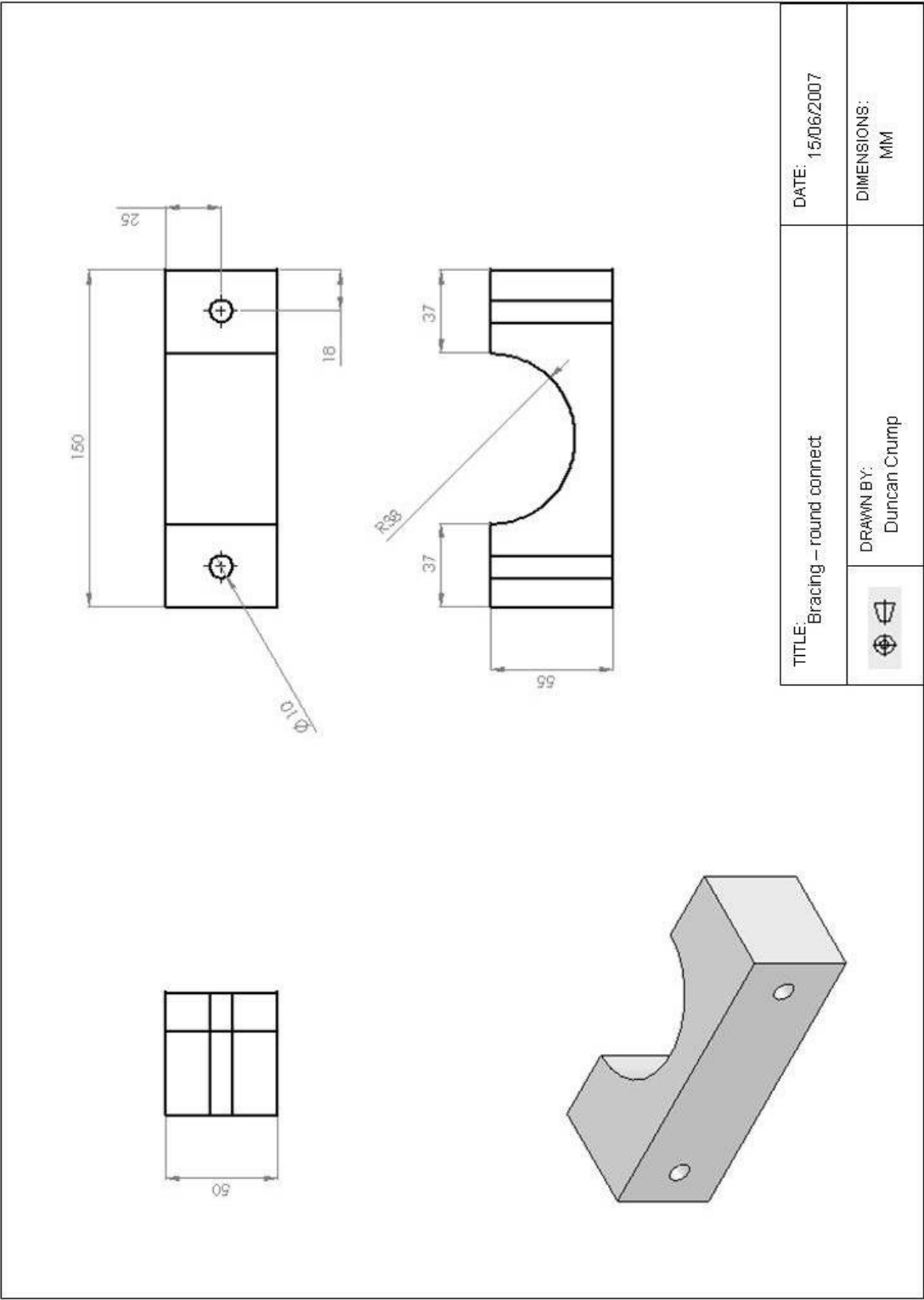
93. Roy, R., et al., *Quantitative and qualitative cost estimating for engineering design*. Journal of Engineering Design, 2001. **12**(2): p. 147-162.
94. Leibl, P., M. Hundal, and G. Hoehne, *Cost calculation with a feature-based CAD system using modules for calculation, comparison and forecast*. Journal of Engineering Design, 1999. **10**(1): p. 93-102.
95. OuYang, C. and T.S. Lin, *Developing an integrated framework for feature-based early manufacturing cost estimation*. International Journal of Advanced Manufacturing Technology, 1997. **13**(9): p. 618-629.
96. Wang, K., Kelly, D. and Dutton, S., *Multi-objective optimisation of composite aerospace structures*. Composite Structures, 2002. **57**: p. 141-148.
97. Park C. H., L., W. I., Han, W. S., and Vautrin, A., *Simultaneous optimisation of composite structures considering mechanical performance and manufacturing cost*. Composite Structures, 2004. **65**: p. 117-127.
98. Gigliotti, M., Riccio, A., Luspa, L., Scaramuzzino, F., Mormile, L., *Weight optimisation of damage resistant composite panels with a posteriori cost evaluation*. Composite Structures, 2009. **88**: p. 312-322.
99. Niu, M., *Composite Airframe Structures*. 1992: Adaso Adastra Engineering Center.
100. Afendi, M.d., Banks, W.M., Kirkwood, D., *Bubble free resin for infusion process*. Composites: Part A, 2005. **36**: p. 739-746.
101. Judd, N.W.C., Wright, W.W., *Voids and their effects on the mechanical properties of composites - An appraisal*. SAMPE Journal, 1978. **14**: p. 10-14.
102. Johannes, M., Dulieu-Barton, J.M., Bozhevolnaya, E., Thomsen, O.T., *Characterisation of local effects at core junctions in sandwich structures using thermoelastic stress analysis*. The Journal of Strain Analysis for Engineering Design, 2008. **43**(6): p. 469-492.
103. Hexcel. www.Hexcel.com. [cited 2006].
104. Jolma, P., Segercrantz, S., Berggreen, C., *Ultimate Failure of Debond Damaged Sandwich Panels Loaded with Lateral Pressure – An Experimental and Fracture Mechanics Study*. Journal of Sandwich Structures and Materials, 2007. **9**: p. 167-196.
105. Anon, *Optical deformation and strain field imaging*, L. Vision, Editor.
106. Corr, D., Accardi, M., Graham-Brady, L., Shah, S., *Digital image correlation analysis of interfacial debonding properties and fracture behavior in concrete*. Engineering Fracture Mechanics, 2007. **74**: p. 109-121.
107. Dulieu-Barton, J.M., Emery, T., Quinn, S. and Cunningham, P., *A temperature correction methodology for quantitative thermoelastic stress analysis and damage assessment*. Measurement Science and Technology, 2006. **17**(6): p. 1627-1637.
108. Dulieu-Barton, J.M., Stanley, P., *Applications of thermoelastic stress analysis to composite materials*. Strain, 1999. **35**(2): p. 41-48.
109. Pitarresi, G., Patterson, E.A., *A review of the general theory of thermoelastic stress analysis*. The Journal of Strain Analysis for Engineering Design, 2003. **38**(5): p. 405-417.
110. Paynter, R.J.H., Dutton, A.G., *The use of a second harmonic correlation to detect damage in composite structures using thermoelastic stress measurements*. Strain, 2003. **39**(2): p. 73-78.
111. Dulieu-Barton, J.M., Quinn, S., Shenoi, R.A., Read, P.J.C.L., and Moy, S.S.J., *Thermoelastic stress analysis of a GRP tee joint*. Applied Composite Materials, 1997. **4**(5): p. 283-303.
112. Boyd, S.W., Dulieu-Barton, Thomsen, O.T. and Gheradi, A., *A development of finite element model for analysis of pultruded structures using thermoelastic data*. Composites Part A: Applied science and manufacturing, 2008. **29**: p. 1311-1321.
113. Cunningham, P.R., Dulieu-Barton, J.M., Shenoi, R.A., *Damage location and identification using infra-red thermography and thermoelastic stress analysis*. Proceedings of SPIE, 2002. **4704**: p. 93-103.
114. Cunningham, P.R., Dulieu-Barton, J.M., Dutton, A.G., Shenoi, R.A., *Thermoelastic characterisation of damage around a circular hole in GRP component*. Key Engineering Materials, 2001. **204-205**: p. 453-463.
115. Fruehmann, R.K., Dulieu-Barton, J.M., Quinn, S., *On the thermoelastic response of woven composite materials*. Journal of Strain Analysis, 2008.
116. <http://www.matweb.com>. Online material database].
117. Systems, G.A.

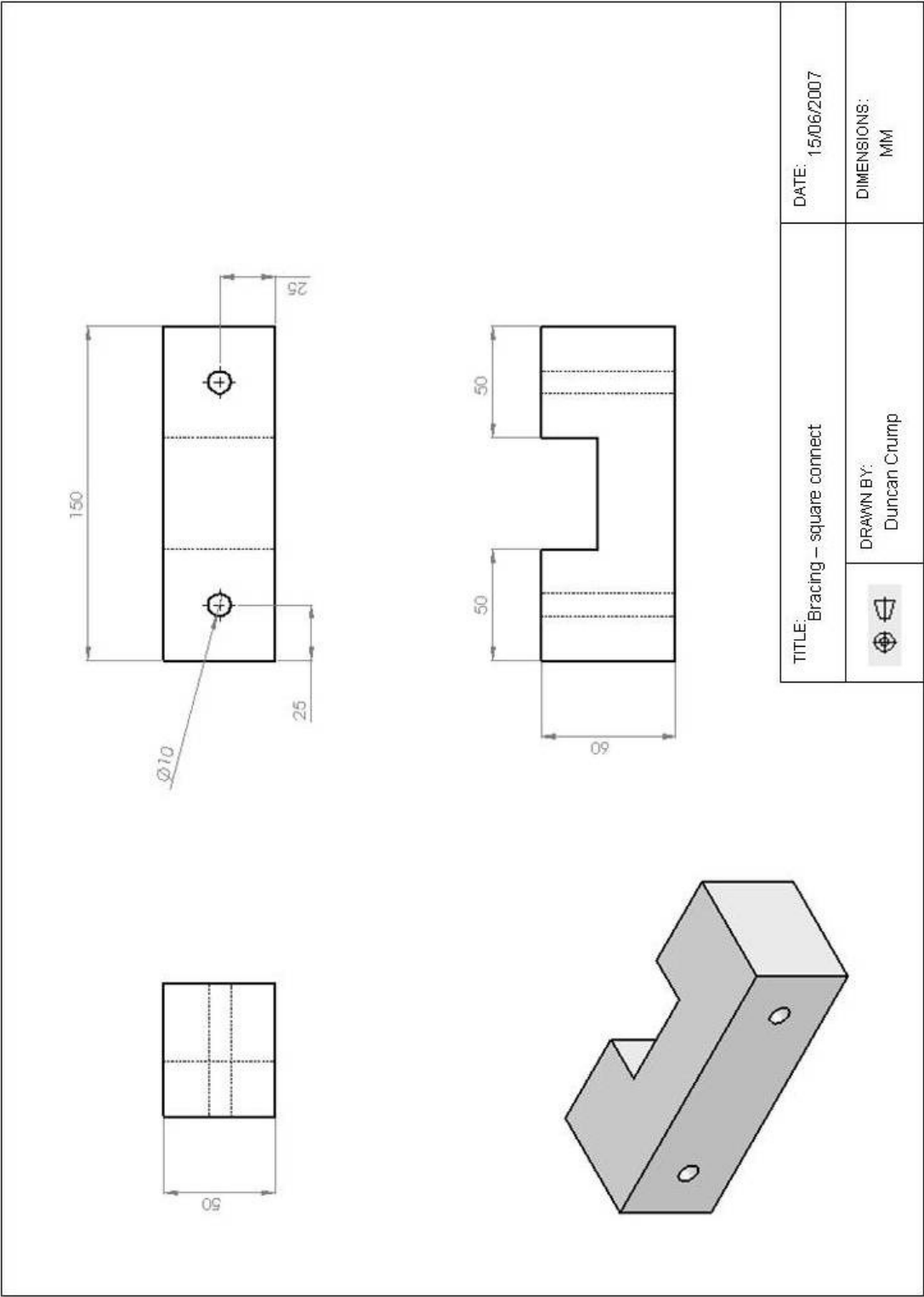
118. Oakeshott, J.L., Iannucci, L., Robinson, P., *Development of a Representative Unit Cell Model for Bi-axial NCF Composites*. Journal of Composite Materials, 2007. **41**(7): p. 801-835.
119. Wilson, R.B., *Continuous feed volumetric heating and convection oven*. 2007: USA.

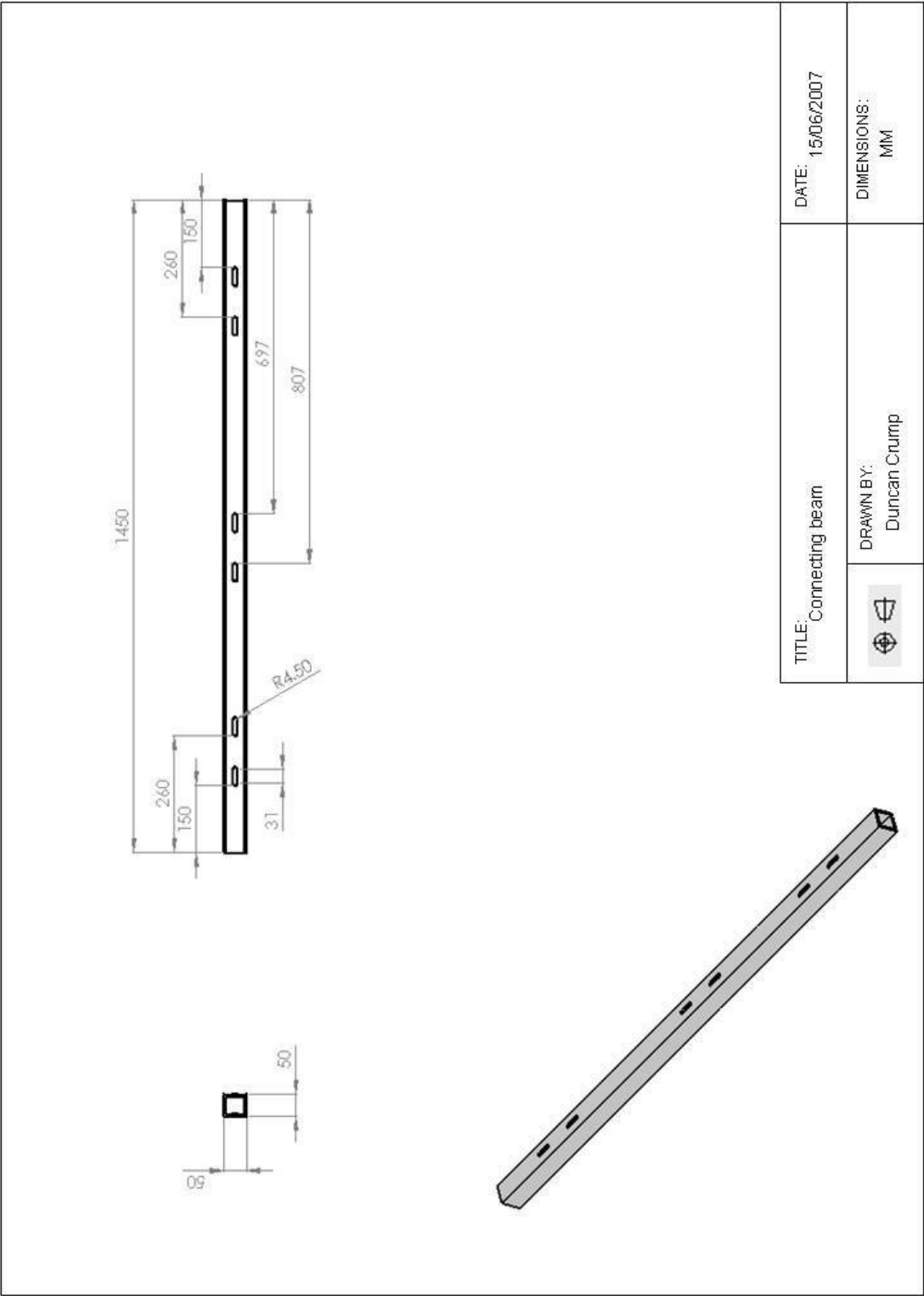
Appendices

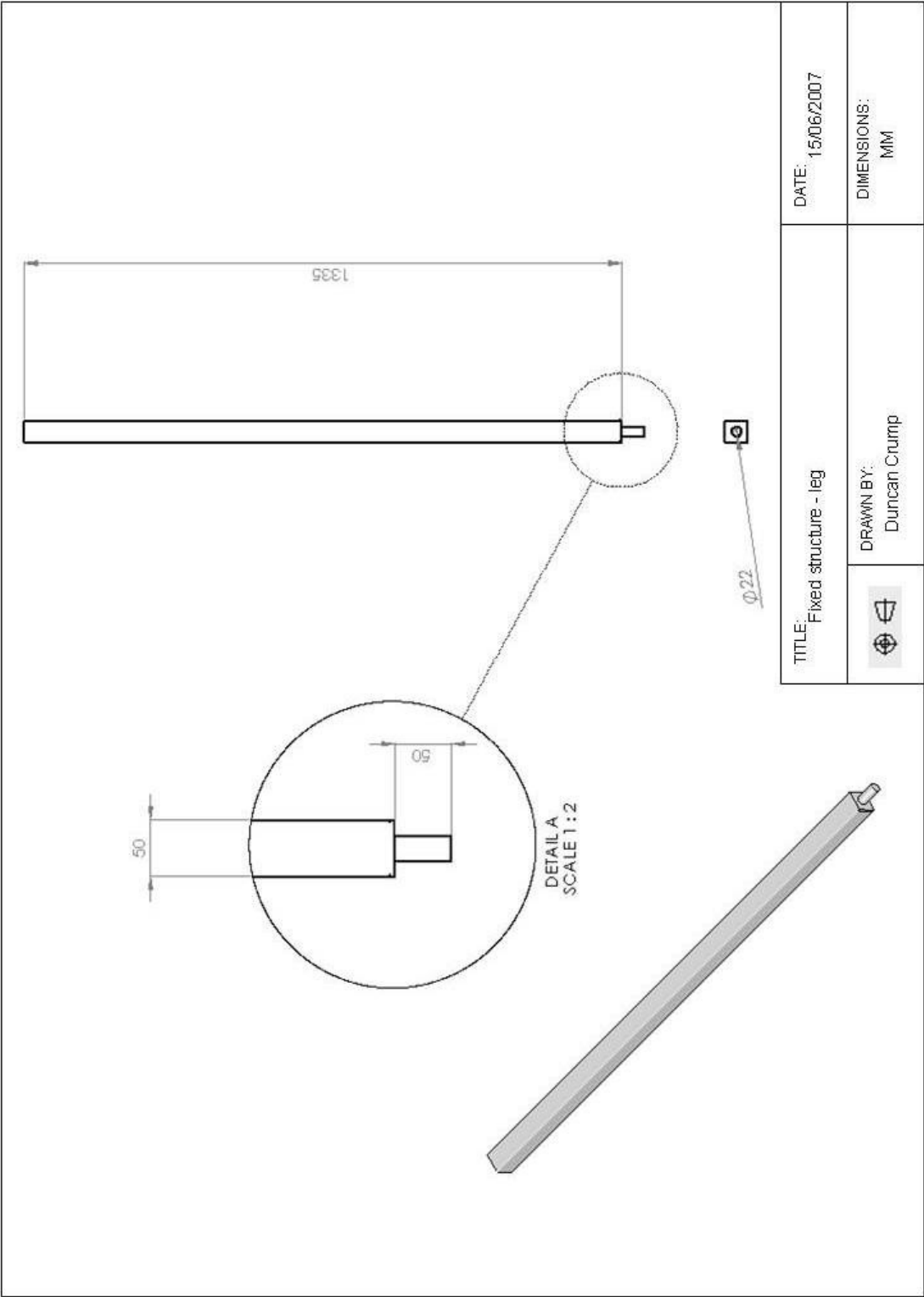
Appendix A – Drawings of Test Rig design

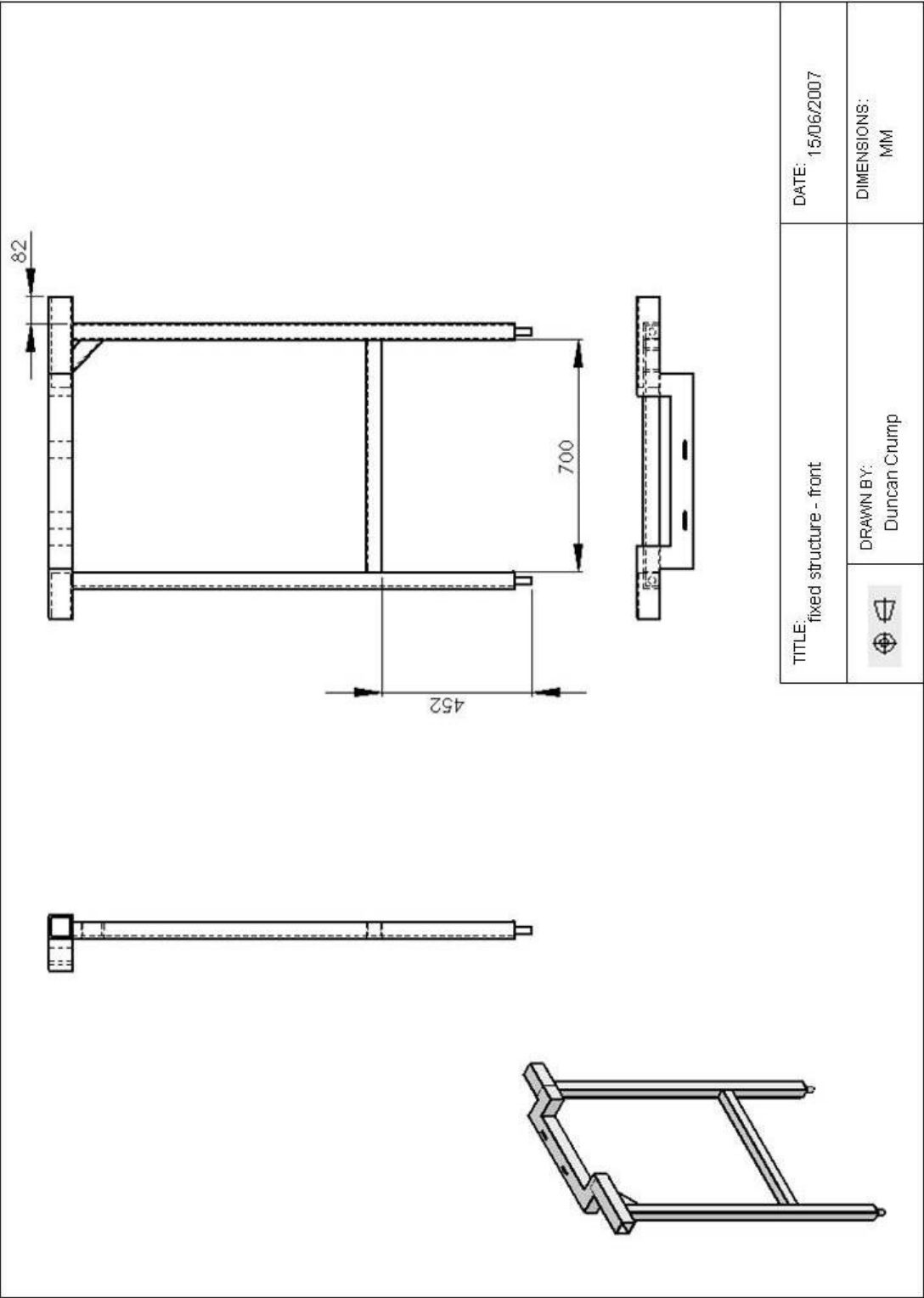


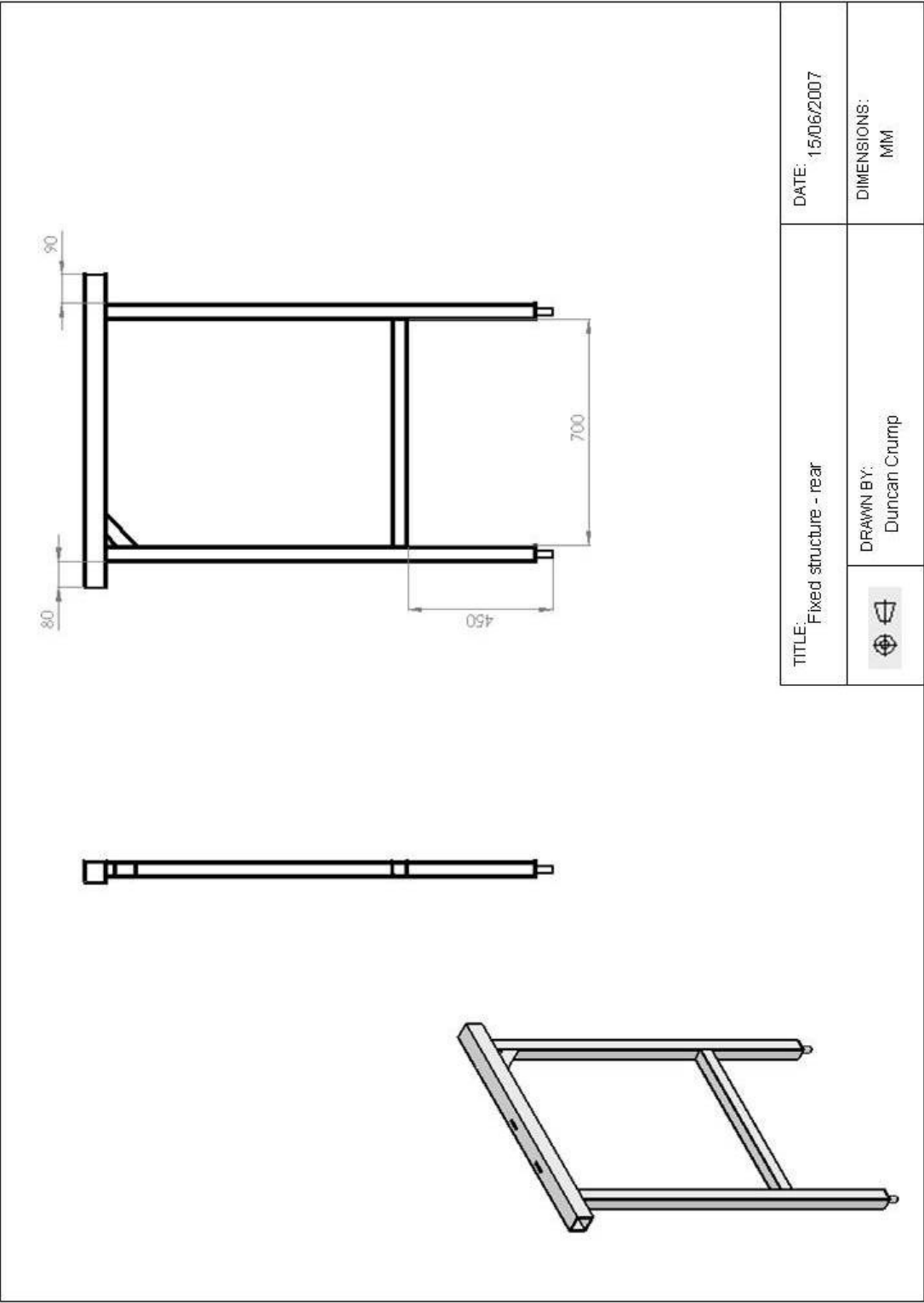


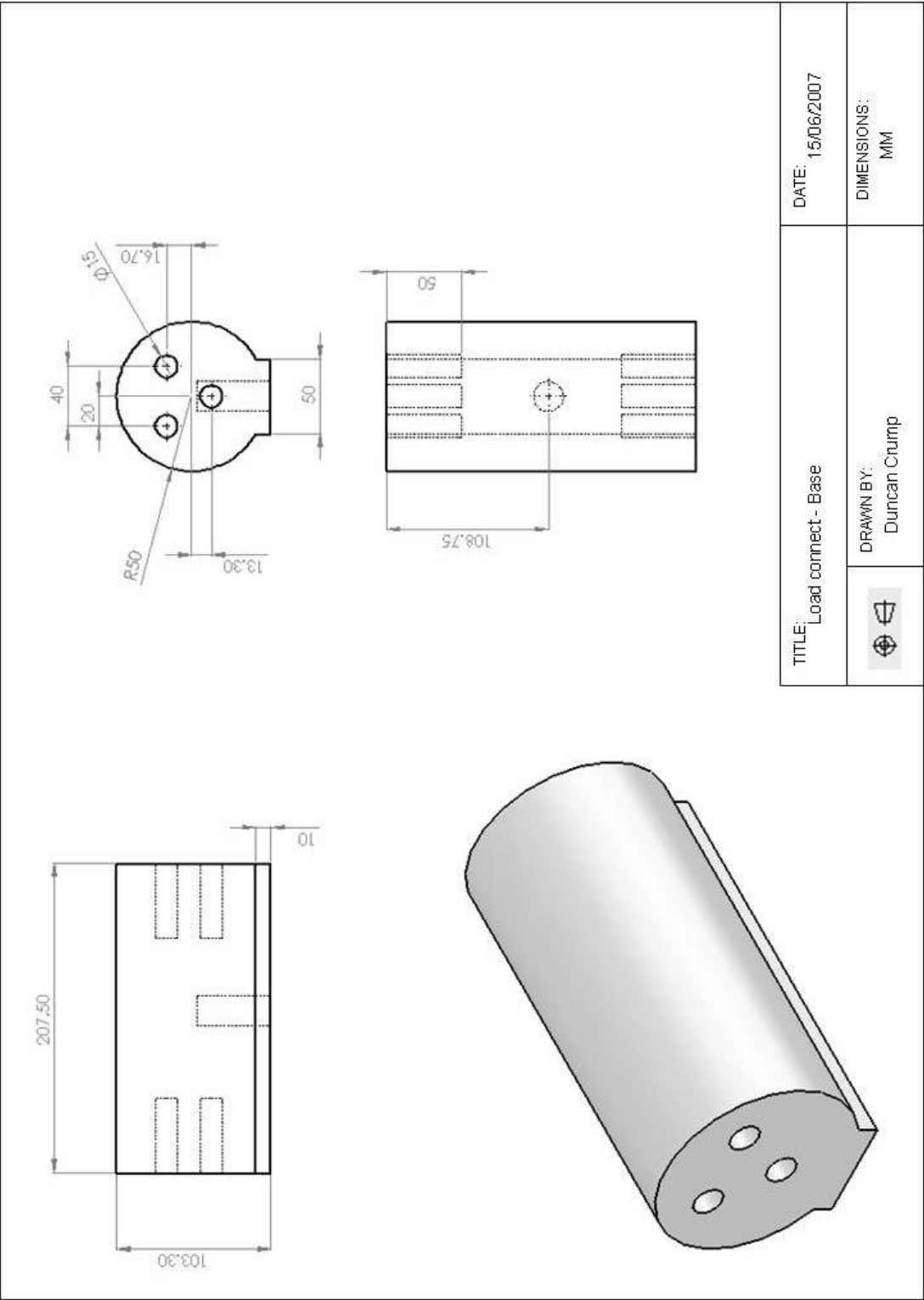


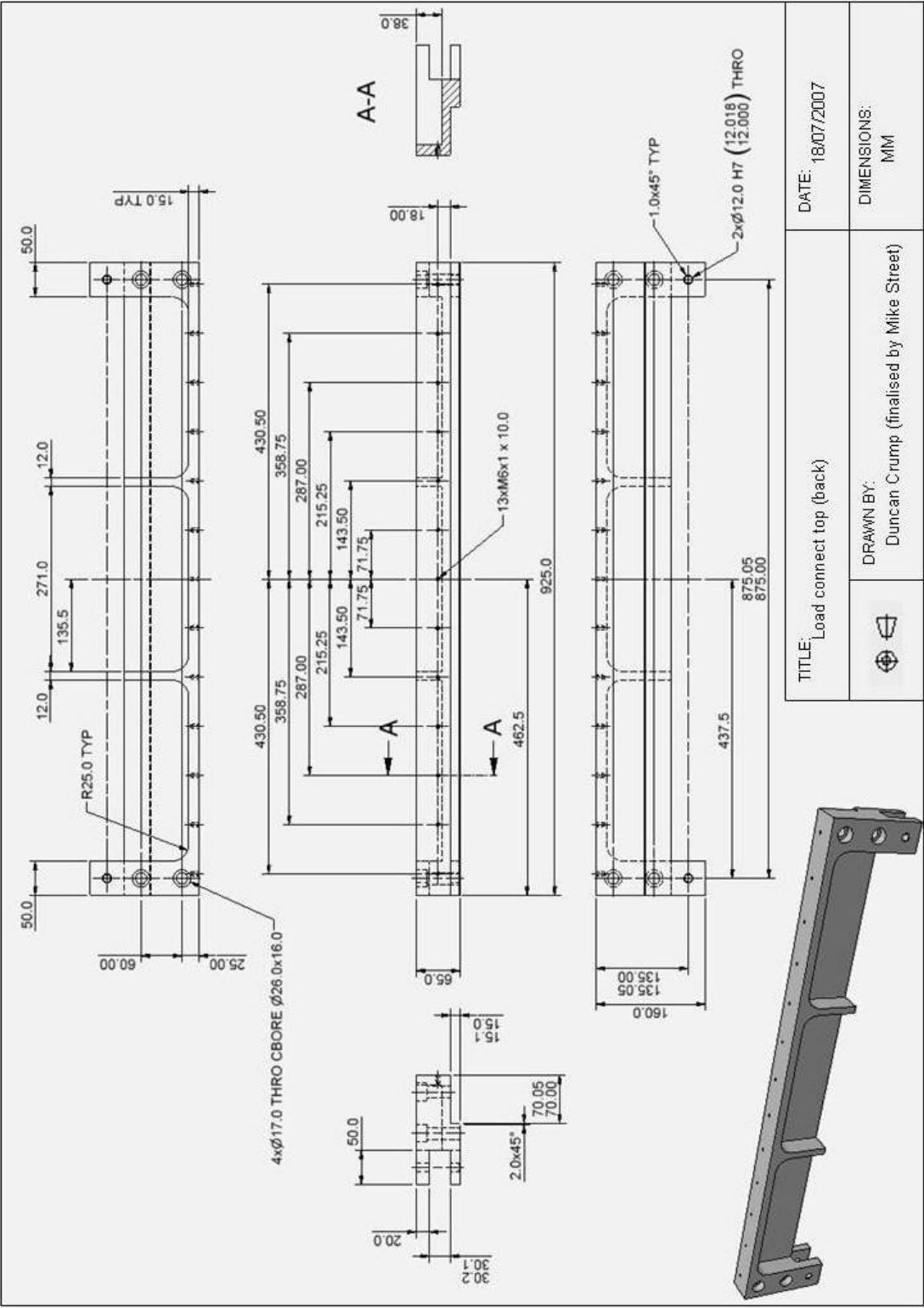


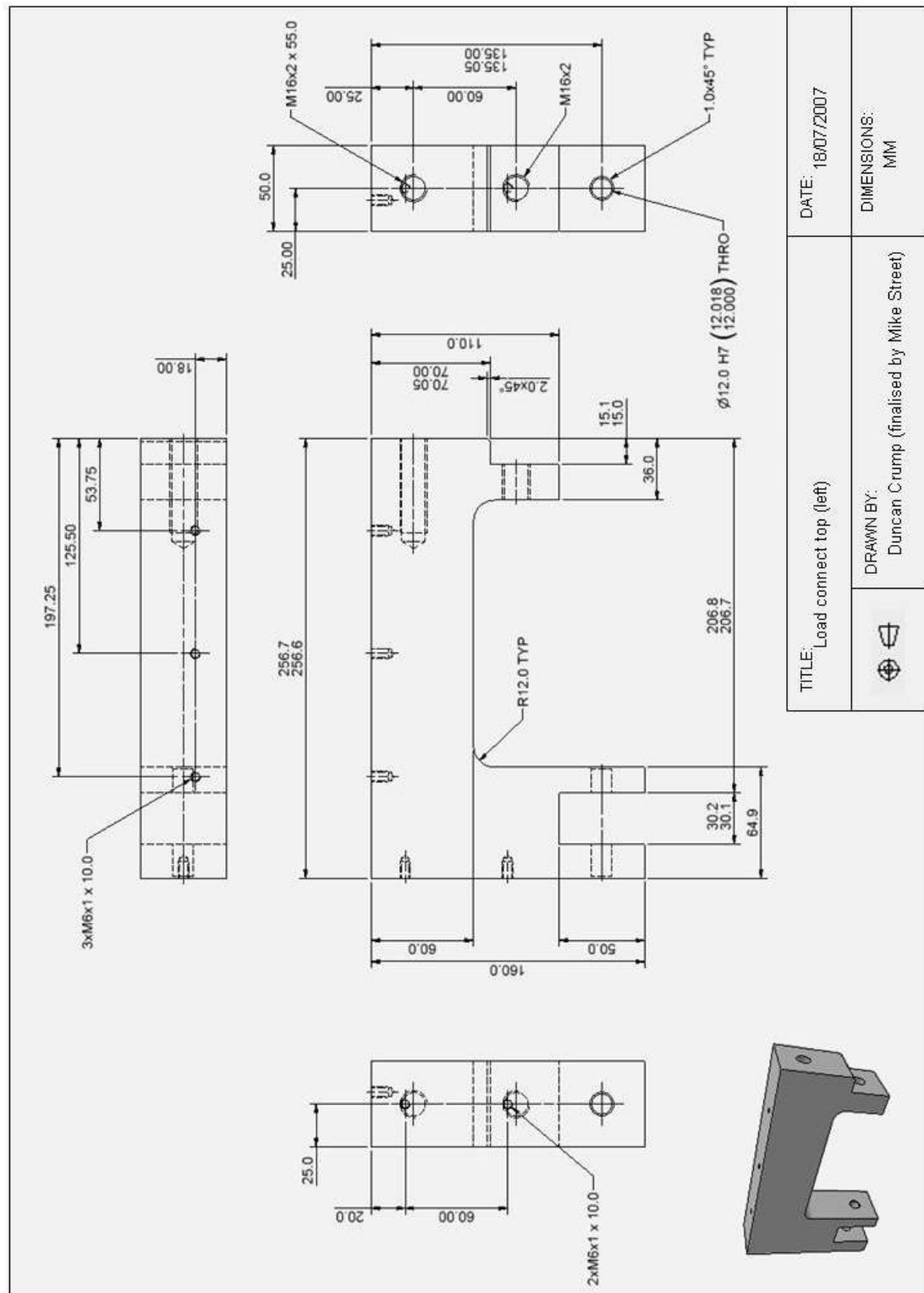


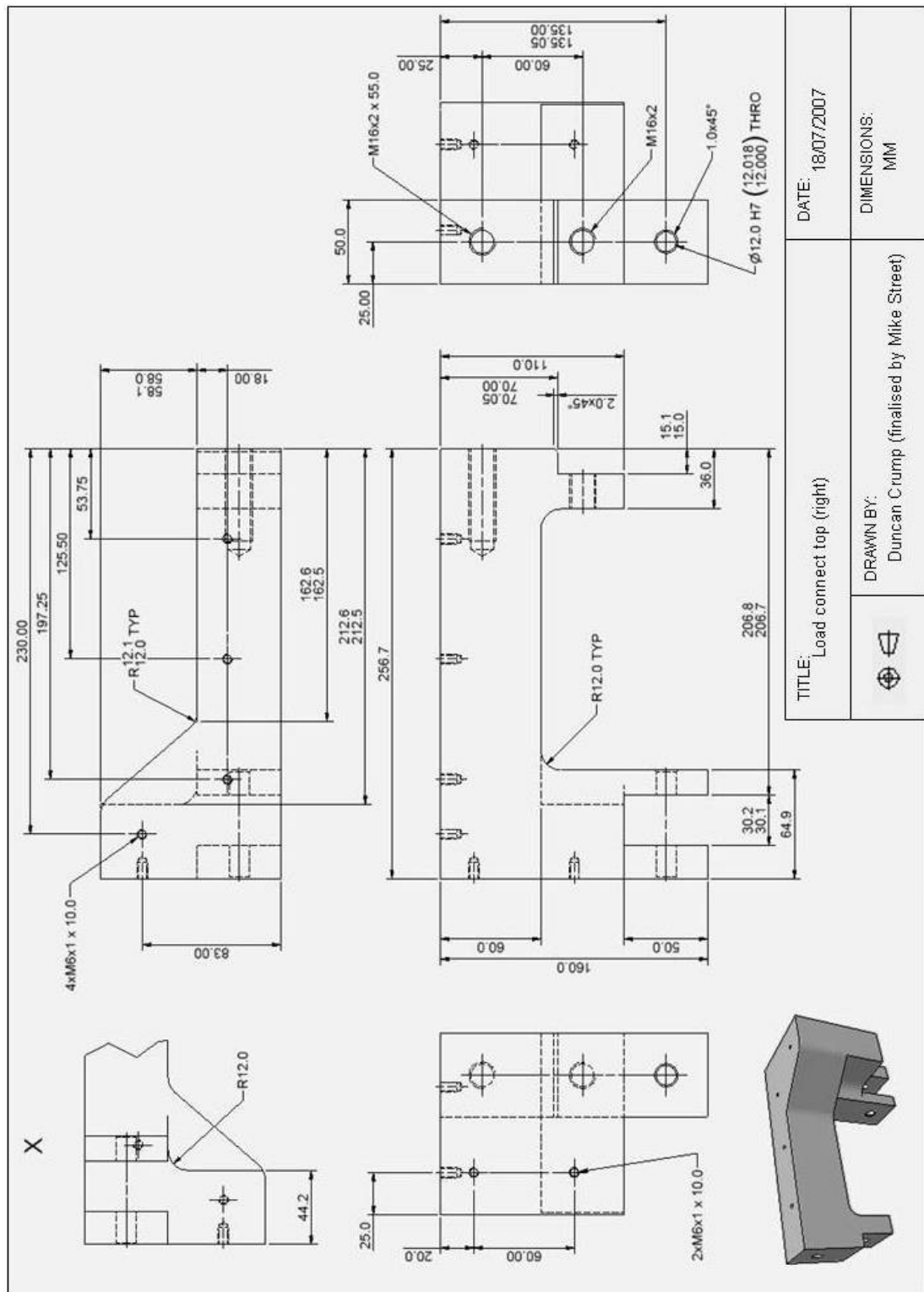


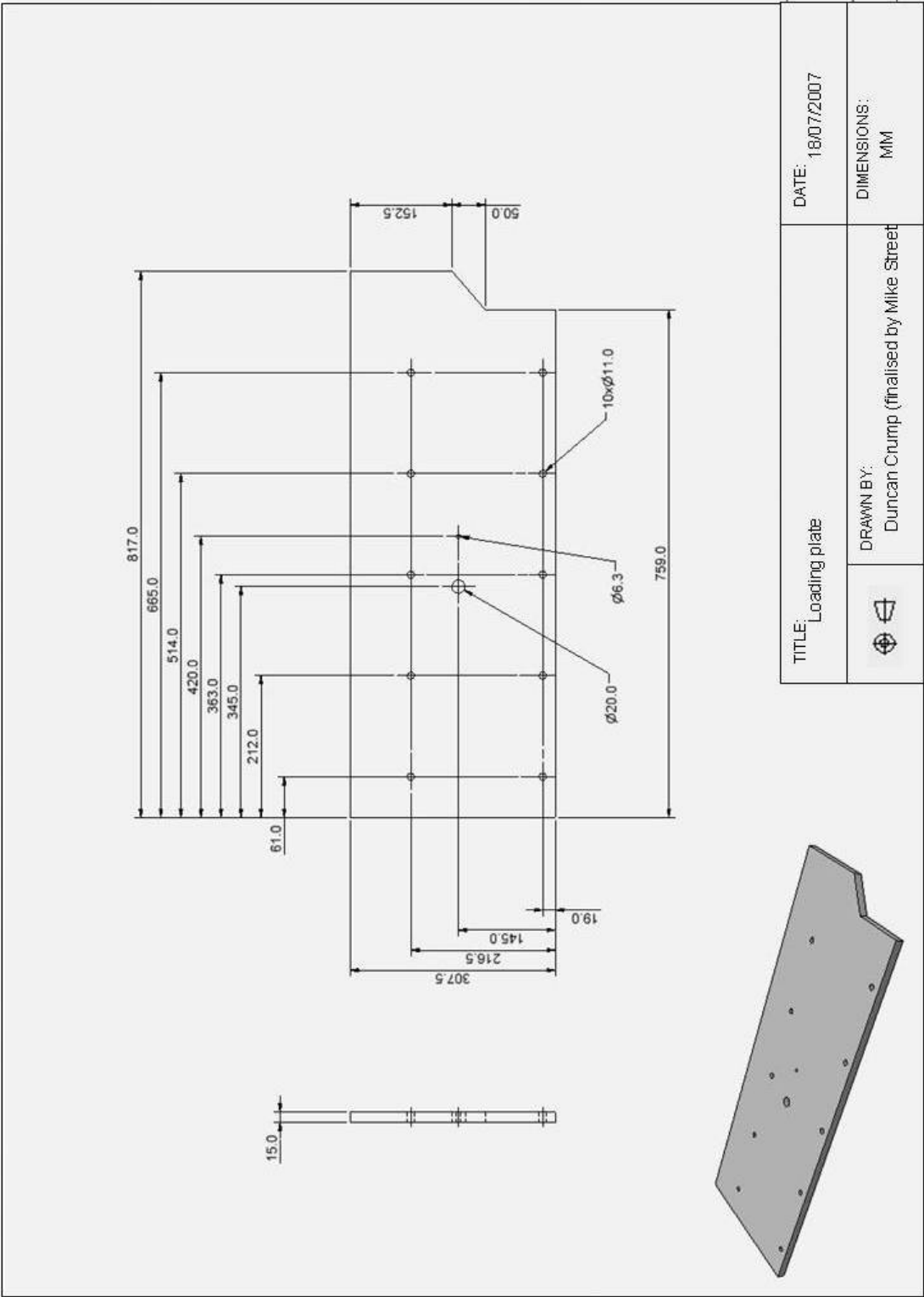




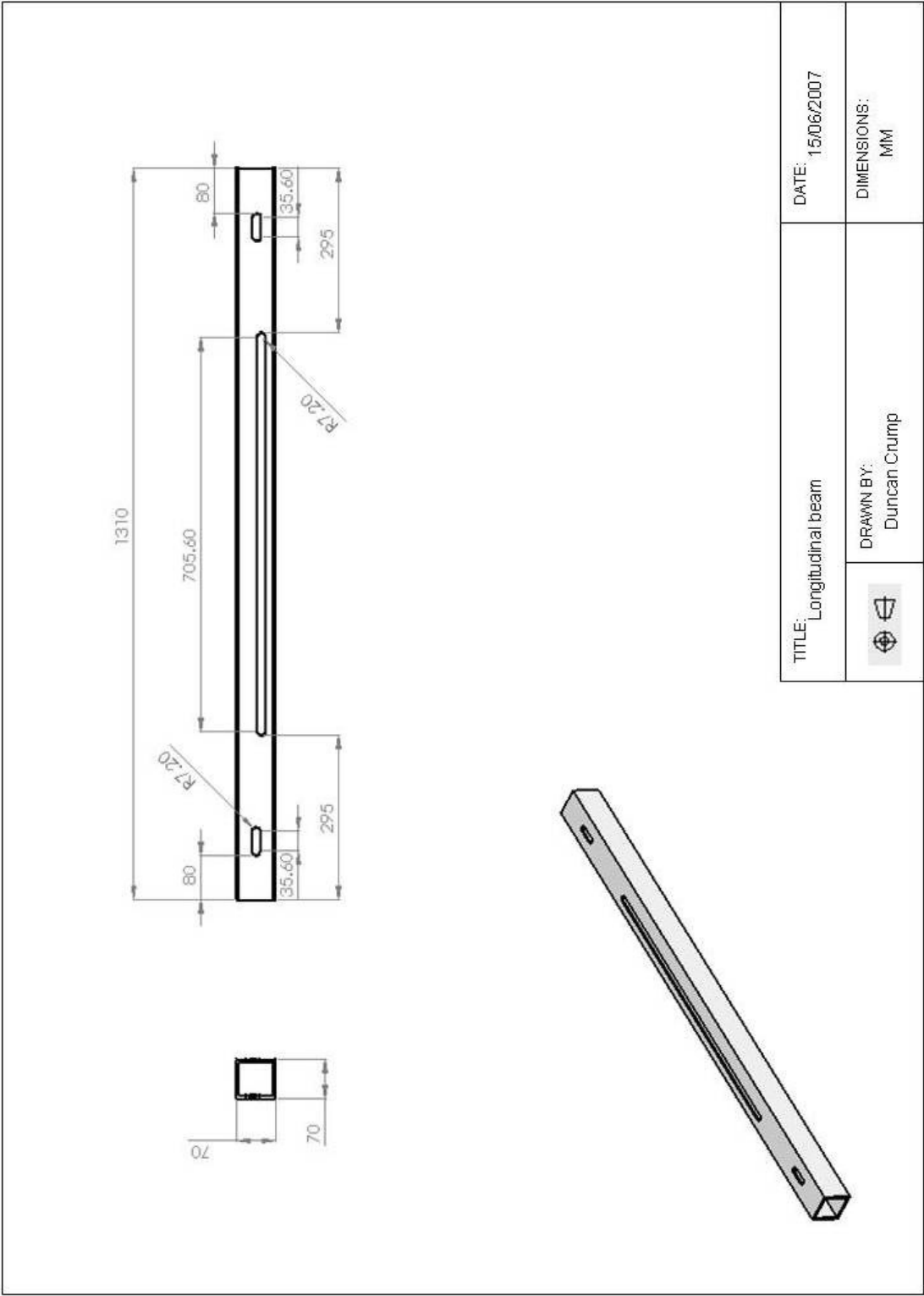


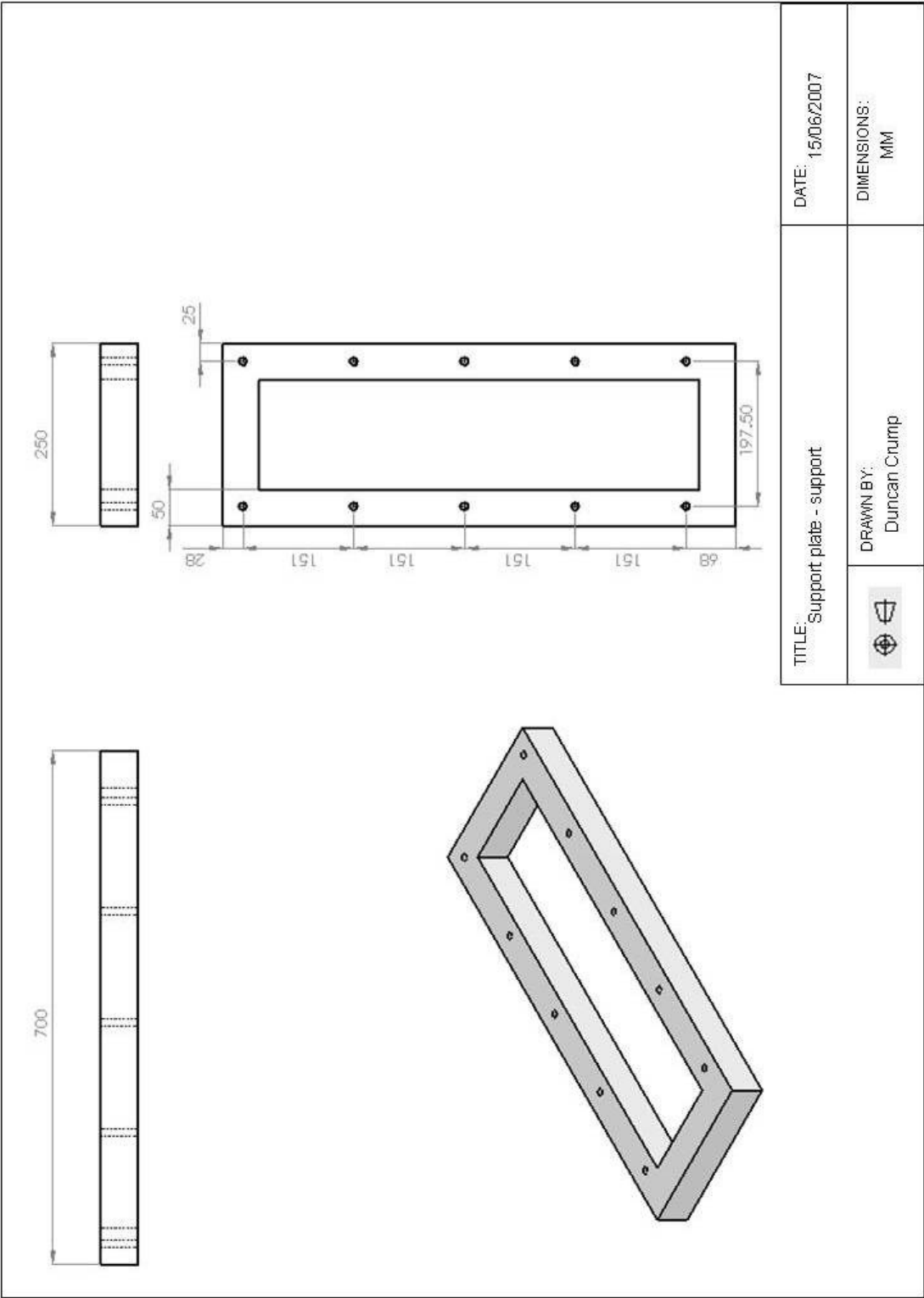


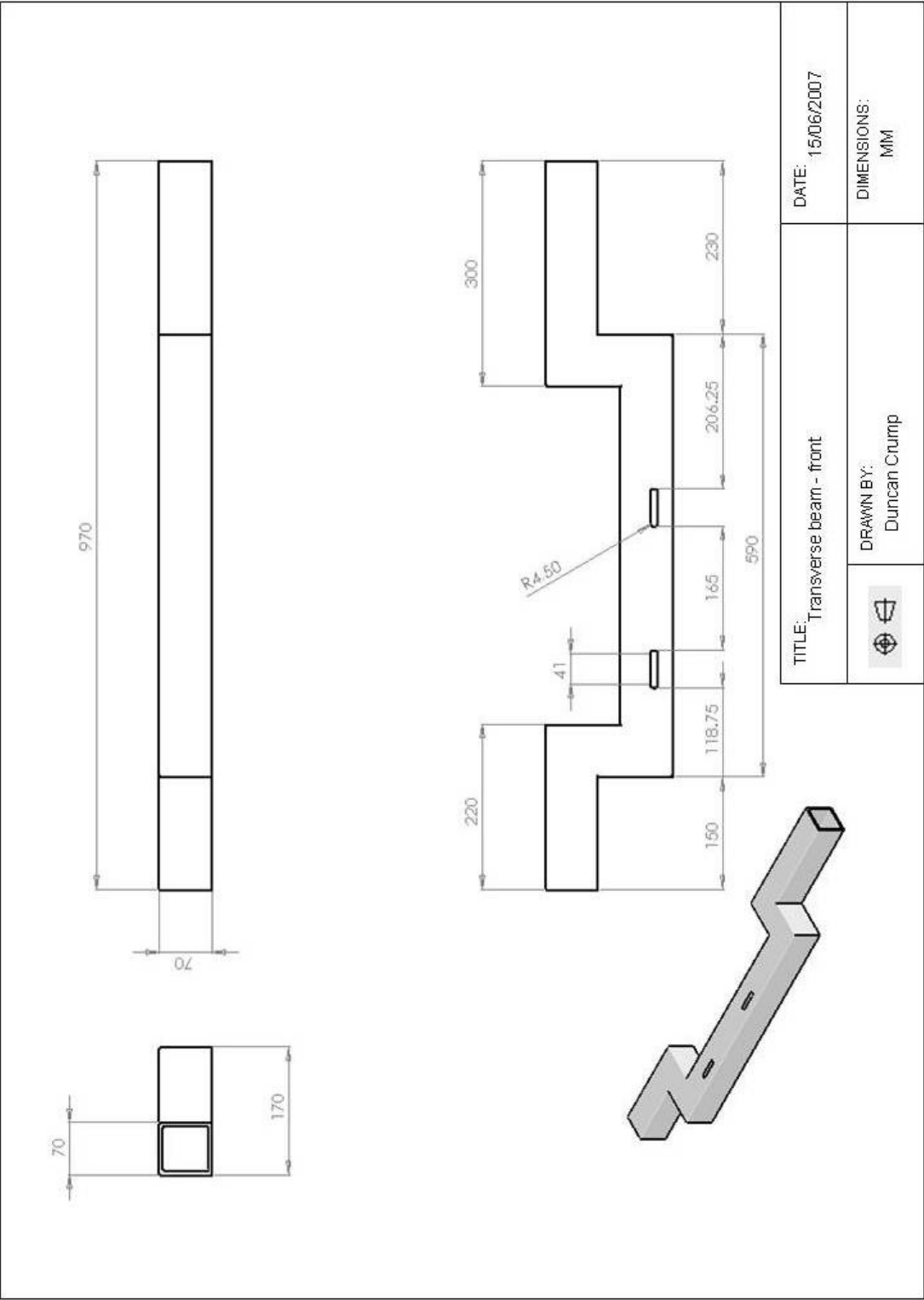


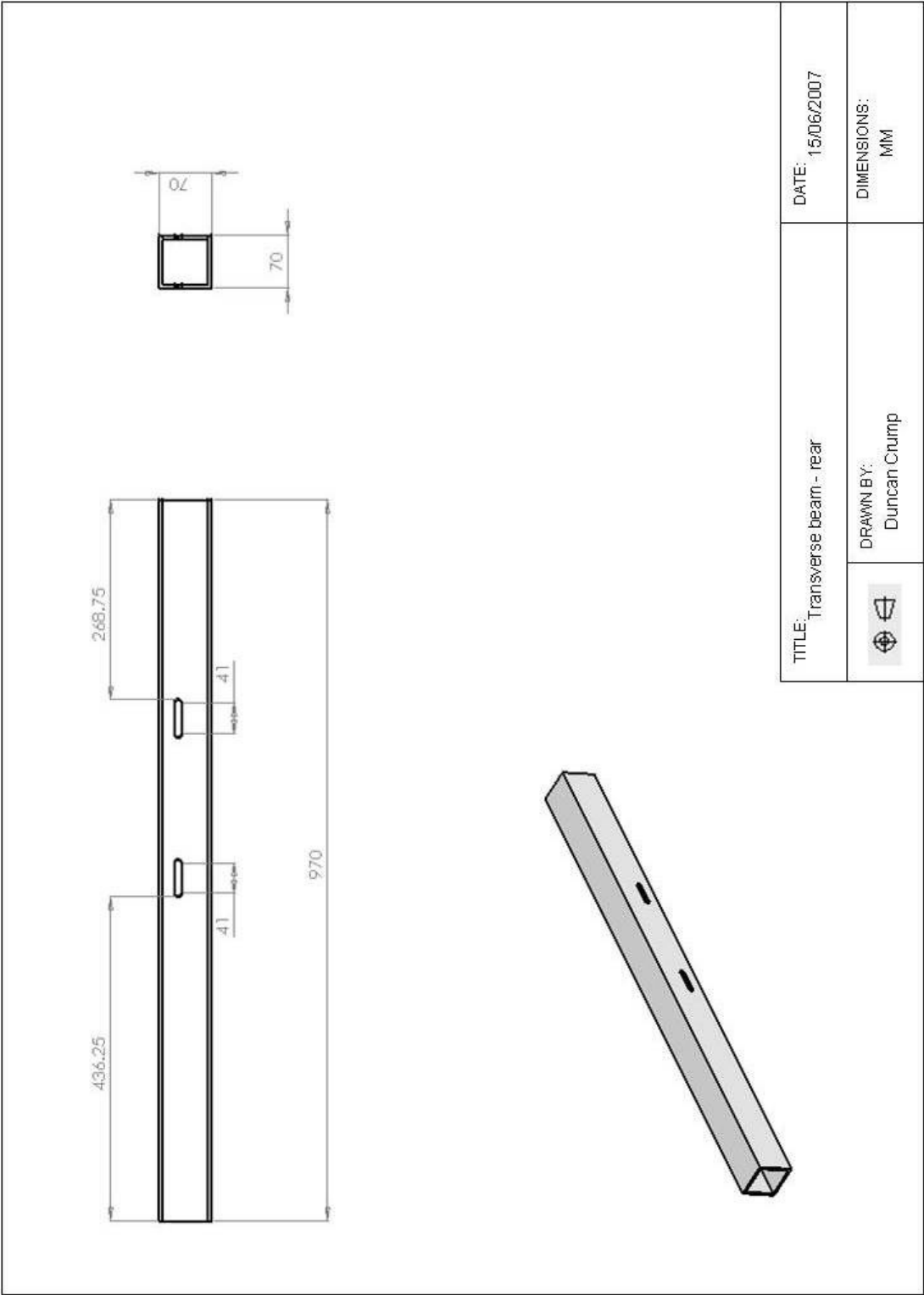



TITLE: Loading plate		DATE: 18/07/2007
	DRAWN BY: Duncan Crump (finalised by Mike Street)	DIMENSIONS: MM









TITLE: Transverse beam - rear		DATE: 15/06/2007
	DRAWN BY: Duncan Crump	DIMENSIONS: MM

Appendix B – Matlab code

B1 – Plotting DIC and FE data on to a regular grid:

```
function plottingcode
xel=900;                                % desired elements in the x direction
yel=300;                                % desired elements in the y direction
a=xlsread('DataplotMO1.xls');           % read in data file with lists of x, y, and value
xlin = linspace(min(a(:,1)),max(a(:,1)),xel); % form scale of regular grid in x
ylin = linspace(min(a(:,2)),max(a(:,2)),yel); % form scale of regular grid in y
[X,Y] = meshgrid(xlin,ylin);            % form regular grid using lines from xlin and ylin
Data= griddata(a(:,1),a(:,2),a(:,3),X,Y,'cubic'); % interpolate the raw data over the regular grid
mesh(X,Y,feplot)                        % plot an image of the interpolated data
```

B2 – Importing TSA image data (from Cedip):

```
%          GETPTWFRAME
% SYNATX:  [data, fileinfo] = GetPTWFrame (filename, frameindex)
% loads frame number "frameindex" from a PTW file "filename"
% result:
% data     contains imagedata on succes, 0 otherwise
% fileinfo is a structure with information about the ptw file
% documentation: see manuelrf.doc by CEDIP
% Copyright (c) Alexander Dillenz 2001

function [data, fileinfo] = GetPTWFrame (filename, frameindex)
data = 0;
s.m_filename = filename;
s = sIdent (s);
fileinfo = s;
if(s.m_format~='cedip')
    disp('Error: file format is not supported');
    result = -1;
else
    s = sCedipFileInfo (s);
    if(frameindex <= s.m_lastframe & frameindex>0) % ok
        s.m_framepointer = frameindex;
        s = sLoadCedip(s);
        data = s.m_data';
        clear s;
    else
        % frameindex exceeds no of frames
        disp('Error: cannot load frame. Frameindex exceeds sequence length.');
```

```
end;
end;

% SEQUENCE :: SIDENT
% identify sequence file
%
% Copyright (c) Alexander Dillenz 2000-2001
function s = sident(s)
if (isempty(s.m_filename))
    error('file not assigned');
end; %if
fid=fopen(s.m_filename,'r');
```



```

info=fread(fid,11,'int8'); %skip the first 11 bytes
fclose(fid); %close file
switch(char(info(1:3)))
case 'AI0' %AGEMA
    s.m_format='agma';
case 'CED'
    s.m_format='cedip';
    s.m_unit='dl';
    s = sCedipFileInfo(s);
otherwise
    s.m_format='unknown';
end; %switch
return;
function s = sCedipFileInfo(s)

% SEQUENCE :: SCEDIPFILEINFO
% Copyright (c) Alexander Dillenz 2000-2001
%
% for documentation see manuelrf.doc
fid=fopen(s.m_filename,'r');
if fid==-1
    error('fileopen');
end; %if
fseek(fid, 11, 'bof');
s.m_MainHeaderSize=fread(fid,1,'int32');
s.m_FrameHeaderSize=fread(fid,1,'int32');
fseek(fid, 27, 'bof');
s.m_nframes=fread(fid,1,'int32');
fseek(fid, 245, 'bof');
s.m_minlut=fread(fid,1,'int16');
s.m_maxlut=fread(fid,1,'int16');
if(s.m_maxlut==-1)
    s.m_maxlut=2^16-1;
end; %if
fseek(fid, 277, 'bof');
s.m_specialscale=fread(fid,1,'uint16'); % Special scale (Echelle Speciale)
scaleunit="";
scaleunit=fread(fid,10,'char');
s.m_scalevalue=fread(fid,17,'float');
if(s.m_specialscale==0)

```

```

        s.m_unit='dl';                % [dl T rad]
    else
        s.m_unit=scaleunit;          % [dl T rad]
    end; %if
    fseek(fid, 377, 'bof');
    s.m_cols=fread(fid,1,'uint16'); % Columns
    s.m_rows=fread(fid,1,'uint16'); % Rows
    if s.m_rows==0
        s.m_rows=128;
    end;%if
    if s.m_cols==0
        s.m_cols=128;
    end;%if
    s.m_bitres=fread(fid,1,'uint16'); % bit resolution
    fseek(fid, 403, 'bof');
    s.m_frameperiode = fread(fid,1,'float'); % frame rate
    s.m_integration = fread(fid,1,'float'); % integration time
    fseek(fid, 563, 'bof');
    s.m_comment=fread(fid,1000,'char');
    fseek(fid, 1563, 'bof');
    s.m_calibration=fread(fid,100,'char'); % calibration file name
    fseek(fid,s.m_MainHeaderSize,'bof'); %skip main header
    fseek(fid,s.m_FrameHeaderSize,'cof'); %skip frame header
    firstline = fread(fid, [s.m_cols, 1], 'uint16'); %read one line
    % look if first line contains lockin information
    if(firstline(1:4)==[1220,3907,1204,2382])
        s.m_cedip_lockin=1;
        s.m_rows=s.m_rows-1;
    else
        s.m_cedip_lockin=0;
    end; %if
    s.m_framepointer=1;
    s.m_firstframe=1;
    s.m_cliprect=[0 0 s.m_cols-1 s.m_rows-1];
    s.m_lastframe=s.m_nframes;
    s.m_FrameSize = s.m_FrameHeaderSize + s.m_cols * s.m_rows * 2;
    fclose(fid); %close file
    clear fid firstline scaleunit;
    return;
function s = sLoadCedip(s)

```

```

% SEQUENCE :: SLOADCEDIP
% loadcedip reads a Cedip-PTW file into matrix result
% Copyright (c) Alexander Dillenz 2000-2001
% for documentation see manuelrf.doc
% check filename
if (isempty(s.m_filename))
    error('file not assigned');
end; %if
% open file
fid=fopen(s.m_filename,'r');
if fid==-1
    error('file open');
end; %if
% skip main header
fseek(fid, s.m_MainHeaderSize,'bof');
if(s.m_cedip_lockin) % lockin -> skip first line
    fseek(fid, (s.m_framepointer-1) * (s.m_FrameSize + 2*s.m_cols), 'cof');
else
    fseek(fid, (s.m_framepointer-1) * (s.m_FrameSize), 'cof');
end; %if
fseek(fid,s.m_FrameHeaderSize,'cof'); %skip frame header
s.m_data = fread(fid, [s.m_cols, s.m_rows],'uint16'); %read one frame
% if a special scale is given then transform the data
if(s.m_specialscale)
    low = min(s.m_scalevalue);
    high = max(s.m_scalevalue);
    s.m_data = s.m_data .* (high-low) ./ 2^16 + low;
    clear low high;
end; %if
if(s.m_cedip_lockin) % lockin -> skip first line
    s.m_cliprect = [0 1 s.m_cols-1 s.m_rows];
end; %if
s.m_minval = min(min(s.m_data(1:s.m_cols,2:s.m_rows)));
s.m_maxval = max(max(s.m_data(1:s.m_cols,2:s.m_rows)));
fclose(fid); %close file
return;

```

B3 – Stitching TSA data:

```
function fullfield=datastitcher
```

```
A = GetPTWFrame('pos012.ptw', 1); % Read in data for each TSA image into a matrix
B = GetPTWFrame('pos013.ptw', 1); % Repeat for required number of images
C = GetPTWFrame('pos014.ptw', 1);
D = GetPTWFrame('pos015.ptw', 1);

for i= 1 : 196 % Select y pixels for each image
    for j= 38 : 320 % Select x pixels for each image
        fullfield(i+53,j-37)=A(i,j); % Copy the required pixels from each image into fullfield
matrix
    end % Repeat for required number of images
end

i = 0;
j = 0;
for i = 1:146
    for j = 38:320
        fullfield(i+249,j-37)=B(i,j);
    end
end

i=0;
j=0;
for i =1:150
    for j =38:320
        fullfield(i+395,j-37)=C(i,j);
    end
end

i=0;
j=0;
for i =1:136
    for j=38:320
        fullfield(i+545,j-37)=D(i,j);
    end
end
end
```

Appendix C –Future generic panel designs

Generic panel 2 (Figure 1) shows an increase in design complexity from the design used in this thesis. The panel has the same plan area as the first generic panel, and uses the same face sheet and core material combination. However, the design includes a cut-out in the middle of one of the long sides and, to accommodate this feature, the core has been split into two squares each 0.2 m x 0.2 m.

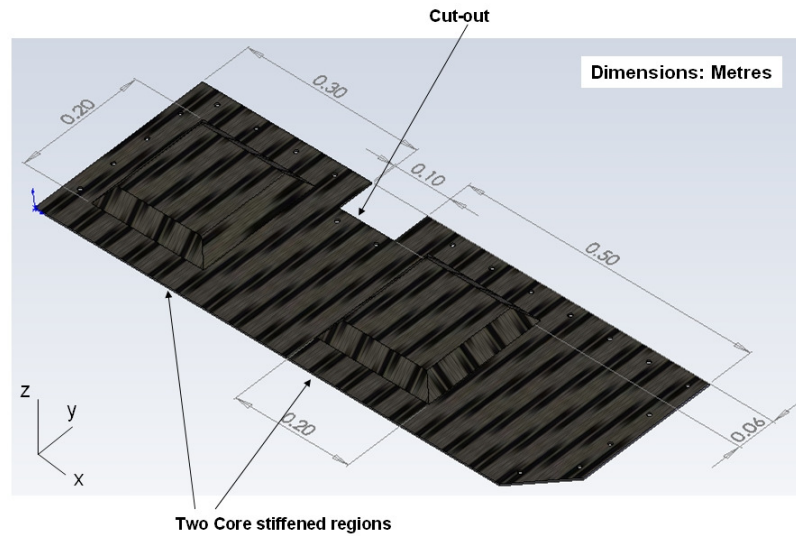


Figure 1: Geometry of generic panel design 2

Finally, generic panel 3 (Figure 2) retains the cut-out from generic panel 2. The core is continued around the cut-out region to stiffen the area seen in panel 2.

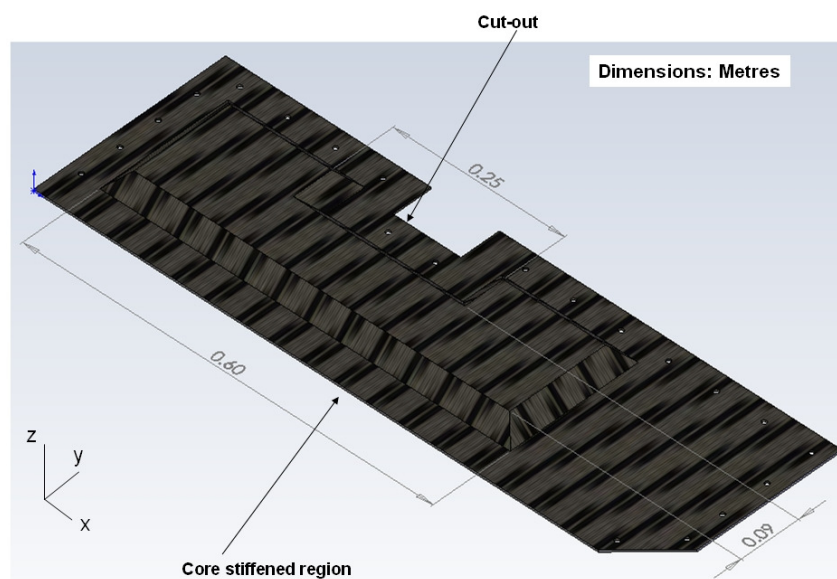


Figure 2: Geometry of generic panel design 3

Appendix D – List of Publications

Journals:

1. Crump, D.A., Dulieu-Barton, J.M., and Savage, J. *Manufacturing procedure for aerospace secondary sandwich panels*. Journal of Sandwich Structures and Materials. 2009, *In press*, DOI: 10.1177/1099636208104531
2. Crump, D.A., Dulieu-Barton, J.M., and Savage, J. *Design and commission of an experimental test rig to apply a full-scale pressure load on composite sandwich panels representative of aircraft secondary structure*. Submitted to Measurement, Science and Technology.
3. Crump, D.A., and Dulieu-Barton, J.M. *Thermoelastic stress analysis of full-scale aircraft secondary sandwich structure*. In preparation for Experimental Mechanics.

Conferences:

1. Crump, D.A., Dulieu-Barton, J.M., and Savage, J. *Manufacturing options for secondary aircraft CFRP sandwich components*. In: 16th International Conference on Composite Materials (ICCM), Kyoto, Japan, 2007.
2. Crump, D.A., Dulieu-Barton, J.M., and Savage, J. *Analysis of full-scale aerospace sandwich panels under pressure loading*. In: 8th International Conference on Sandwich Structures (ICSS), Porto, Portugal, 2008
3. Crump, D.A., Dulieu-Barton, J.M., and Savage, J. *Full field strain analysis of aircraft sandwich structures*. In: 11th International Congress of the Society for Experimental Mechanics (SEM), Orlando, USA, 2008.
4. Crump, D.A., Dulieu-Barton, J.M., and Savage, J. *Full-scale performance assessment of aircraft secondary sandwich structure using thermoelastic stress analysis*. Accepted in: 17th International Conference on Composite Materials (ICCM), Edinburgh, UK, 2009.